



HAL
open science

Molecular tectonics based on fluorinated porphyrins

Elena Vulpe

► **To cite this version:**

Elena Vulpe. Molecular tectonics based on fluorinated porphyrins. Other. Université de Strasbourg, 2015. English. NNT : 2015STRAF048 . tel-01292409

HAL Id: tel-01292409

<https://theses.hal.science/tel-01292409>

Submitted on 23 Mar 2016

HAL is a multi-disciplinary open access archive for the deposit and dissemination of scientific research documents, whether they are published or not. The documents may come from teaching and research institutions in France or abroad, or from public or private research centers.

L'archive ouverte pluridisciplinaire **HAL**, est destinée au dépôt et à la diffusion de documents scientifiques de niveau recherche, publiés ou non, émanant des établissements d'enseignement et de recherche français ou étrangers, des laboratoires publics ou privés.

ÉCOLE DOCTORALE DES SCIENCES CHIMIQUES

UMR 7140

THÈSE présentée par :

Elena VULPE

soutenue le : 29 septembre 2015

pour obtenir le grade de : **Docteur de l'université de Strasbourg**

Discipline/ Spécialité : Sciences Chimiques

**Tectonique Moléculaire à base de
Porphyrines Fluorées**

THÈSE dirigée par :

M. HOSSEINI Mir Wais
Mme BULACH Véronique

Professeur, université de Strasbourg
Professeur, université de Strasbourg

RAPPORTEURS :

M. BOITREL Bernard
M. GROS Claude

Directeur de recherche, université de Rennes
Professeur, université de Bourgogne

AUTRES MEMBRES DU JURY :

M. REGNOUF de VAINS Jean-Bernard
M. WEISS Jean

Professeur, université de Lorraine
Directeur de recherche, université de Strasbourg

**“If I have seen further it is by standing on the shoulders of
giants.”**

Isaac Newton

Acknowledgments

I would like to express my gratitude to the members of the jury: Dr. Bernard Boitrel, Prof. Claude P. Gros, Prof. Jean-Bernard Regnouf de Vains and Dr. Jean Weiss for the time they took to evaluate my thesis and for the interesting discussions during the thesis defense.

I would like to thank my thesis supervisors: to Prof. Mir Wais Hosseini for the opportunity to work on this project, for the scientific enthusiasm and motivation during the thesis. Special thanks to Prof. Véronique Bulach for the patience during the past three years, for the discussions, the support (especially before presentations) and the expertise in porphyrin chemistry.

An individual recognition to Isabelle Wessely, Dr. Alexandra Schade, Dr. Sylvain Grosjean and Prof. Stefan Braese, our collaborators within the Chiranet framework, without whom a part of the work described in this manuscript wouldn't be possible.

The laboratory members have been a great source of inspiration and motivation. Thanks to Prof. Sylvie Ferlay, Dr. Abdelaziz Jouaiti, Dr. Stéphane Baudron, Dr. Aurélie Guenet and Audrey Fluck for keeping their door open for questions and discussions and for their advices. Special thanks to Nathalie Kyritsakas, for finding time and performing a part of the X-Ray crystallographic measurements and to Valérie Rey, our secretary, for all the administrative help and her encouraging attitude. I would like to thank all my lab mates, past and present: Fabien, Nicolas Z, Nicolas "le petit", Patrick, Mohamed, Antoine, Bowen, Liwen, Fan, Yanan, Takumi, Hervé, Romain, Berangere, Cyril, Sasha, Georges, Maxime, Dimby (for the morning snacks), Nico (for the amazing French music culture), Chaojie (for all the presentations together), Ivan (for the homely spirit) and many more whom I missed to note, for the warm welcome and making the past three years unforgettable.

I would like to thank my friends, in Strasbourg or scattered around the globe, for being a constant source of inspiration and motivation, for their support, for the challenges and the happy moments shared together.

All my gratitude goes to my parents and my brother for encouraging me to pursue my dreams and always persevere, for their moral support and understanding.

Last but not the least, my love and recognition goes to Teo, for fully sharing this experience.

Contents

Introduction	10
Supramolecular Chemistry	10
Chirality	10
Enantioselective synthesis	11
Separation of enantiomers	11
Fluorine-“the siren of the elements”	12
Research Project	14
Chapter I.....	20
I.1. Molecular Tectonics	20
I.2. Molecular Networks.....	22
I.3. Coordination polymers or coordination networks.....	24
I.4. MOFs and Enantioselective separation.....	26
I.5. Halogen Bonding	29
Chapter II.....	38
II.1. Porphyrins.....	38
II.2. Synthesis of fluorinated and/or chiral porphyrin based tectons	43
Conclusion	53
Chapter III. Coordination Networks based on halogenated or/and Chiral Porphyrins.....	58
III. 1. Coordination networks and porphyrins: Some examples.....	58
III. 2. MOFs and Porphyrins: Synthetic strategy	63
III. 3. Self-assembly of new Zinc (II) Porphyrin tectons.....	64
III. 4. Double component systems composed of Porphyrin and Cd (II)	78
III. 5 Conclusion	81
Chapter IV.....	84
IV. 1. Halogen bonded networks involving pyridine derivatives.....	84
IV. 2. Halogen bonded networks involving porphyrins.....	91
General Conclusion	102
Experimental Part.....	105
Crystallographic Data	125
Résumé.....	161

Introduction

Contents

Introduction	10
Supramolecular Chemistry	10
Chirality	10
Enantioselective synthesis	11
Separation of enantiomers	11
Fluorine-“the siren of the elements”	12
Pharmaceuticals	12
Magnetic resonance imaging	13
Research Project	14
References	16

Introduction

“...that one might as well say that mankind is divisible into two great classes: hosts and guests. “

Hosts and Guests (1918), Max Beerbohm

The 20th century in chemistry started with the invention of chromatography, the development of Haber Bosch process for making ammonia, the development of X-ray Crystallography, Nuclear Magnetic Resonance, the determination of molecular structure of myoglobin and continued with the use of chiral transition metal centers for asymmetric catalysis, the olefin metathesis, stereoselective oxidation reactions, the discovery of fullerenes and the rise of new fields such as supramolecular chemistry and nanotechnology among many other advances. Yet many other discoveries are to come. Still, numerous processes need constant improvements in order to fulfill the on growing needs of the humanity.

Supramolecular Chemistry

The concept of molecular recognition was first mentioned in 1894 by Emil Fischer,¹ in his approach on receptor-substrate binding in enzymes. He described this by a *lock and key* image of steric fit in which the guest possesses a specific size and shape complementarity to the receptor or host receptor site. Later on, the concept of molecular recognition was stated as the basis of supramolecular chemistry. Originally, it was defined as non-covalent interaction between ‘host’ and ‘guest’ molecules. Supramolecular chemistry was introduced by Professor Jean-Marie Lehn in 1978,² 1987 Nobel Prize Winner. The concept is described as follows: “Just as there is the field of *Molecular Chemistry* based on the covalent bond, there is a field of *Supramolecular Chemistry*, the chemistry of molecular assemblies and of the intermolecular bond”.

Supramolecular chemistry has become a truly interdisciplinary topic influencing many fields such as: polymer chemistry^{3, 4} and material science, solid-state chemistry and crystal engineering, biological interactions and drug design.⁵

Chirality

Chiral organic molecules have an important role in biological systems where they are involved in numerous biochemical reactions. For example, all natural amino acids forming proteins (except glycine) are of the same enantiomeric configuration (L), or the folding of the DNA in a helical arrangement. In medicine and pharmacology, it becomes increasingly important to administer the enantiomerically pure compound as the presence of the second enantiomer can induce side effects. As a result, the development of processes (enantiospecific synthesis or enantioseparation of racemate) leading to enantiomerically pure species is of prime importance.

Enantioselective synthesis

One of the most frequently used methods for obtaining chiral compounds on lab scale is by far the homogeneous asymmetric catalysis, which usually uses chiral metallic complexes as catalysts.⁶ The catalysts are typically rendered chiral by using chiral ligands, however it is also possible to generate chiral-at-metal complexes⁷ using achiral ligands. This method allows the synthesis of optically pure molecules starting from achiral components. Some of the efficient reactions reported are enantioselective hydrogenation, epoxidation or reduction.⁸ However, this approach is not always transposable to industrial production due to the high costs of the catalysts, and the difficulties in recovering and reusing the catalyst.⁹ A possible solution is to perform asymmetric catalysis in heterogeneous phase. Usually, this is achieved by immobilization of the catalyst on a solid support *via* covalent bonds or other physical interactions. Some of the most used supports are mesoporous silica, zeolites or organic polymers.^{10, 11} Although, this method is a promising alternative, nevertheless, it has some disadvantages, namely the difficulty to control the arrangement of the active sites on the support and their distribution. The efficiency and the enantioselectivity of the catalytic process will be reduced if the active sites are inaccessible to the substrate.^{11, 12}

Separation of enantiomers

Enantioselective synthesis is not the only method to obtain chiral materials, chiral resolution can be an interesting alternative. This involves the isolation of one enantiomer from a racemic mixture by different methods.¹³ The cost of preparing racemic mixtures is low; furthermore, if both enantiomers are useful, the strategy is more cost-effective. Some of the most used methods are:

1. Liquid-liquid extraction¹⁴
2. Chiral resolution through crystallization (*via* an inclusion processes for example)¹⁵⁻¹⁷
3. Chromatography (HPLC,GC) or chiral electrophoresis with chiral stationary phases (cellulose (chiralpack@) β -cyclodextrine)^{18, 19}

Even though the cost to separate optically pure molecules is lower than the cost of enantioselective synthesis, some of the methods mentioned above require specific instruments, enhancing thus the overall cost. The quest for more accessible highly efficient methods is of current interest and is a challenging research topic. Molecular tectonics²⁰ is a possible and interesting approach to tackle this important issue. The design and synthesis of porous enantiomerically pure materials in the solid state capable of selectively uptake one of the two enantiomers may be an interesting possibility. Some examples of chiral coordination networks for asymmetric heterogeneous catalysis^{21, 22} or enantioselective separation²³ have been reported. Advantages of this strategy are combining enantioselective processes in homogeneous phase (efficiency and reproducibility) with heterogeneous systems (stability and recoverability). Crystalline coordination networks are highly ordered architectures with well-defined chiral cavities, which in principle, offer the possibility to adapt the size of pores and the number of chiral centers within cavities which can lead to higher yields and selectivity.

The use of inhalation anesthetics worldwide has risen to almost 50 million surgeries/year. Among them, fluoroether anesthetics: R-enflurane, R-isoflurane and R-desflurane (figure 1) bear a single chiral center. However, in practical use, they are still administered as racemic mixtures,²⁴ although in some cases the second enantiomer leads to undesired side effects.

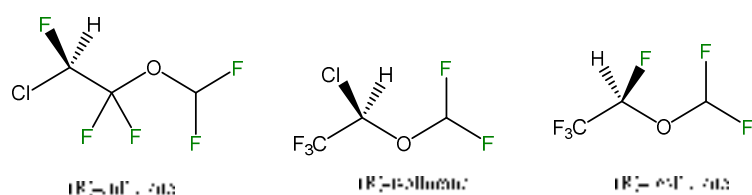


Figure 1. Fluoroether inhalation anesthetics.

The enantioselective synthesis of inhalation anesthetics presented above is difficult and costly. Yet, no efficient separation technique has been developed so far. One of the issues aside the chirality which should be considered when searching for a separation method is the nature of substituents on the molecule's backbone. The presence of fluorine and chiral centers as a whole should be treated as equally important features when screening for an adequate separation technique.

Further on, it is worth to point out that the presence of fluorine atom, owing to its peculiarity, could play an important role in the design and formation of coordination networks capable of separating aforementioned molecules.

Fluorine-“the siren of the elements”

“Fluorine leaves nobody indifferent; it inflames emotions such as affections or aversions. As a substituent, it is rarely boring, always good for a surprise, but often completely unpredictable.”²⁵ Among the elements, it ranks 24th in universal abundance and 13th in terrestrial abundance, but its uniqueness comes from an unprecedented combination of small size, very low polarizability and the strongest inductive effect found among the chemical elements. These result in a set of interesting applications and make fluorine an indispensable for all parts of our daily life, such as food, health care as well as the alternative energy, which is becoming of importance in the times of limited resources and climate change.²⁶

Pharmaceuticals

Since the introduction of a fluorine atom to the 9 α position of cortisol in 1954,²⁷ that showed that indeed the presence of fluorine improved the therapeutic index as an anti-inflammatory by an order of magnitude, fluorine is found in *ca* 15-20% of new chemicals licensed each year in pharmaceutical products and up to 30% in agrochemicals.²⁸ As illustrated in the diagram below (figure 2), fluorine accounts for about 57% of the total amount of halogens used in drug compounds.²⁹

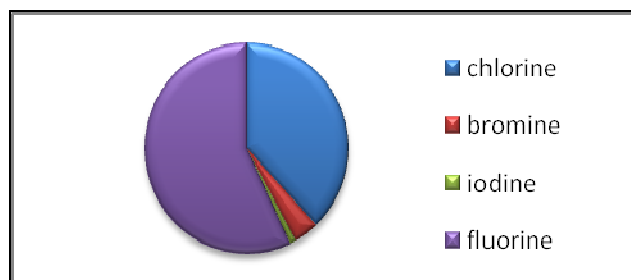


Figure 2. Classification of halogenated drugs according to the kind of halogen used.

Some of the top-selling fluorinated pharma products include Prozac (antidepressant), Lipitor (cholesterol lowering drug) and Ciprobay an antibacterial compound. The introduction of fluorine atoms in pharmaceuticals was boosted also by the introduction of safe and selective fluorinating agents during 70's which on its own became a highly researched subject.^{30, 31} One of the main reasons why the introduction of fluorine atoms is such a “hit” is due to the delay of inactivation and lengthened dosage periods owing to the carbon–fluorine bond stability³² as well as increased lipophilicity owing to its more hydrophobic nature when compared to carbon–hydrogen bond. This often helps in cell membrane penetration and hence in bioavailability.³³

Positron emission tomography (PET)

Positron emission tomography is an imaging technique used both as a medical and research tool. PET is heavily used in clinical oncology and neuroimaging as a diagnosis tool for certain brain diseases. It creates a three dimensional image of functional processes in the body, by detecting gamma rays emitted by a positron emitting short-lived radioactive tracer, which is introduced in the body with a biologically active molecule.³⁴ Depending on their purpose a series of tracers have been developed and fluorine-18 radioisotope, with a half life of about 20 minutes have been extensively used. Among the most known tracers one can cite Fluorodeoxyglucose (FDG) a standard tracer in cancer patient management, Fallypride and Desmethoxyfallypride for dopamine D2/D3 receptors, Mefway for serotonin 5HT1A etc.

Magnetic resonance imaging

The need to detect and monitor various diseases in real time and the development of targeted therapeutics are currently major challenges in medicine. Imaging techniques play a key role in settling these issues and magnetic resonance imaging is one of the most promising amongst them. The basics of imaging by nuclear magnetic resonance (NMR) were laid by Lauterbur in the early 1970s³⁵ and rely on the ability of hydrogen atoms to align in an external magnetic field. Though it is a very powerful technique it also has its limits, the use of contrast agents needed to improve the low sensitivity, can generate toxicity issues. One of the strategies used to overcome this point is the development of a second color or hot spot imaging using heteronuclear MRI atoms in addition to hydrogen. ¹⁹F seems to be one of the most promising imaging nucleus, it has 100% natural abundance and a ½ spin with sensitivity of 83% that of the proton. ¹⁹F chemical shifts vary in a broad range and only trace amounts are present in the human body. As in the case of proton

magnetic resonance imaging (MRI), the presence of contrast agents is needed to generate a good-quality image. Thus the use of high density of ^{19}F nuclei in the tracers is one of the strategies employed. So far a vast range of contrast agents have been tested ranging from small fluorinated molecules to polymeric tracers and fluorinated metallic nanoparticles; some of them are even FDA approved and currently used in clinical treatments.³⁶ ^{19}F MRI is a relatively young technique, however intense efforts, particularly in research of biocompatible highly fluorinated molecules, show an encouraging picture for the future of this technique.

The last but not the least, relatively recent studies discussing the influence of the fluorine on the protein structures and protein-protein interactions, show that fluorinated amino acids have become an important tool in the field of protein engineering.³⁷ There is an acute need to understand and generalize the effects of introducing fluorinated aminoacids into naturally occurring protein sequences.

One could argue that there is no connection between the inhalation anesthetics, the importance of fluorine in pharmaceuticals, Magnetic Resonance Imaging and protein engineering field. However the point unifying these components is the question of how fluorine influences the structure, and, how it interacts with its surrounding media. Concerning the design of porous crystals for inhalation anesthetics separation, fluorinated medicine administered to patients or molecules used for imaging, we lack knowledge on how exactly the presence of fluorine influences the interactions within the network or generically with the human body.

Research Project

Considering features discussed so far: molecular recognition and supramolecular chemistry, chirality, fluorine and inhalation anesthetics, a key point is missing in order to conceptualize the aim of this work: molecular tectonics, which will be discussed in the next chapter in detail. This approach deals with the design and synthesis of crystalline materials with tunable properties. As mentioned before, the crystalline coordination networks are highly ordered architectures that can offer porosity. This particular property can be used to generate materials with specifically designed chiral pores for separation of chiral anesthetics. The “success” of this separation procedure is based on molecular recognition between the network and the molecule of interest, not only due to the chirality of the network but also through specific F---F contacts between the finely customized networks and the fluorinated molecules to be separated.

This work is focused on the design and generation of molecular networks resulting either from combinations of organic tectons with metallic centers/complexes or organic tectons and iodo-fluoroarenes, with the aim of fabricating porous crystalline materials. The selection of the organic tectons as well as the metal centers is a key issue, as it will influence the final molecular network. In this PhD project, we have focused on porphyrin based molecules as organic tectons. Indeed, the porphyrin backbone offers particular properties such as thermal stability, robust nature and relatively easy functionalization.³⁸⁻⁴⁰ The incorporation of fluorine atoms into the porphyrin

backbone leads to interesting electron deficient systems with a variety of applications such as NMR imaging, catalysis and biomedical applications.^{36, 41, 42} However, so far only few investigations dealing with the formation of coordination networks with this class of fluorinated tectons have been reported. The porphyrin molecule offers also specific coordination abilities and, depending on the number of the coordinating substituents present on the backbone, the tetraaza core offers a perfectly suitable core for binding a wide range of metal ions. As mentioned before, the possibility to functionalize “easily” the porphyrin backbone either in the *meso* positions or in their β positions with fluorinated and chiral substituents is crucial for generating networks with fluorinated, chiral or fluorinated and chiral cavities that could increase the interactions between the molecules of interest and the walls of the cavities and channels.

Building on previous studies of our group,⁴³⁻⁴⁶ we focused on the design of porphyrin based building blocks bearing neutral coordinating sites such as pyridyl units on the one hand and fluorinated/halogenated and chiral alkyl chains in the opposite *meso* positions of the porphyrin on the other. The structural characterization of the materials was possible by generation of crystalline materials, precisely single crystals. Their analysis by X-Ray diffraction gave information on the dimensionality and the geometry adopted by molecular networks and their organization in the crystal.

For the separation techniques, we can divide the approaches into two pathways:

The first one consists in generating the molecular network by combining the functionalized organic tecton with a suitable metal ion, in a first step. Afterwards, the obtained crystals can be emptied from the potential solvent present in the architecture under vacuum. The empty crystals thus obtained are then exposed to a racemic mixture of molecules to be separated (figure 3).

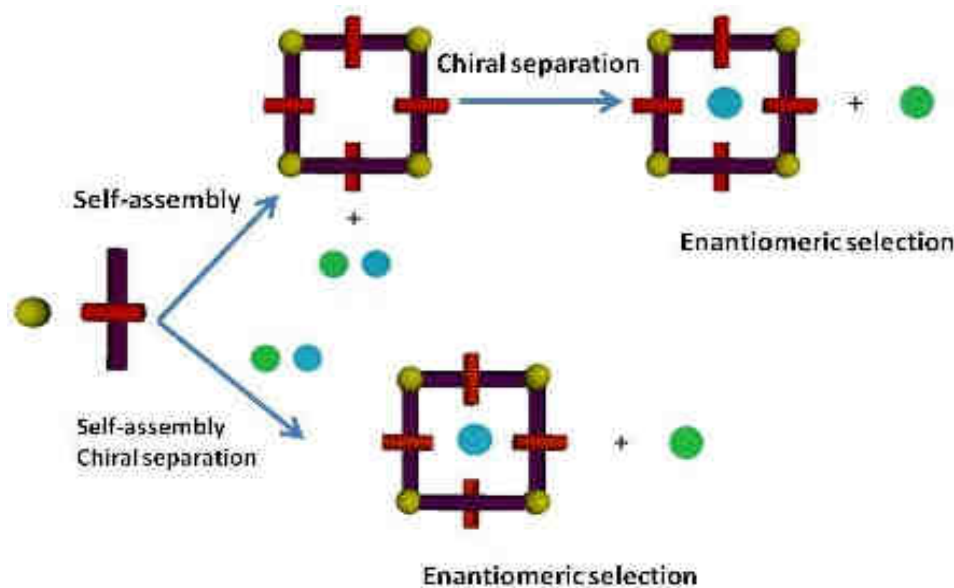


Figure 3. A schematic representation of the project's objectives (the blue and green circles represent the separated molecules).

The second strategy is a “one pot” approach, where the racemic mixture of molecules is used during the self-assembly process. Thus, the self-assembly process and the chiral separation occur in

a single step through the formation of the network, and the separation is achieved through the selective encapsulation of one of the two enantiomers within the network.

This manuscript is separated in four chapters as follows:

Chapter one is focused on principles of molecular tectonics and halogen bonding for a better understanding of the network formation. It also focuses on several examples reported in the literature that discuss the aforementioned strategies of separation.

Chapter two presents first a general introduction to porphyrin macrocycle, its synthesis and characterization. Then the second part is fully dedicated to the synthetic work achieved during the course of this project as well as structural investigations.

Chapter three describes the coordination networks obtained through assembly of the porphyrin based tectons and Zn(II) or Cd(II) salts. A detailed structural characterization of the networks and the influence of the fluorinated substituents on packing of networks are given.

Chapter four concerns partly with the description of halogen bonded networks reported in the literature as well as the results obtained in the framework of our investigations on new porphyrin based tectons, focusing on the importance of the fluorine substituents. A series of bipyridine ligands, obtained through collaboration with the group of Pr Stefan Bräse (Karlsruhe Institute of Technology, Germany), were also used to generate molecular networks with iodo-fluoroarenes and are described in detail in this chapter.

References

1. E. Fischer, *Ber. Dtsch. Chem. Ges.*, 1894, **27**, 2985-2993.
2. J. M. Lehn, in *Pure Appl. Chem.*, 1978, vol. 50, p. 871.
3. N. Roy, E. Buhler and J.-M. Lehn, *Polym. Int.*, 2014, **63**, 1400-1405.
4. P. Cordier, F. Tournilhac, C. Soulie-Ziakovic and L. Leibler, *Nature*, 2008, **451**, 977-980.
5. D. Y. W. Ng, Y. Wu, S. L. Kuan and T. Weil, *Acc. Chem. Res.*, 2014, **47**, 3471-3480.
6. P. Pino and G. Consiglio, in *Fundamental Research in Homogeneous Catalysis*, ed. M. Tsutsui, Springer US, 1979, pp. 519-536.
7. E. B. Bauer, *Chem.Soc.Rev.*, 2012, **41**, 3153-3167.
8. T. Inagaki, A. Ito, J.-i. Ito and H. Nishiyama, *Angew. Chem. Int.Ed.*, 2010, **49**, 9384-9387.
9. H. U. Blaser, F. Spindler and M. Studer, *Appl. Catal., A* 2001, **221**, 119-143.
10. M. Heitbaum, F. Glorius and I. Escher, *Angew. Chem. Int.Ed.*, 2006, **45**, 4732-4762.
11. P. McMorn and G. J. Hutchings, *Chem.Soc.Rev.*, 2004, **33**, 108-122.
12. D. Pini, A. Mandoli, S. Orlandi and P. Salvadori, *Tetrahedron: Asymmetry* 1999, **10**, 3883-3886.
13. E. Tesarova and D. W. Armstrong, in *Journal of Chromatography Library*, eds. I. M. F. T. Zdeněk Deyl and T. Eva, Elsevier, 1998, vol. Volume 60, pp. 197-256.
14. B. Schuur, B. J. V. Verkuijl, A. J. Minnaard, J. G. de Vries, H. J. Heeres and B. L. Feringa, *Org. Biomol. Chem.*, 2011, **9**, 36-51.
15. X. X. Zhang, J. S. Bradshaw and R. M. Izatt, *Chem. Rev.*, 1997, **97**, 3313-3362.
16. F. Faigl, E. Fogassy, M. Nógrádi, E. Pálovics and J. Schindler, *Tetrahedron: Asymmetry* 2008, **19**, 519-536.
17. M. Leeman, G. Brasile, E. Gelens, T. Vries, B. Kaptein and R. Kellogg, *Angew. Chem. Int.Ed.*, 2008, **47**, 1287-1290.
18. T. Jira, A. Bunke, M. G. Schmid and G. Gübitz, *J. Chromatogr. A* 1997, **761**, 269-275.
19. V. A. Davankov, *J. Chromatogr. A* 1994, **666**, 55-76.
20. M. W. Hosseini, *Acc. Chem. Res.*, 2005, **38**, 313-323.
21. M. Yoon, R. Srirambalaji and K. Kim, *Chem. Rev.*, 2012, **112**, 1196-1231.

22. L. Ma, C. Abney and W. Lin, *Chem.Soc.Rev*, 2009, **38**, 1248-1256.
23. J.-R. Li, J. Sculley and H.-C. Zhou, *Chem. Rev.*, 2011, **112**, 869-932.
24. H. Y. Aboul-Enein, J. Bojarski and J. Szymura-Oleksiak, *Biomed. Chromatogr.* , 2000, **14**, 213-218.
25. M. Schlosser, *Angew. Chem. Int.Ed*, 1998, **37**, 1496-1513.
26. R. Berger, G. Resnati, P. Metrangolo, E. Weber and J. Hulliger, *Chem.Soc.Rev*, 2011, **40**, 3496-3508.
27. J. Fried and E. F. Sabo, *J. Am. Chem. Soc*, 1954, **76**, 1455-1456.
28. D. O'Hagan, *J. Fluorine Chem.* , 2010, **131**, 1071-1081.
29. M. Z. Hernandez, S. M. T. Cavalcanti, D. R. M. Moreira, W. F. de Azevedo Junior and A. C. L. Leite, *Current Drug Targets*, 2010, **11**, 303-314.
30. R. E. Banks, *J. Fluorine Chem.* , 1998, **87**, 1-17.
31. T. Umemoto, *J. Fluorine Chem.* , 2000, **105**, 211-213.
32. W. K. Hagmann, *J. Med. Chem.* , 2008, **51**, 4359-4369.
33. J. Swinson, *PharmaChem*, 2005, 26-30.
34. Dale L. Bailey, David W. Townsend, Peter E. Valk and M. N. Maisey, *Positron Emission Tomography*, Eds. Springer-Verlag London, 2005.
35. P. C. Lauterbur, *Nature*, 1973, **242**, 190-191.
36. I. Tirota, V. Dichiarante, C. Pigliacelli, G. Cavallo, G. Terraneo, F. B. Bombelli, P. Metrangolo and G. Resnati, *Chem. Rev.*, 2015, **115**, 1106-1129.
37. M. Salwiczek, E. K. Nyakatura, U. I. M. Gerling, S. Ye and B. Kokschi, *Chem.Soc.Rev*, 2012, **41**, 2135-2171.
38. M. d. G. H. Vicente and K. M. Smith, *Current organic synthesis*, 2014, **11**, 3-28.
39. W.-Y. Gao, M. Chrzanowski and S. Ma, *Chem.Soc.Rev*, 2014, **43**, 5841-5866.
40. V. Bulach and M. W. Hosseini, *Handbook of Porphyrin Science*, Eds. K. Kadish, K. Smith and R. Guilard, *World Scientific*, 2011, **13**, 299-391.
41. T. Goslinski and J. Piskorz, *J. Photochem. Photobiol., C* 2011, **12**, 304-321.
42. I. Hatay, B. Su, M. A. Méndez, C. Corminboeuf, T. Khoury, C. P. Gros, M. Bourdillon, M. Meyer, J.-M. Barbe, M. Ersoz, S. Záliš, Z. Samec and H. H. Girault, *J. Am. Chem. Soc*, 2010, **132**, 13733-13741.
43. E. Deiters, V. Bulach and M. W. Hosseini, *Chem. Commun.*, 2005, 3906-3908.
44. E. Kuhn, V. Bulach and M. W. Hosseini, *Chem. Commun.*, 2008, 5104-5106.
45. F. Sguerra, V. Bulach and M. W. Hosseini, *Dalton Trans.*, 2012, **41**, 14683-14689.
46. N. Marets, V. Bulach and M. W. Hosseini, *New J. Chem.* , 2013, **37**, 3549-3558.

Chapter 1

Contents

Chapter I	20
I.1. Molecular Tectonics	20
I.1.A. Endo-receptors	20
I.1.B. Exo-receptors	21
I.1.C. Intermolecular Recognition	22
I.2. Molecular Networks	22
I.2.A. Dimensionality and geometry	23
I.3. Coordination polymers or coordination networks	24
1.3.A. Organic tectons or ligands	24
I.3.B. Metallic centers	25
I.4. MOFs and Enantioselective separation	26
I.5. Halogen Bonding	29
1.5.A. Halogen bonding in Liquid crystals	31
1.5. B. Halogen bonding and Anion sensing	32
1.5.C. Halogen bonding and Supramolecular networks	32
References	33

Chapter I.

I.1. Molecular Tectonics

Molecular tectonics (from the Greek tekton: builder) is an approach which combines supramolecular chemistry and the solid state chemistry. The term was proposed in 1993 by S. Mann¹ and deals with molecular scale building of large scale architectures in crystalline phase. The formation of such constructions is based on interactions between tectons (building blocks) possessing complementary or auto-complementary recognition sites both in terms of energy and geometry. The iteration of the interaction processes leads to the translation of the recognition pattern and generates molecular networks possessing translational symmetry (figure I.1). The dimensionality of the network (one, two or three) depends on the number of translations of recognition patterns in the 3 directions of space.² A prerequisite for the self-assembly processes is the reversible interactions between tectons. Indeed, the use of non-covalent interactions allows self-repairing processes correcting connectivity mistakes during the construction event.

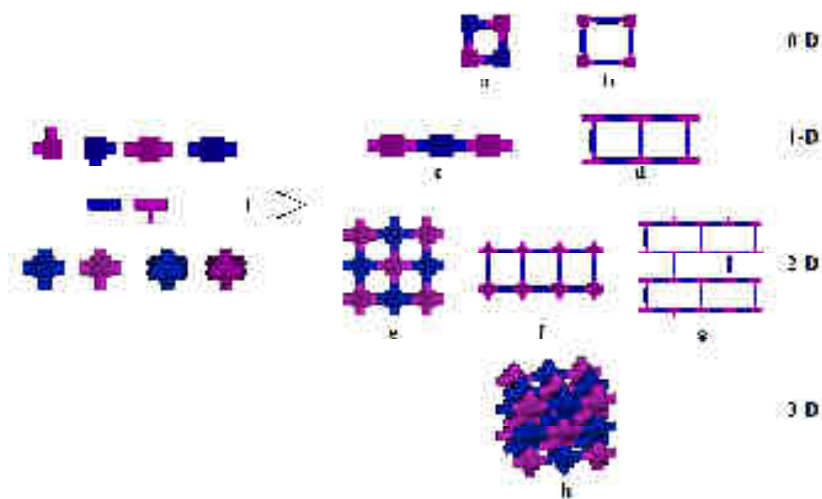


Figure I.1. Schematic representation of supramolecular extended and periodic architectures and their dimensionality depending on the geometry of tectons.

The role of the chemist is to control the self-assembly process through the design of molecular tectons using classical covalent chemistry. One may control energetic factors (intermolecular interactions) leading to molecular recognition processes, as well as the number of different tectons and the relative orientation of the interaction sites. Considering the last parameter two distinct families of tectons, mainly endo and exo, can be considered.

I.1.A. Endo-receptors

For this type of receptors, interaction sites are located in a convergent manner leading to formation of “host-guest” complexes called inclusion complexes³ in the presence of suitable substrates. Some of the most popular systems includes: cavitands,^{4, 5} cryptands,⁶ cages⁷ and of course crown ethers.⁸ Since these complexes are discrete entities, they will not be discussed further (figure I.2).

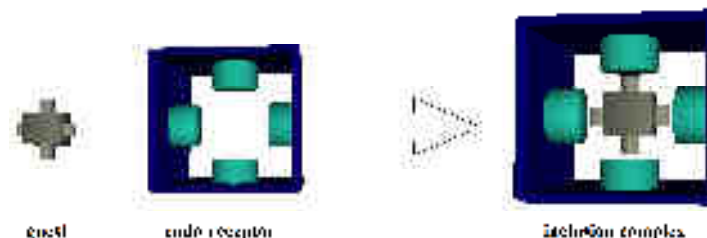


Figure I.2. A schematic representation of the formation of an inclusion complex by combining an endo-receptor with a substrate.

I.1.B. Exo-receptors

Exo-receptors are tectons with their interaction sites arranged in a divergent fashion and lead to the formation of a molecular network if the orientation and the number of connecting sites allows the translation of the interaction pattern (figure I.3b), otherwise a discrete complex can be formed (figure I.3a).

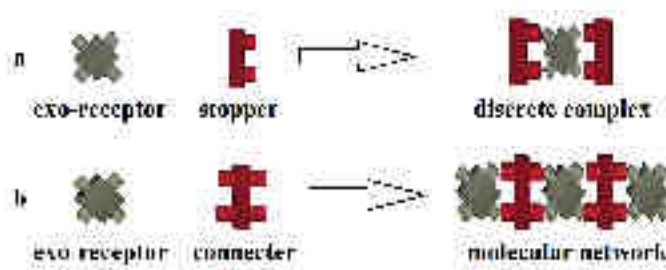


Figure I.3. A schematic representation of the formation of a discrete complex (a) and of a molecular network (b) using an exo-receptor.

By changing the number of interaction sites on the tecton and adjusting their orientation, it is possible to design infinite two-dimensional or three-dimensional architectures (figure I.4).

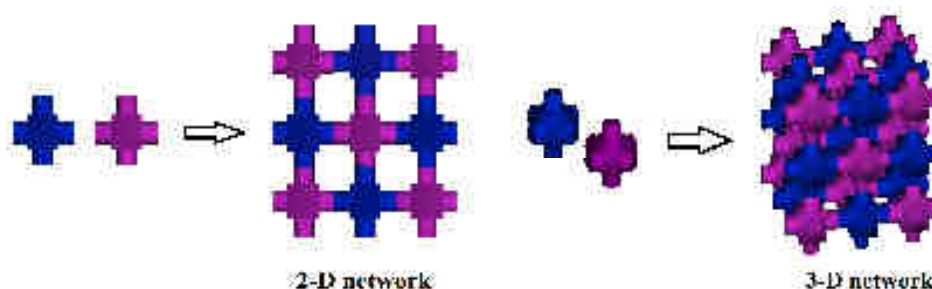


Figure I.4. Schematic representations of 2D and 3D molecular networks by self-assembly processes.

Lastly, one can distinguish between self-complementary and complementary tectons (figure I.5). The former represents a single entity equipped with complementary connecting sites capable of forming a network on its own. The latter implies the need of at least two complementary tectons in order to generate a network.

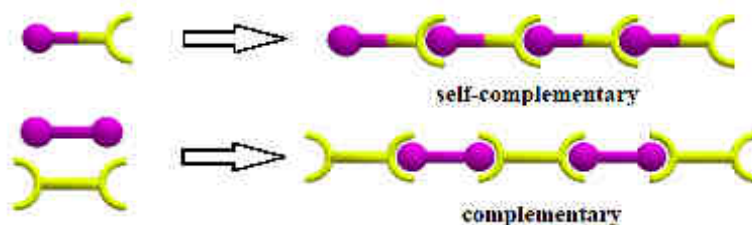


Figure I.5. A schematic representation of molecular networks formed by complementary and self-complementary tectons.

I.1.C. Intermolecular Recognition

A second essential point in molecular tectonics is the self-healing processes allowing the system to repair eventual structural defects that appeared during the self-assembly process, therefore the interactions between tectons need to be reversible. Thus, interconnection through the formation of covalent bonds cannot be employed due to their irreversible nature and high energetic requirements. However, the less energetic and reversible interactions (figure I.6), such as coordination bonds or H-bonds allowing bond breaking and making leading to the formation of the most stable assembly under thermodynamic control may be used. The toolbox used by molecular tectonics is based on reversible non covalent interactions which vary in strength from 0.5 kJ/mol up to 400 kJ/mol, from stronger interactions such as coordination bonds⁹ to weaker intermolecular interactions like π - π stacking¹⁰ and van der Waals forces.¹¹ In recent years, halogen bond^{12, 13} have been added to this list.

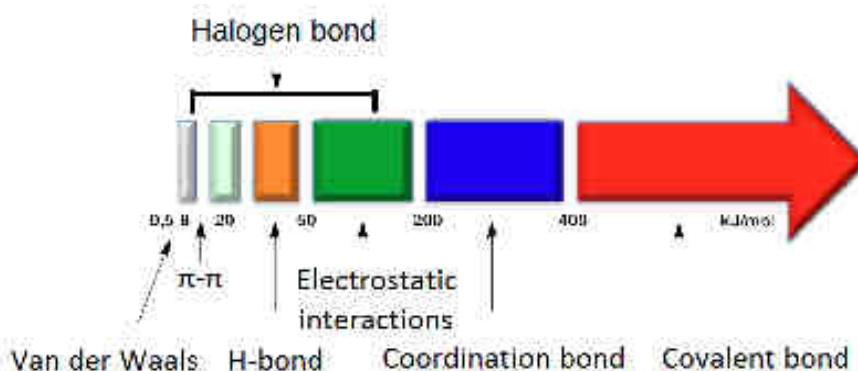


Figure I.6. An energy scale of molecular interactions used for building supramolecular assemblies.

I.2. Molecular Networks

Molecular tectonics is a rational approach to the design and formation of periodic infinite architectures, also called molecular networks. It is based on self-assembly processes between programmed tectons in the crystalline phase. The self-assembly processes take place between either complementary or self-complementary tectons and depend on the chemical nature, the number and the orientation of connecting sites. Thus the topology and dimensionality of molecular network may be controlled by iteration of the recognition process in the one-, two- or three-dimensions of space.

I.2.A. Dimensionality and geometry

1D networks

The 1-D networks are one of the simplest geometries to imagine and need tectons possessing at least two divergently oriented recognition sites. Among a variety of possible 1-D geometries, some appear more frequently than others. An infinite chain can, amongst others, adopt a linear,¹⁴⁻²⁰ a zig-zag,^{21, 22} wavy^{23, 24} or helical geometries (figure I.7).²⁵



Figure I.7. Schematic representations of possible 1-D geometry: linear (A), zig-zag (B), wavy (C,D) and helical (E).

2D networks

2-D networks are generated when the iteration of the recognition process is translated in two dimensions of the space. In order for it to occur the tectons have to possess at least 3 recognition sites oriented in a divergent manner. The most recurrent geometries found in the literature are: planar,²⁶ sine wave²⁷ or zig-zag (figure I.8).^{28, 29}



Figure I.8. Schematic representations of possible 2-D sheets: linear (A), zig-zag (B), sine wave (C,D).

Depending on the nature of the building blocks, one can expect several motifs for two-dimensional architectures. The generation of these motifs depends on the number and orientation of the recognition sites. For example, three recognition sites can give a honeycomb arrangement (figure I.9 (C)),^{30, 31} while four recognition sites leads to the formation of square-grids^{26, 32} or rectangular grids (figure I.9 (A,B)).^{33, 34}

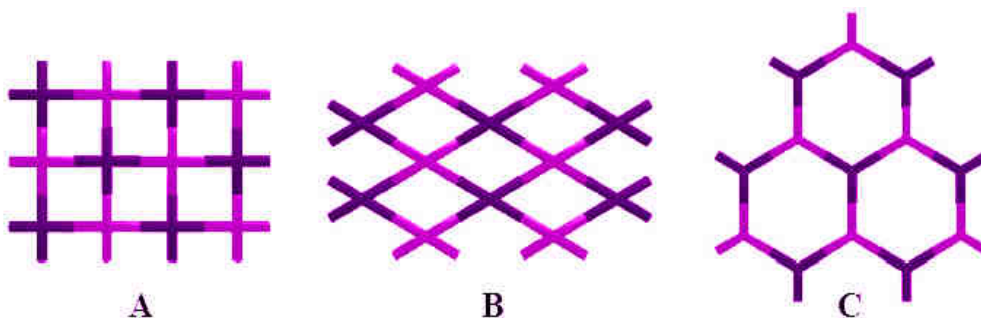


Figure I.9. Schematic representations of possible 2-D architectures: square grid (A), rectangular grid (B), honeycomb arrangement (C).

3D networks

In order to generate a 3-D network, thus assure the iteration of the interaction process in the three directions of the space, one of the tectons have to possess four non-coplanar recognition sites oriented in a divergent fashion. Given the complexity of these architectures compared to the 1-D and 2-D, it is much more difficult to predict their formation. Among the possible topologies of the 3-D networks are: cubic, diamondoid and gyroid (figure I.10). The cubic and diamondoid³⁵ networks are more often reported, yet the gyroid networks³⁶⁻³⁸ are more difficult to design, thus fewer examples are described.



Figure I.10. Schematic representations of possible 3-D topology: cubic (A), gyroid (B), diamondoid (C).

All the reversible interactions presented in Figure I.6 can be used to generate molecular networks, among some of the most used so far we can find hydrogen bonds,³⁹ coordination bonding^{40, 41} and lately halogen bonding.⁴² The last two will be discussed more in detail as they represent the topic of this thesis.

1.3. Coordination polymers or coordination networks

A coordination polymer, as recommended by IUPAC in 2013 “is a compound with repeating coordination entities in 1, 2 or 3 dimensions”,⁴³ including the pure inorganic networks as well as “hybrid” organic-inorganic networks such as MOFs.⁴⁴ The former are molecular networks containing metallic centers as construction nodes connecting organic or inorganic entities.⁴⁵

After the communication of R. Robson in 1989⁴⁶ followed by a full paper in 1990⁴⁷ this subject has attracted lots of interest among scholars due to the huge variety of possible combinations between organic tectons and metallic centers or complexes that can lead to a large diversity of possible networks with tuneable properties.

1.3.A. Organic tectons or ligands

Supramolecular chemistry relies on the classic organic chemistry for the design of the tectons with various coordinating sites such as: pyridine or nitriles (which are neutral moieties) or carboxylates and phenolates as charged moieties. As seen previously in order to design 1-D, 2-D or 3-D network the number and orientation of coordinating sites has to be controlled. The term that describes the spatial arrangement (convergent or divergent) and the number of the coordinating sites is called denticity. Thus the tectons with one, two, three or four divergently oriented coordinating sites will be called monodentate, bidentate, tridentate or tetradentate ligands tectons respectively. For more

The diversity of organic tectons and metallic centers or complexes, as described above, leads to infinite possibilities of combining these two for the formation of coordination polymers.

Crystal engineering of coordination polymers is a rational approach to generate solid-state structures that is of fundamental and practical importance. Several groups have pioneered^{47, 49-52} the development of the field. By finely adapting the organic tectons and the metallic centers one can not only play with the dimensionality of the generated network but also “imprint” a specific property. Recently it has become of outmost interest to be able to obtain porous materials with well defined cavity dimensions, in order to modify these cavities with different substituents depending on the ultimate property one needs to generate. One of the strategies, also known as post-synthetic modification,⁵³ is broadly defined as chemical derivatization of the networks involving covalent bond formation with the framework. Furthermore, recently post-synthetic metallation⁵⁴ procedures have been successfully employed which relied on the coordinating ability of the network and not on covalent bonding.

Porosity is one of the properties that have been extensively studied towards applications such as gas storage^{55, 56} and gas sensing,⁵⁷ catalysis,^{58, 59} gas adsorption and separation,⁶⁰ luminescence⁶¹ and others.⁶² Understanding intermolecular interactions and recognition phenomena in crystalline materials should establish a reliable baseline for generating desired properties starting from the simple building blocks.

I.4. MOFs and Enantioselective separation

The advantages in the use of crystalline materials as possible hosts for enantioselective recognition processes have been described in the Introduction of this thesis, thus this part will focus on several literature examples that have been proven of potential use. The group of Che *et al*⁶³ reported in 2001 the formation of a homochiral 3-D diamondoid type network with large cavities able to recognize selectively one enantiomer from a racemic mixture (figure I.13).

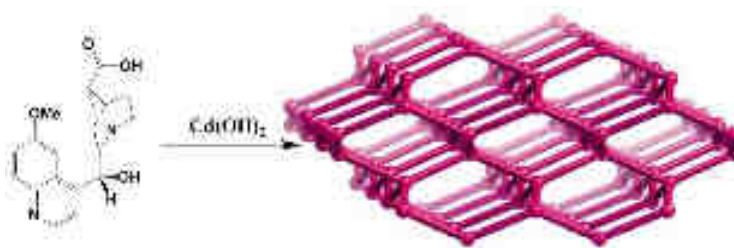


Figure I.13. Schematic representation of the topology of the 3-D diamondoid network resulting from the combination of the chiral organic tecton with Cd^{2+} cation.

When added to a racemic mixture of 2-butanol, the crystalline powder leads to the selective inclusion of one of the two enantiomers, the butan-2-ol and thus to enantiomeric separation. The (S)-butan-2-ol desorbed from the network, showed specific optical rotation identical to that of a pure (S)-butan-2-ol standard. The *ee* value was estimated to be approximately 98.2 %. The same

experiment with a racemic mixture of 2-methylbutan-1-ol gave similar results, with the selective inclusion of S enantiomer (figure I.14).

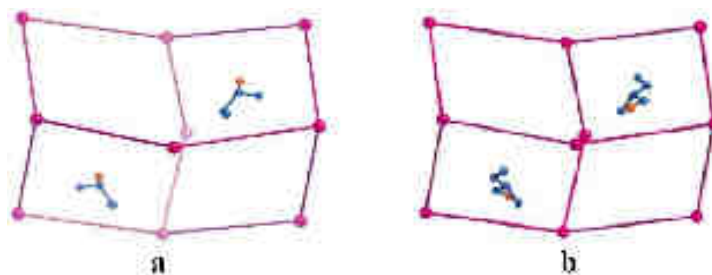


Figure I.14. A simplified representation of the diamondoid network with the selective inclusion of (S)-2-butanol (a) and (S)-2-methylbutan-1-ol (b).

A more recent example by Yuan *et al*⁶⁴ describes a successful use of a homochiral network as a stationary phase for enantio-separation of alcohols and ketones. This is a particularly interesting example as the stationary phase was filled with particles of the coordination network (5 μm), thus excluding the use of silica as support (figure I.15).

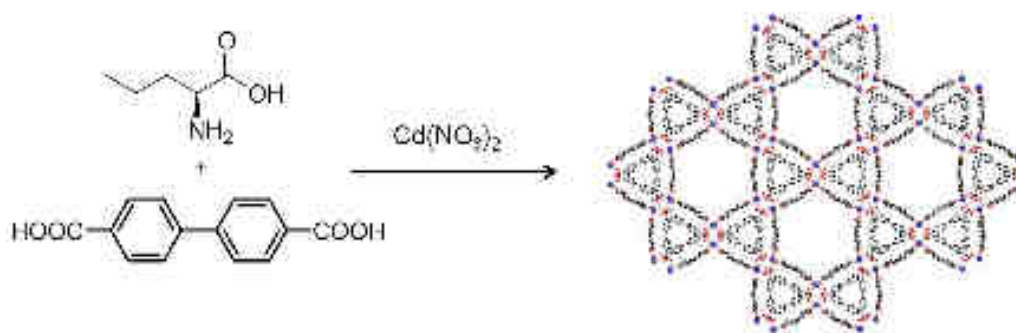


Figure I.15. A portion of the 3-D network presenting tubular channels used as stationary phase for chiral separation.

In our group, this subject has been intensely developed by Dr. Patrick Larpent⁶⁵ and more recently by Nicolas Marets⁶⁶ on chiral porphyrin based tectons. The strategy used by Dr. Larpent was to employ rigid neutral or charged organic tectons of different length bearing two chiral substituents per molecule. The latter were used with a great variety of metal salts to generate chiral networks with different geometry for chiral separation. Few examples of 3-D cuboid coordination polymers are presented in figure I.16. Here, rigid neutral chiral tectons with two divergently oriented pyridine moieties with $\text{Zn}(\text{II})$ (metallic node) and SiF_6^{2-} dianion behaving as inorganic tecton form the 3-D architectures.

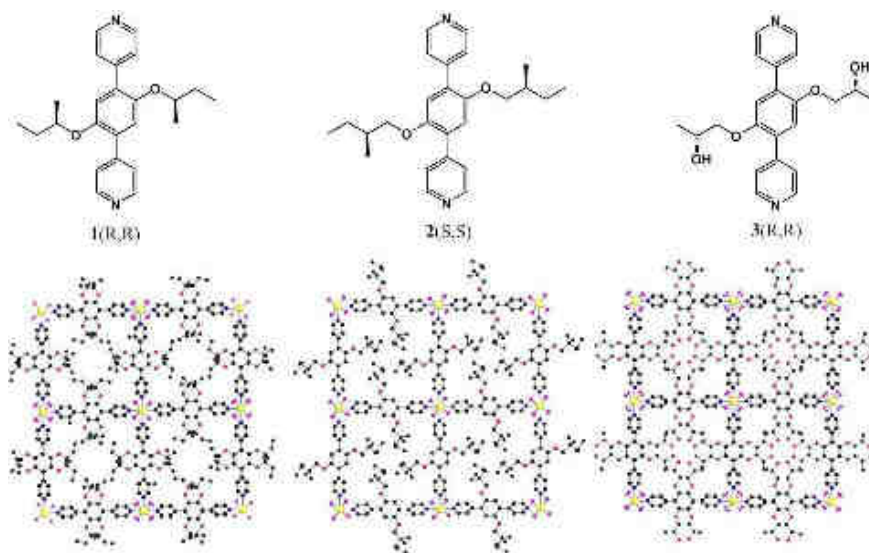


Figure I.16. Portion of the three dimensional crystalline structures, the view along the c axis.

Owing to the chiral substituents on the organic ligands, the porous crystals contain chiral channels occupied by solvent molecules. Interestingly it is possible to tune the hydrophobicity and hydrophilicity of chiral channels due to the convergent orientation of the OH groups. Unfortunately all the crystalline architectures were found to be unstable, and collapsed upon removal of solvent molecules.⁶⁷

As mentioned before, first tests on generating chiral networks by using chiral porphyrins in our group have already been made. The porphyrin units, aside their robust nature, can be functionalized either at the β pyrrolic or *meso* positions. A particular property of the porphyrin ring is its ability to coordinate a variety of metal ions, thus alongside with the coordinating sites introduced into the porphyrin backbone during the synthesis, the tetraaza core offers another four convergently oriented coordinating sites. By using zinc salts, a Zn-porphyrin metallatecton capable of self-assembly is formed. Depending on the Zn^{2+} geometry, mono-, bi- and three-dimensional networks can be obtained. Using chiral metallatectons 1-D and 2-D networks were obtained, the Zn^{2+} cation is located in the centre of the tetraaza core of the porphyrin and is either pentacoordinated adopting a square based pyramidal geometry with a pyridyl unit belonging to the neighbouring metallatecton occupying the axial position on the Zn(II) ion, or is hexacoordinated with two pyridyl units in the axial positions (figure I.17a).

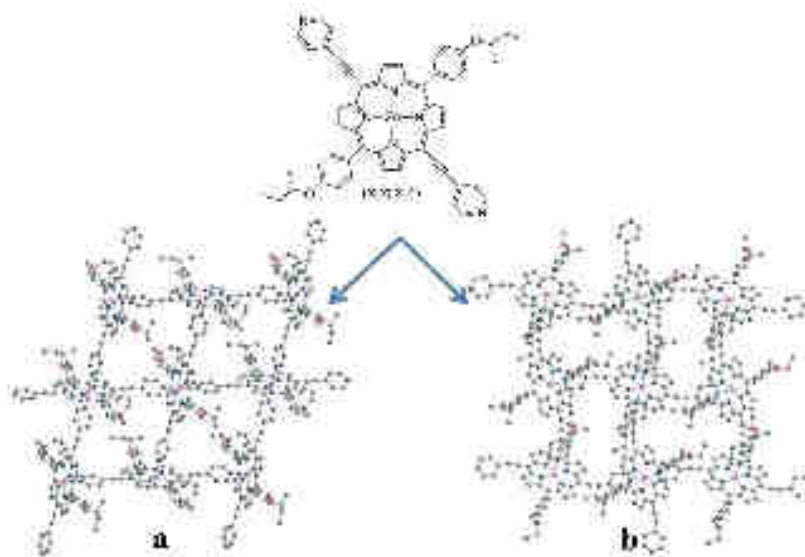


Figure I.17. A portion of the grid type 2-D network formed by self-assembly of self-complementary porphyrin based chiral tectons with included solvent molecules (a) and its solvent free equivalent (b). As in the previous case, the removal of solvent from the 2-D network leads to the loss of the structural integrity, although a solvent-free structure was generated by changing the crystallization conditions (figure I.17b). The introduction of the chiral center in this case was achieved in a first step, by synthesizing a chiral aldehyde which subsequently was used to generate the porphyrin based tectons. For this project, as presented in detail in the next chapter, the first challenge was to introduce the chiral center at the end of the synthetic pathway.

I.5. Halogen Bonding

The term halogen bond (XB) indicates a non-covalent interaction between an electrophilic region associated with a halogen atom in a molecular entity and a nucleophilic region in another or the same molecular entity.⁶⁸ A typical halogen bond can be represented as $R-X\cdots Y$, where $R-X$ is the halogen bond donor (X is any halogen atom with an electrophilic region and R is a group covalently bond to X) and Y is the halogen bond acceptor, possessing at least one nucleophilic region (figure I.18). The first report of adducts that now can be attributed to the formation of halogen bond, dates back to 1814⁶⁹ when M. Collin described iodine reacting with ammonia. In 1863, F. Guthrie defined the diiodine/ammonia system as a NH_3-I_2 adduct.⁷⁰ By 1893 I. Remsen and J.F. Norris demonstrated the tendency of methylamines to form similar adducts with chlorine, bromine and iodine.⁷¹

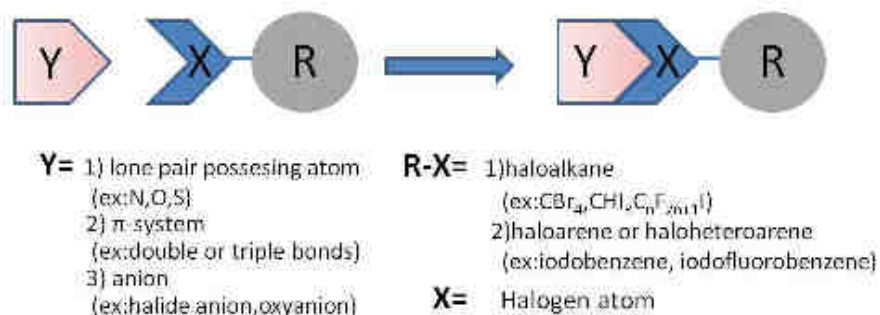


Figure I.18. Schematic representation of halogen bond.

The field began to be systematized after the crystallographic studies of O. Hassel in the 1950s⁷² showing a 1:1 complex between bromine and 1,4-dioxane with a short Br---O (2.71Å) distance within the network. Until the end of 90s, several groups (Murray-Rust, Desiraju and Parthasarathy) gathered further information on halogen bonded systems in the solid state by analysing structures reported in the Cambridge Structure Database (CSD).⁷³⁻⁷⁵ A major breakthrough in the conceptualization of XB resulted in 1998 when G. Resnati rediscovered this interaction and further developed its use in solid state supramolecular chemistry.⁷⁶ A huge interest from the scientific community in the field followed thereafter, as evidenced by an incremental growth of publications titled halogen bonding with each passing year (figure I.19).

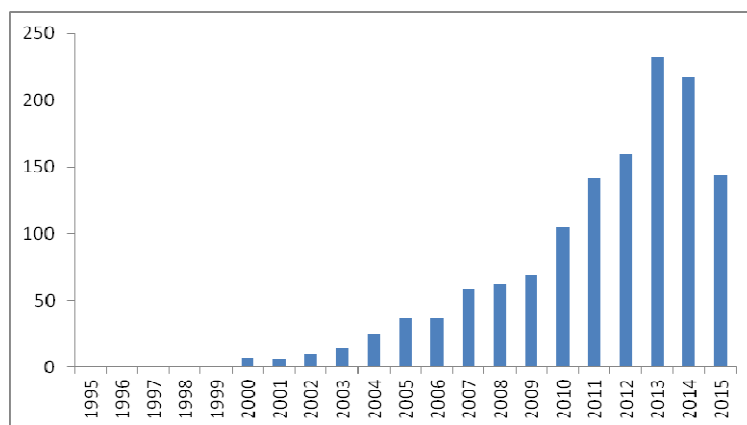


Figure I.19. Incremental growth of articles titled “halogen bonding”.

Based on a multitude of X-Ray crystal structures, P. Metrangolo and G. Resnati developed the concept that halogen bonding is a strong specific and directional interaction^{77, 78} that in some cases can overrule other intermolecular interactions. The XB interaction energy spans over a wide range, from 5 kJ to 180 kJ, the weak Cl---Cl interaction between chlorocarbons and the very strong I---I₂ interaction between I₃⁻ being the extremes.⁷⁹ Iodine, bromine and chlorine are traditionally accepted as XB donors and a consensus emerged recently that also fluorine under some circumstances, can work as XB donor^{80, 81} (tendency to form strong interactions I>Br>Cl>F).

The homo and hetero halogen-halogen (X---X) interactions belong to a special class of XB, wherein halogen atoms act both as bond donor and acceptor. On the basis of geometrical features, halogen-halogen interactions have been classified into two types: type I with angles θ_1 (C-X₁---X₂) and θ_2 (C-X₂---X₁) equal and type II, $\theta_1=180^\circ$ and $\theta_2=90^\circ$ (figure I.20).⁸²

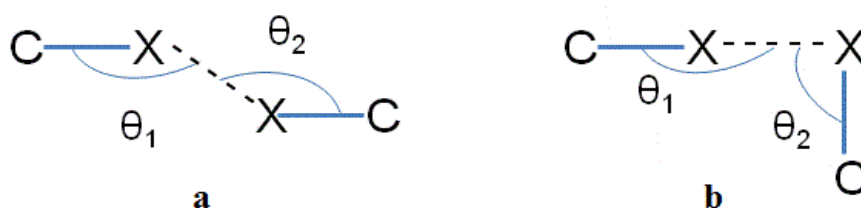


Figure I.20. Schematic representation of halogen-halogen interactions: a) type I interaction ($\theta_1=\theta_2$), b) type II interaction ($\theta_1=180^\circ$, $\theta_2=90^\circ$).

A CSD search shows that, while homo-halogen interactions have no real preferred type, both types I and II are present, most of the hetero-halogen contacts belong to type II geometry and are highly directional. Type I contacts are considered as van der Waals type and occur due to decreased repulsion, whereas type II are caused by attractive interaction between the electrophilic region of one halogen atom and the nucleophilic region of the other.⁸³ The likelihood of a type II interaction increases over type I, on proceeding from chlorine to iodine, as the halogen atoms becomes more polarizable. Also, in unsymmetrical halogen-halogen interaction of the type II contacts, the θ_2 angle occurs more often at the lighter halogen atom due to different polarization of the heavier halogen (positive) and lighter halogen (negative).⁸⁴ The ability of fluorine to form hetero halogen-halogen contacts was questioned although in a more recent paper it was shown that organic fluorine can be polarized and act as a halogen bond donor rather than simply a halogen bond acceptor in suitable electronic environment.⁸⁵

In the landscape of non-covalent interactions the halogen bonding seems to be an appealing strategy for the design of new soft materials. Several examples will be discussed hereafter.

1.5.A. Halogen bonding in Liquid crystals

In the field of liquid crystalline materials, non-covalent interactions have been used in order to generate new mesomorphic supramolecular species by self-assembly. Halogen bond has proven a successful tool in directing the self-assembly of supramolecular mesogens. In particular the N---I interactions have been consistently exploited by using non-mesomorphic alkoxystilbazoles and iodofluorobenzene⁸⁶ or iodoperfluoroalkanes.⁸⁷ In figure I.21 a list of employed entities used to generate liquid crystalline properties is shown.

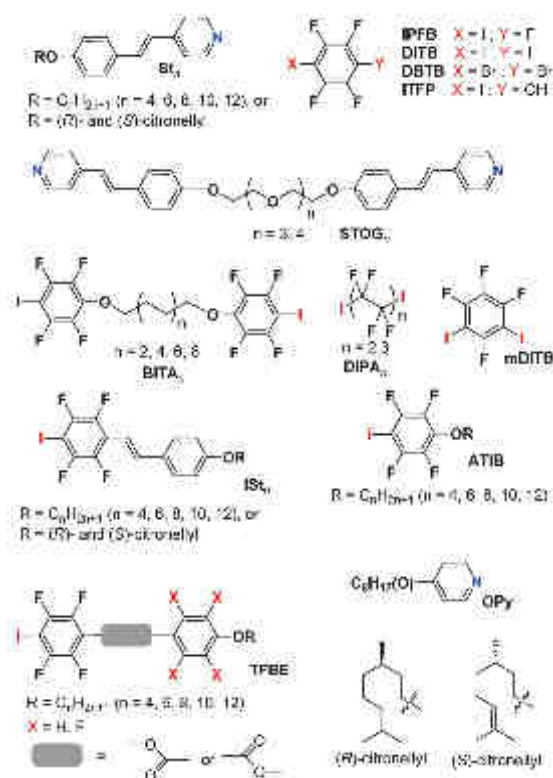


Figure I.21. Schematic representation of mesogens involved in XB liquid crystals.⁸⁸

1.5. B. Halogen bonding and Anion sensing

In 2005, a tripodal receptor possessing tetrafluoriodobenzene groups was constructed in order to bind Γ and Na^+ by two different recognition arrays of atoms (figure I.22).⁸⁹ Strong $\Gamma \cdots \text{I}$ XB interactions drive the anion exo-binding. Γ anions bridge two iodopentafluorophenyls of two different podand molecules, and forms infinite chains (figure I.22c). Na^+ is completely surrounded by the three arms of the receptor, accepting six ligands namely N, O₁, O₂, O₃, O₄ and O₅.

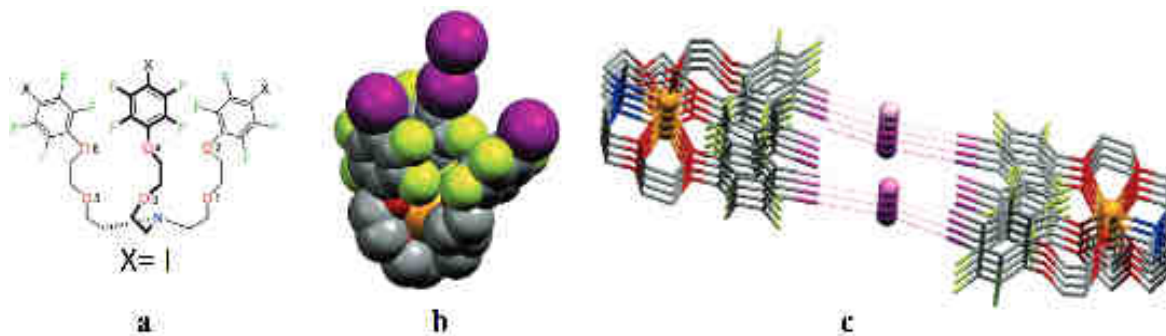


Figure I.22. Tripodal receptor (a), single-crystal X-ray structure of the receptor binding NaI (b), crystal packing of the complex showing the infinite chain. Color code: gray=C, red=O, green=F, blue=N, violet=I, orange=Na.

Further on, ditopic ion transport system in lipid bilayers, which rely on both halogen bonds and anion- π interactions, have been explored.⁹⁰

1.5.C. Halogen bonding and Supramolecular networks

Halogen bonding is emerging as a new tool in crystal engineering and in the last 15 years has proven to be reliable in constructing supramolecular architectures.¹³ There are numerous examples using bipyridine type ligands with iodofluorinated-phenyls which will be discussed in more detail in chapter 4. However an interesting example showing the use of halogen bond to direct the self-assembly of an anionic supramolecular network is given below. By slow evaporation of an equimolar solution of trifluorotriiodobenzene and trimethylsulfonium iodide a colorless heteromeric crystal was formed.⁹¹ Single crystal X-Ray analysis revealed the formation of a honeycomb-like supramolecular anionic network in which I and Γ are tridentate and the $\text{I} \cdots \Gamma$ interaction ranges between 3.38 Å and 3.50 Å (15-18% shorter than sum of van der Waals and Pauling radii). The small trimethylsulfonium cation sits perfectly in the centre of the formed hexagonal framework, where it is “locked” by electrostatic interactions and weak $\text{H} \cdots \text{F}$ contacts (figure I.23). The overall crystal packing displays the 2D honeycomb-like networks layered in a planar fashion, with a distance of 3.608 Å between layers. Various other onium iodides were studied in order to depict the critical cation size needed to form the supramolecular assemblies, which seems to lie between the dimensions of tetra-*n*-propylammonium and tetra-*n*-butylammonium cations.

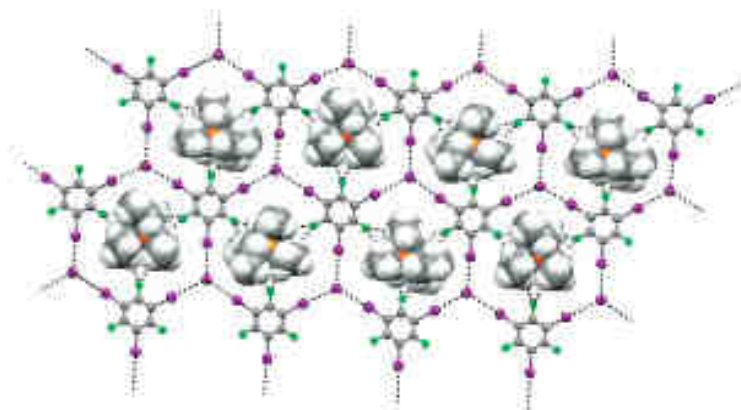


Figure I.23. Overall crystal structure of the hexagonal honeycomb network with cations accommodated in the hexagonal frames. Color code: gray=C, green=F, blue=N, violet=I, orange=S.

This field, despite being a “young” one, has offered extensive insight into the use of halogens specifically: iodine, bromine, chlorine for various applications through halogen bonding, yet fluorine due to its special nature has been disfavoured. However its peculiar nature makes it an interesting candidate for further research.

References

1. S. Mann, *Nature*, 1993, **365**, 499-505.
2. M. W. Hosseini, *Acc. Chem. Res.*, 2005, **38**, 313-323.
3. D. J. Cram and J. M. Cram, *Container Molecules and Their Guests*, *The Royal Society of Chemistry, Cambridge*, 1997.
4. D. M. Rudkevich, G. Hilmersson and J. Rebek, *J. Am. Chem. Soc.*, 1997, **119**, 9911-9912.
5. A. Rafai Far, D. M. Rudkevich, T. Haino and J. Rebek, *Org. Lett.*, 2000, **2**, 3465-3468.
6. B. Dietrich, J. M. Lehn and J. P. Sauvage, *Tetrahedron Lett.*, 1969, **10**, 2889-2892.
7. L. R. MacGillivray and J. L. Atwood, *Angew. Chem. Int. Ed.*, 1999, **38**, 1018-1033.
8. C. J. Pedersen, *J. Am. Chem. Soc.*, 1967, **89**, 7017-7036.
9. M. Fujita, *J. Synth. Org. Chem. Jpn.*, 1996, **54**, 953-963.
10. A. Arnaud, J. Belleney, F. Boué, L. Bouteiller, G. Carrot and V. Wintgens, *Angew. Chem. Int. Ed.*, 2004, **43**, 1718-1721.
11. M. Wais Hosseini and A. De Cian, *Chem. Commun.*, 1998, 727-734.
12. P. Metrangolo, F. Meyer, T. Pilati, G. Resnati and G. Terraneo, *Angew. Chem. Int. Ed.*, 2008, **47**, 6114-6127.
13. P. Metrangolo, G. Resnati, T. Pilati and S. Biella, in *Halogen Bonding*, eds. P. Metrangolo and G. Resnati, Springer Berlin Heidelberg, 2008, vol. 126, pp. 105-136.
14. F. Hajek, E. Graf and M. W. Hosseini, *Tetrahedron Lett.*, 1996, **37**, 1409-1412.
15. F. Hajek, M. W. Hosseini, A. De Cian and J. Fischer, *Angew. Chem. Int. Ed.*, 1997, **36**, 1760-1762.
16. A. Harriman and R. Ziessel, *Coord. Chem. Rev.*, 1998, **171**, 331-339.
17. J. Martz, E. Graf, M. Wais Hosseini, A. De Cian and J. Fischer, *J. Mater. Chem.*, 1998, **8**, 2331-2333.
18. G. Mislin, E. Graf, M. Wais Hosseini, A. De Cian, N. Kyritsakas and J. Fischer, *Chem. Commun.*, 1998, 2545-2546.
19. S. Ferlay, A. Jouaiti, M. Loi, M. W. Hosseini, A. De Cian and P. Turek, *New J. Chem.*, 2003, **27**, 1801-1805.
20. M. N. Kozlova, S. Ferlay, S. E. Solovieva, I. S. Antipin, A. I. Konovalov, N. Kyritsakas and M. W. Hosseini, *Dalton Trans.*, 2007, 5126-5131.
21. A. S. Batsanov, M. J. Begley, P. Hubberstey and J. Stroud, *J. Chem. Soc., Dalton Trans.*, 1996, 1947-1957.

22. E. Deiters, V. Bulach, N. Kyritsakas and M. W. Hosseini, *New J. Chem.* , 2005, **29**, 1508-1513.
23. M. J. Irwin, J. J. Vittal, G. P. A. Yap and R. J. Puddephatt, *J. Am. Chem. Soc.*, 1996, **118**, 13101-13102.
24. M. A. Beswick, C. Lopez-Casideo, M. A. Paver, P. R. Raithby, C. A. Russell, A. Steiner and D. S. Wright, *Chem. Commun.*, 1997, 109-110.
25. P. Grosshans, A. Jouaiti, V. Bulach, J.-M. Planeix, M. W. Hosseini and J.-F. Nicoud, *CrystEngComm*, 2003, **5**, 414-416.
26. K. Biradha, Y. Hongo and M. Fujita, *Angew. Chem. Int.Ed.*, 2000, **39**, 3843-3845.
27. B. F. Abrahams, T. A. Hudson and R. Robson, *J. Mol. Struct.* , 2006, **796**, 2-8.
28. S. Ferlay, T. Mallah, J. Vaissermann, F. Bartolome, P. Veillet and M. Verdaguer, *Chem. Commun.*, 1996, 2481-2482.
29. J. T. Brewer, S. Parkin and R. B. Grossman, *Crystal Growth & Design*, 2004, **4**, 591-594.
30. G. B. Gardner, D. Venkataraman, J. S. Moore and S. Lee, *Nature*, 1995, **374**, 792-795.
31. M.-L. Tong, S.-L. Zheng and X.-M. Chen, *Chem. Commun.*, 1999, 561-562.
32. K. Biradha and M. Fujita, *J. Chem. Soc., Dalton Trans.* , 2000, 3805-3810.
33. A. Neels, H. Stoeckli-Evans, A. Escuer and R. Vicente, *Inorg. Chem.*, 1995, **34**, 1946-1949.
34. A. Escuer, R. Vicente, M. A. S. Goher and F. A. Mautner, *Inorg. Chem.*, 1997, **36**, 3440-3446.
35. R. Mondal, M. K. Bhunia and K. Dhara, *CrystEngComm*, 2008, **10**, 1167-1174.
36. A. B. Mallik, S. Lee and E. B. Lobkovsky, *Crystal Growth & Design*, 2005, **5**, 609-616.
37. A. L. Mackay, *Nature*, 1985, **314**, 604-606.
38. X.-P. Zhou, M. Li, J. Liu and D. Li, *J. Am. Chem. Soc.*, 2012, **134**, 67-70.
39. D. S. Lawrence, T. Jiang and M. Levett, *Chem. Rev.*, 1995, **95**, 2229-2260.
40. G. F. Swiegers and T. J. Malefetse, *Chem. Rev.*, 2000, **100**, 3483-3538.
41. B. Moulton and M. J. Zaworotko, *Chem. Rev.*, 2001, **101**, 1629-1658.
42. P. Metrangolo and G. Resnati, *Crystal Growth & Design*, 2012, **12**, 5835-5838.
43. S. R. Batten, N. R. Champness, X.-M. Chen, J. Garcia-Martinez, S. Kitagawa, L. Öhrström, M. O'Keeffe, M. P. Suh and J. Reedijk, *Pure and Applied Chemistry*, 2013, **85**, 1715-1724.
44. J. R. Long and O. M. Yaghi, *Chem.Soc.Rev*, 2009, **38**, 1213-1214.
45. Stuart R Batten, Suzanne M Neville and D. R. Turner, *Coordination Polymers : Design, Analysis and Application*, Royal Society of Chemistry, 2009.
46. B. F. Hoskins and R. Robson, *J. Am. Chem. Soc.*, 1989, **111**, 5962-5964.
47. B. F. Hoskins and R. Robson, *J. Am. Chem. Soc.*, 1990, **112**, 1546-1554.
48. O. M. Yaghi, M. O'Keeffe, N. W. Ockwig, H. K. Chae, M. Eddaoudi and J. Kim, *Nature*, 2003, **423**, 705-714.
49. M. Fujita, Y. J. Kwon, S. Washizu and K. Ogura, *J. Am. Chem. Soc.*, 1994, **116**, 1151-1152.
50. S. Subramanian and M. J. Zaworotko, *Angew. Chem. Int. Ed.*, 1995, **34**, 2127-2129.
51. O. M. Yaghi and H. Li, *J. Am. Chem. Soc.*, 1995, **117**, 10401-10402.
52. C. Kaes, M. W. Hosseini, C. E. F. Rickard, B. W. Skelton and A. H. White, *Angew. Chem. Int.Ed.*, 1998, **37**, 920-922.
53. Z. Wang and S. M. Cohen, *Chem.Soc.Rev*, 2009, **38**, 1315-1329.
54. J. D. Evans, C. J. Sumbly and C. J. Doonan, *Chem.Soc.Rev*, 2014, **43**, 5933-5951.
55. Y. Peng, V. Krungleviciute, I. Eryazici, J. T. Hupp, O. K. Farha and T. Yildirim, *J. Am. Chem. Soc.*, 2013, **135**, 11887-11894.
56. M. P. Suh, H. J. Park, T. K. Prasad and D.-W. Lim, *Chem. Rev.*, 2012, **112**, 782-835.
57. D. J. Wales, J. Grand, V. P. Ting, R. D. Burke, K. J. Edler, C. R. Bowen, S. Mintova and A. D. Burrows, *Chem.Soc.Rev*, 2015.
58. J. Liu, L. Chen, H. Cui, J. Zhang, L. Zhang and C.-Y. Su, *Chem.Soc.Rev*, 2014, **43**, 6011-6061.
59. J. Lee, O. K. Farha, J. Roberts, K. A. Scheidt, S. T. Nguyen and J. T. Hupp, *Chem.Soc.Rev*, 2009, **38**, 1450-1459.
60. J.-R. Li, R. J. Kuppler and H.-C. Zhou, *Chem.Soc.Rev*, 2009, **38**, 1477-1504.
61. M. D. Allendorf, C. A. Bauer, R. K. Bhakta and R. J. T. Houk, *Chem.Soc.Rev*, 2009, **38**, 1330-1352.

62. P. Horcajada, R. Gref, T. Baati, P. K. Allan, G. Maurin, P. Couvreur, G. Férey, R. E. Morris and C. Serre, *Chem. Rev.*, 2012, **112**, 1232-1268.
63. R.-G. Xiong, X.-Z. You, B. F. Abrahams, Z. Xue and C.-M. Che, *Angew. Chem. Int.Ed.*, 2001, **40**, 4422-4425.
64. M. Zhang, Z.-J. Pu, X.-L. Chen, X.-L. Gong, A.-X. Zhu and L.-M. Yuan, *Chem. Commun.*, 2013, **49**, 5201-5203.
65. P. Larpent, *Tectonique moléculaire: Conception et Formation de Polymères de Coordination Chiraux*, Thèse Université de Strasbourg, 2013.
66. N. Marets, V. Bulach and M. W. Hosseini, *New J. Chem.* , 2013, **37**, 3549-3558.
67. P. Larpent, A. Jouaiti, N. Kyritsakas and M. W. Hosseini, *Chem. Commun.*, 2013, **49**, 4468-4470.
68. R. Desiraju Gautam, P. S. Ho, L. Kloo, C. Legon Anthony, R. Marquardt, P. Metrangolo, P. Politzer, G. Resnati and K. Rissanen, in *Pure and Applied Chemistry*, 2013, vol. 85, pp. 1711-1713.
69. M. Collin, *Ann. Chim.* , 1814, **91**, 252-272.
70. F. Guthrie, *J. Chem. Soc.*, 1863, **16**, 239-244.
71. I. Remsen and J. F. Norris, *Am. Chem. J.* , 1896, **18**, 90-95.
72. O. Hassel and J. Hvoslef, *Acta Chemica Scandinavica*, 1954, **8**, 873-873.
73. P. Murray-Rust, W. C. Stallings, C. T. Monti, R. K. Preston and J. P. Glusker, *J. Am. Chem. Soc.*, 1983, **105**, 3206-3214.
74. N. Ramasubbu, R. Parthasarathy and P. Murray-Rust, *J. Am. Chem. Soc.*, 1986, **108**, 4308-4314.
75. G. R. Desiraju and R. Parthasarathy, *J. Am. Chem. Soc.*, 1989, **111**, 8725-8726.
76. V. Amico, S. V. Meille, E. Corradi, M. T. Messina and G. Resnati, *J. Am. Chem. Soc.*, 1998, **120**, 8261-8262.
77. P. Metrangolo and G. Resnati, *Chem. Eur. J.*, 2001, **7**, 2511-2519.
78. P. Metrangolo, H. Neukirch, T. Pilati and G. Resnati, *Acc. Chem. Res.*, 2005, **38**, 386-395.
79. E. Corradi, S. V. Meille, M. T. Messina, P. Metrangolo and G. Resnati, *Angew. Chem. Int.Ed.*, 2000, **39**, 1782-1786.
80. D. Chopra, *Crystal Growth & Design*, 2011, **12**, 541-546.
81. D. Chopra and T. N. G. Row, *CrystEngComm*, 2011, **13**, 2175-2186.
82. T. T. T. Bui, S. Dahaoui, C. Lecomte, G. R. Desiraju and E. Espinosa, *Angew. Chem. Int.Ed.*, 2009, **48**, 3838-3841.
83. P. Metrangolo and G. Resnati, *IUCrJ*, 2014, **1**, 5-7.
84. V. R. Pedireddi, D. S. Reddy, B. S. Goud, D. C. Craig, A. D. Rae and G. R. Desiraju, *J. Chem. Soc., Perkin Trans. 2* 1994, 2353-2360.
85. A. G. Dikundwar and T. N. G. Row, *Crystal Growth & Design*, 2012, **12**, 1713-1716.
86. H. L. Nguyen, P. N. Horton, M. B. Hursthouse, A. C. Legon and D. W. Bruce, *J. Am. Chem. Soc.*, 2004, **126**, 16-17.
87. P. Metrangolo, C. Prasang, G. Resnati, R. Liantonio, A. C. Whitwood and D. W. Bruce, *Chem. Commun.*, 2006, 3290-3292.
88. F. Meyer and P. Dubois, *CrystEngComm*, 2013, **15**, 3058-3071.
89. A. Mele, P. Metrangolo, H. Neukirch, T. Pilati and G. Resnati, *J. Am. Chem. Soc.*, 2005, **127**, 14972-14973.
90. A. Vargas Jentzsch, D. Emery, J. Mareda, P. Metrangolo, G. Resnati and S. Matile, *Angew. Chem. Int.Ed.*, 2011, **50**, 11675-11678.
91. P. Metrangolo, F. Meyer, T. Pilati, G. Resnati and G. Terraneo, *Chem. Commun.*, 2008, 1635-1637.

Chapter 2

Contents

Chapter II.....	38
II.1. Porphyrins	38
II.1.A. Structure and general properties	38
II.1.B. Coordination Properties and Deformation	38
II.1.C. Synthesis	39
II.1.D. Characterization NMR-Spectroscopy	41
II.1.E. Porphyrin and Chirality	43
II.1.F. Fluorinated porphyrins	43
II.2. Synthesis of fluorinated and/or chiral porphyrin based tectons	43
II.2.A. Synthesis of A ₂ B ₂ porphyrins through classic [2+2] condensation reaction	44
II.2.B. Synthesis of A ₂ B ₂ porphyrins through cross-coupling reaction.....	46
II.2.C. Crystal Structures	49
Conclusion	53
References.....	54

Chapter II

II.1. Porphyrins

II.1.A. Structure and general properties

Porphyrin chemistry is a research field that has been honored with several Nobel prizes and shares a rich history with numerous monographs and books dealing with porphyrin synthesis, characterization and properties.

Basically, a porphyrin is a biologically relevant macrocycle consisting of four pyrrole rings linked by methylene bridges. Following the IUPAC nomenclature,¹ the macrocycle is numbered from 1 to 20 and the four pyrrole rings are labeled from A to D (figure II.1). The significant property of the porphyrin backbone is that it can be substituted with various functionalities either in the 8 available β - positions or the 4 *meso*-positions, which can influence its electronic properties as well as the chemical reactivity.

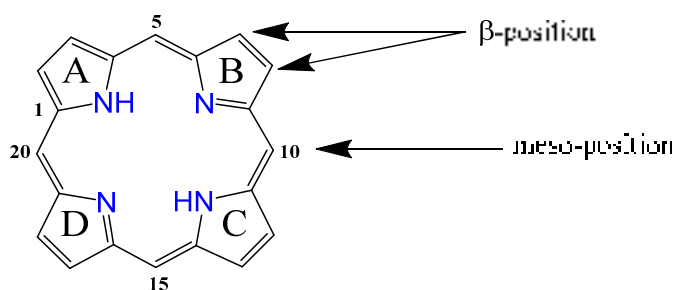


Figure II.1. Chemical structure of the porphyrin and its nomenclature.

The inner ring contains four nitrogen atoms and two protons, also known as the free-base porphyrin, and shows a great propensity to coordinate to a wide range of transition metals. Considering the number of functionalizable sites, the size of the macrocycle and the coordination abilities of its core it becomes obvious why porphyrins are an interesting platform for studies in various fields like catalysis,^{2,3} biomimetic chemistry⁴ and molecular tectonics.⁵

II.1.B. Coordination Properties and Deformation

As mentioned before the porphyrin core has the ability to coordinate metal ions, by deprotonation of the two inner nitrogens, the macrocycle cavity forms a tetradentate dianionic ligand, perfectly suited for transitional metals and the lanthanides.⁶ Metallic centers can have additional ligands, external or belonging to the porphyrin, coordinated in the axial position in order to complete the coordination sphere (from 0 to 5 depending on the metal ion).

The transition metals of the first row are a perfect fit for the porphyrin cavity (figure II.2a), while the metal ions with higher volume are located out of the porphyrin cavity, often causing deformation of the porphyrin core (figure II.2b).

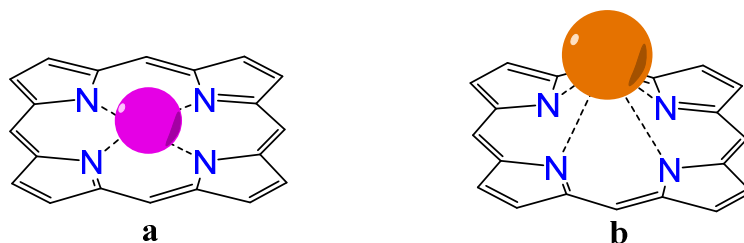


Figure II.2. Schematic representation of the metal position within the porphyrin core with respect to its size.

Due to the relative flexibility of the backbone, the macrocycle can deform at some extent. It was possible to identify several conformations in the solid state depending on the nature of the substituents in the *meso* and β -positions and the metal ions in the cavity (figure II.3).^{7, 8}

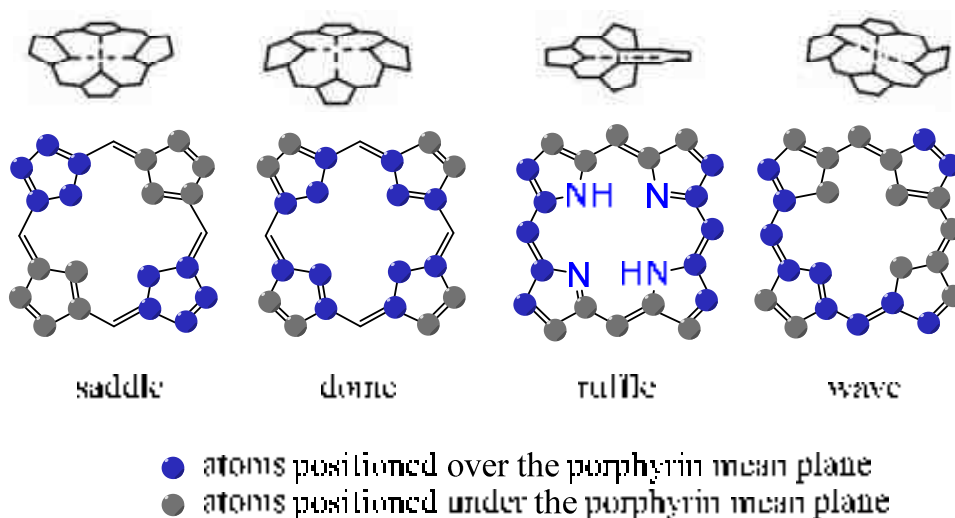


Figure II.3. Most frequent porphyrin deformations of the porphyrin macrocycle (24 atoms) in the solid state.

II.1.C. Synthesis

It is generally known in porphyrin chemistry that TPP (tetraphenylporphyrin) is the easiest synthesizable porphyrin, yet back in 1935 that took a sealed glass tube filled with pyrrole and benzaldehyde in pyridine at 220°C for 48 hours.⁹ Rothmund's work was a breakthrough for porphyrin synthesis and started a new "chase" towards easier and more efficient methods. In 1967 Adler and Longo reported the synthesis of TPP with better yields and lower reaction time.¹⁰ They developed a new method which used propionic acid as solvent and by refluxing pyrrole and an aldehyde for only 30 min, a simple filtration and methanol wash led to elevated yields of TPP. This method was indeed more convenient, yet the use of high temperature and the acidic environment limited the number of used aldehydes. Later, Lindsey *et al* developed a different method using milder reaction conditions, in which the ring closure of the tetrapyrrole and the oxidation of the porphyrinogen are two separate reaction steps.¹¹ This strategy doesn't require high temperatures, the pyrrole and the aldehyde are reacting at room temperature in CH₂Cl₂ or CHCl₃ in the presence of boron trifluoride etherate or trifluoroacetic acid as acid catalyst and benzoquinone derivatives such as DDQ or p-chloranil as oxidizing agents. All these methods are useful for the synthesis of

highly symmetric A_4 porphyrins (the four meso positions being occupied by the same group) using only one aldehyde, A-CHO.

In order to obtain porphyrins with different *meso* substituents (figure II.4), a different approach was needed, thus Little *et al.* have adapted the synthesis of Adler and Longo named the “mixed aldehyde” method and leads usually to a statistic mixture of 6 porphyrins, that are difficult and time consuming to separate.¹²

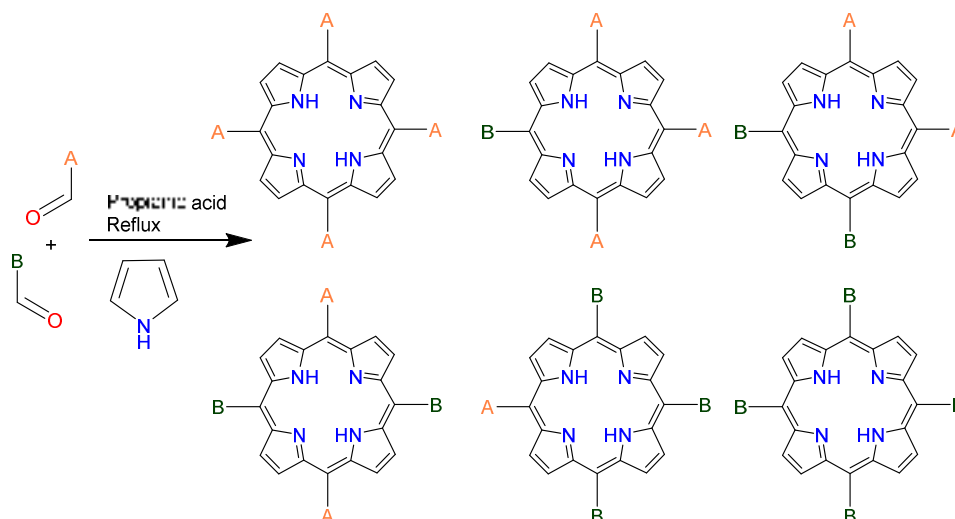


Figure II.4. Mixture of porphyrins generated by the so-called “mixed aldehyde method”.

A more selective method for porphyrins with two distinct substituents was described by MacDonald *et al.* in 1960 using a two steps procedure: in the first one, dipyrromethane is synthesized from one aldehyde using an excess of pyrrole. The A_2B_2 porphyrin is generated in the second step in a [2+2] condensation reaction, where the dipyrromethane reacts with the second aldehyde, in acid conditions (figure II.5).¹³ This method, however, has one downside: the dipyrromethane units in acid catalyzed media can undergo fragmentation and recombination with the unconsumed starting material which leads to the phenomenon called “scrambling” that usually mean complex separation techniques, thus figure II. 5 represents an “ideal” version of the reaction.

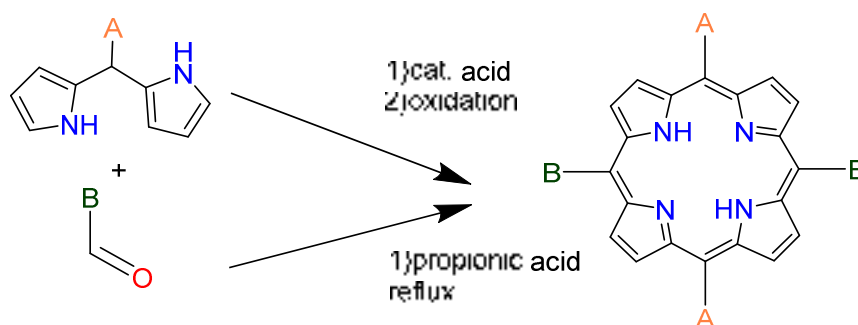


Figure II.5. A representation of [2+2] condensation reaction.

A_2B_2 porphyrins of high purity and moderate yields can be obtained by combining the Adler and the MacDonald methods and refluxing the dipyrromethane in propionic acid in the presence of a second aldehyde.¹⁴ The success of this reaction will depend on the stability and the reactivity of the

functionalized dipyrromethane and the aldehydes under the reaction conditions. Depending on the target porphyrin one of these methods can be applied.

Another approach to functionalized porphyrins is to use the primary substituents as a platform to construct superstructural entities such as biomimetic heme analogues,¹⁵⁻¹⁸ perpendicular to the porphyrin mean plane, usually using 5, 10, 15, 20-tetrakis (*o*-aminophenyl)porphyrin. This type of porphyrin ligands have been used for near infra-red emission¹⁹ or as chelating ligands for cation binding.²⁰

The last approach has its roots in the early 90's and was inspired by the developments in metal mediated cross-coupling reactions. It opens the lane for both mixed meso-substituted porphyrins and unsymmetrical porphyrins.^{21, 22} Despite the fact that this procedure needs usually 4 steps, it provides several important advantages for the synthesis of elaborated porphyrins. The key step is a pallado-catalyzed coupling between the brominated meso positions and the precursor of the substituent B which may lead to quantitative conversion of reactants. It enables a straightforward purification and isolation of products and finally it decouples the porphyrin ring cyclization chemistry from porphyrin derivatization (figure II.6).

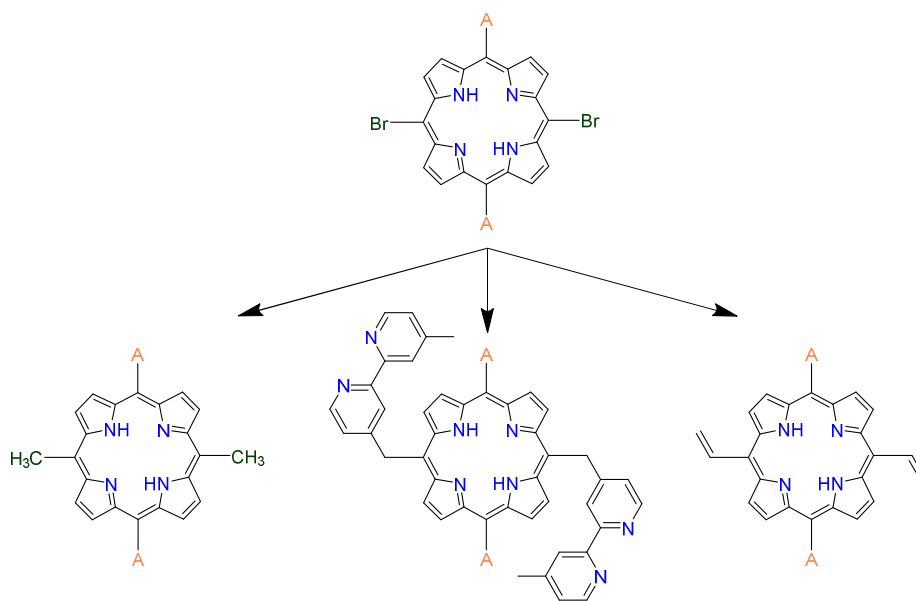


Figure II.6. First examples of A_2B_2 type porphyrins obtained by cross-coupling reactions.

Later on Zhang and co-workers developed several general and efficient methods for the synthesis of a variety of heteroatom-substituted porphyrins including amino,²³ amido,²⁴ sulfo²⁵ and oxo²⁶ by palladium-catalyzed cross-coupling reactions. The introduction of different functionalities in the porphyrin periphery allows modulating its properties, as well as providing possible reaction sites for further transformations.

II.1.D. Characterization

NMR-Spectroscopy

Porphyrins are easily recognizable by NMR spectroscopy due to two specific signals in proton NMR:

- The protons of the inner core attached to the nitrogen get a broad signal at -2 ppm.
- The β -pyrrolic protons are situated around 8-9 ppm and their multiplicity is depending on the nature of the substituents in the *meso* positions and the porphyrin symmetry.

These shifts are the results of a large magnetic anisotropy of the cyclic conjugated π -electron system of the aromatic porphyrin ring. The external magnetic field going through the aromatic ring sets up a current of mobile π -electrons, this circulation give rise to a secondary magnetic field coming from the center of the macrocycle with a strong anisotropic effect.²⁷ Thus the protons inside the ring (NH protons) current will be shielded, while the one located outside (β -pyrrolic protons) will not.

In the case of ^{13}C NMR-Spectroscopy, the small effective frequency of the ^{13}C isotope and low intensity of the signals, especially the signals of quaternary carbon atoms have very weak signals due to their long relaxation time,²⁸ becomes problematic for porphyrin characterization and higher concentrations are usually needed. The low solubility of several porphyrins resulting from self aggregation often interferes with the need of higher concentrations for the NMR measurements.

UV-visible Spectroscopy

Porphyrins, due to their 22 π -electron system, show very distinctive absorption spectra. All the absorption bands in the UV-Vis spectrum of the free-base porphyrin result from π - π^* electronic transitions. Typically the resulting spectrum can be divided in two parts²⁹ (figure II.7):

- The Soret band, a very intense absorption band around 420 nm ($\epsilon \sim 4.10^5 \text{ L/mol.cm}$) , named after the swiss chemist and physicist Jacques Louis Soret who observed this band for the first time in Hemoglobin in 1883.³⁰
- The Q bands, those are usually weaker than Soret band, and can be found between 500-700 nm ($\epsilon \sim 1.10^4 \text{ L/mol.cm}$). In general, there are four bands for the free base porphyrin and two for the metallated one.

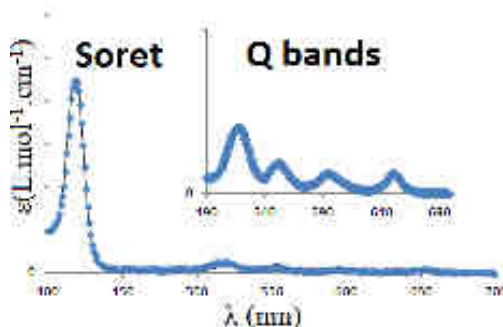


Figure II.7. Absorption spectrum of a substituted porphyrin at room temperature in chloroform. The structure of the porphyrin as well as the position and electronic nature of the substituents have a great influence on the resulting absorption bands.

II.1.E. Porphyrin and Chirality

In terms of decorating the periphery of the porphyrin, the four meso and/or eight β -pyrrolic positions can be functionalized with a variety of substituents, including chiral groups. Porphyrins can become intrinsically chiral due to the presence of a chiral substituent group, due to restricted rotation leading to atropisomerism, or to asymmetric disposition of a strap or methylation of the inner hydrogen. Chiral porphyrins have been used as an important platform for circular dichroic (CD) spectroscopy,³¹ due to the intense extinction coefficients, facile modification of substituents and the ease of metal incorporation into the porphyrin ring (metalloporphyrins can provide extra stereo differentiation due to their Lewis acid sites for binding OH, NH₂, COO⁻ and other functional groups). Another interesting application is chiral recognition, as the porphyrin scaffold offers a rigid platform to construct guest-recognition pockets.³²⁻³⁴ Among other application for chiral porphyrins one can list their use as catalyst for: diastereoselective cyclopropanation,^{35, 36} enantioselective epoxidation^{37, 38} or their use in formation of coordination networks.³⁹⁻⁴¹ This brief description of possible applications is far from being comprehensive, nevertheless it shows the vastness of possibilities that the porphyrin scaffold affords.

II.1.F. Fluorinated porphyrins

The incorporation of fluorine atoms into the porphyrin backbone leads to interesting electron deficient systems with a variety of applications such as imaging,⁴² catalysis^{43, 44} and biomedical applications.⁴⁵ There were several reports^{46, 47} on meso-tetrakis (perfluoroalkyl)porphyrins in the mid 90's and the group of DiMaggio emphasized on the use of these molecules as photosensitizers due to higher molar absorption coefficients.⁴⁸ The majority of reported studies is still focused on the use of fluoroaryl substituents or introduces the fluoroalkyl substituents in the β -positions, which might be explained by the low commercial availability of fluorinated aldehydes. It is worth mentioning that the introduction of the fluoroalkyl substituents in the β -positions can be synthetically challenging,⁴⁹ which is why a method introducing this substituents in the *meso* position without using aldehydes could be a good alternative.

II.2. Synthesis of fluorinated and/or chiral porphyrin based tectons

Our aim is to synthesize porphyrin tectons of the A₂B₂ type bearing two divergently oriented pyridine coordinating sites in the trans *meso* positions, in order to build coordination networks, and two chiral or/and fluorinated substituents in the other two trans *meso* positions. As seen previously, we can either use the straight forward MacDonald [2+2] condensation yielding an A₂B₂ porphyrin with pyridine and chiral/fluorinated substituents in two steps or a four steps procedure using the brominated derivative as a scaffold for further functionalization (figure II.8).

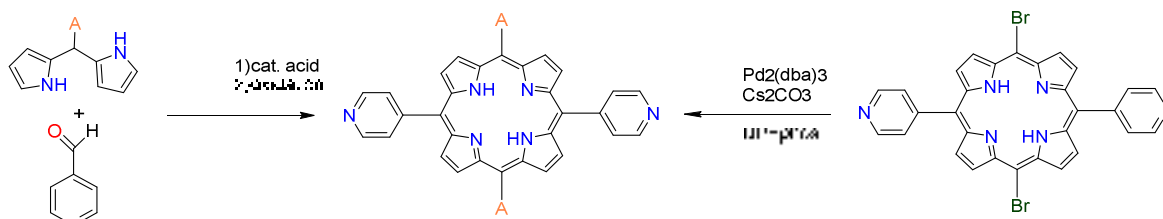


Figure II.8. The two possible synthetic pathways (A- generically stands for the chiral and/or fluorinated substituents).

II.2.A. Synthesis of A₂B₂ porphyrins through classic [2+2] condensation reaction

For the synthesis of the desired A₂B₂ porphyrins, our first approach was to use commercially available aldehydes and to perform a MacDonald [2+2] condensation reaction.

For the chiral substituent, we chose the citronellal aldehyde for several reasons: commercial availability, acceptable price range and the presence of flexible substituents (like alkyl chains) within the cavities of the potential networks.

The reaction of an excess of pyrrole with R-citronellal leads to the formation of the corresponding DPM (dipyrromethane) **1**, in 67% yield. It reacts with 4-pyridinecarboxaldehyde in the presence of TFA (trifluoroacetic acid) to form the porphyrin **2** in a poor yield (16%). No increase of the yield could be observed in the presence of boron trifluoride diethyl etherate (BF₃·OEt₂) (figure II.9). Porphyrin **2** was characterized by ¹H-, ¹³C-, UV-vis and Mass Spectrometry described in the experimental part. It is worth noting that due to the symmetry of the tecton, the β-pyrrolic protons appear as two doublets around 8-9 ppm with integration of four, for each doublet.

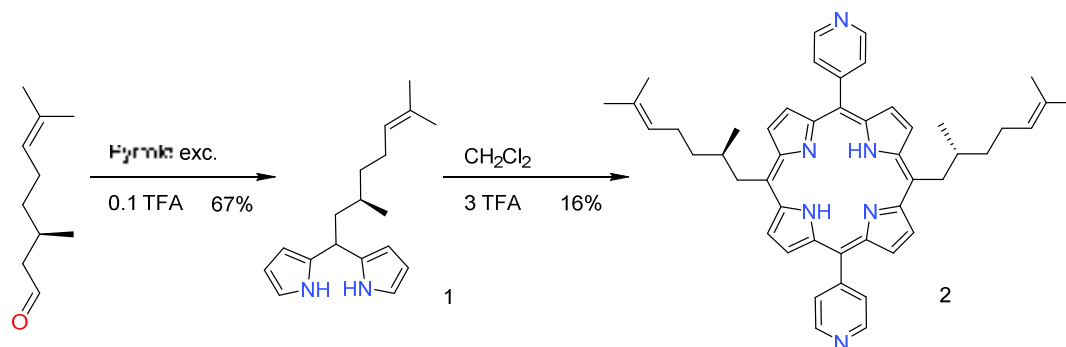


Figure II.9. Synthetic pathway for the synthesis of porphyrin **2**.

In the case of the fluorinated derivative a similar approach was tested with the only commercially available aldehyde, 4, 4, 4-Trifluorobutylaldehyde. The DPM **3** is formed in 53% yield in the presence of excess pyrrole and TFA as acid catalyst (figure II.10). In a second step the pyridine carboxaldehyde is reacted with **3** in a stoichiometric amount to yield the porphyrin **4** with a poor yield (6%).

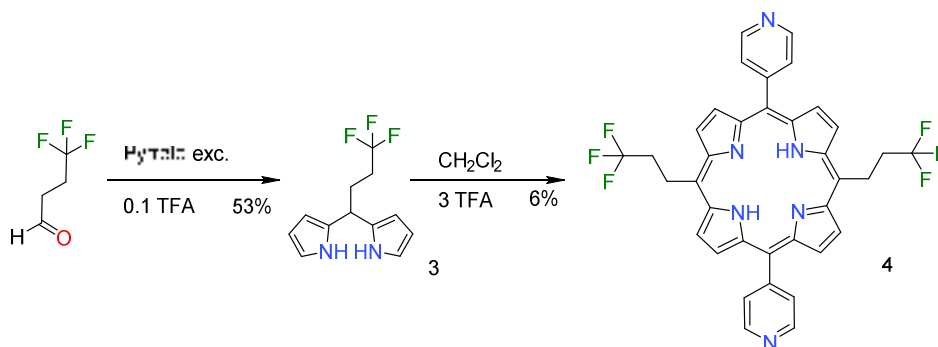


Figure II.10. Synthetic procedure for the porphyrin **4**.

The porphyrin **4** was characterized by ^1H -, ^{13}C -, and ^{19}F - NMR, UV-vis and Mass Spectrometry described in the experimental part. It is worth noting that due to the symmetry of the tecton the β -pyrrolic protons appear as two doublets around 8-9 ppm with integration of four. Single crystals of **4** have been obtained and analyzed by X-Ray diffraction. Two sets of single crystals have been obtained from slow diffusion of diethyl ether or ethanol into a solution of the porphyrin in chloroform. In both structures, no intermolecular F---F contacts were observed.

In the presence of Et_2O , the porphyrin crystallizes in the P-1 space group without any solvent molecules; two porphyrin entities are present in the asymmetric unit. The porphyrin core adopts a saddle shape deformation (max deviation of $\text{C}\beta$ of 0.39 Å for 1st porphyrin present in the asymmetric unit and 0.49 Å max deviation of $\text{C}\beta$ for the 2nd porphyrin in the unit). The dihedral angles between the porphyrin mean plane (24 atoms) and the meso-pyridyl groups are ranging between 48°-53°. Interestingly, in the solid state, the fluorinated chains are both located on the same side of the porphyrin plane in a “convergent” manner. (figure II.11) A closer look at the packing revealed the formation of H---F intermolecular hydrogen bonds (between 3.32 Å and 3.50 Å for C---F distances) between the fluorine atoms on the alkyl chains and the β -pyrrolic protons within porphyrin layers (4 fluorines involved/porphyrin).

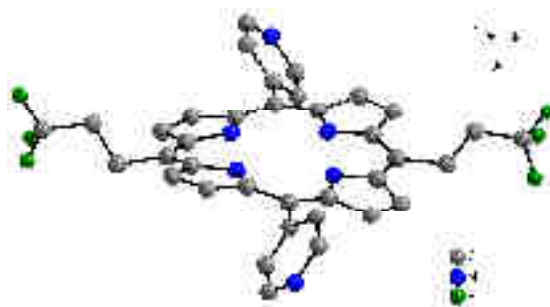


Figure II.11. Crystal structure of **4**, its saddle form. Hydrogen atoms are omitted for clarity.

In the presence of EtOH the porphyrin crystallizes in P21/c space group with solvent molecules (ethanol) present in the architecture, with a ratio of one solvent molecule per porphyrin. There is only one planar macrocycle unit in the asymmetric unit. The dihedral angles between the pyridine moieties and the porphyrin mean plane (24 atoms) are around 71° and 86°. In this case the fluorinated chains are located in a divergent fashion relative to the mean plane of the porphyrin. (figure II.12). The ethanol molecule is hydrogen bonded to one pyridine moiety of the porphyrin molecule (distance N---O equal to 2.85 Å). The crystal packing reveals the formation of additional

weak intermolecular H---F bonds (the C---F distances ranging from 3.22 Å to 3.50 Å) between the fluorine atoms on the alkyl chain and the β -pyrrolic protons within porphyrin layers (4 fluorines involved/porphyrin) as well as π - π interactions between pyrrolic units within the layers (3.38 Å).

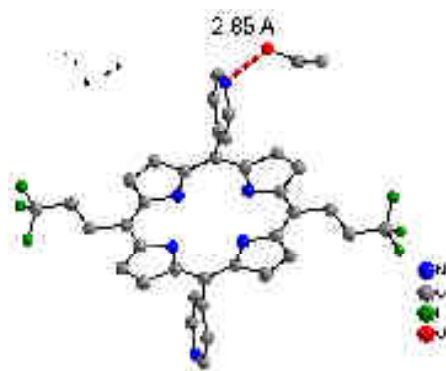


Figure II.12. Crystal structure of **4**, highlighting the solvent porphyrin interaction. Hydrogen atoms are omitted for clarity.

In both cases, this two steps approach has one major disadvantage. Indeed, due to the low yields of the second step the use of costly fluorinated or chiral aldehydes in big amounts is required. Considering also the limited commercial availability of the fluorinated aldehydes and the synthetic difficulties that could be met during the attempt to synthesize them in the lab (low boiling point) a different reaction pathway was required.

II.2.B. Synthesis of A_2B_2 porphyrins through cross-coupling reaction

The aim is to try to introduce the chiral and/or fluorinated substituents in a last step in order to avoid excessive use of costly precursors.

The second strategy involved a 4 steps procedure : the synthesis of a dipyrromethane bearing a pyridine moiety⁵⁰ in the first step. The second step required the synthesis of the 5,15-dipyridylporphyrin. This synthesis was already performed in the group of J. Sanders⁵¹ few years ago, thus it was a matter of adjusting the reaction conditions. By using TFA instead of trichloroacetic acid we observed a slightly higher yield (20-21 %); unfortunately the tests to scale up the reaction (x2) gave no desired product. (figure II.13). Bromination of the two *meso* positions of the porphyrin is an established procedure (notably 0°C and 2.1 equivalents of NBS in chloroform),⁵² although no bromination of the 5,15-dipyridylporphyrin was described before this work. The tecton **7** is thus a previously unreported scaffold which was further used as a platform for the synthesis of a large variety of porphyrins.

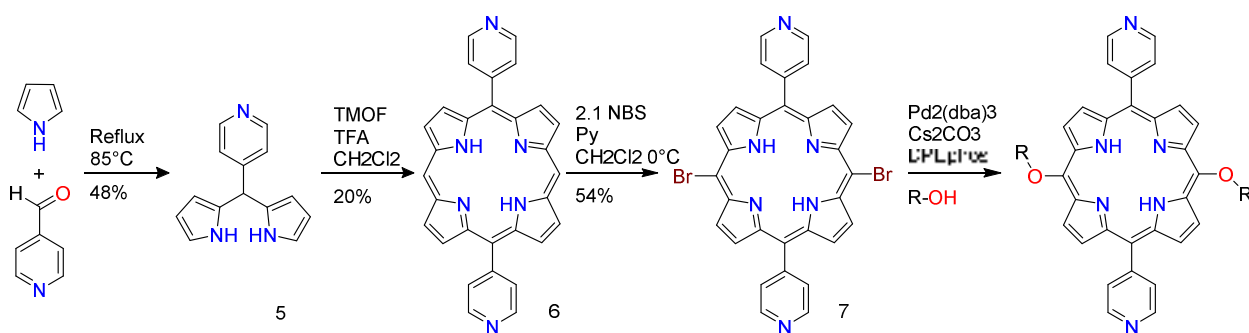


Figure II.13. A four steps procedure for the synthesis of substituted 5, 5-dipyridylporphyrin.

By adapting the conditions of the palladium mediated cross-coupling reported by Zhang²⁶ used for aryl alcohols but also several examples of simple alkyl alcohols and 2,2,2-trifluoroethan-1-ol, we successfully synthesized a series of 11 new fluorinated and/or chiral porphyrins that are depicted figure II.14.

Regarding the substituents we used, it is possible to divide the new tectons in three categories: the first row shows 4 building blocks (**8-11**) with an increasing number of fluorine atoms on the backbone ranging from 6 to 16 fluorines per porphyrin. The second row (**12** and **13**) comprises chiral non fluorinated tectons and the last row is formed by chiral and fluorinated or brominated molecules. The 2, 2, 3, 4, 4, 4-hexafluorobutan-1-ol (racemate) and (*R*)-(-)-3-bromo-2-methylpropan-1-ol are commercially available while the 4, 4, 4-trifluoro-3-methylbutan-1-ol and 3-(trifluoromethyl) pentan-1-ol (racemate) were synthesized in the group of Prof. Stefan Bräse in Karlsruhe Institute of Technology. It is worth to mention that the compounds **14**, **15** and **16** were synthesized by using racemic mixtures of the alcohols, **14**, **15**, and **16** have thus been obtained as a mixture of two enantiomers (*R,R* and *S,S*) together with the non chiral meso form (*R,S*) while tecton **17** was obtained as a pure enantiomer (*R,R*-**17**).

Both enantiomers (*R,R* and *S,S*) of **12** have been obtained while the synthesis of **13** has only been performed starting from the (*S*)-2-methylbutan-1-ol due to commercial availability.

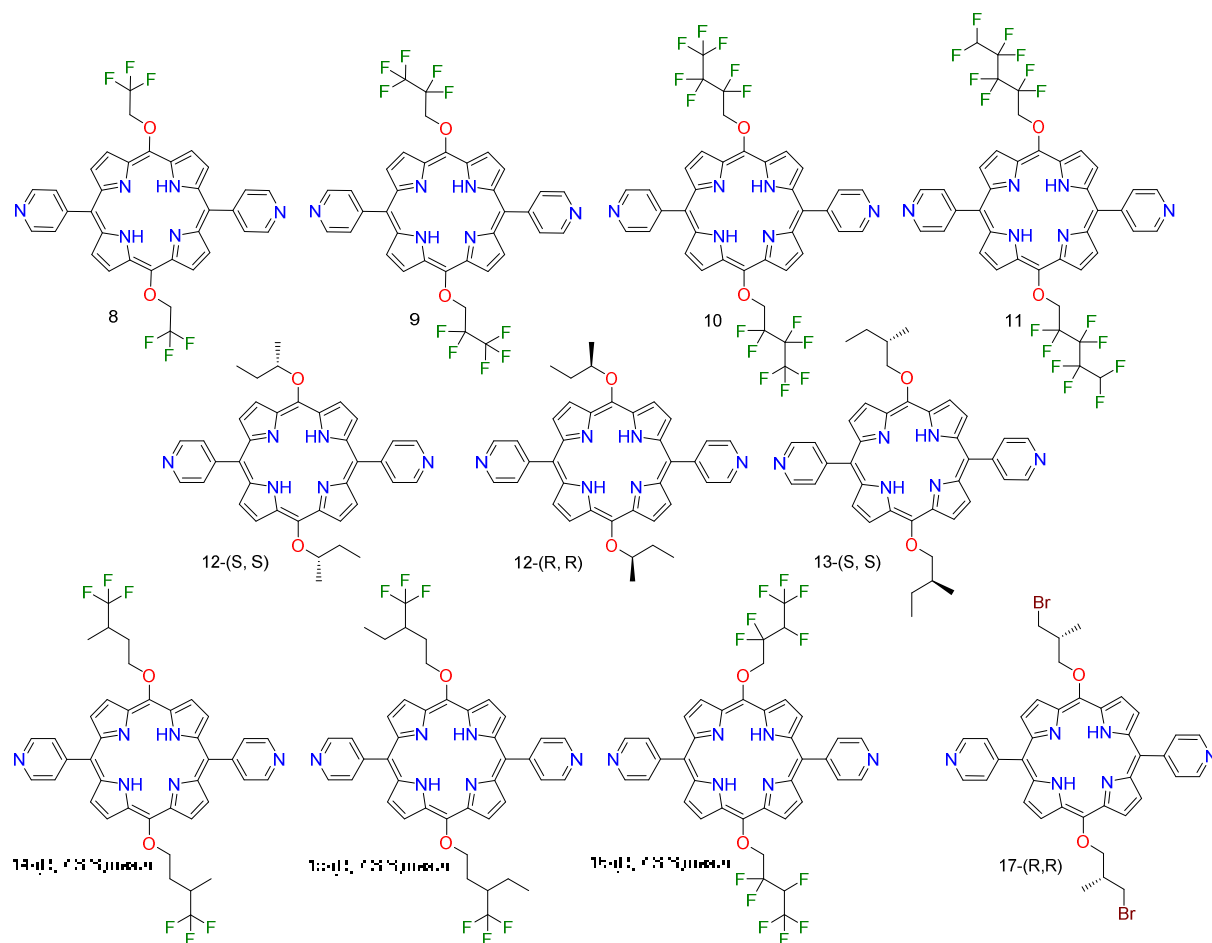


Figure II.14. Ten new porphyrin based tectons synthesized.

All eleven new tectons were characterized by ¹H-, ¹³C-, and ¹⁹F- NMR, UV-vis and Mass Spectrometry. It is worth mentioning that in the case of ligand **14,15** and **16** a mixture of the 3

stereoisomers (racemate + meso) with a statistic mix corresponding to 25% of R,R, 25% of S,S and 50% of R,S is formed. For ligand **14**, the NMR spectrum of the mixture shows the presence of only one porphyrin. The same is observed for ligand **15** and **16**.

Based on the scheme above, we could observe that by applying this method we have access to a wide variety of new porphyrins bearing different substituents in a simple and elegant manner. This synthetic pathway allows diversifying the pool of neutral coordinating tectons, by finely tuning the substituents that are introduced in the final step. Table II. 1 gives a comparative view on the synthesis of the 11 different tectons including the details on the reaction times and the corresponding yields.

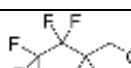
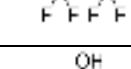
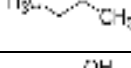
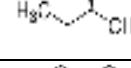
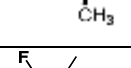
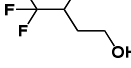
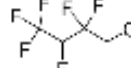
Tecton	Alcohol	Yield	Time	Temperature
8		31%	48h	100°C
9		28%	5h	80°C
10		36%	7h	80°C
11		45%	7h	100°C
(R,R)-12		69%	4h	80°C
(S,S)-12		69%	4h	80°C
(S,S)-13		85%	5h	80°C
14		55%	8h	100°C
15		40%	48h	100°C
16		51%	24h	100°C
(R,R)-17		61%	4h	80°C

Table II.1.

By comparing the yield in the table II.1 we can observe that the highest yield is observed for the chiral tecton **13** while the lowest goes to the fluorinated tecton **9**.

It was observed that in several cases, increasing the reaction time leads to the formation of the non-brominated porphyrin **6**.

However, within the fluorinated porphyrins we observe that depending on the number of fluorine atoms yields are varying from 28% to 55%, and by comparing tectons **9**, **10** and **11** it seems that for primary alcohols the yield is increasing with the number of fluorines. Also the comparison of the yield obtained for **12** and **13** seems to indicate that the use of primary alcohol leads to better yield than secondary alcohol.

II.2.C. Crystal Structures

Despite extensive crystallization tests, up to now, we succeed in growing single crystals for only 6 porphyrins among the eleven new tectons that we synthesized. Moreover for all the tectons we tried to grow single crystals in the presence of additional fluorinated solvents such as 2,2,2-trifluoroethan-1-ol, but unfortunately, none of them leads, up to now, to the formation of single crystals.

In the following part, the six corresponding crystal structures obtained by X-ray diffraction are presented in the order of increasing number of fluorine atoms present on the backbone, thus the first analyzed will be tecton **15** with 6 fluorine atoms, followed by **9** with 10 fluorine atoms per porphyrin, **16** with 12 fluorine atoms then **10** with 14 fluorines and finally **11** with 16 fluorine atoms. The structure of the chiral tecton **17** is given last.

Tecton 15

Single crystals of **15** were obtained by slow diffusion of acetonitrile into a solution of **15** (RR, SS and the meso) in CHCl_3 . Under those conditions, the meso form crystallizes in the P21/n space group with no solvent molecules included in the asymmetric unit. The porphyrin core is almost planar and the dihedral angle between the porphyrin mean plane (24 atoms) and the *meso*-pyridyl groups is close to 78° . The relative orientation in the solid state of the fluorinated chains for **15** is above and below the porphyrin mean plane (figure II.15).

As in the case of tecton **4**, no F---F interaction is observed, yet the formation of weak intermolecular hydrogen bonds between the fluorine atoms and the β -pyrrolic protons (4 fluorine involved/porphyrin) can be observed (the C---F distances range between 3.17 Å and 3.56 Å).

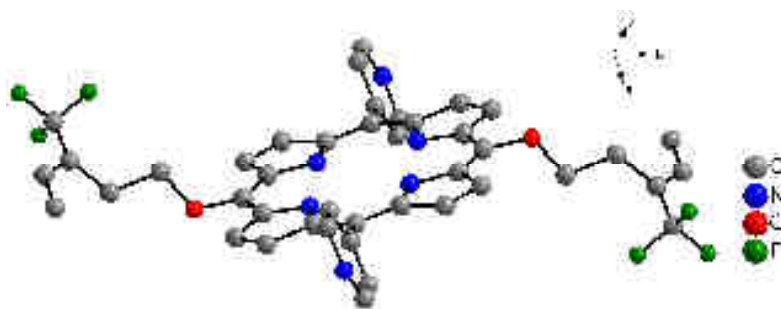


Figure II.15. Crystal structure of the tecton **15**. Hydrogen atoms are omitted for clarity.

Tecton 9

Single crystals of **9** have been obtained by slow diffusion of EtOH into a chloroform solution of the porphyrin and analyzed by X-Ray diffraction. The porphyrin crystallizes in the absence of solvent. The porphyrin core is almost planar and the fluorinated chains are situated above and under the porphyrin mean plane (figure II.16a). No F---F contacts are observed. Moreover no intermolecular hydrogen bonds involving fluorine are present. In this case, despite an increasing number of fluorine atoms present in the periphery of **9** compared to **15**, we do not observe an increasing number of interactions involving fluorine. Instead, in the structure, there are weak π - π interactions in the β -pyrrolic regions of the porphyrin (3.67 Å). Another interesting feature is the arrangement of the macrocycles in a parallel manner resulting in the formation of “fluorous” layers (oriented along the *ab* plane), as it can be seen in figure II.16 b.

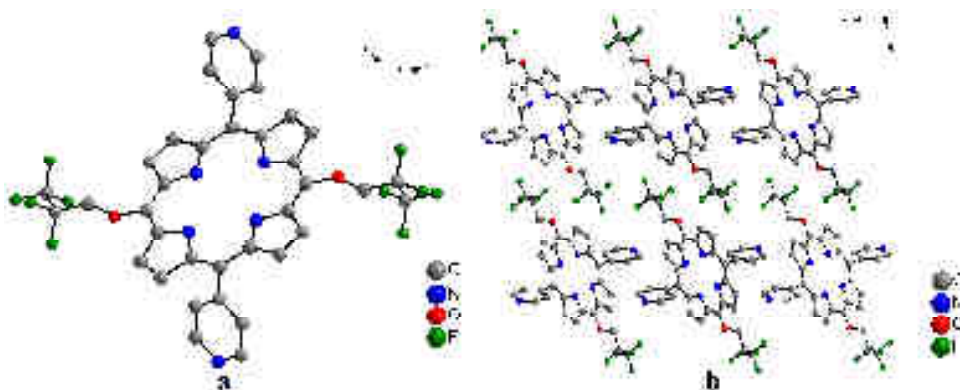


Figure II.16. a) Crystal structure of the tecton **9**; b) Crystal packing. Hydrogen atoms are omitted for clarity.

Tecton 16

Single crystals of **16** were obtained by slow diffusion of ethanol into a solution of the **16** in CHCl_3 . Under those conditions, **16** crystallizes in the P-1 space group with two independent porphyrin units and no solvent molecules included in the asymmetric unit. One moiety has the alkyl chains disordered over two positions. The porphyrin core is almost planar and the dihedral angle between the porphyrin mean plane (24 atoms) and the *meso*-pyridyl groups is close to 61° . Fluorinated alkyl chains are situated under and over the plane for the non-disordered porphyrin moiety. (Figure II.17a) Unlike tecton **15**, we observe for the non-disordered porphyrin moiety six, type one, F---F contacts/Po (d F---F= 2.72 Å and 2.80 Å) and intermolecular hydrogen bonds between fluorine atoms on the alkyl chains and the protons on the pyridine moiety of the porphyrin (the C---F distances close to 3.36 Å) (figure II.17b). The second moiety is involved only in intermolecular hydrogen bonds between the fluorine atoms and the β pyrrolic protons (the C---F distances are close to 3.30 Å).

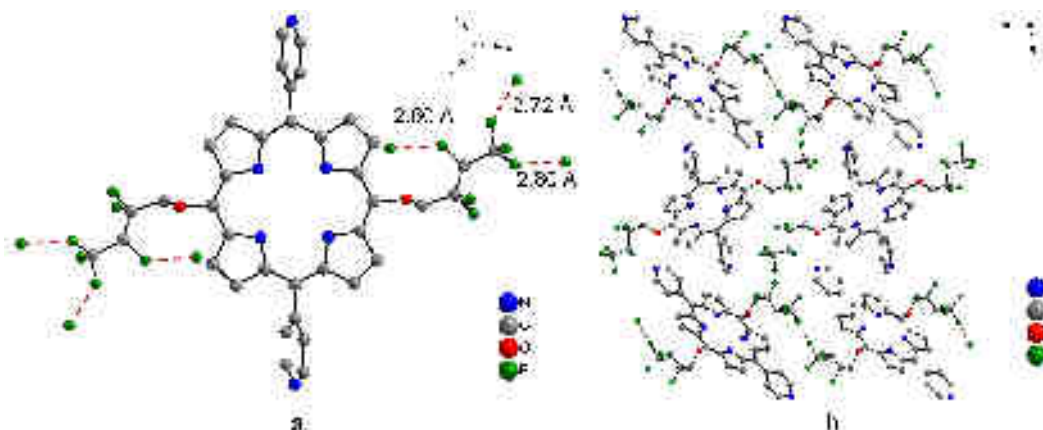


Figure II.17. a) Crystal structure of the tecton **16**, the non-disordered porphyrin moiety; b) crystal packing highlighting the only two F...F contacts (red dotted line). The disorder in the alkyl chains and hydrogen atoms are omitted for clarity.

Tecton 10

Single crystals of **10** were obtained by slow diffusion of ethanol into a solution of the **10** in CHCl_3 . Under those conditions, **10** crystallizes in the $P21/n$ space group with $\frac{1}{2}$ porphyrin and no solvent molecules included in the asymmetric unit. The porphyrin core is planar and the dihedral angle between the porphyrin mean plane (24 atoms) and the *meso*-pyridyl groups is close to 62° (figure II.18a). Fluorinated alkyl chains are disordered over two positions (multiplicity $\frac{1}{2}$).

The F...F interactions couldn't be assigned due to the disorder on the alkyl chains, yet the formation of intermolecular hydrogen bonds between the fluorine atoms and the CH_2 protons on the alkyl chains (2 fluorines involved/porphyrin) can be observed (the C...F distances are close to 3.0 \AA). Moreover, in the structure, there are π - π interactions between the mean planes of the pyridine moieties of the porphyrins (3.30 \AA). (figure II.18b)

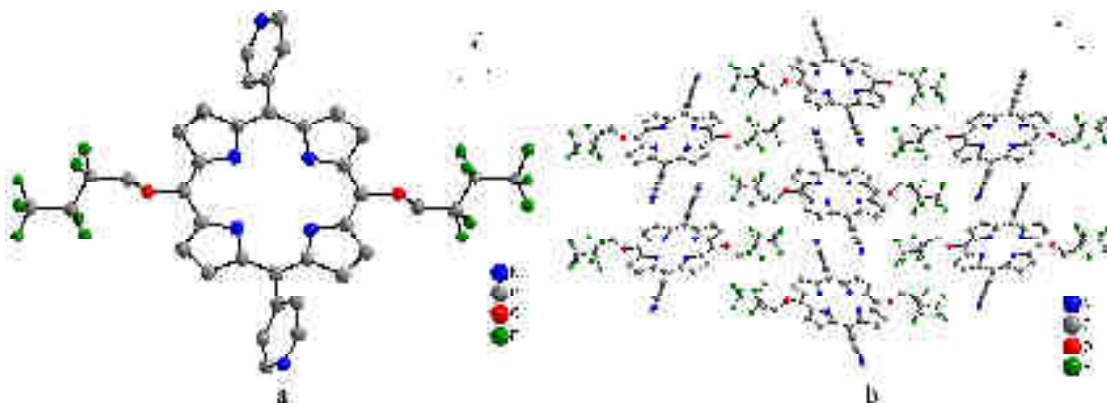


Figure II.18. a) Crystal structure of the tecton **10**; b) crystal packing. The disorder in the alkyl chains and hydrogen atoms are omitted for clarity.

Tecton 11

The most densely fluorinated porphyrin **11**, bearing a total of 16 fluorine atoms in the *meso* positions, crystallizes in the $P-1$ space group and the asymmetric unit contains no solvent molecules. The porphyrin core is planar and the dihedral angles between the porphyrin mean plane (24 atoms) and the *meso*-pyridyl groups is *ca* 74° . The two *trans* chains are situated above and

under the tecton mean plane. In the solid state, no π - π stacking is observed within porphyrin layers but numerous F---F contacts are present between adjacent porphyrins with up to 12 F---F interactions per porphyrin (figure II.19a) with distances varying from 2.83 Å to 2.94 Å (the upper limit of the sum of the van der Waals radii). Moreover, three of the four contacts have θ_1 and θ_2 (discussed in chapter 1) quite close to each other (118° and 127°) while for the F---F contact of 2.86 Å, $\theta_1 = 170^\circ$ and $\theta_2 = 110^\circ$, which is near to the value expected for type II halogen bonding. Focusing only on these F---F contacts, one may describe the structure as a monodimensional network (figure II.19b).

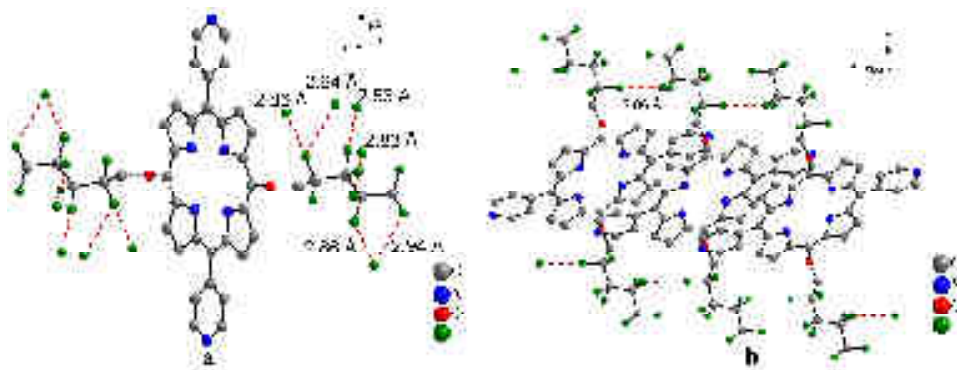


Figure II.19. a) A portion of the crystal structure of **11** highlighting all the F---F contacts (red dotted line); b) Crystal packing of the porphyrin focusing on short F-F contact and the 1D supramolecular network. Hydrogen atoms are omitted for clarity.

Tecton 17

Last but not least, it was also possible to crystallize the chiral brominated tecton, by slow diffusion of EtOH into a chloroform solution of the porphyrin. **17** crystallizes in a chiral space group P1 without any solvent molecules present in the asymmetric unit. X-Ray analysis confirms the R configuration of the two stereogenic carbon atoms (Flack parameter). The porphyrin core is planar and the *meso*-pyridyl groups are almost perpendicular (87° - 88°) to the porphyrin mean plane (24 atoms). The *meso*-alkyl substituents are oriented on opposite sides with respect to the porphyrin mean plane.(Figure II.20 a) In the crystal packing no π - π interactions are observed and the only intermolecular interactions are hydrogen bonds, notably involving Br and β -pyrrolic CH (distance of Br---C *ca* 3.67 Å) (figure II.20 b).

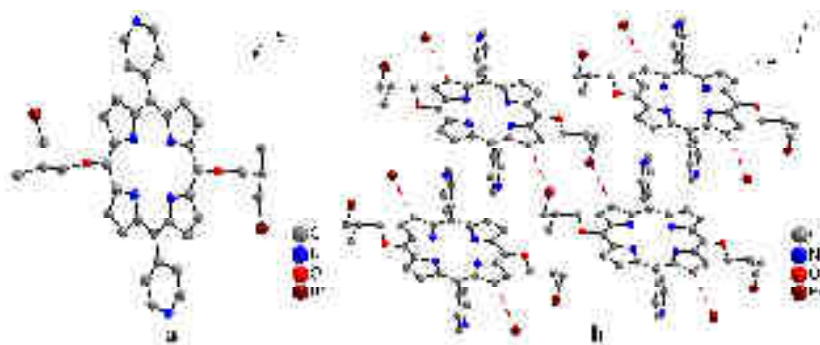


Figure II.20. a) Crystal structure of the chiral tecton **17** b) Crystal packing highlighting the hydrogen bonds (red dotted line).

Conclusion

A series of 13 new fluorinated and/or chiral tectons were synthesized, either by using a [2+2] MacDonald condensation reaction, where the chiral and fluorinated substituents are introduced in the first step, or by using a dibromo-porphyrin derivative as an intermediate for metal catalyzed cross-couplings. The first method was applied only for two commercially available aldehydes and leads to poor yields. The second method allowed the design of a new family of tectons, which have two coordinating sites in two opposite *meso* positions on one hand and a series of fluorinated and/or chiral alkyl chains on the other hand. This synthetic pathway is quite handy as the number of reported porphyrins with fluorinated alkyl chains in the *meso* positions is scarce. The tectons synthesized by this method can be divided in three groups; the first one (tectons **8-11**) is a set of porphyrins with varying number of fluorine substituents on the alkyl chains (from 6 to 16 fluorine atoms), a second group of chiral tectons (**12** and **13**) and the last one is a sequence of chiral and halogenated porphyrins (tectons **14-17**). This synthetic pathway seems to be suitable for the introduction of a large variety of substituents in the *meso* positions of porphyrin and it will be used in the laboratory in the near future in order to generate new porphyrin tectons.

Seven tectons have been characterized by X-Ray diffraction analysis. This solid state study has shed some light on the specific interactions in the crystal packing of the tectons depending on their structure. Obviously, the conformations of the tectons in the crystal are influenced by intermolecular interactions such as H-bonds or π - π stacking and can thus be different depending on the packing or on the presence of solvent molecules in the asymmetric unit.

Concerning intermolecular interactions and more specifically halogen contacts, we do observe numerous intermolecular F---F contacts ranging from 2.72 Å to 2.94 Å in length, for two tectons **16** and **11**.

Tecton **16** has six, type one, F---F contacts and considering the shortest one 2.72 Å a monodimensional supramolecular networks is built. For tecton **11** among the 12 F---F contacts present most of them (8) are type I halogen bond contacts (θ_1 and θ_2 are equal), while four contacts (F---F distance equal to 2.86 Å) are close to type II with $\theta_1=170^\circ$ and $\theta_2=110^\circ$. A 1-D supramolecular network can be built through these interactions. F---F contacts for tecton **10**, that has an intermediate number of fluorine atoms between **16** and **11**, couldn't be assigned due to the disorder on the alkyl chains.

Considering the X-ray structures, the presence of fluorine atoms in the periphery of the porphyrin could influence the crystal packing in the solid state but is definitely not the only interaction to consider in order to describe the organization of such molecules in the solid state. Considering that the energy of halogen bond is ranging from 5kJ to 180 kJ/ mol, the lower limit is comparable to the energy of π --- π interactions. Thus, even for tecton **11**, during the crystallization process F---F contacts are certainly not the only and probably not the main driving force for the organization of the porphyrins in the crystal.

Interestingly some of these trends in the crystal structure of the free ligand will be observed in the subsequent networks obtained from their metal complexes, discussed in next chapter.

References

1. G. P. Moss, *Pure & Appl. Chem.*, , 1987, **59**, 779—832.
2. J.T.Groves, K.Shalyaev and J.Lee, *Oxometalloporphyrins in oxydative catalysis, The Porphyrin Handbook*, Ed. K.M. Kadish, K.M. Smith, R. Guilard, Academic Press, 2000, **Vol. 4**
3. T.Aida and S.Inoue, *Metalloporphyrins as Catalysts for Precision Macromolecular Synthesis, The Porphyrin Handbook* , Ed. K.M. Kadish, K.M. Smith, R. Guilard, Academic Press, 2000, **Vol.6**.
4. B. Morgan and D. Dolphin, in *Metal Complexes with Tetrapyrrole Ligands I*, ed. J. Buchler, Springer Berlin Heidelberg, 1987, vol. 64, pp. 115-203.
5. V. Bulach and M. W. Hosseini, *Handbook of Porphyrin Science*, Eds. K. Kadish, K. Smith and R. Guilard, World Scientific, 2011, **13**, 299-391.
6. J. K. M. Sanders, N.Bampos, Z.Clyde-Watson, S. L. Darling, J.C.Hawley, H.J.Kim, C.C.Mak and SJ.Webb, *Axial Coordination Chemistry of Metalloporphyrins, The Porphyrin Handbook* , Ed. K.M. Kadish, K.M. Smith, R. Guilard, Academic Press, 2000, **Vol. 3**.
7. W. R. Scheidt, *Systematics of the Stereochemistry of Porphyrins and Metalloporphyrins, The Porphyrin Handbook* , Ed. K.M. Kadish, K.M. Smith, R. Guilard, Academic Press, 2000, **Vol.24**.
8. D. J. Nurco, C. J. Medforth, T. P. Forsyth, M. M. Olmstead and K. M. Smith, *J. Am. Chem. Soc.*, 1996, **118**, 10918-10919.
9. P. Rothmund, *J. Am. Chem. Soc.*, 1935, **57**, 2010-2011.
10. A. D. Adler, F. R. Longo, J. D. Finarelli, J. Goldmacher, J. Assour and L. Korsakoff, *J. Org. Chem.*, 1967, **32**, 476-476.
11. J. S. Lindsey, I. C. Schreiman, H. C. Hsu, P. C. Kearney and A. M. Marguerettaz, *J. Org. Chem.*, 1987, **52**, 827-836.
12. R. G. Little, J. A. Anton, P. A. Loach and J. A. Ibers, *J. Heterocycl. Chem.* , 1975, **12**, 343-349.
13. G. P. Arsenault, E. Bullock and S. F. MacDonald, *J. Am. Chem. Soc.*, 1960, **82**, 4384-4389.
14. S. J. Lee, R. A. Jensen, C. D. Malliakas, M. G. Kanatzidis, J. T. Hupp and S. T. Nguyen, *J. Mater. Chem.* , 2008, **18**, 3640-3642.
15. V. Bulach, D. Mandon and R. Weiss, *Angew. Chem. Int. Ed.*, 1991, **30**, 572-575.
16. J. P. Collman, X. Zhang, P. C. Herrmann, E. S. Uffelman, B. Boitrel, A. Straumanis and J. I. Brauman, *J. Am. Chem. Soc.*, 1994, **116**, 2681-2682.
17. J. P. Collman, P. C. Herrmann, L. Fu, T. A. Eberspacher, M. Eubanks, B. Boitrel, P. Hayoz, X. Zhang, J. I. Brauman and V. W. Day, *J. Am. Chem. Soc.*, 1997, **119**, 3481-3489.
18. J. P. Collman, B. Boitrel, L. Fu, J. Galanter, A. Straumanis and M. Rapta, *J. Org. Chem.*, 1997, **62**, 2308-2309.
19. V. Bulach, F. Sguerra and M. W. Hosseini, *Coord. Chem. Rev.* , 2012, **256**, 1468-1478.
20. Z. Halime, M. Lachkar, N. Matsouki, G. Charalambidis, M. di Vaira, A. G. Coutsolelos and B. Boitrel, *Tetrahedron*, 2006, **62**, 3056-3064.
21. S. G. DiMugno, V. S. Y. Lin and M. J. Therien, *J. Org. Chem.*, 1993, **58**, 5983-5993.
22. S. G. DiMugno, V. S. Y. Lin and M. J. Therien, *J. Am. Chem. Soc.*, 1993, **115**, 2513-2515.
23. G. Y. Gao, Y. Chen and X. P. Zhang, *J. Org. Chem.*, 2003, **68**, 6215-6221.
24. G.-Y. Gao, Y. Chen and X. P. Zhang, *Org. Lett.*, 2004, **6**, 1837-1840.
25. G.-Y. Gao, A. J. Colvin, Y. Chen and X. P. Zhang, *J. Org. Chem.*, 2004, **69**, 8886-8892.
26. G.-Y. Gao, A. J. Colvin, Y. Chen and X. P. Zhang, *Org. Lett.*, 2003, **5**, 3261-3264.
27. D. P. Arnold, *J. Chem. Educ.* , 1988, **65**, 1111.
28. S. J. Shaw, S. Shanmugathan, O. J. Clarke, R. W. Boyle, A. G. Osborne and C. Edwards, *J. Porphyrins Phthalocyanines* 2001, **5**, 575-581.
29. M. Gouterman, *J. Mol. Spectrosc.* , 1961, **6**, 138-163.
30. J. L. Soret, *Comp. Rendu.*, 1883, **97**, 1269.
31. X. Huang, K. Nakanishi and N. Berova, *Chirality*, 2000, **12**, 237-255.

32. Y. Mizuno, T. Aida and K. Yamaguchi, *J. Am. Chem. Soc.*, 2000, **122**, 5278-5285.
33. I. Nicolas, S. Chevance, P. L. Maux and G. Simonneaux, *Tetrahedron: Asymmetry* 2010, **21**, 1788-1792.
34. X. Wu and S. D. Starnes, *Org. Lett.*, 2012, **14**, 3652-3655.
35. D. Intriери, S. Le Gac, A. Caselli, E. Rose, B. Boitrel and E. Gallo, *Chem. Commun.*, 2014, **50**, 1811-1813.
36. B. Boitrel, V. Baveux-Chambenoît and P. Richard, *Eur. J. Inorg. Chem.*, 2002, 1666-1672.
37. S. Gazeau, J. Pécaut, R. Haddad, John A. Shelnutz and J.-C. Marchon, *Eur. J. Inorg. Chem.*, 2002, **2002**, 2956-2960.
38. S.-Q. Liu, J. Pécaut and J.-C. Marchon, *Eur. J. Inorg. Chem.*, 2002, 1823-1826.
39. N. Marets, V. Bulach and M. W. Hosseini, *New J. Chem.* , 2013, **37**, 3549-3558.
40. P. Iavicoli, H. Xu, L. N. Feldborg, M. Linares, M. Paradinas, S. Stafström, C. Ocal, B. Nieto-Ortega, J. Casado, J. T. López Navarrete, R. Lazzaroni, S. D. Feyter and D. B. Amabilino, *J. Am. Chem. Soc.*, 2010, **132**, 9350-9362.
41. C. Chappaz-Gillot, G. Canard, F. Andreoli, N. Vanthuyne, M. Giorgi, J.-V. Naubron, V. Monnier, R. Rosas, C. Roussel and T. S. Balaban, *Eur. J. Org. Chem.*, 2012, 6526-6536.
42. J. C. P. Grancho, M. M. Pereira, M. d. G. Miguel, G. A. M. Rocha and H. D. Burrows, *Photochem. Photobiol.* , 2002, **75(3)**, 249-256.
43. I. Hatay, B. Su, M. A. Méndez, C. Corminboeuf, T. Khoury, C. P. Gros, M. Bourdillon, M. Meyer, J.-M. Barbe, M. Ersoz, S. Záliš, Z. Samec and H. H. Girault, *J. Am. Chem. Soc.*, 2010, **132**, 13733-13741.
44. E. Porhiel, A. Bondon and J. Leroy, *Eur. J. Inorg. Chem.*, 2000, 1097-1105.
45. T. Goslinski and J. Piskorz, *J. Photochem. Photobiol., C* 2011, **12**, 304-321.
46. S. G. DiMagno, R. A. Williams and M. J. Therien, *J. Org. Chem.*, 1994, **59**, 6943-6948.
47. T. P. Wijesekera, *Can. J. Chem.* , 1996, **74**, 1868-1871.
48. S. G. DiMagno, P. H. Dussault and J. A. Schultz, *J. Am. Chem. Soc.*, 1996, **118**, 5312-5313.
49. W.-B. Yi, J.-J. Ma, L.-Q. Jiang, C. Cai and W. Zhang, *J. Fluorine Chem.* , 2014, **157**, 84-105.
50. D. Gryko and J. S. Lindsey, *J. Org. Chem.*, 2000, **65**, 2249-2252.
51. D. P. N. Goncalves, S. Ladame, S. Balasubramanian and J. K. M. Sanders, *Org. Biomol. Chem.* , 2006, **4**, 3337-3342.
52. L. Yu, K. Muthukumar, I. V. Sazanovich, C. Kirmaier, E. Hindin, J. R. Diers, P. D. Boyle, D. F. Bocian, D. Holten and J. S. Lindsey, *Inorg. Chem.*, 2003, **42**, 6629-6647.

Chapter 3

Contents

Chapter III. Coordination Networks based on halogenated or/and Chiral Porphyrins.....	58
III. 1. Coordination networks and porphyrins: Some examples.....	58
III. 2. MOFs and Porphyrins: Synthetic strategy.....	63
III. 3. Self-assembly of new Zinc (II) Porphyrin tectons.....	64
III. 3. A. Zn-Tecton 4.....	65
III. 3. B. Zn-Tecton 8-11.....	68
III. 4. Double component systems composed of Porphyrin and Cd (II).....	78
III. 5 Conclusion.....	81
References.....	82

Chapter III. Coordination Networks based on halogenated or/and Chiral Porphyrins

This chapter deals with porphyrin-based tectons for building coordination networks. Our goal, as stated in the introduction, is to build functional networks for efficient separation of mixtures through specific interactions. We focused on the use of chiral and/or fluorinated tectons to decorate the interior of channels within coordination networks. In particular our aim was to design porous materials capable of trapping fluorinated and/or chiral molecules. In chapter II, we described the formation of a series of chiral and/or fluorinated porphyrin based tectons. Here we describe their use in the generation of fluorinated and/or chiral networks.

III. 1. Coordination networks and porphyrins: Some examples

In this part, only few relevant examples of coordination networks formed by porphyrin based tectons are discussed. A more complete description of the state of the art concerning this topic could be found in recent reviews.^{1, 2, 3}

The first porphyrin-based coordination polymer was reported by Robson and co-workers in 1991.⁴ A palladium tetrapyrrolyl porphyrin moiety leads to the formation of a 3-D arrangement in the presence of cadmium cation (figure III. 1). One Cd^{2+} is coordinated by two *cis* pyridyl, while the second cadmium cation is connected by two *trans* pyridyl donors. The square bipyramidal geometry is formed by two pyridine moieties and four water molecules. This contribution is not only a milestone for porphyrin based coordination networks, but also represents the first reported heterometallic architecture.

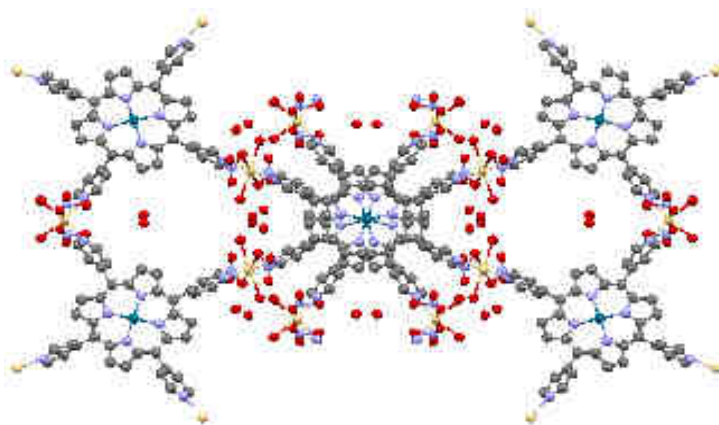


Figure III. 1. A view of the first coordination network based on porphyrins (N=blue, Cd=light yellow, Pd=green, O=red). Hydrogen atoms are omitted for clarity.

In 1994, Robson *et al.* proved that the crystal engineering approach can be successfully used to generate three dimensional networks with large channels, starting from porphyrin building blocks.⁵ These results were at the origin of the rapid increase in the number of reports dealing with porphyrin based frameworks (figure III. 2).

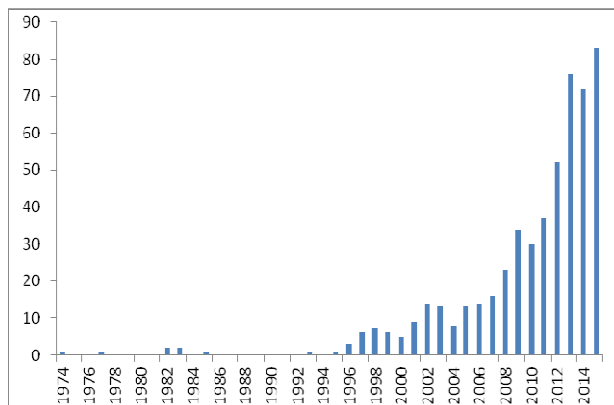


Figure III. 2. Number of articles including “porphyrin frameworks” in the title in recent years.

The most frequent groups used as coordinating sites are 4-pyridine and 4-benzoic acid located at the *meso* positions. One particular interest in the porphyrin backbone is related to the possibility of tuning the number (1 to 4) and the positions of the coordination sites at the meso positions. This leads to many possibilities in terms of geometry and denticity for the design of tectons. Moreover, the position of the coordinating atoms, the number of coordinating sites, the nature of the spacer linking the coordinating site to the porphyrin backbone may be varied leading thus to an infinity of possibilities for the design of tectons and for their combinations with a variety of metal centers leading to an infinity of coordination networks with different topology and geometry (figure III.3).³

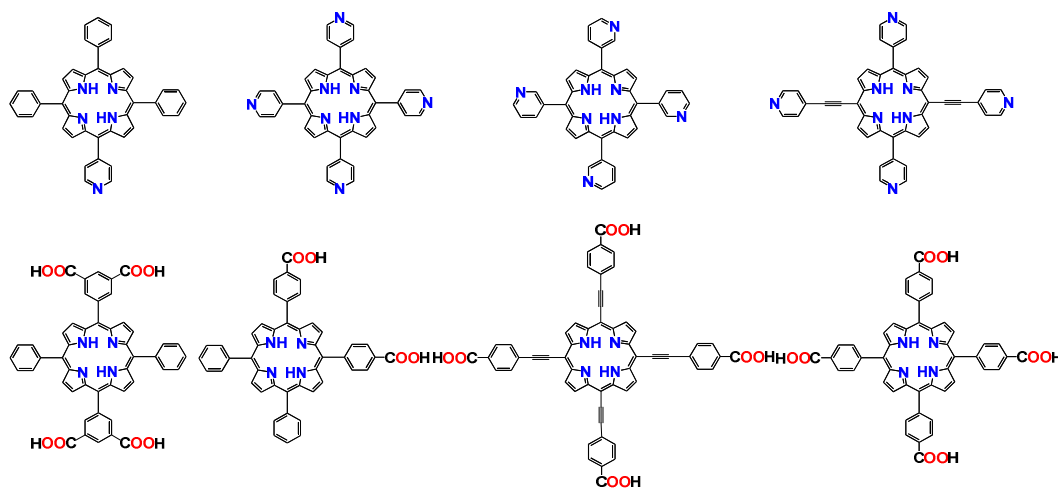


Figure III. 3. An overview of the most exploited tectons.

In 2002, Suslick and co-workers described the formation of a porphyrin based coordination polymer for selective sorption of guest solvent molecules.⁶ The zeolite like analogue (PIZA-1: Porphyrin Illinois Zeolite Analogue) was generated under solvothermal conditions, *via* self-assembly of a cobalt tetrakis (4-carboxyphenyl) porphyrin with cobalt chloride. This stable and robust framework displays large voids with accessible hydrophilic channels perfectly suitable for a

large variety of molecules (amines, alcohols) with different affinity for solvents depending on their size (figure III. 4).

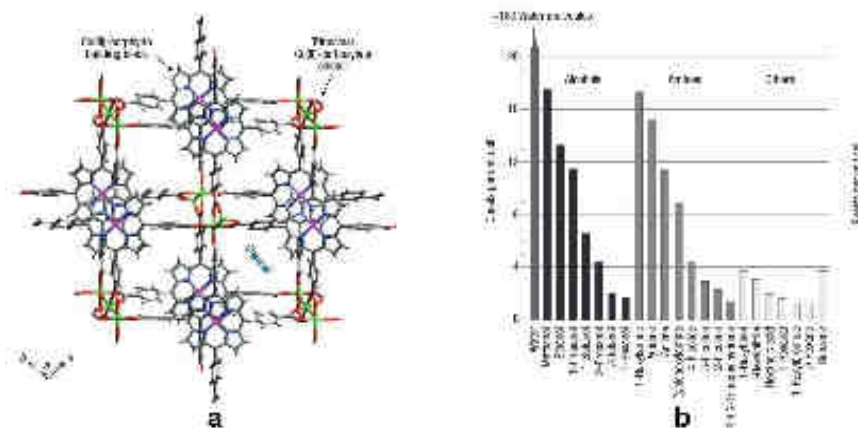


Figure III. 4. a) Structure of PIZA-1 showing channels; b) incorporation capacity of the networks observed for different molecules.

Later on, the same group showed that PIZA-3, an analogue of PIZA-1 for which cobalt cation was replaced by manganese, catalyzes the oxidation of linear and cyclic alkanes and epoxidation of cyclic alkenes with yields varying from 20 to 74%. The catalysis occurs on the MOF surface as the cavities were too narrow to allow substrate diffusion.⁷

More recently, the group of Hupp described the synthesis of a MOF using two organic ligands: a porphyrin possessing two pyridine moieties in the *trans meso* positions and a tetrakis (4-carboxyphenyl)benzene⁸ and tetra (p-carboxyphenyl)porphyrin (figure III. 5).⁹ In this case, the pyridine bearing porphyrins act as pillars connecting consecutive layers. A series of different MOFs can be synthesized applying this approach and more interestingly a wide variety of metal ions can be used. The ability to incorporate two different metal ions into a framework could enable the presence of two distinct catalysts capable of accelerating multiple steps complex reactions.

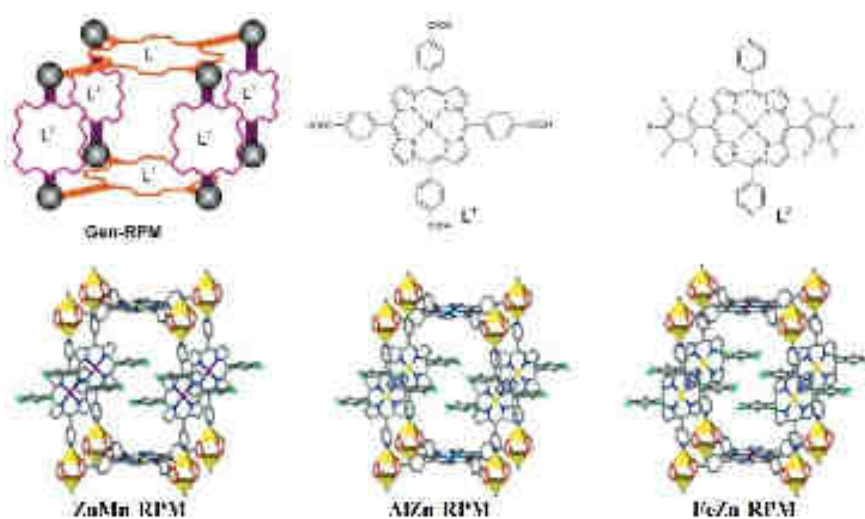


Figure III. 5. Structure of Robust Porphyrinic Materials (RPM), top left: a schematic representation of RPM unit cell, top center and right: the structures of porphyrin building blocks; bottom: the three RPM representatives with different metal centers.

As mentioned before, the biological importance of the porphyrin macrocycle makes it an attractive scaffold for assembling crystalline MOFs for light harvesting properties. In 2012, the group of Hupp reported¹⁰ porphyrin based MOFs showing exciton migration over up to ~45 porphyrin units. This remarkably efficient exciton migration is attributed to enhanced π -conjugation through the addition of two acetylene moieties within the porphyrin molecule (figure III. 6). In this case, it was not possible to have full structure determination, but the cell parameters indicate that the Zn-Porphyrin acts as pillars between the Zn-paddlewheel sheets formed by the carboxylate co-ligand.



Figure III. 6. Structure of a porphyrin based MOF and its use in light harvesting properties, highlighting the exciton migration within the framework.

Emphasis on two and three dimensional networks and their possible applications has been a focal point in the chemistry of coordination polymers, yet it can be quite difficult to predict or to push a system towards the formation of these structures. Recently the importance of mono dimensional porous structures has been rising due to high occurrence of this type of architectures as well as easiness in anticipating their formation. A recent example of 1D double chain dipyrindyl-porphyrin based porous coordination polymers (figure III. 7) showed interesting results towards CO₂ sorption.¹¹

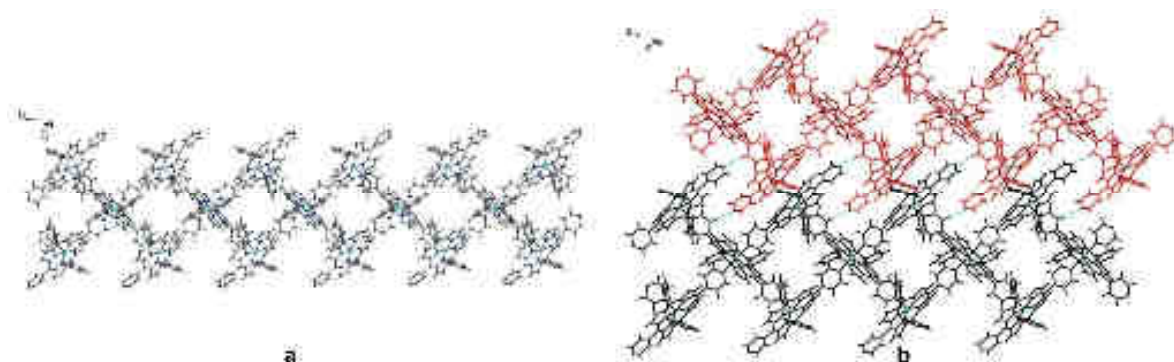


Figure III. 7. a) 1D double chain structure of Co²⁺-Porphyrin; b) two 1D double chains (represented in red and black) connected through hydrogen bonds (blue dotted line).

Two isostructural networks based on Co²⁺-Porphyrin and Zn²⁺-Porphyrin in DMF showed adsorption selectivity for CO₂ over N₂, H₂, and CH₄ at low temperature and low pressure. It is

worth noting that structural changes during adsorption processes are highly metal dependent. This is only a brief discussion on possible applications of porphyrin based networks, an ampler review on the functional materials composed of metal-metalloporphyrin frameworks has been published by Ma and co-workers² in 2014.

In our group,¹²⁻¹⁸ numerous studies have focused on the formation of MOFs based on porphyrin building units. Especially, those obtained through self-assembly of Zn(II) [5,15-(4-pyridyl) porphyrins], (Zn-Po), possessing different aryl substituents in *trans* 10 and 20 positions. The 3D coordination networks were obtained through pyridine coordination of two adjacent porphyrins in axial positions of the metal ion (Zn^{2+}). The hexagonal architectures possess cavities that can be filled with solvent molecules. (figure III. 8)

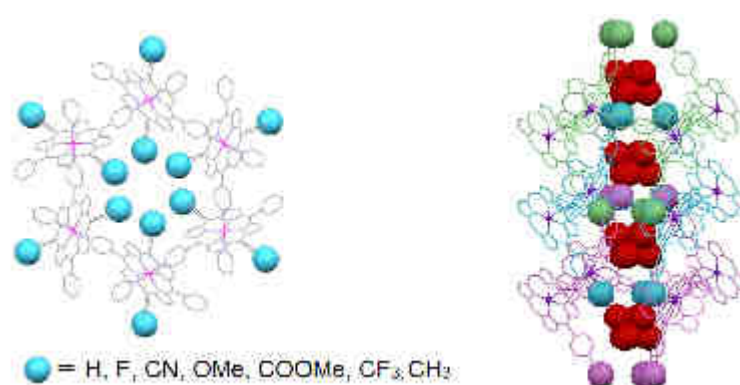


Figure III. 8. On the right, view on the channels with solvent molecules (only one pyridine is represented); on the left, the view on the hexagonal network formed (C=grey, Zn^{2+} =purple, blue ball= *para* substituents of the meso phenyl).

These architectures are robust enough to allow solvent exchange in single-crystal-to-single crystal transformations. The amount of solvent exchanged (ethanol, methanol, cyclohexane) depends on the *para*-substituents and on the cavity dimensions. As the substituents in the *para* position of the phenyl are pointing inside the channels, one can imagine altering the pore dimensions and the affinity towards polar or non-polar solvents, by varying the nature of these substituents (figure III. 9).

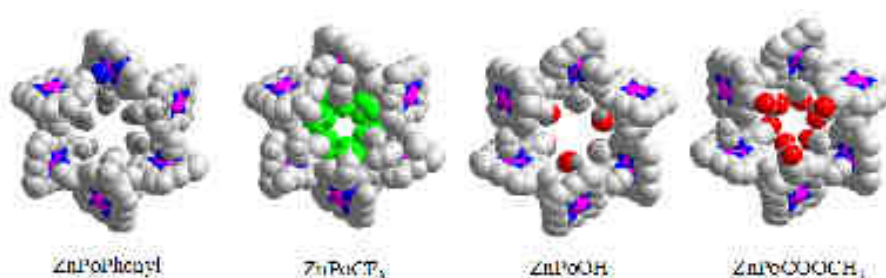


Figure III. 9. Influence of the nature of substituents in *para* position of *meso* phenyls on the channel size.

The research topic of my PhD was inspired by these studies. Indeed, the introduction of chiral or highly fluorinated substituents could lead to the formation of similar hexagonal coordination networks possessing channels that are well suited for the trapping of chiral and/or fluorinated species such as inhalation anaesthetics.

III. 2. MOFs and Porphyrins: Synthetic strategy

Dealing with coordination networks based on porphyrin tectons, one may use mainly two strategies differing by the localization of the metal ion: in the porphyrin cavity or outside of the core. The first one is called: single component strategy because it involves the self-assembly of a self-complementary tecton. The multiple component strategy involves necessarily an external metal cation and leads to the formation of either homometallic or heterometallic coordination frameworks depending on the absence or presence of a metal cation within the porphyrin precursor.

In order to reduce the number of components and to avoid the inclusion of counter ions, one might use self-complementary neutral metallotectons. For self-complementary metalloporphyrins, the generation of networks takes place through the formation of coordination bond (usually one or two) involving the axial position(s) of the metal cation.

When dealing with porphyrins bearing three coordinating poles: the tetradentate porphyrin core and the two monodentate pyridyl units (such as the tectons described in the previous chapter), the binding of metal ions such as Zn(II) cation by these porphyrin cores leads to the formation of a neutral self-complementary tectons due to the possibility of further interactions, using the axial position of the Zn²⁺ cation, with substituents such as pyridine present at the porphyrin periphery. Their self-assembly generates 1-D, 2-D,^{12, 13} and 3-D^{14, 18} coordination networks depending on the coordination geometry (either 5 or 6-coordinated) of the Zn(II) cation (figure III. 10).

Indeed, the coordination of only one pyridine in the axial position on the Zn(II) cation may lead to the formation of 1D networks, while the presence of two pyridyl units in the apical positions of the Zn²⁺ generates either two- or three-dimensional networks depending on the angle between the porphyrin mean plane and the pyridyl substituents.

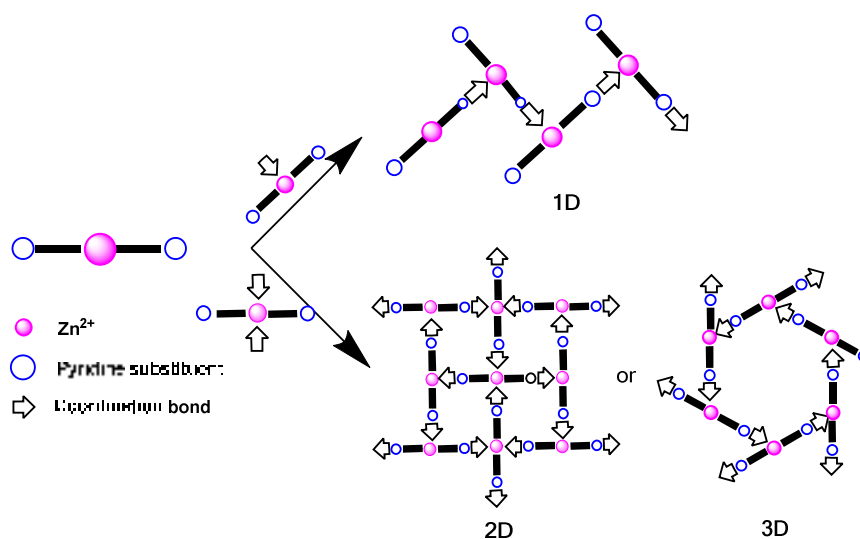


Figure III. 10. Schematic representation of the topology of the coordination networks formed by self-complementary Zn-porphyrins.

A great majority of coordination networks are based on two or three component systems. When employing external metal cations and organic tectons, if charge neutrality is not assured by the organic part, in order to balance the charge of the metal ions, the crystal will include additional anions either coordinated to the metal cations or located in the cavities. Systems based on two components require both a porphyrin-based unit and an external metal ion or a metal complex. Depending on the nature, number and position of the coordinating sites located at the porphyrin periphery and the coordination requirements of the external metal center (number and relative position of free coordination sites), the formation of either 1-D, 2-D or 3-D architectures is possible.

III. 3. Self-assembly of new Zinc (II) Porphyrin tectons

The formation of coordination networks by combining the 13 new tectons described in chapter 2 and Zn^{2+} salts was studied. Many parameters could be varied: the crystallization procedure (liquid/liquid diffusion, solvothermal synthesis, and slow evaporation), the solvents, the temperature and the metal salts. Many attempts have been made, yet for most of them, the formation of amorphous powder was observed. Nevertheless, in 11 cases, we observed the formation of single crystals that were analyzed by the method of choice to characterize such assemblies: X-Ray diffraction on single crystals. In a first part, we will focus on structures obtained using 4-Zn, then the structures concerning the self-assembly of zinc complexes with the ether bonded alkyl chains porphyrins will be presented.

III. 3. A. Zn-Tecton 4

By slow diffusion of $\text{Zn}(\text{OAc})_2 \cdot 2\text{H}_2\text{O}$ in methanol into a chloroform solution of tecton **4**, crystals suitable for X-Ray diffraction were formed. Their analysis revealed that the crystal was of low quality leading thus to high refinement parameters ($R1 = 0.17$ and $wR2 = 0.43$). However, their analysis revealed that a 1D network is formed upon self-assembly of the **4**-Zn. The asymmetric unit contains one Zn-porphyrin moiety and one methanol and disordered water molecules. The Zn^{2+} cation is pentacoordinated and adopts the square based pyramidal geometry with a pyridyl unit belonging to the neighboring metallatecton occupying the axial position of the Zn(II) ion. The average Zn-N distance within the porphyrin core is 2.04 \AA , whereas the axial Zn-N bond distance is slightly longer (2.15 \AA). The porphyrin backbone is planar and the Zn(II) is slightly displaced from the PMP (porphyrin mean plane, 24 atoms) by 0.32 \AA toward the axial pyridyl moiety. Among the two pyridyl units of the tecton, only one is involved in the formation of the coordination network, the second one is “blocked” by a hydrogen bond (2.78 \AA) with a methanol molecule present in the structure (figure III. 11). Within the 1D chain, the dihedral angle between the mean plane of the axial pyridyl unit and the PMP is equal to 81° and the average tilt angle between consecutive porphyrins (PMP) is 82° . Within the tecton, the dihedral angles between the porphyrin mean plane and the *meso* pyridyl substituents are 60° and 87° . As in the case of the free base ligand, presented in the Chapter II, the alkyl chains are situated on the same side of the porphyrin mean plane.

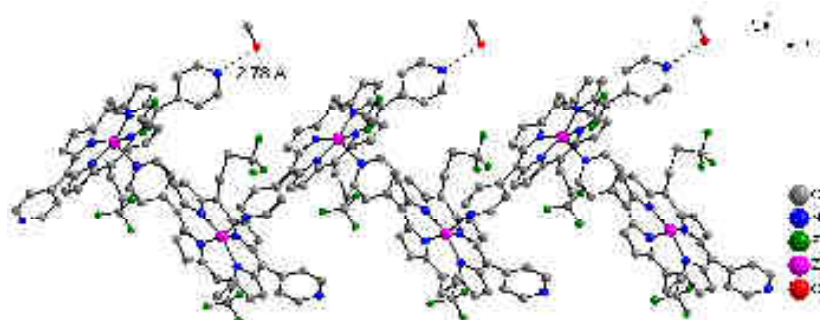


Figure III. 11. A portion of the 1-D coordination network (hydrogen atoms are omitted for clarity) formed by self-complementary **4**-Zn tectons (the dotted line represents the H-bond between pyridine and methanol). Interestingly, unlike the structures of the free tecton reported in the previous chapter, F---F contacts are present in the crystal. Indeed, the chains are connected through F---F contacts (type I) with distance of 2.58 \AA and the angles θ_1 and θ_2 are equal to 111° (figure III. 12). No π - π interactions are spotted.

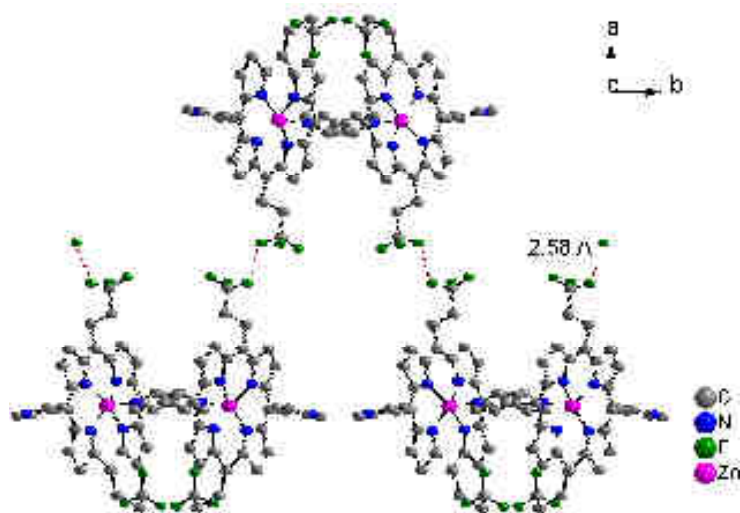


Figure III. 12. Crystal packing of the network, highlighting the F...F contacts in green. Hydrogen atoms and solvent molecules are omitted for clarity.

We tried to trap fluorinated molecules within the network, and, for that purpose, added some drops of 2,2,2-trifluoroethan-1-ol in the methanolic solution of $\text{Zn}(\text{OAc})_2 \cdot 2\text{H}_2\text{O}$. Stable crystals were obtained and studied by X-Ray diffraction. The asymmetric unit contains one Zn-porphyrin together with one 2,2,2-trifluoroethan-1-ol and one CHCl_3 molecules. The structural study revealed the formation of a one-dimensional network similar to the previous one discussed above. The metal ion is pentacoordinated and adopts a square based pyramidal geometry, with an axial pyridyl unit belonging to the neighboring metallatecton. The porphyrin backbone is planar and the Zn(II) is slightly displaced from the PMP by 0.32 Å toward the axial pyridyl moiety. Among the two pyridyl units of the tecton, only one is involved in the formation of the coordination network, while the non-coordinated moiety, as showed in the previous case, is involved in hydrogen bonds (2.75 Å) with the 2,2,2-trifluoroethan-1-ol present in the network (figure III. 13).

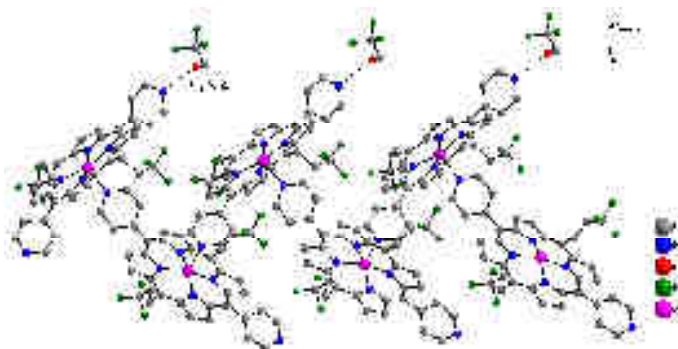


Figure III. 13. A portion of the 1-D coordination network (hydrogen atoms and chloroform molecules are omitted for clarity) formed by self-complementary 4-Zn (the dotted line represents the H-bond between non coordinated pyridine and 2,2,2-trifluoroethan-1-ol).

Within the 1D chain, the average angle between the axial pyridyl unit and the PMP is 77° and the average tilt angle between consecutive porphyrins is 84° . Within the tecton, the dihedral angles between the PMP and the meso pyridines are 58° and 89° , values really close to the one in the first

example. Like in the first case the crystal packing reveal the formation of F---F contacts between the chains with a distance of 2.77 Å, and the θ_1 and θ_2 values (102°) suggest type I halogen-halogen contacts (figure III. 14). Moreover, weak intermolecular H---F contacts are formed between the fluorine atoms of the porphyrin and solvent molecules ($d_{C...F} = 3.45$ Å) as well as the β -pyrrolic protons ($d_{C...F} = 3.16$ Å).

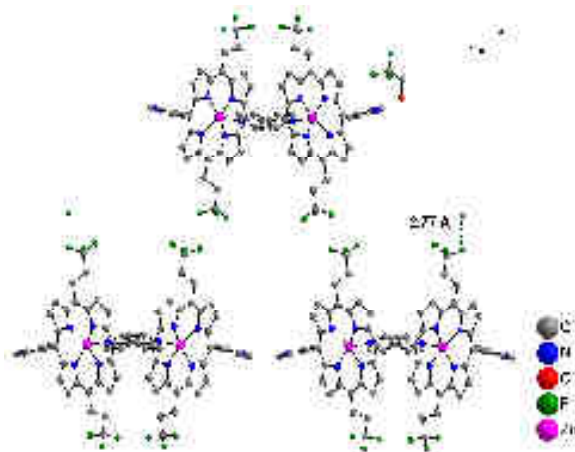


Figure III. 14. Crystal packing of the network, highlighting the F---F contacts in green. Hydrogen atoms and chloroform molecules are omitted for clarity.

Using slightly modified crystallization conditions (DMSO as an interlayer phase between MeOH and CHCl_3), it was possible to isolate two types of crystals in the crystallization tube: the major ones with parameter metrics and stability similar to the 1D network reported previously and a more stable crystalline form as a minor product. The analysis of the minor crystals by XRD revealed the formation of a 2D coordination network of the grid type. The formation of this architecture is possible due to mutual bridging between consecutive **4-Zn** self-complementary tectons through the coordination of two appended pyridyl units, belonging to adjacent units, to the axial positions of Zn^{2+} cations. Each **4-Zn** moiety is surrounded by four neighbouring tectons. The tilt angles between the meso pyridyl groups and the porphyrin mean plane are equal to 77° . The Zn^{2+} ion is 6-coordinated and its coordination sphere is composed in the equatorial plane of four $\text{N}_{\text{pyrrolic}}$ atoms ($d_{\text{Zn-N}}$ of *ca* 2.06 Å) and two $\text{N}_{\text{pyridine}}$ atoms in the axial positions ($d_{\text{Zn-N}}$ of *ca* 2.47 Å). The axial pyridyl units make a 47° angle with the PMP (figure III. 15). Within the 2D grid the dihedral angle between the mean planes of the two adjacent porphyrins is close to 79° and a Zn-Zn distance between two consecutive porphyrin molecules of *ca* 9.87 Å is observed.

In this case the alkyl chains are situated under and over the porphyrin mean plane, unlike the 1D networks, where in both cases the chains were located on the same side of the porphyrin plane.

Unlike the previous 1D networks obtained using **4-Zn**, there are no F---F contacts present in the crystal.

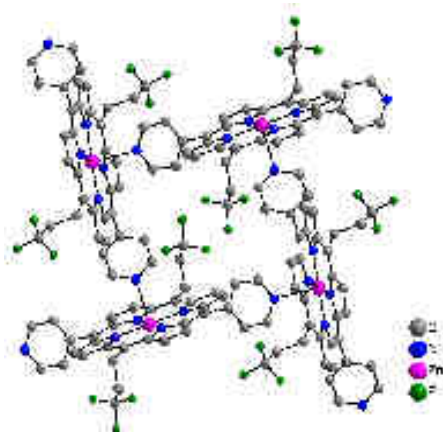


Figure III. 15. A view on the 2-D network with fluorinated chains pointing into the cavity. Hydrogen atoms are omitted for clarity.

Within the network, no solvent molecules were found and attempts to fill the cavities with solvent molecules such as fluorinated alcohol failed and lead to the formation of amorphous powders.

Based on crystallization conditions, it was possible to switch the dimensionality and to influence intermolecular interactions. By varying the crystallization conditions, it was also possible to switch between a crystal with methanol as solvent and 2,2,2-trifluoroethan-1-ol. Although it isn't a single-crystal-to-single crystal transformation, it is important to discover how to influence the networks formation by varying the growth conditions. It is also important to emphasize that in the monodimensional networks, along the coordination bond and solvent molecules, we could observe intermolecular interactions such as F---F contacts and F---H bonds. On the other hand, the two-dimensional network presents no intermolecular interactions and no solvent molecules are included within cavities. These results are also encouraging; they show that even with a relatively simple tecton: two recognition sites and six fluorine atoms on the backbone we can build monodimensional or two dimensional networks, although this issue remains challenging, with F---F contacts. The next step is to be able to fill the cavities with molecules of interest through specific interactions involving fluorine atoms on the backbone.

III. 3. B. Zn-Tecton 8-11

We do observe the formation of single crystals for seven Zn-Porphyrin self-complementary tectons bearing alkyl chains through ether junctions. The corresponding structures are not presented in numerical order but with respect to the increasing number of fluorine atoms on the chains.

Zn-Tecton 8

By slow diffusion of ZnSiF_6 in MeOH into a solution of the **8** in CHCl_3 through an interface composed of a solution of DMSO containing few drops of 2, 2, 3, 4, 4, 4-hexafluorobutan-1-ol, single crystals suitable for measurement were obtained. The X-ray diffraction analysis revealed the formation of a 1D network, formed upon self-assembly of the Zn-metallated porphyrin (figure III.

16). The asymmetric unit ($P2_1/n$ space group) contains one Zn-porphyrin moiety and solvent molecules (DMSO and 2,2,3,4,4,4-hexafluorobutan-1-ol). The Zn^{2+} cation is pentacoordinated and adopts a square based pyramidal geometry with a pyridyl unit belonging to the neighboring metallatecton occupying the axial position of the Zn(II) ion. The porphyrin backbone is planar and the Zn(II) is slightly displaced from the PMP by 0.27 Å toward the axial pyridyl moiety. The average Zn-N distance within the porphyrin core is 2.06 Å, whereas the axial Zn-N bond distance is slightly longer (2.19 Å). Among the two pyridyl units of the tecton, only one is involved in the formation of the coordination network. Within the tecton, the dihedral angles between the porphyrin mean plane and the meso pyridyl substituents are 57° and 68°. Within the 1D chain, the average angle between the axial pyridyl unit and the porphyrin mean plane is 79° and the average tilt angle between consecutive porphyrins (PMP) is 78°.

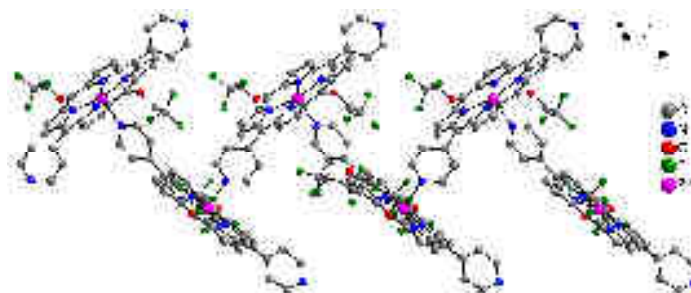


Figure III. 16. A portion of the 1-D coordination network (hydrogen atoms and solvent molecules are omitted for clarity) formed by self-complementary **8-Zn**.

One DMSO and one hexafluorobutanol molecules per **8-Zn** are present in the crystal. It is worth noting that the space group is not chiral and the hexafluorobutanol present in the structure is present as a racemate. The crystal packing reveals the formation of F...F contacts between the alkyl chains of adjacent porphyrin based tectons with a distance of 2.93 Å, and the θ_1 and θ_2 values (124° and 114°) suggest type I halogen-halogen contacts. There are also several hydrogen bonds between solvent molecules and the porphyrin moiety. β -pyrrolic protons are hydrogen bonded with fluorine atoms of hexafluorobutanol ($d_{C...F} = 3.20$ Å), the non-coordinated pyridine molecule forms hydrogen bonds with the DMSO ($d_{C...O} = 3.34$ Å) and finally the fluorine atoms of the alkyl chains form F...H bonds with DMSO molecule ($d_{C...F} = 3.4$ Å). Crystal packing is mostly influenced by π - π stacking within consecutive 1-D zig-zag chains, with plane distances around 3.48 Å (figure III. 17).

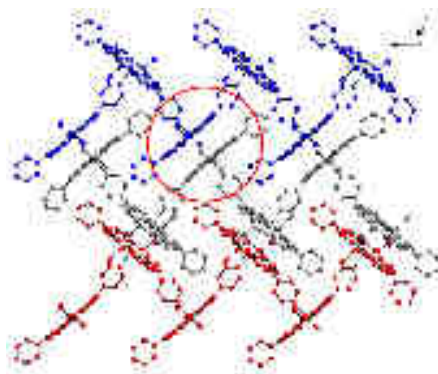


Figure III. 17. Crystal packing of the network, highlighting the π - π stacking in red circle. Hydrogen atoms, solvent molecules and alkyl chains are omitted for clarity.

Zn-Tecton 14

Tecton **14** contains 6 fluorine atoms/ porphyrin and is present as a racemate (RR and SS) and of the *meso* compound (R, S). Crystallization tests were made using this mixture and single crystals obtained were measured by X-ray diffraction. The crystal structure described below is a preliminary structure since the refinement was not totally finalized at the time of writing this chapter. We observe the formation of a 1-D network containing the *meso* form of **14-Zn**. The Zn(II) is pentacoordinated and located slightly above the porphyrin plane (0.33 Å) toward the axial pyridine. No solvent molecule is present in the crystal (figure III. 18).

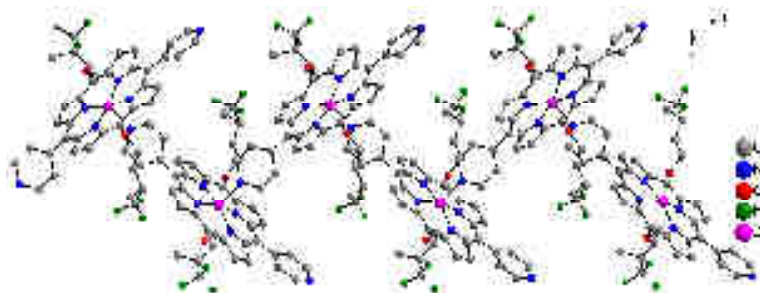


Figure III. 18. A portion of the 1-D coordination network (hydrogen atoms are omitted for clarity) formed with the self-complementary **14-Zn**.

Within the 1D chain, the average angle between the axial pyridyl unit and the PMP is 70° , one of the closest angles seen as yet in this chapter, approaching the value that could lead to hexagonal 3-D networks. The average tilt angle between consecutive porphyrins (PMP) is 74° . Within the tecton, the dihedral angles between the porphyrin mean plane and the meso pyridyl substituents are 51° and 61° . Unlike the other ether bonded porphyrins described so far (free base or coordination networks) alkyl chains are situated on the same side of the porphyrin mean plane. Neither F---F contacts nor hydrogen bonds are present. The crystal packing reveals formation of 1-D stacked layers through π - π interactions with distance of 3.4 Å, similar to the one presented for tecton **8** (figure III. 17).

Zn-Tecton 15

The difference between the tectons **14** and **15** is the presence of an ethyl group instead of a methyl group at the stereogenic carbons. The X-ray structure of crystal by self-assembling of **15-Zn** (*meso* form) indeed showed several similarities with the previous structure. The structure is an unfinished version with no solvent molecules depicted in the architecture. The 1-D network is formed by coordination of one pyridyl moiety to the axial position of a Zn(II), located 0.35 Å above the porphyrin mean plane. Like in the previous case, the average angle between the axial pyridine moiety and the porphyrin mean plane is quite small and close to 69°. The average tilt angle between consecutive porphyrins is 77°. Within the tecton, the dihedral angles between the porphyrin mean plane and the *meso* pyridyl substituents are equal to 54° and 59°. Unlike the structure obtained for **15**, the fluorinated chains are positioned on the same side of the porphyrin plane (figure III. 19).

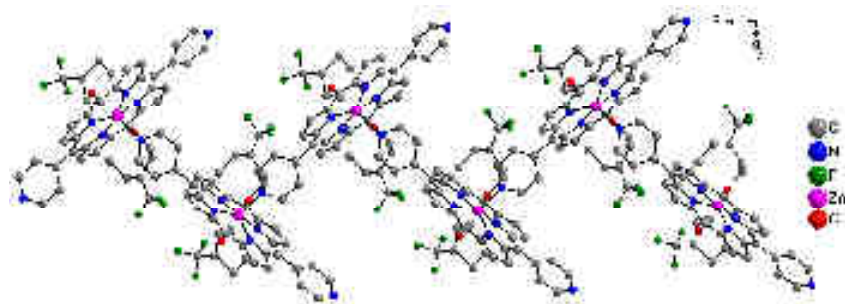


Figure III. 19. A portion of the 1-D coordination network (hydrogen atoms are omitted for clarity) formed by self-complementary **15-Zn**.

The crystal packing reveals formation of 1-D stacked layers with a distance of 3.49 Å between the stacked porphyrin rings, similar to the one presented for tecton **8** (figure III. 17). Comparable with its free base structure, the packing reveals the formation of intermolecular H-bonds between fluorine atoms on the alkyl chains and the β -pyrrolic protons ($d_{C\cdots F} = 3.30$ Å) as well as between the fluorine atoms and the protons belonging to the non coordinated pyridine ($d_{C\cdots F} = 3.43$ Å), but no F---F contacts between the porphyrin are observed.

Using slightly modified crystallization conditions (DMSO with some drops of hexafluorobutanol at the $\text{CHCl}_3/\text{MeOH}$ interface), it was possible to isolate, in its crystalline form as a minor product, a 2D grid network, composed of self-complementary, **15-Zn(R,S)**.

The Zn^{2+} ion is 6-coordinated, its coordination sphere is composed of the four N atoms constituents of the tetraaza core of the porphyrin ($d_{\text{Zn-N}}$ of *ca* 2.06 Å) and two N atoms belonging to the two apical pyridyl units of two consecutive **15-Zn** tectons (2.35 Å). The axial pyridyl units are almost perpendicular to the porphyrin mean plane with dihedral angles of *ca* 82°. The tilt angles between the *meso* pyridyl groups and the porphyrin mean plane are identical and equal to 80°. The alkyl chains are situated under and over the porphyrin mean plane. Within the 2D grid, the dihedral angle between the mean planes of the two adjacent porphyrins is close to 89°. A Zn-Zn distance between two consecutive porphyrin moieties of *ca* 10.11 Å is observed (figure III. 20). Like the previous 1D

networks obtained with **15-Zn**, in this case there are no F---F or F---H contacts present in the crystal.

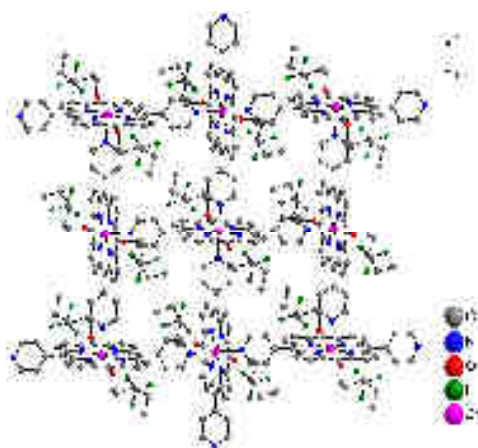


Figure III. 20. A view on the 2-D network with fluorinated chains pointing into the cavity. Hydrogen atoms are omitted for clarity.

Zn-Tecton 9

Crystals were obtained by slow diffusion of $\text{Zn}(\text{OAc})_2 \cdot 2\text{H}_2\text{O}$ into a solution of tecton **9**. **9-Zn** crystallizes with no solvent molecules in the asymmetric unit. The self-complementary metallatecton self-assembles into a 1D network (figure III. 21). The porphyrin backbone is planar and the Zn(II) is slightly displaced from the PMP by 0.21 Å toward the axial pyridyl moiety. The average Zn-N distance within the porphyrin core is 2.07 Å, whereas the axial Zn-N bond distance is slightly longer (2.18 Å). Within the 1D chain, the average angle between the axial pyridyl unit and the porphyrin mean plane is 77° and the average tilt angle between consecutive porphyrins (PMP) is 73°. Within the tecton, the dihedral angles between the porphyrin mean plane and the pyridine substituents are 54° and 67°. The alkyl chains are situated under and over the porphyrin mean plane. A distance of *ca.* 15.5 Å between the N atoms of the pyridyl groups belonging to the same tecton is observed.

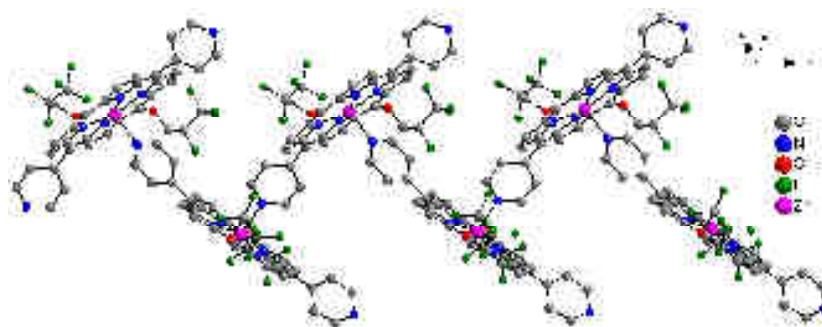


Figure III. 21. A portion of the 1-D coordination network (hydrogen atoms are omitted for clarity) formed by self-complementary **9-Zn**.

The non-coordinating pyridine moiety is involved in hydrogen bonds ($d_{C\cdots N} = 3.18 \text{ \AA}$) with the β -pyrrolic protons of adjacent porphyrins. Interestingly, we also observe H-bonds involving fluorine atoms on the alkyl chains (4 contacts per porphyrin) and β -pyrrolic protons ($d_{C\cdots F} = 3.22 \text{ \AA}$), coordinating pyridine moiety ($d_{C\cdots F} = 3.40 \text{ \AA}$), non-coordinating pyridine moiety ($d_{C\cdots F} = 3.23 \text{ \AA}$) and even protons on the alkyl chain ($d_{C\cdots F} = 3.29 \text{ \AA}$). The packing revealed π - π interactions between porphyrin mean planes of adjacent 1-D chains (3.45 \AA) (figure III. 22).

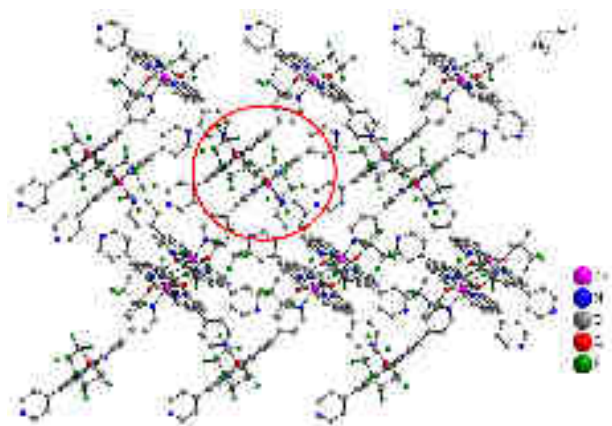


Figure III. 22. Crystal packing of the network, highlighting the π - π stacking in red circle. Hydrogen atoms are omitted for clarity.

Zn-Tecton 16

Tecton **16** contains a total of 12 fluorines together with two stereogenic centers. Like tecton **14** and **15**, the crystallization in the presence of Zn(II) was performed starting with the mixture of the racemate (R,R and S,S) and the *meso* forms. The 1-D network shows similarities with the previously described zig-zag chains. The asymmetric unit contains one *meso* **16**-Zn moiety and one methanol solvent molecule. The Zn^{2+} is pentacoordinated and slightly displaced from the PMP by 0.33 \AA toward the axial pyridyl moiety. The average equatorial Zn-N distance is 2.06 \AA , and the axial Zn-N distance is equal to 2.15 \AA . Among the two pyridyl units of the tecton, only one is involved in the formation of the coordination network, the second one is “blocked” in hydrogen bonds ($d_{N\cdots O} 2.82 \text{ \AA}$) with the hydrogen belonging to methanol molecules, present in the structure (figure III. 23).

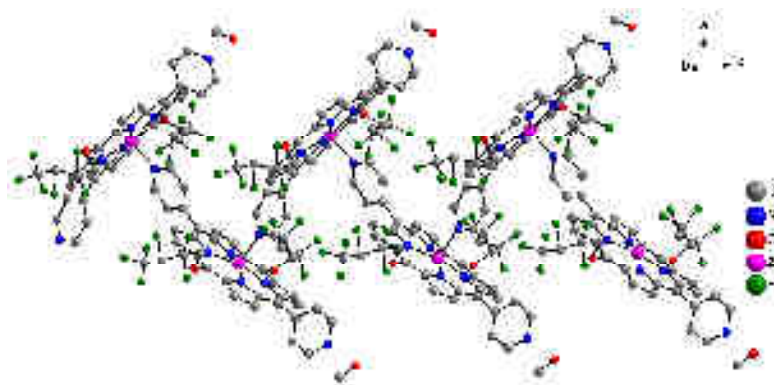


Figure III. 23. A portion of the 1-D coordination network (hydrogen atoms are omitted for clarity) formed by self-complementary **16**-Zn.

Within the 1D chain, the average angle between the axial pyridyl unit and the porphyrin mean plane is 85° and consecutive porphyrins are almost perpendicular (tilt angle of 84°). Within the tecton, the angle between the PMP and the *meso*-pyridine is equal to 80° . The alkyl chains are situated on the same part of the porphyrin plane. There are three F---F contacts per porphyrin with a distance of 2.91 \AA and 2.92 \AA , and like before the θ_1 and θ_2 values (122° and 108°) suggest type I halogen-halogen contacts. As observed in several cases discussed above, the fluorinated chains tend to assemble into a “fluorous” layer (figure III. 24).

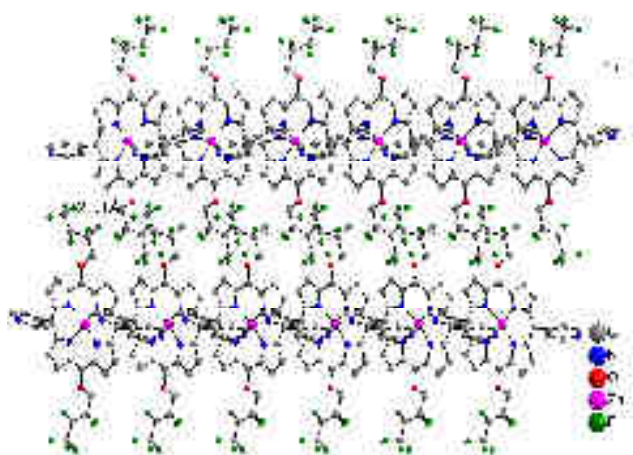


Figure III. 24. A portion of the crystal packing highlighting the F---F contacts (red dotted line).

The crystal structure also contains intermolecular F---H bonds, between the fluorine atoms and the protons of the coordinating pyridine moiety ($d_{\text{C}\cdots\text{F}} = 3.42 \text{ \AA}$) as well as the protons on the alkyl chains ($d_{\text{C}\cdots\text{F}} = 3.31 \text{ \AA}$). The crystal packing reveals also the formation of stacked 1-D chains, with a distance of 3.33 \AA between the porphyrin mean planes (figure III. 25).

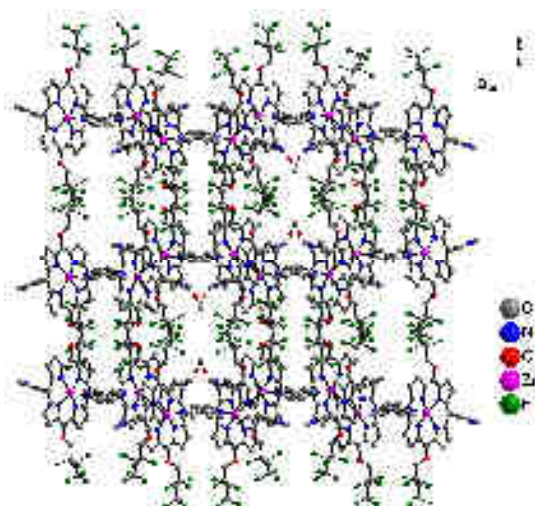


Figure III. 25. Crystal packing of the network, hydrogen atoms are omitted for clarity.

Attempts to empty the cavities lead to decomposition of the crystalline structure. Crystallizations with fluorinated solvents are still in progress.

Zn-Tecton 10

Tecton **10** has one more fluorine atom per substituent than **16**, thus leading to a total of 14 fluorine atoms in the periphery of the porphyrin. By using the usual crystallization conditions (liquid diffusion of a methanolic solution of ZnSiF_6 into a solution of **10** in chloroform with an interlayer of DMSO), a 1-D network was obtained. The asymmetric unit contained the Zn-porphyrin and disordered solvent molecules: two chloroform molecules and one MeOH, with no interaction with the porphyrin framework. The structure was treated with the SQUEEZE command for solving the structure. Like in the previous 1D assemblies, Zn(II) is 5-coordinated with 4 Zn-N_{pyrrolic} bonds (2.06 Å), and one axial Zn-N_{pyridine} bond (2.18 Å), while the second pyridine moiety belonging to the *meso* position of the porphyrin is not involved in coordination. Within the tecton, the dihedral angles between the porphyrin mean plane and the *meso* pyridyl substituents are 55° and 67°. The alkyl chains are situated under and over the porphyrin mean plane (figure III. 26). Within the 1D chain, the average angle between the axial pyridyl unit and the PMP is 78° and the tilt angle between consecutive porphyrins is 75°.

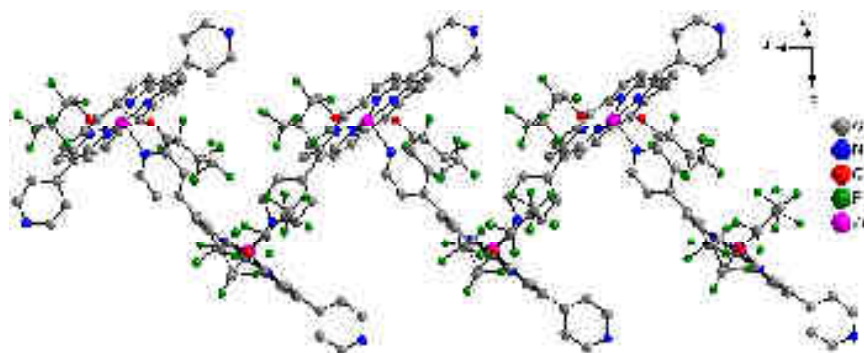


Figure III. 26. A portion of the 1-D coordination network (hydrogen atoms are omitted for clarity) formed by self-complementary **10**-Zn.

Each porphyrin has three F---F contacts (figure III. 30a), with two F---F distances of 2.92 Å and one shorter with 2.74 Å distance (figure III. 27). The angles θ_1 and θ_2 values suggest type I halogen-halogen contacts ($\theta_1 = \theta_2 = 141^\circ$). There is no intermolecular H---F contacts observed in the crystal structure. The crystal packing reveals also the formation of π - π stacking between the consecutive mono-dimensional chains, with a distance between the porphyrin mean planes of 3.43 Å.

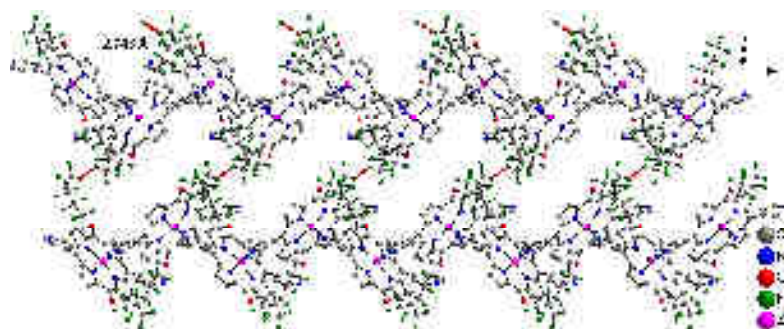


Figure III. 27. Crystal packing of the network, highlighting only the shortest F---F contacts in red. Hydrogen atoms are omitted for clarity.

Zn-Tecton 11

Tecton **11** is the most heavily fluorinated tecton synthesized, with a total of 16 F atoms per porphyrin macrocycle. Single crystals were grown in the presence of CHCl_3 , MeOH and DMSO. Formation of a 1D zig-zag chains **11**-Zn is observed. The asymmetric unit contains one Zn-porphyrin moiety and one DMSO molecule. The four equatorial Zn-N bonds are equal to *ca* 2.06 Å while the axial bond length is 2.17 Å. Among the two pyridyl units of the tecton, only one is involved in the formation of the coordination network. Within the 1D chain, the average angle between the axial pyridyl unit and the porphyrin mean plane is 80° and the average tilt angle between consecutive porphyrins (24 atoms of the mean plane) is 87°. Within the tecton, the dihedral angles between the porphyrin mean plane and the meso pyridyl substituents are 64° and 87°. The alkyl chains are situated under and over the porphyrin mean plane (figure III. 28).

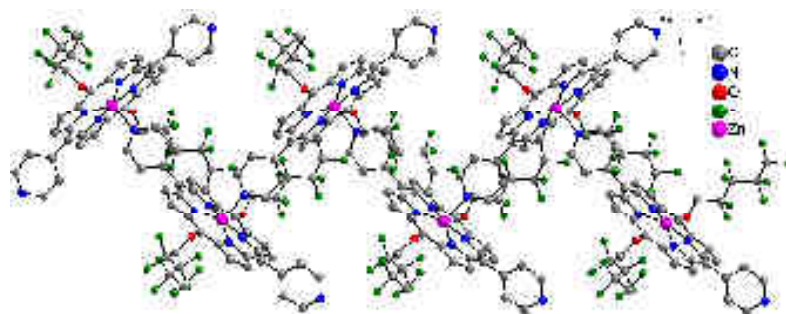


Figure III. 28. A portion of the 1-D coordination network (hydrogen atoms and solvent molecules are omitted for clarity) formed by self-complementary **11**-Zn.

As in the previous case, the packing reveals the formation of π - π stacked mono-dimensional layers, with a distance between porphyrin mean planes of *ca* 3.52 Å.

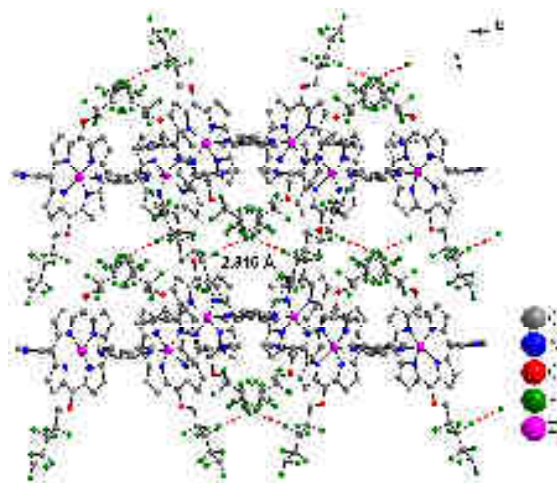


Figure III. 29. Crystal packing of the network, highlighting only one F---F contact in red. Hydrogen atoms are omitted for clarity.

For the free base structure, we observed up to 12 F---F contacts per porphyrin, with no π - π stacking, for the coordination network, 8 F---F contacts (figure III. 30b) and π - π interactions are observed. More curious is the existence of θ_1 and θ_2 equal to 161° and 87° for the F---F distance of 2.81 Å and θ_1 and θ_2 equal to 152° and 87° for the distance of 2.83 Å that are close to type II interactions. These values indicate that by increasing the number of fluorine atoms present on the porphyrin backbone, the number and strength of intermolecular F---F contacts are enhanced.

Interestingly, through these interactions, the 1-D chains are interconnected forming thus a supramolecular 2-D network (figure III. 29). Intermolecular H---F contacts are formed between the solvent molecules ($d_{C\cdots F} = 3.14 \text{ \AA}$) and the protons of the adjacent chains ($d_{C\cdots F} = 3.17 \text{ \AA}$).

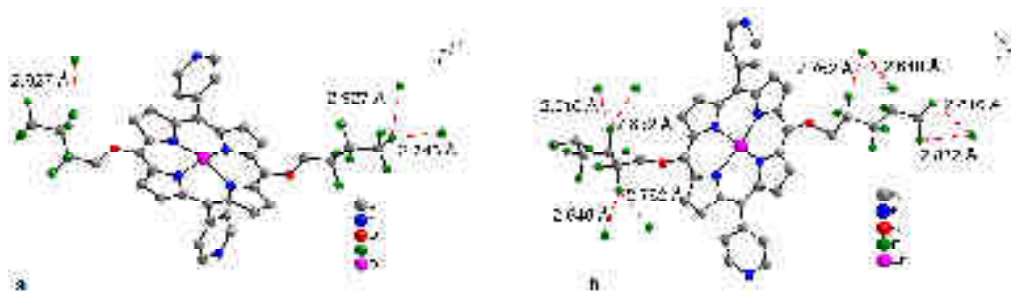


Figure III. 30. View on the tecton **10** (a) and tecton **11** (b) in their zinc networks with a highlight on the F---F contacts in red. Hydrogen atoms are omitted for clarity.

Table 1 summarizes relevant structural features obtained by X-ray analysis for this series of Zn based self-complementary tectons.

Tecton nr.	Nr of F atoms/Po	Presence of the solvent	Topology	F---F contacts	H---F interactions (d C---F)	$\pi - \pi$ interactions
4	6	MeOH	1D	1/Po 2.58 Å	no	no
4	6	CHCl ₃ 2,2,2-trifluoroethan-1-ol	1D	1/Po 2.77 Å	3/Po 3.15 Å 3.45 Å	3.41 Å
4	6	no	2D	no	no	no
8	6	2, 2, 3, 4, 4, 4-hexafluorobutanol DMSO	1D	4/Po 2.93 Å	2/Po 3.2 Å 3.4 Å	3.48 Å
14	6	no	1D	no	no	3.40 Å
15	6	no	1D	no	4/Po 3.30 Å 3.43 Å	3.49 Å
15	6	no	2D	no	no	no
9	10	no	1D	no	8/Po 3.22 Å 3.23 Å 3.29 Å 3.45 Å	3.45 Å
16	12	MeOH	1D	3/Po 2.91 Å	4/Po 3.31 Å 3.42 Å	3.33 Å
10	14	CHCl ₃ MeOH	1D	3/Po 2.74 Å 2.93 Å	no	3.43 Å
11	16	DMSO	1D	8/Po 2.64 Å 2.76 Å 2.81 Å 2.83 Å	3/Po 3.14 Å 3.17 Å	3.52 Å

Table III. 1.

Focusing on the F---F contacts present in the solid state, although weak in nature, one may notice that they are already present in **4-Zn** and in **8-Zn** for which the two tectons contain only 6 fluorine atoms. On the other hand, increasing the number of F atoms on the porphyrin periphery does not necessarily lead to an increase in the number of F---F contacts. Indeed, in crystal structures of **9-Zn**, **14-Zn** and **15-Zn** no F---F contacts are present. These observations suggest that while the number of fluorine atoms is a relevant parameter to consider when seeking specific interactions involving fluorine atom, other factors influence also the overall packing of the networks in the crystalline phase. For example, the packing of most of the 1-D chains also display π - π interactions. For the last 3 representatives networks, with increasing number of fluorine atoms (tectons **16**, **10** and **11** bear 12, 14 and 16 fluorine atoms respectively), a more clear-cut trend is observed. While for the **16-Zn**, only three F---F (type I) contacts with quite long F---F distance are spotted, for **10-Zn** three shorter contacts per porphyrin (type I) are observed, finally, for and **11-Zn**, up to 8 contacts per porphyrin with one of the shortest F---F distance are detected.

Concerning the halogen-halogen bond type, most of the 1-D networks revealed type I contacts. Only in the case of **11-Zn**, F---F distances of 2.81 Å and 2.83 Å and angles closer to 180° for θ_1 and 90° for θ_2 indicate a type II contact. A result in accordance with the one obtained for the free base porphyrin **11**, for which a similar tendency for one F---F contact is observed. It is important to notice that structural investigations of the fluorinated ligand itself give insight into possible interactions within the networks.

The results obtained for the self-assembled zinc networks shine light on how the number of fluorine atoms may influence the interactions present within the networks and this knowledge may be further used to test the trapping capacity of crystals based on molecular networks towards fluorinated solvents. For several examples, the use of chiral and fluorinated solvents was already tested. We have not yet observed the formation of chiral networks using chiral solvents, while for fluorinated solvent containing networks, solvent trapping takes place through hydrogen bonding.

The two 2-D networks **4-Zn** and **15-Zn** formed through self-assembly, formation of cavities decorated with fluorinated alkyl chains is observed. However, cavities were found to be empty in both cases. Unfortunately, attempts to fill the cavities with solvent molecules failed.

III. 4. Double component systems composed of Porphyrin and Cd (II)

Many attempts have been made to grow single crystals by combining fluorinated or/and chiral porphyrin based tectons bearing two pyridyl units in the *meso* positions with external metal cations such Cu^{2+} , Co^{2+} , Ni^{2+} , Cd^{2+} , Hg^{2+} , Ag^+ . In most cases, amorphous powders were obtained. Some crystallizations are still in progress.

So far, we have obtained single crystals suitable for XRD in only two cases involving Cd(II) as external metallic cations and tectons **4** and **10**.

Cd-Tecton 4

Slow diffusion of CdBr_2 in EtOH into a chloroform solution of tecton **4** in the presence of DMSO containing drops of 2,2,2-trifluoroethan-1-ol generated suitable crystals for X-ray diffraction. The asymmetric unit contained the porphyrin interconnected by CdBr_2 moieties and three disordered water molecules with no specific interactions with the porphyrin framework. Since the solvent could not be refined, the structure was treated with the SQUEEZE command and then solved.

The structural investigation revealed the formation of a 2D coordination network with a Cd/porphyrin ratio of 1/2. The external Cd^{2+} cation is six-coordinated with four pyridyl units belonging to four distinct porphyrin based tectons in the equatorial plane ($d_{\text{Cd-N}}$ of *ca* 2.43 Å) and two bromide anions located in the axial positions ($d_{\text{Cd-Br}} = 2.70$ Å) (figure III. 31). The average tilt angle between the PMP of the 4 porphyrins that connect to the same cadmium center is *ca* 22°. The porphyrin core remains non-metallated, adopting a saddle-shaped conformation. The dihedral angles between porphyrin and *meso*-pyridyl substituents are close to 75° and the alkyl chains are situated over and under the porphyrin backbone.

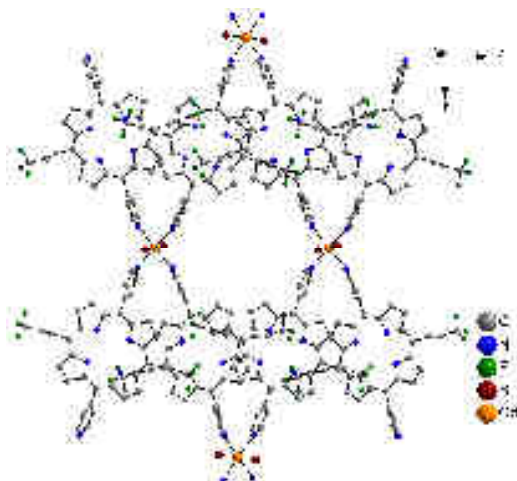


Figure III. 31. The 2D coordination network formed upon combining tecton **4** and CdBr_2 . Hydrogen atoms are omitted for clarity.

Fluorine atoms are involved in hydrogen bonds with the β -pyrrolic protons ($d_{\text{C}\cdots\text{F}} = 3.30$ Å) and the pyridine protons ($d_{\text{C}\cdots\text{F}} = 3.19$ Å), no F---F contacts are observed. The 2-D layers are π - π stacked with distances of 3.47 Å between porphyrin mean planes (figure III. 32).

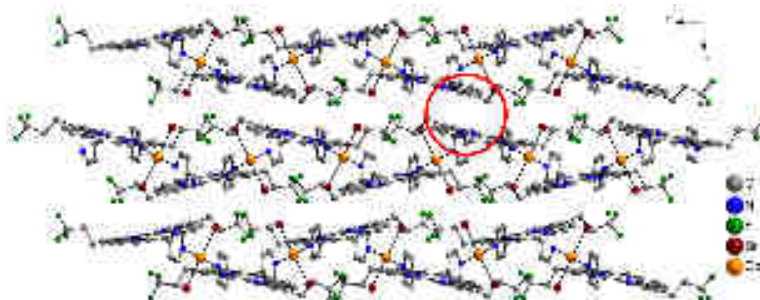


Figure III. 32. The packing of the 2D network highlighting the zone of π - π stacking with a red circle. Hydrogen atoms are omitted for clarity.

Cd-Tecton 10

Single crystals were obtained by combining the tecton **10** with CdBr₂ in the presence of CHCl₃, MeOH, DMSO and few drops of 2,2,2-trifluoroethan-1-ol. XRD analysis revealed the formation of a 3D coordination network (figure III. 33) composed of tectons **10** bridged by Cd(Br₂)_n polymeric chains and disordered water molecules with no interactions with the coordination network. No fluorinated solvent is present in the asymmetric unit. The ratio between the cadmium cation and porphyrin is 1/1. Cd(II) is 6-coordinated with two pyridyl units in *cis* positions ($d_{\text{Cd-N}} = 2.37 \text{ \AA}$) and 4 Br⁻ anions ($d_{\text{Cd-Br}}$ of *ca* 2.75 Å). The four bromides are acting as bridging ligands between adjacent Cd(II) cations thus leading to (CdBr₂)_n chains along the *c* axis with a distance between two consecutive metal centres of 3.77 Å (figure III. 34). The tilt angle between the PMP of the two porphyrins connected in the *cis*-position of the same Cd(II) is equal to 37°.

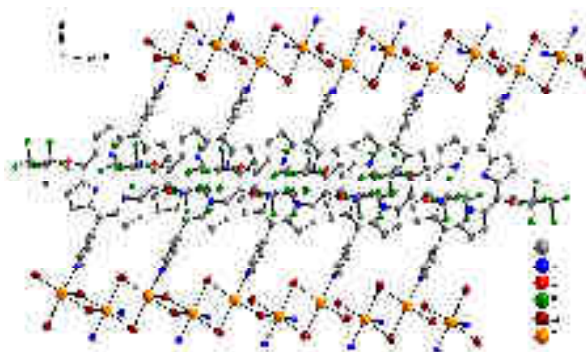


Figure III. 33. The view on the infinite (CdBr₂)_n chains. Hydrogen atoms and solvent molecules are omitted for clarity.

Within the tecton, the porphyrin center remains non metallated during the diffusion process, and the porphyrin is almost planar. The dihedral angles between the PMP and the *meso* pyridyl substituents are equal to 64°. The alkyl chains are situated over and under the porphyrin backbone. In figure III. 34, a view of the 2-D layers shows very short F---F contacts of 2.61 Å ($\theta_1 = \theta_2 = 125^\circ$). Interestingly here, the fluorinated chains decorating the channels do not interact with the solvent molecules.

By increasing the number of fluorine atoms, as discussed above, F---F contacts between the porphyrin based tectons are observed. Despite the presence of CF₃CH₂OH, the latter is not trapped within the crystal. Attempts to trap other solvent molecules are still ongoing.

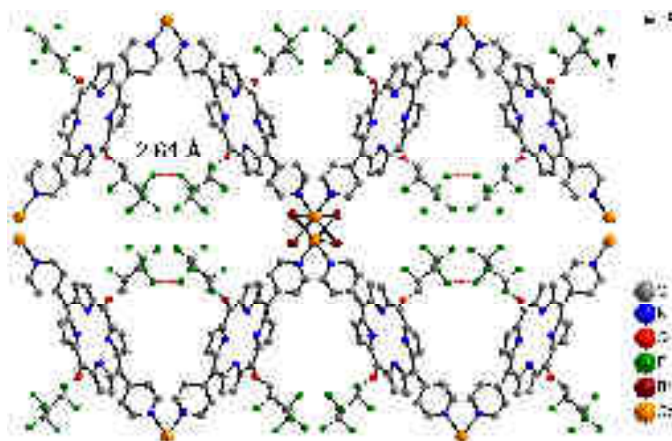


Figure III. 34. The view along the *c* axis which shows the 2D layers highlighting the F---F contacts (red dotted line). Hydrogen atoms and solvent molecules are omitted for clarity.

In summary, the double component systems based on porphyrins as tectons and CdBr_2 as the external metal and connecting node were explored for the formation of coordination networks. Although many attempts have been done by varying the crystallization conditions and the nature of the metal cation, only two coordination networks could be characterized by X-ray diffraction. The use of tecton **4** lead to the formation of a 2-D network, where the Cd^{2+} /Porphyrin ratio is $\frac{1}{2}$. For the tecton **10**, a 3-D network was generated, and the Cd^{2+} /Porphyrin ratio was 1/1. We can again observe that for six fluorine atoms on the backbone, no F...F contacts are observed while for 14 fluorine atoms per porphyrin, very short F...F contacts of 2.61 Å are detected. It is worth mentioning that in both arrangements, the fluorinated alkyl chains decorate the cavities, which is an important feature if we want to have specific interactions between guest molecules of interest and the networks. While both networks are stable, we were not successful in filling the channels with different solvent molecules, either during the crystallization process or after the formation of crystals.

III. 5 Conclusion

By using single component based systems composed of self-complementary tectons or the double component strategy based on two complementary tectons, a series of mono-, bi- and three-dimensional networks were generated. The self-complementary metallatectons, Zn metallated porphyrins, under self-assembly conditions lead to the formation of 1D networks for all the tectons used. However, occasionally the formation of 2-D networks was also observed. The coordination number and thus geometry of Zn(II) imposes the dimensionality of networks. Indeed, whereas pentacoordinated metal centre leads to the formation of monodimensional architectures, hexacoordinated Zn^{2+} cation affords bidimensional structures. In contrast with the solid state structure of free base porphyrin **4**, for crystals based on **4**-Zn, F...F contacts of the type I were observed. Depending on the crystallization conditions, tecton **4** leads to two different types of 1-D networks and one 2D network. The 1D networks differ from the other by the solvent molecules trapped within the network through H-bonding with the non-coordinated pyridyl unit. The propensity to trap fluorinated solvent molecules within the network through hydrogen bonding clearly demonstrates the possibility of using such systems for separation processes. Even though, we did not observe any F...F contacts between the fluorinated chains and the fluorinated solvent, this result is a promising start. For porphyrins containing fluorinated and chiral alkyl chains, the 1-D networks formed display the same zig-zag type geometry resulting from the pentacoordination of the metal cation and participation of one of the two pyridyl coordinating units. The second pyridyl moiety is usually hydrogen bonded to solvent molecules present in the networks. It is interesting to notice that, unlike in the case of free base porphyrin structures, for which F...F contacts were observed only with highly fluorinated tectons (14 fluorine atoms on the porphyrin), in the presence of Zn(II) or Cd(II) cations leading to the formation of coordination networks, a closer packing of

porphyrin tectons takes place leading thus to an increase in the number of intermolecular interactions, especially F---F contacts.

This study shows that the strategy based on the use of fluorinated alkyl chains or fluorinated and chiral alkyl chains is viable and leads to the formation of coordination networks displaying specific interactions between the porphyrin substituents and potential fluorinated guest molecules. Although so far no F---F contacts have been observed with solvent molecules, we are still trying to tune the crystallization conditions to hopefully observe successful trapping of fluorinated species. In order to increase the affinity of networks for fluorinated guests, we have also tried to increase the number of fluorine atoms to 36 per porphyrin. So far, due to solubility problems, we were not able to isolate and characterize the porphyrin based tectons.

References

1. V. Bulach and M. W. Hosseini, *Handbook of Porphyrin Science*, Eds. K. Kadish, K. Smith and R. Guilard, *World Scientific*, 2011, **13**, 299-391.
2. W.-Y. Gao, M. Chrzanowski and S. Ma, *Chem.Soc.Rev.*, 2014, **43**, 5841-5866.
3. Z. Guo and B. Chen, *Dalton Trans.*, 2015.
4. B. F. Abrahams, B. F. Hoskins and R. Robson, *J. Am. Chem. Soc.*, 1991, **113**, 3606-3607.
5. B. F. Abrahams, B. F. Hoskins, D. M. Michail and R. Robson, *Nature*, 1994, **369**, 727-729.
6. M. E. Kosal, J.-H. Chou, S. R. Wilson and K. S. Suslick, *Nat. Mater.*, 2002, **1**, 118-121.
7. K. S. Suslick, P. Bhyrappa, J. H. Chou, M. E. Kosal, S. Nakagaki, D. W. Smithenry and S. R. Wilson, *Acc. Chem. Res.*, 2005, **38**, 283-291.
8. A. M. Shultz, O. K. Farha, J. T. Hupp and S. T. Nguyen, *J. Am. Chem. Soc.*, 2009, **131**, 4204-4205.
9. O. K. Farha, A. M. Shultz, A. A. Sarjeant, S. T. Nguyen and J. T. Hupp, *J. Am. Chem. Soc.*, 2011, **133**, 5652-5655.
10. H.-J. Son, S. Jin, S. Patwardhan, S. J. Wezenberg, N. C. Jeong, M. So, C. E. Wilmer, A. A. Sarjeant, G. C. Schatz, R. Q. Snurr, O. K. Farha, G. P. Wiederrecht and J. T. Hupp, *J. Am. Chem. Soc.*, 2013, **135**, 862-869.
11. H.-C. Kim, Y. S. Lee, S. Huh, S. J. Lee and Y. Kim, *Dalton Trans.*, 2014, **43**, 5680-5686.
12. F. Sguerra, V. Bulach and M. W. Hosseini, *Dalton Trans.*, 2012, **41**, 14683-14689.
13. N. Marets, V. Bulach and M. W. Hosseini, *New J. Chem.*, 2013, **37**, 3549-3558.
14. E. Kuhn, V. Bulach and M. W. Hosseini, *Chem. Commun.*, 2008, 5104-5106.
15. E. Deiters, *Tectonique moléculaire: Réseaux moléculaires à base de porphyrines*, Thèse Université de Strasbourg, 2006.
16. E. Kuhn, *Molecular Tectonics: 2- and 3-D molecular organisations based on porphyrins*, Thèse Université de Strasbourg, 2009.
17. F. Sguerra, *Variations autour de la porphyrine*, Thèse Université de Strasbourg, 2012.
18. E. Deiters, V. Bulach and M. W. Hosseini, *Chem. Commun.*, 2005, 3906-3908.

Chapter 4

Contents

Chapter IV.....	83
IV. 1. Halogen bonded networks involving pyridine derivatives.....	84
IV. 1. A. Literature overview.....	84
IV. 1. B. Halogen bonded networks.....	86
IV. 1. C. Conclusion.....	90
IV. 2. Halogen bonded networks involving porphyrin.....	91
IV. 2. A. Literature overview.....	91
IV. 2. B. New Halogen bonded networks	93
IV. 2. C. Conclusion.....	99
References.....	100

Chapter 4

This chapter focuses on halogen-bonded networks using organic building blocks such as porphyrins or bipyridine molecules and iodofluoroarenes. The first part deals with the use of bipyridyl based tectons synthesized in the group of Prof. Stefan Bräse (Karlsruhe Institute of Technology, Germany) by Dr. Sylvain Grossjean.

The second part describes the use of porphyrin derivatives as tectons, a short overview on the few examples present in the literature and our results in the field.

IV. 1. Halogen bonded networks involving pyridine derivatives

This section of the chapter deals with the use of three bipyridyl based tectons differing by their length, synthesized in the group of Pr Stefan Bräse (Karlsruhe Institute of Technology, Germany) by Dr. Sylvain Grossjean. In figure IV.1, an overview of the tectons used to generate supramolecular networks is presented. Several reports in literature are dealing with the use of haloarenes and 4,4'-bipyridine molecules, only few examples will be presented here.

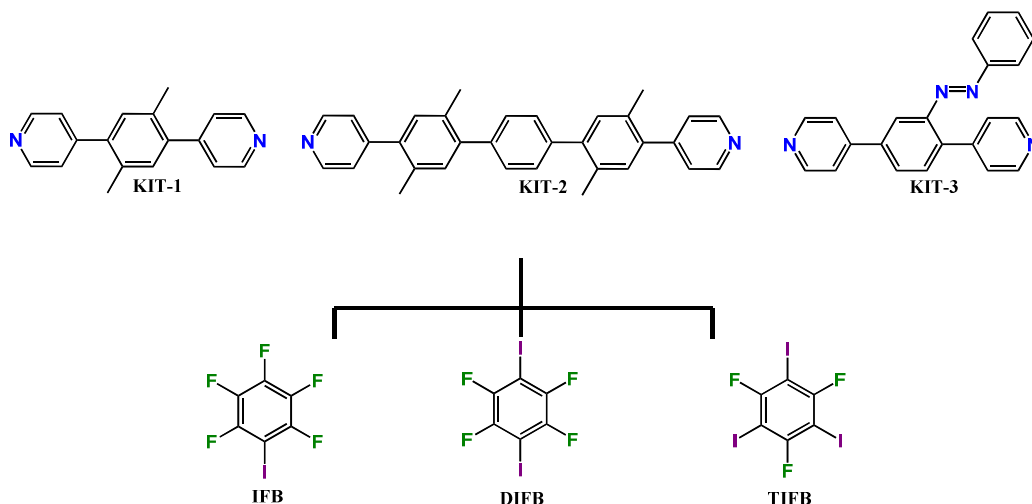


Figure IV.1. Tectons used for generating supramolecular networks.

IV. 1. A. Literature overview

DIFB and TIFB have been largely employed to generate molecular networks with different topologies and dimensionalities.¹ About 60% of structures filed in the CCDC data base involving these compounds deals with networks based on nitrogen compounds. It started of course with 4,4'-bipyridine but more complex examples have been reported enlarging the group with tripyridyl² or tetrapyridyl^{3, 4} compounds. When, both donor and acceptor molecules are bidentate in nature, we can expect, as seen for porphyrin based tectons, infinite 1-D chains. In principle, the dimensionality of the network, *i.e.* extension from 1- to 2-D architectures, should be possible by using the triiodobenzene such as TIFB. However, as an example published in 2007, a report⁵ concerning variable lengths of bipyridyl ligands and the use of TIFB revealed that irrespective of the molar ratio and the tecton used, a 1:1 adduct was formed through only two N---I bonds instead of three, the third Iodine atoms being involved in I---F interactions (figure IV.2). The authors argued that the

gain in enthalpy from close packing is larger than the benefit from a third halogen bond, which could generate 2D open layers.

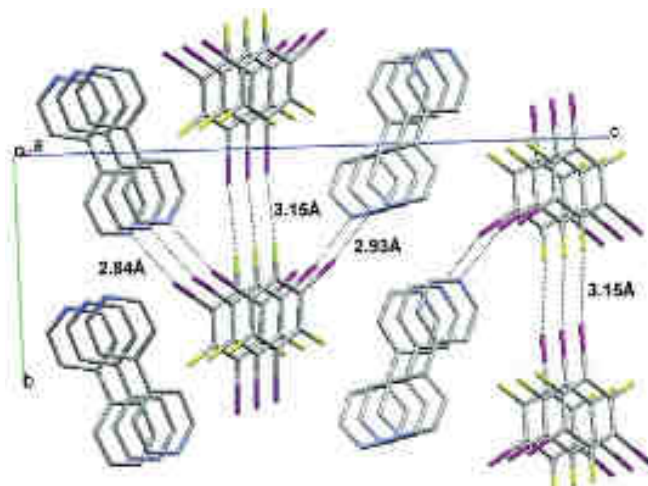


Figure IV.2. View of the co-crystal between 4,4'-bipyridine and TIFB pointing out the N---I and I---F contacts (hydrogen atoms are omitted, iodine in purple, fluorine in green, nitrogen in blue, carbon in grey).

One year later, the group of M. Fourmigué⁶ showed that by using Bu_4NX or Ph_4PX , where $\text{X} = \text{Cl}$ or Br , it was possible to engage all three iodine in halogen bonding interactions with the chlorine or bromine ions, affording a two dimensional motif (figure IV.3).

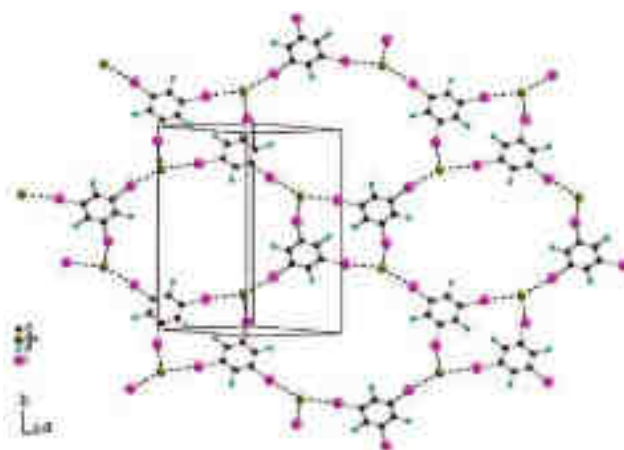


Figure IV.3. A detail view of one polymeric halogen bonded plane (cations have been omitted for clarity, iodine in purple, fluorine in green, bromine in brown, carbon in black).

This topic has so far been focused on understanding the formation of this kind of systems and discovering parameters controlling the dimensionality of halogen bonded networks. Only recently the use of such interactions to generate functional materials (aside from examples presented in chapter 1) has been reported. The group of M.E. van der Boom has recently demonstrated a solvent free crystal-to-co-crystals conversion on surface through physical vapour deposition involving halogen bonding (figure IV.4). The stepwise formation of multicomponent organic thin films through physical vapour deposition was explored.⁷

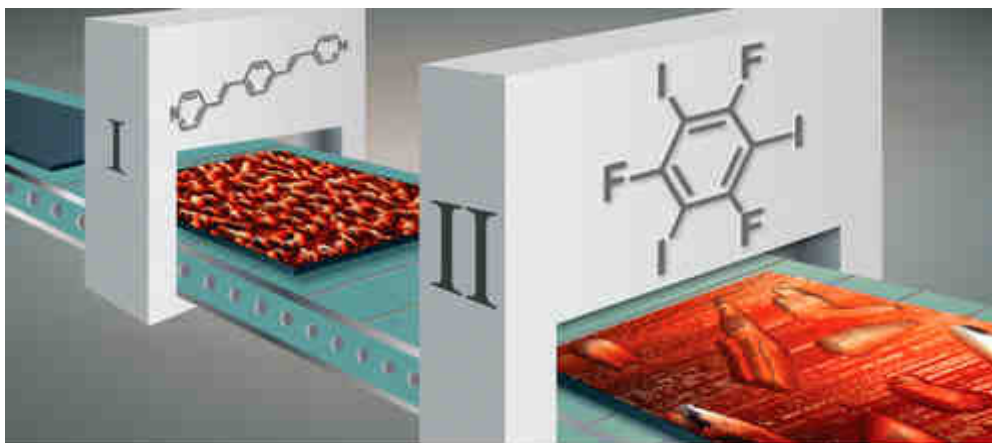


Figure IV.4. Representation of the formation of halogen bonded co-crystal on surface.

IV. 1. B. Halogen bonded networks

We have studied the interaction of ligands KIT-1, KIT-2 and KIT-3 (figure IV.1.) with IFB (mono iodoiodofluorobenzene), DIFB, and TIFB.

In the presence of 4,4'-bipyridyl ligands such as KIT-**X** ($X = 1-3$), the monoiodo IFB acts, as expected, as a stopper and does not lead to the formation of a network. Nevertheless, these structures may serve as references in order to compare the influence of the N---I interactions on the overall angles and distances.

Several crystallization conditions with different KIT-**X** ($X = 1-3$)/IFB ratio were employed. The same holds for TIFB. In the case of DIFB an equimolar stoichiometry was used. When a 1:2 tecton/TIFB ratio was used, for both KIT-**1** and KIT-**2**, crystals were obtained. The 3/2 ratio of KIT-**1**/TIFB, leads to the formation of a network, while KIT-**2** crystallizes alone without any halogenated compound. Finally, tecton KIT-**3** forms an amorphous powder.

Co-crystals of compound KIT-**1** and KIT-**2** with IFB were obtained by adding an ethanol solution of KIT-**1** or KIT-**2** to a solution of IFB. After 2-3 days, light yellow crystals appeared and were measured by single X-Ray diffraction. The analysis revealed the formation, in both cases, of discrete halogen bonded complexes with 2:1 ratio for IFB and bipyridyl based tecton. For the two supramolecular entities, the N---I bonds are equal to 3.53 Å, 19 - 20% shorter than the sum of van der Waals radii. The connectivity is the same in both structures, however, the crystal packing shows tecton dependent differences. For the shorter tecton KIT-**1**, a herringbone arrangement with IFB molecules between the layers is observed (figure IV.5a), while for the longer pyridine ligand, linear type chains packed in a parallel fashion are formed (figure IV.5b).

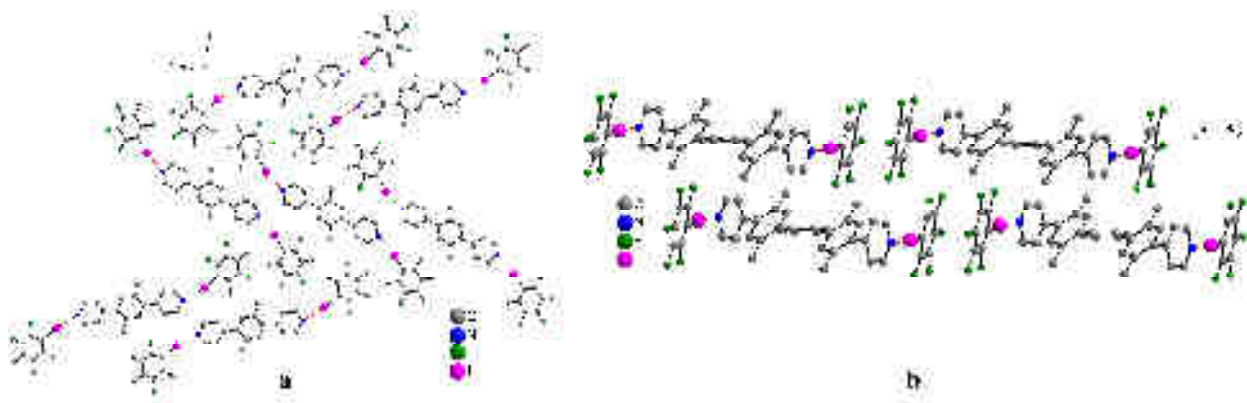


Figure IV.5. View of packing of networks formed between IFB and tecton KIT-1 (a) and tecton KIT-2 (b).

Interestingly, for the herringbone structure, no π - π interactions are observed, C-F---H-C contacts with $d_{\text{C}\cdots\text{F}}$ distances close to 3.5 Å are identified. Within the ligand KIT-1, the $N_{\text{py}}\text{-}N_{\text{py}}$ distance is equal to 11.4 Å, and the tilt angle between the pyridine mean plane and the xylene moiety is about 47°, a feature subject to significant changes depending on the coordinating iodine based tectons, as will be described later on. The tilt angle between the pyridine and the IFB is 23°.

For the tecton KIT-2, the $N_{\text{py}}\text{-}N_{\text{py}}$ distance is equal to 20.1 Å and the dihedral angle between pyridine moiety mean planes and xylene moiety is about 40° while the tilt angle between the xylene moieties and the benzene ring is 44°. The tilt angle between the pyridine and the IFB is 18°. As for tecton KIT-1 no π - π or C-F---H-C interactions are observed.

By combining ligand KIT-1 or KIT-2 with DIFB, the formation of two infinite linear chains of the same topology is observed (figure IV.6). Both structures present the same N---I distance of 2.78 Å with stabilizing C-F---H-C contacts ($d_{\text{C}\cdots\text{F}}$ of *ca* 3.4 Å) connecting neighbouring layers.

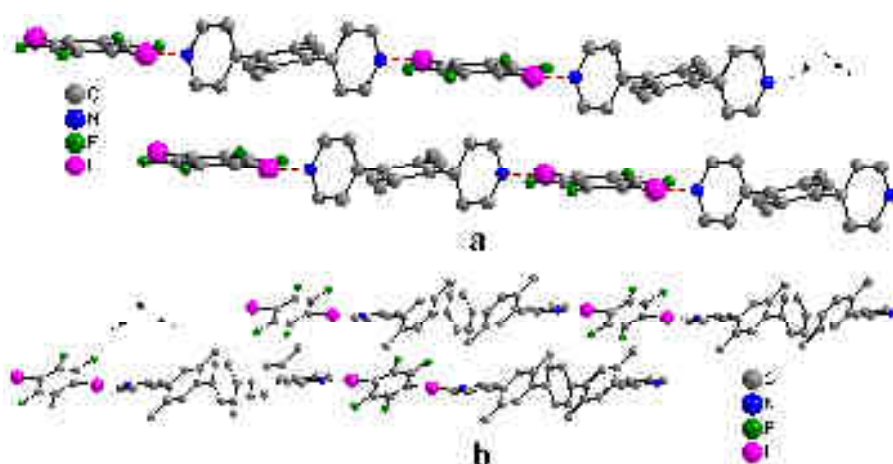


Figure IV.6. View of 1-D chains formed between DIFB and tecton KIT-1 (a) and with tecton KIT-2 (b).

The structural differences become apparent when looking at the angles between the pyridine mean plane and the DIFB moiety, for the shorter tecton the angle is *ca* 77° while for the longer tecton KIT-2, the angle is 32°. Within the tecton KIT-1, as emphasized before, there is also a shift of about 19° for the angle between the mean plane of the pyridine (Py_{mp}) and the mean plane of the xylene (Xy_{mp}) moiety. For the ligand KIT-2, the change is in the 5-7° range (Table 1).

Comp	Angle Py _{mp} / Xy _{mp} (deg)	Angle Py _{mp} / HBdonor _{mp} (deg)	Angle N---I- C (deg)	Comp	Angle Py _{mp} / Xy _{mp} (deg)	Angle Xy _{mp} / Bz _{mp} (deg)	Angle Py _{mp} / HBdonor _{mp} (deg)	Angle N---I-C (deg)
KIT-1	-	-	-	KIT-2	58	-	-	-
IFB	47	23	170	IFB	40 40	44	18	174
DIFB	66	77	176	DIFB	43	51	31	176
TIFB (1:2 ligand: TIFB)	86	83	171	TIFB (1:2 ligand: TIFB)	52	42	46	174
TIFB (3:2 ligand: TIFB)	50 42	43 46	167 178	TIFB (3:2 ligand: TIFB)	-	-	-	-

Table IV.1. Py_{mp}-pyridine mean plane, Xy_{mp}-xylene moiety mean plane, Bz_{mp}-benzene moiety mean plane, HBdonor_{mp}- mean plane of the DIFB moiety.

Due to the presence of the azobenzene moiety, the tecton **KIT-3** is of particular interest. Azobenzene has been used in photo-responsive functional devices for various applications.⁸ We are interested in light control of size and shape of cavities and channels in self-assembled materials in the crystalline phase. Indeed, by switching between the two *cis* and *trans* conformers of the azobenzene moiety, one could change the specific uptake of host molecules. By combining tecton **KIT-3** and DIFB, a 1-D chain, resulting from two N---I bonds with 2.85 Å and 2.88 Å distances with angles between C-I-N around 170° is formed. Within the network, as expected, the *E* isomer (or *trans*) of azobenzene is found. Attempts to switch to the *Z* (*cis*) conformer are currently under investigation (figure IV.7). The angles between the mean plane of the DIFB and the connecting pyridine moiety are 41° and 42°. Within the tecton, the angle between the two pyridyl moieties is 82° and the dihedral angle between the pyridyl units and the central benzene moiety is 39°. The DIFB moieties belonging to the same plane are π - π stacked (centroid distance of 3.6 Å) with a benzene moieties of the azobenzene group of consecutive layers. The fluorine atoms of the DIFB also form intermolecular H---F bonds with pyridyl units ($d_{C...F}$ in the 3.12 - 3.5 Å range), as well as between DIFB moiety and the protons of the benzene moiety from the azobenzene function ($d_{C...F}$ = 3.27 Å).

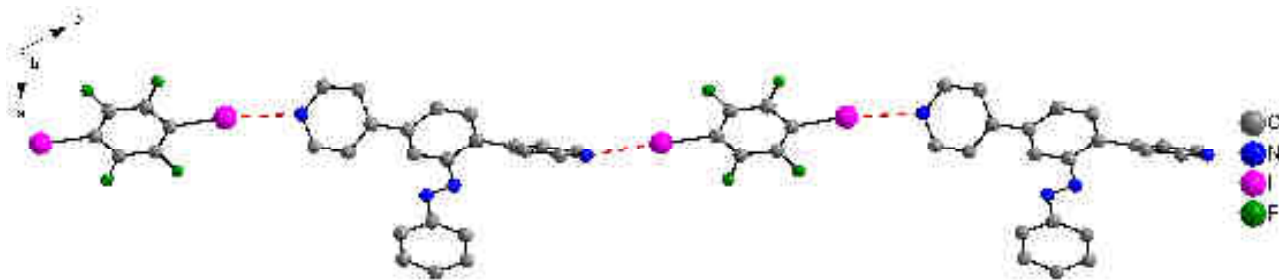


Figure IV.7. View of the 1-D chains formed through two N---I halogen bonds. Hydrogen atoms are omitted for clarity.

By combining tecton KIT-1 or KIT-2 with TIFB, the formation of only 2 halogen bonds is observed, confirming, as already mentioned above, that only two out of the three iodine centres take part in the formation of the network.

Using a 3:2 tecton/TIFB ratio, in the case of KIT-2, crystals were only composed of the tecton. However, in the case of the tecton KIT-1, the formation of a 1D chain was observed. The co-crystal displays two distinct N---I bonds of 2.85 and 2.91 Å, with two different angles between the mean plane of the pyridyl moiety and the TIFB plane of *ca* 43° and 47°. The overall packing shows π - π stacking interactions between TIFB moieties with a distance of *ca* 3.5 Å (figure IV.8a).

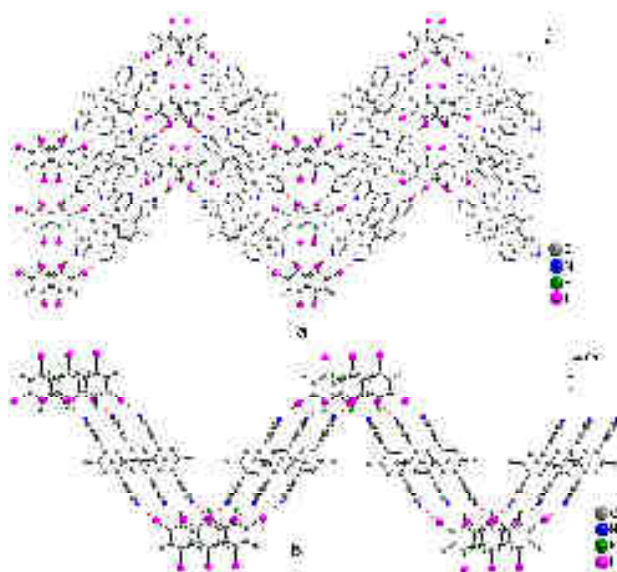


Figure IV.8. a) View of the 1-D chains formed through two N---I halogen bonds between KIT-1 and TIFB (3:2 ratio); b) A portion of the 1-D chains formed through two N---I halogen bonds between KIT-1 and TIFB (1:2 ratio). Hydrogen atoms are omitted for clarity.

A 1/1 chloroform/ethanol mixture of KIT-1 or KIT-2 with TIFB affords two types of networks. In the case of KIT-1, a network with a 1:2 ratio of tectons is formed. Whereas, for KIT-2 a network with a 2:1 ratio is generated. For the 1D network based on tecton KIT-1, the formation of two N---I halogen bonds is observed (figure IV.8b). Within the halogen bond acceptor tecton, as emphasized above, a change in the angle of *ca* 19° between the mean plane of the pyridyl and the xylene molecule is observed. This may be attributed to a less restrained overall π -system when compared

to tecton KIT-2, for which the difference in angles is much less pronounced. No interactions between chains could be detected in this case.

For the co-crystal based on tecton KIT-2, only one N---I halogen bond per TIFB molecule is observed. For this 2:1 adduct, the 1D chains are arranged in a herringbone fashion. The TIFB within consecutive layers are stacked in an offset manner (figure IV.9). In contrast with the above-mentioned structure obtained with the tecton KIT-1, two F---I (3.11 Å) intermolecular contacts (distance shorter by 10% with respect to the sum of van der Waals radii) are formed. In this case, the C-F-I angles are almost identical and close to *ca* 163° which suggests a type I halogen-halogen interaction.

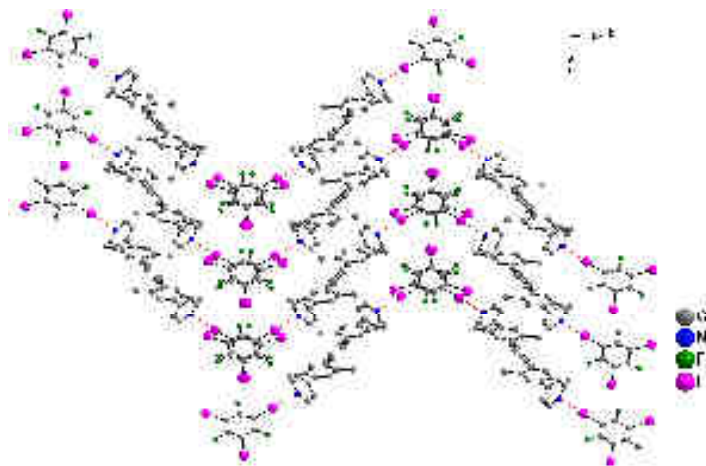


Figure IV.9. A portion of the structure obtained by combining the tecton KIT-2 and TIFB through one N---I halogen bonds. Hydrogen atoms are omitted for clarity.

IV. 1. C. Conclusion

This study was focused on the formation of halogenated networks based on combinations of tectons bearing two bipyridyl units and displaying different lengths with iodofluorinated benzene derivatives. In the presence of the mono iodo compound (IFB), a 2:1 tecton/IFB ratio was obtained in both cases in the solid state, the iodo compound acting as a stopper. However, the packing of the two [(tecton)(IFB)₂] species in the crystal is different: intermolecular weak H---F bonds are only present for [(KIT-1)(IFB)₂] thus leading to a herringbone arrangement while for **2**, [(KIT-2)(IFB)₂] units are arranged in a parallel fashion with no specific interactions between components.

In the case of the ditopic tectons, the self-assembling of KIT-1 or KIT-2 with DIFB leads to the formation of the expected 1D chains through N---I interactions and hydrogen bonding between consecutive layers.

In the presence of the triiodobenzene for the 2:3 (TIFB:tecton) ratio, the tecton KIT-1 forms a 1D chain with π - π stacking between the layers, while the tecton KIT-2 crystallizes alone. By changing the ratio to 2:1 (TIFB/tecton), the tecton KIT-1 generates a similar wavy 1-D chain without any interactions between them, while ligand KIT-2 generates a 1D network with 2:1 (TIFB/tecton) ratio with their packing in a herring bone manner, with π - π staking of TIFB moieties belonging to consecutive layers. It is also interesting to notice that, for tecton KIT-1, the change in stoichiometry

leads to the formation of a similar 1D architecture. The co-crystals formed between the pyridyl based tectons and iodofluoroarenes are stable in air. So far, no attempts to test their trapping abilities have been made. KIT-3, as mentioned before, is a particular tecton bearing two azobenzene moieties. So far, a 1D network with the *E* isomer combined to DIFB was generated. The photo switching to the *Z* isomer is currently under investigation.

IV. 2. Halogen bonded networks involving porphyrins.

IV. 2. A. Literature overview

Only very few reports, dealing with the use of porphyrins as scaffolds for halogen-bonding, have been published, in particular by the group of I. Goldberg. In 2008, this group reported one of the first examples of two different combinations of a porphyrin bearing both pyridyl and iodophenyl groups: 5-(4-pyridyl)-10,15,20-tris(4-iodophenyl)porphyrin (figure IV.10) and 5,15-bis(4-pyridyl)-10,20-bis(4-iodophenyl)porphyrin (figure IV.11).^{9, 10} It has been shown that, while the 1:3 substituted porphyrin self-assembles into a 2-D network for which the N---I interactions are directing the structure (figure IV.1), the porphyrin bearing two iodophenyl moieties yields a compact layered organization sustained by various types of porphyrin-porphyrin interactions, including I--- π , π --- π and C-H---N contacts (figure IV.11). More interesting is the chiral nature of the PyTIPP architecture, as all the molecules are oriented in the same direction and they lack inversion and mirror symmetries.

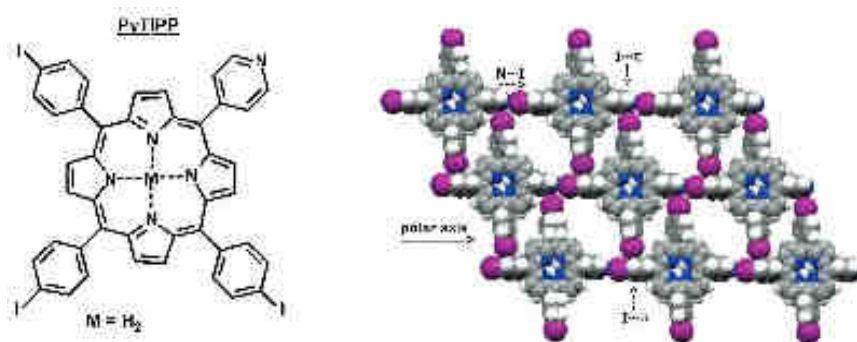


Figure IV.10. Self assembly of the PyTIPP into chiral layers by N---I halogen bonds and I--- π interactions.

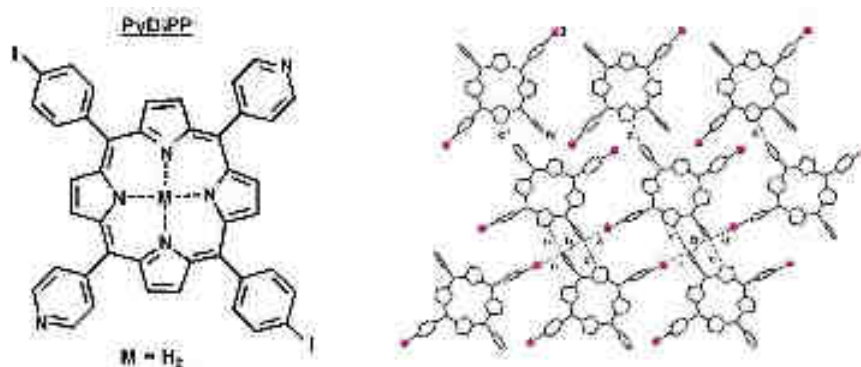


Figure IV.11. Layered structure formed through self-assembly of the PyDIPP with the specific I--- π contacts (dotted lines) noted with “a”, π --- π interactions (dotted lines) noted with “b” and weak C-H---I contacts(dotted lines) between the layers marked with c.

More recently, the same group has extended their studies to the corresponding metalloporphyrin.¹¹⁻¹³ In these cases, the target is mostly the formation of halogen bonds between the porphyrin substituents and axially coordinated metal ligands.

A particularly interesting example was recently reported by the group of B. Schöllhorn.¹⁴ An extended porphyrin network with nanosized linear channels was obtained by using tetrakis (4-iodoperfluoro-phenyl) porphyrin (I₄-PFTPP) and hexamethylenetetramine (HMTA) (figure IV.12a). The structure involves eight crystallographically different iodine atoms (I1 to I8). Each iodine atom of the porphyrin is involved in halogen bonds with the nitrogen of HMTA. The halogen bonds, show relatively long interatomic I...N distances of 2.85 to 3.17 Å (the sum of van de Waals radii for nitrogen and iodine is *ca* 3.53 Å). The ladders formed by N...I interactions are also connected through short I...I contacts and the angles between C-I...I suggest type II halogen bonding. An interesting feature of the network is the presence of a linear helical structure pattern in the *b* direction, which is sustained through short C-H...F contacts; however the overall structure is not chiral because of the presence of left and right handed helices (figure IV.12b).

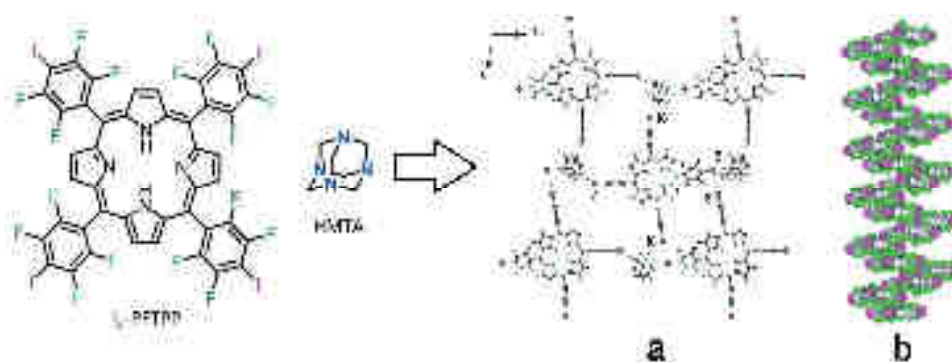


Figure IV.12. A portion of the supramolecular layer formed by N...I and I...I interactions (a), the helical structure of the porphyrins forming a channel in the *b* direction (b) (carbon in grey, fluorine in green, iodine in violet and nitrogen in blue).

The channels are filled with disordered solvent molecules (chloroform and acetone) and attempts to exchange the solvent were made. Unfortunately no crystal structure with the exchanged solvent could be resolved.

The group of C. Arunkumar has reported recently on the use of fluorinated porphyrins for halogen-bonding. Their contributions focus on the intermolecular interactions in fluorinated tetraarylporphyrins and their metallated equivalents¹⁵⁻¹⁷ highlighting the stabilizing nature of F...H, F...C and F...F contacts in crystal packing. In their examples, the theoretical calculations (Hirshfeld surface analysis) showed that the weak interactions involving fluorine atoms can comprise up to 50% of the stabilizing energy of the crystal packing. As for the F...F contacts, in particular the shortest distance observed in the crystal structures corresponds to 2.84 Å, these contacts represent about 6-7 % of the intermolecular interactions.¹⁶

As stated above, the use of halogen bonds in constructing networks with porphyrin based tectons has been scarcely explored and no studies dealing with the use of fluorinated alkyl chains have been reported. Having in hand a series of highly fluorinated porphyrin based tectons bearing two *meso* pyridyl units, in order to generate halogenated supramolecular networks through halogen bonds, their interactions with iodofluoroarenes were investigated. The idea pursued was the generation of porous networks containing high number of fluorine atoms for the encapsulation of halogenated species.

IV. 2. B. New Halogen bonded networks

Based on tectons described in Chapter II, the approach followed to generate supramolecular networks was to exploit N---I interaction in the presence of a series of iodofluoroarenes.

Iodopentafluorobenzene (IFB), 1,4-diiodotetrafluorobenzene (DIFB) and 1,3,5-triiodo-2,4,6-trifluorobenzene (TIFB) were considered for the crystallization process. The use of fluorinated iodoarenes was further rationalized by the influence of fluorine atoms on the iodine ability to form stronger halogen bonds. Indeed, fluorine's electronegativity should affect the electron density on iodine, thus creating a more pronounced σ hole which would lead to stronger halogen bonds. Furthermore, by varying the number and localization of iodine atoms, it should be possible to control the dimensionality of architectures. IFB is a blocking unit that should lead to discrete species, DIFB, bearing two iodine atoms, could behave as a ditopic tecton and depending on the complementary tecton used, should lead to the formation of supramolecular networks, finally, the same holds for TIFB which forms up to three bonds.

Various crystallization conditions were tested. The formation of single crystals suitable for XRD was observed for combinations of DIFB with tectons **4**, **9**, **10**, **11** and **16** containing 6, 10, 14, 16 and 12 fluorine atoms at their periphery respectively.

While crystals obtained from the tecton **4** have a Porphyrin/DIFB ratio of 2:1, tectons **9**, **10**, **11** and **16** crystallize in the presence of 2 DIFB moieties leading to the reverse 1:2 ratio. Many attempts were made in order to change the ratio and in particular to obtain a 1:1 adduct, but in all cases with lower concentration of DIFB, the formation of crystals solely composed of the free-base porphyrin was observed. On the other hand, higher concentrations of DIFB did not change the Po: DIFB ratio. The description of the structures given below is organized according to the number of fluorine atoms present on the backbone.

DIFB-Tecton 4

Slow diffusion of an ethanol solution of DIFB into a chloroform solution of the porphyrin **4** in a 4:1 DIFB/**4** ratio followed by slow evaporation afforded in 3-4 days single crystals suitable for X-ray diffraction measurements. The mixture crystallizes in the *P-1* space group ($Z = 1$), the asymmetric unit contains two halves porphyrin moieties and one half DIFB moiety. In the crystal, the ratio between the tecton **4** and DIFB is 2:1. Among the two crystallographically non equivalent porphyrin based tectons P1 and P2, only P1 is involved in N---I interactions with a distance of *ca*

3.00 Å and C-I-N angle of 172°. The infinite 1-D network is of the stair type (figure IV.13); the second porphyrin (P2) is located between layers (figure IV.14).



Figure IV.13. A portion of the structure obtained upon combining the tecton **4** with DIFB, only specific interactions between the porphyrin based tecton P1 and DIFB are shown. Hydrogen atoms are omitted for clarity.

The angle between the P1 and the DIFB moiety is 40° and the angle between the mean plane of pyridyl moieties attached to P1 and the mean plane of the DIFB moieties is 85°. The angle between the mean planes of P2 and of DIFB situated under and above P2 plane is 29°.



Figure IV.14. A portion of the structure obtained upon combining the tecton **4** with DIFB focusing on a halogen bonded chain resulting from N---I interactions (red dotted lines). Hydrogen atoms are omitted for clarity.

For both P1 and P2 porphyrin based tectons, the alkyl chains are located above and under their mean planes. The angle between the mean planes of P1 and P2 is around 12°, while the P1 type porphyrins forming the 1-D chain are parallel to each other. The dihedral angle between the P1 mean plane and its pyridyl moieties is 80°, while for P2, the angle is 71°. The non-connected porphyrin P2 forms intermolecular F---H bonds between fluorine atoms of the DIFB moiety and the protons of the pyridyl unit of the porphyrin ($d_{C...F} = 3.00 \text{ \AA}$) and the protons on the alkyl chains ($d_{C...F} = 3.48 \text{ \AA}$).

DIFB-Tecton 9

Under similar crystallization conditions with a different stoichiometry (Po/DIFB ratio of 1:1.6), suitable single-crystals were obtained after several days. The X-ray diffraction measurement revealed the formation of a 1-D chain type network based on N---I bonds. The mixture crystallizes in the *P-1* space group ($Z = 1$), the asymmetric unit contains $\frac{1}{2}$ porphyrin moiety and two $\frac{1}{2}$ moieties of DIFB. The ratio between the tecton and the DIFB is 1:2 and only one of the DIFB moiety is connected to the porphyrin (figure IV.15) through two N---I interactions (2.75 Å) with the C-I-N angle of 172° involving the pyridyl units. The angle between the pyridyl moiety and DIFB is *ca* 80° and the angle between the porphyrin mean plane and DIFB involved in the formation of the network is 42° . Within the tecton the dihedral angle between the porphyrin mean plane and the *meso* pyridyl substituents is 59° . Both alkyl chains are situated above and under the porphyrin mean plane.

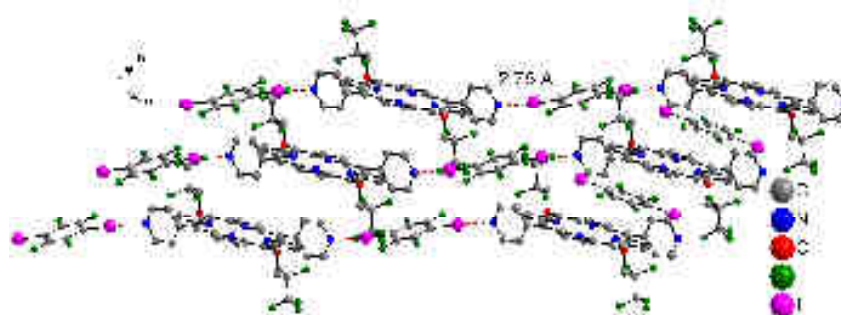


Figure IV.15. A portion of the structure obtained upon combining the tecton **9** with DIFB focusing on the halogen-bonded chain resulting from N---I interactions (red dotted lines). Hydrogen atoms are omitted for clarity.

The DIFB molecule not involved in the network formation is engaged in two I---I interactions with the DIFB molecule connected to the porphyrin with a distance of 3.95 Å, which is at the limit of the sum of van der Waals radii for iodine (3.96 Å).

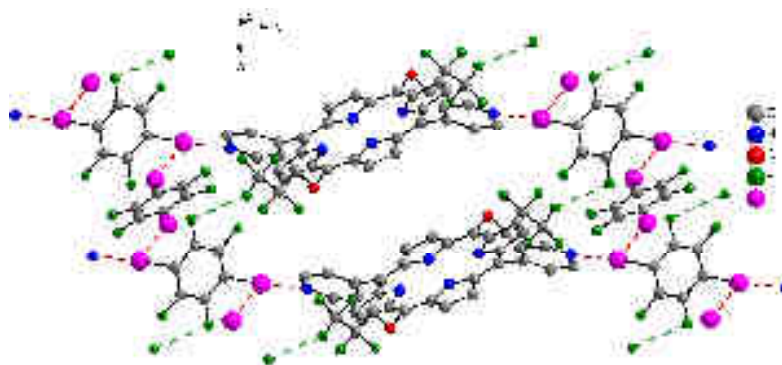


Figure IV.16. A portion of the structure obtained upon combining the tecton **9** with DIFB focusing on N---I and I---I (red dotted lines) and F---F bonds (green dotted lines). Hydrogen atoms are omitted for clarity.

Considering both N---I and I---I interactions, the overall structure may be described as a 2D network (figure IV.16). The fluorine atoms on the alkyl chains are involved in two F---F contacts

with a distance of 2.93 Å (type one) with the fluorine atoms on the DIFB moiety in the plane of the 2D network. Intermolecular F---H ($d_{C...F} = 3.40$ Å) contacts are as well formed between fluorine atoms on the DIFB belonging to the network and the β protons of porphyrin backbone belonging to consecutive layers. The porphyrin planes are also π - π stacked with the DIFB moieties (3.5 Å).

DIFB-Tecton 16

Tecton **16** (as a mixture of *meso* and racemate) possesses 12 fluorine atoms on its backbone. By using a Po/DIFB ratio of 1:5, suitable crystals for X-ray structural investigations were obtained within a few days. The mixture crystallizes in the *P-1* space group ($Z = 1$), the asymmetric unit contains $\frac{1}{2}$ porphyrin (*meso* form) moiety and two $\frac{1}{2}$ DIFB units. As for the tecton **9**, the ratio between the tecton and the DIFB moiety is 1:2 and only one of the two DIFB moieties takes place in the formation of the network through N---I interactions (2.73 Å) with a C-I-N angle of 178° involving the pyridyl substituents (figure IV.17). The angle between the pyridyl moiety and the DIFB unit is *ca* 88° and the angle between the porphyrin mean plane and the connected DIFB moiety is 30° . Within the tecton, the dihedral angles between the porphyrin mean plane and the *meso* pyridyl substituents are equal to 58.5° . Both alkyl chains are situated above and under the porphyrin mean plane (figure IV.17).

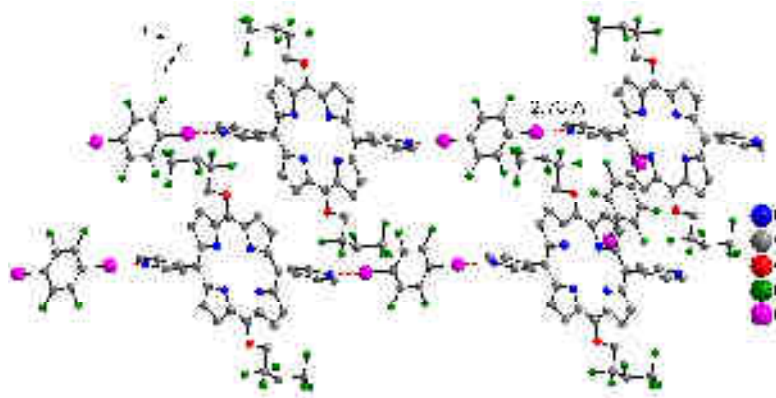


Figure IV.17. A portion of the structure obtained upon combining the tecton **16** with DIFB focusing on the halogen-bonded chain formed through N---I interactions (red dotted lines). Hydrogen atoms are omitted for clarity.

The DIFB molecule not involved in the network formation is engaged in two I---I interactions with the DIFB molecule connected to the porphyrin with a distance of 3.90 Å, which is shorter than the sum of van der Waals radii for iodine (3.96 Å). The fluorine atoms of the alkyl chains, alike for tecton **9**, are involved in two F---F contacts with a distance of 2.84 Å (type one) with the fluorine atoms of the DIFB unit belonging to consecutive layers (figure IV.18). The angle between the two mean planes of the DIFB units is *ca* 34° . Intermolecular F---H ($d_{C...F} = 3.30$ Å) contacts are as well formed between fluorine atoms of the DIFB connected moiety and the β -pyrrolic protons of the porphyrin from the consecutive layers. The porphyrin planes are also π - π stacked with the DIFB moieties (3.5 Å).

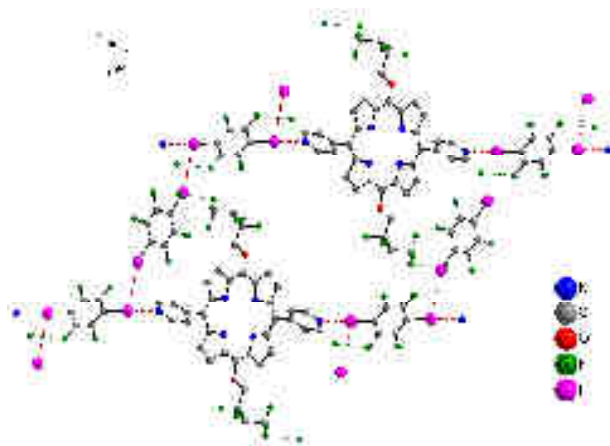


Figure IV.18. A portion of the structure obtained upon combining the tecton **16** with DIFB focusing on N---I (red dotted lines) and F---F (green dotted lines) interactions. Hydrogen atoms are omitted for clarity.

DIFB-Tecton 10

After diffusion of an ethanol solution of DIFB into a chloroform solution of porphyrin with a Po/DIFB ratio of 1:5 followed by slow evaporation of solvents, single-crystals were formed within 3-4 days. The X-ray diffraction analysis revealed the formation of a 1D chain type network resulting from halogen-bonding similar to the one described above. The mixture crystallizes in the *P-1* space group ($Z = 1$), the asymmetric unit contains $\frac{1}{2}$ porphyrin moiety and two $\frac{1}{2}$ DIFB moieties. The ratio between the tecton and the DIFB is 1:2 with only one DIFB moiety involved in N---I interactions (2.74 Å) (figure IV.19). The C-I-N angle involving the pyridyl substituents is 178° . The angle between the pyridyl moiety and the DIFB unit is *ca* 83° and the angle between the porphyrin mean plane and the connecting DIFB molecule is 30° . Within the tecton, the dihedral angles between the porphyrin mean plane and the *meso* pyridyl substituents is 68° . The alkyl chains are situated under and above the porphyrin mean plane.

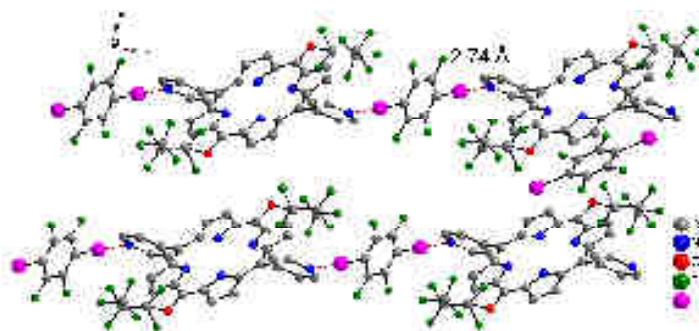


Figure IV.19. A portion of the structure obtained upon combining the tecton **10** with DIFB focusing on the halogen-bonded chain formed through N---I interactions (red dotted lines). Hydrogen atoms are omitted for clarity, only one non connecting DIFB is shown to give a clear picture.

The DIFB molecule not involved in the network formation is engaged in two I---I interactions with the second DIFB moiety (3.81 Å) and interacts with the porphyrin through π - π interactions (3.4 Å). The angle between the two mean planes of the DIFB units is *ca* 34° . Each porphyrin moiety has

four F---F contacts, two with the DIFB within the same plane (2.85 Å) and the other two with the DIFB connecting moieties (2.87 Å) from the next layer (figure IV.20). Intermolecular F---H ($d_{C\cdots F} = 3.5$ Å) contacts are as well formed between fluorine atoms on the porphyrin alkyl chains and the β -pyrrolic protons of the porphyrin from the subsequent layer.

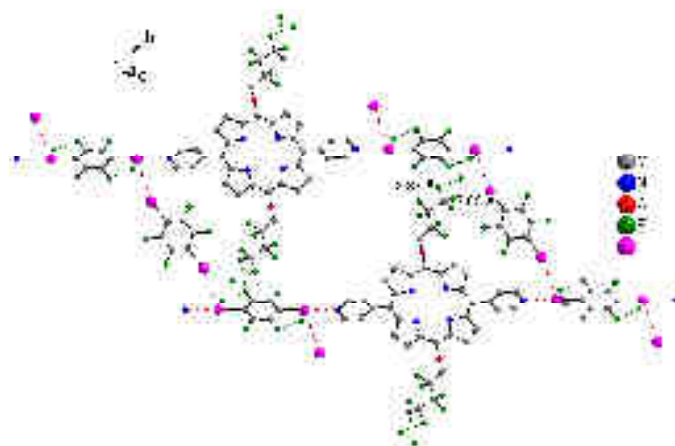


Figure IV.20. A portion of the structure obtained upon combining the tecton **10** with DIFB focusing on N---I/I---I (red dotted lines) and F---F contacts (green dotted lines). Hydrogen atoms are omitted for clarity.

DIFB-Tecton 11

The last representative tecton **11** possesses 16 fluorine atoms. Under the same conditions as described above (Po/DIFB ratio of 1:5), single crystals were obtained. As in the previous cases, a 1-D supramolecular chains is formed through N---I interactions. The space group is *P-1* ($Z = 1$). The asymmetric unit contains two $\frac{1}{2}$ non-equivalent porphyrin moieties and two DIFB moieties leading to an overall porphyrin/DIFB ratio of 1:2. Each porphyrin based tecton is bridging one molecule of DIFB through the pyridyl substituents. The N---I distance is *ca* 2.74 Å and the angle is close to 173° (figure IV.21). The angle between the pyridine moiety and the DIFB unit is *ca* 90°. The angle between the porphyrin mean planes and the connecting molecule is 29° and 35° for the two independent porphyrin moieties in the asymmetric unit respectively. Within the tectons, the dihedral angles between the PMP and the *meso*-pyridyl are close to 60°. The alkyl fluorinated chains are situated under and above the porphyrin mean plane, due to the centrosymmetry of the unit cell. For one porphyrin, the chains are disordered over two positions.

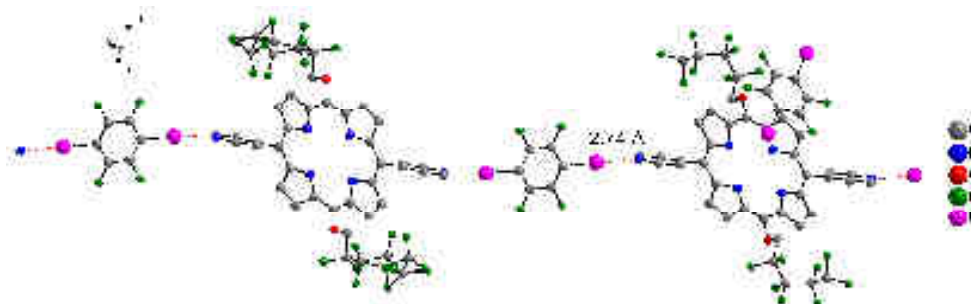


Figure IV.21. A portion of the structure obtained upon combining the tecton **11** with DIFB focusing on halogen-bonded chain formed through N---I interactions (red dotted lines). Hydrogen atoms are omitted for clarity.

The DIFB molecule not involved in the network formation is forming as in the previous case two I---I interactions with the second DIFB moiety with a distance of 3.86 Å and 3.91 Å (figure IV.22), thus forming the 2D network discussed above for the tecton **10**. The angle between the two mean planes of the DIFB moieties is *ca* 37°. Considering the disorder on the fluorinated chains no description of F---F contacts is given.

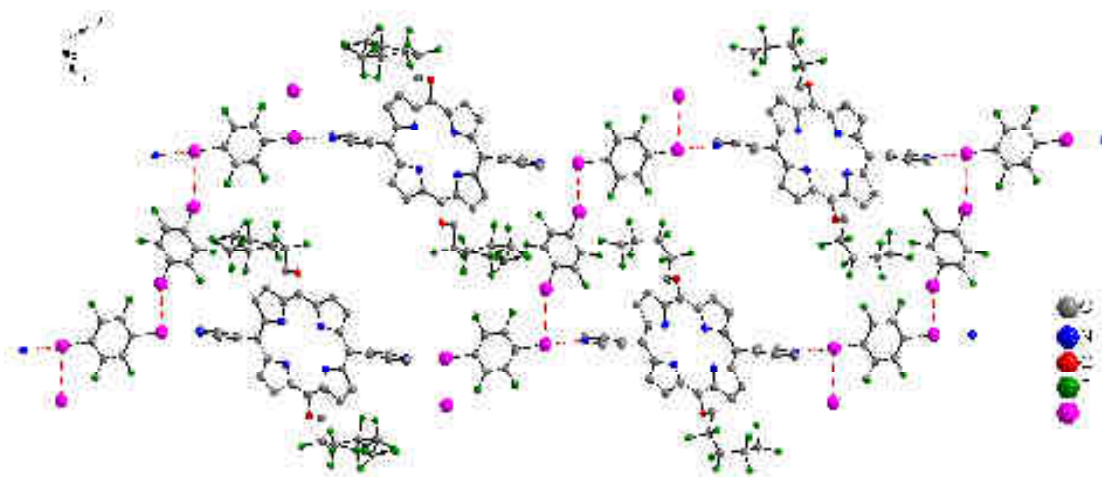


Figure IV.22. A portion of the structure obtained upon combining the tecton **11** with DIFB focusing on N---I / I---I (red dotted lines). Hydrogen atoms are omitted for clarity.

IV. 2. C. Conclusion

The use of *trans meso* substituted porphyrin based tectons bearing pyridyl sites capable of connecting organic tectons carrying iodine atoms led to the formation of a series of supramolecular networks. The role played by the number of fluorine atoms on the backbone, on establishment of non-covalent interactions such as F---F contacts guiding the overall packing of the networks was investigated. Based on the use of six different tectons (**4**, **9**, **10**, **11** and **16**), a difference in the ratio of components within the networks was observed. While tecton **4** leads to a Po/DIFB 2:1 ratio, the *meso* ether bonded porphyrin series all adopt a Po/DIFB 1:2 ratio, thus in the first case, a non-connected porphyrin is present. For the second series, one DIFB moiety is not involved in N---I bonds. By adding more fluorine atoms at the periphery of the porphyrin based tecton, it was noticed that the N---I interaction distance is decreased from 3.01 Å for tecton **4** to 2.74 Å for tectons **10** and **11**. This may be related to the electron withdrawing nature of the fluorine atoms. The number of fluorine, as seen in previous chapters, also influences the number and the distance of F---F contacts, the same trend is observed here. In order to fully elucidate the reason of this particular network formation, theoretical calculations could provide helpful insights.

Crystals for all the tectons investigated are stable during the measurements, however upon leaving them in air overnight, the formation of amorphous powder is observed. Attempts to introduce a third fluorinated or chiral solvent molecules are still undergoing.

References

1. P. Metrangolo, G. Resnati, T. Pilati and S. Biella, in *Halogen Bonding*, eds. P. Metrangolo and G. Resnati, Springer Berlin Heidelberg, 2008, vol. 126, pp. 105-136.
2. M. Vartanian, A. C. B. Lucassen, L. J. W. Shimon and M. E. van der Boom, *Crystal Growth & Design*, 2008, **8**, 786-790.
3. F. C. Pigge, P. P. Kapadia and D. C. Swenson, *CrystEngComm*, 2013, **15**, 4386-4391.
4. M. Baldrighi, P. Metrangolo, F. Meyer, T. Pilati, D. Proserpio, G. Resnati and G. Terraneo, *J. Fluorine Chem.*, 2010, **131**, 1218-1224.
5. A. C. B. Lucassen, A. Karton, G. Leitus, L. J. W. Shimon, J. M. L. Martin and M. E. van der Boom, *Crystal Growth & Design*, 2007, **7**, 386-392.
6. S. Triguero, R. Llusar, V. Polo and M. Fourmigué, *Crystal Growth & Design*, 2008, **8**, 2241-2247.
7. M. Boterashvili, M. Lahav, S. Shankar, A. Facchetti and M. E. van der Boom, *J. Am. Chem. Soc.*, 2014, **136**, 11926-11929.
8. F. Hamon, F. Djedaini-Pilard, F. Barbot and C. Len, *Tetrahedron*, 2009, **65**, 10105-10123.
9. S. Lipstman, S. Muniappan and I. Goldberg, *Crystal Growth & Design*, 2008, **8**, 1682-1688.
10. S. Muniappan, S. Lipstman and I. Goldberg, *Chem. Commun.*, 2008, 1777-1779.
11. H. M. Titi, R. Patra and I. Goldberg, *Chem. Eur. J.*, 2013, **19**, 14941-14949.
12. G. Nandi, H. M. Titi and I. Goldberg, *Crystal Growth & Design*, 2014, **14**, 3557-3566.
13. G. Nandi and I. Goldberg, *CrystEngComm*, 2014, **16**, 8327-8333.
14. J.-L. Syssa-Magale, K. Boubekeur, J. Leroy, L.-M. Chamoreau, C. Fave and B. Schollhorn, *CrystEngComm*, 2014, **16**, 10380-10384.
15. R. Soman, S. Sujatha and C. Arunkumar, *J. Fluorine Chem.*, 2014, **163**, 16-22.
16. R. Soman, S. Sujatha, S. De, V. C. Rojisha, P. Parameswaran, B. Varghese and C. Arunkumar, *Eur. J. Inorg. Chem.*, 2014, **2014**, 2653-2662.
17. F. R. Kooriyaden, S. Sujatha, B. Varghese and C. Arunkumar, *J. Fluorine Chem.*, 2015, **170**, 10-16.

General Conclusion

General Conclusion

The work presented in this thesis is focused on the design of neutral porphyrin based tectons and their use for the generation of chiral and/or fluorinated molecular networks that could be used as functional materials towards the separation of chiral and/or fluorinated molecules.

The formation of coordination networks is based on combinations of metallic centers with chiral/fluorinated tectons while the supramolecular networks are generated by halogen bonds by using iodofluoroarenes. For the formation of crystals, several methods have been tested. For the operational ones, experimental conditions have been optimized. Overall, 34 new crystal structures of novel porphyrin based ligands, coordination networks and supramolecular networks have been obtained and discussed in different chapters.

Chapter one is a general introduction on topics such as Molecular tectonics, Molecular networks, Halogen bonding and Enantioselective separation. This gives an overview of the state of the art of the subject and some crucial notions for the next chapters.

The second chapter deals with the synthesis of neutral porphyrin based tectons bearing two neutral coordinating sites (4-pyridyl) in the two *trans meso* positions and either fluorinated or chiral substituents in the other two remaining positions. Two different strategies have been used to prepare the tectons. The first one was based on the use of commercially available aldehydes in the classic [2+2] MacDonald condensation. The second method, a four-step transformation, is based on a *trans meso* brominated porphyrin as a platform for palladium mediated coupling reactions with a series of fluorinated and/or chiral alcohols. Seven new tectons have been characterized by X-Ray diffraction analysis on single crystals which revealed that the presence of fluorine atoms in the periphery of the porphyrin influences the crystal packing in the solid state. Two of the tectons with a high number of fluorine atoms on the backbone display F...F contacts in the solid state. Attempts to incorporate fluorinated solvent within the porphyrin containing crystals cavities through specific interactions have been unsuccessful so far.

Chapter three describes the formation of coordination networks based on tectons discussed in chapter two. Depending on the localization of the metal center: inside the porphyrin cavity or at the periphery, two approaches have been explored: i) the self-assembly based on self-complementary metallatectons, ii) the multicomponent strategy involving an external metal cation leading to the formation of either homometallic or heterometallic coordination frameworks depending on the absence or presence of a metal cation within the porphyrin core. For the first strategy Zn-Po self-complementary metallatectons have been used to generate eleven 1-D and 2-D coordination networks. For the monodimensional networks, we have investigated the role played by the number of fluorine atoms in intramolecular interactions, specifically the F...F contacts, within the crystal. Taking advantage of this type of interactions, the trapping fluorinated solvents was explored.

Several attempts using chiral and fluorinated solvents have been made. Unfortunately, so far, no chiral networks have been obtained using chiral solvents. However, for networks containing fluorinated solvent, the latter are trapping through hydrogen bonding. The two 2-D networks obtained through self-assembly of Zn-Po, showed the formation of cavities decorated with fluorinated alkyl chains. However, in both cases, cavities are empty and attempts to fill them with solvent molecules have failed. For the multiple component strategy, external metal cations such Cu^{2+} , Co^{2+} , Ni^{2+} , Cd^{2+} , Hg^{2+} , Ag^+ were tested and, so far, two coordination networks (one 2-D and one 3-D) with Cd^{2+} have been obtained and characterized. We observe that for six fluorine atoms on the backbone no F---F contacts are found while for 14 fluorine atoms per porphyrin, short F---F contacts of 2.61 Å are observed. Although both crystalline materials appeared to be stable, the inclusion of solvent molecules within the channels either during the crystallization process or after the formation of the crystals was unsuccessful.

Chapter four is divided in two parts: the first one describes the use of bipyridyl based tectons, synthesized in the group of Prof. Stefan Bräse by Dr. Sylvain Grossjean (Karlsruhe Institute of Technology, Germany), with three haloarenes (iodopentafluorobenzene, 1,4-diiidotetrafluorobenzene and 1,3,5-triiodo-2,4,6-trifluorobenzene). Co-crystals formed between the bipyridyl based tectons and iodofluoroarenes are stable in air. Their propensity to uptake solvent molecules is currently under investigation. Among all tectons prepared, the one bearing an azobenzene moiety seems particularly interesting. Indeed, one might exploit its E/Z photoisomerization ability “to light tune” structures of networks in the crystalline phase and thus their solvent trapping capacity. The second part focuses on the synthesis of halogen bonded networks based on porphyrin based tectons, a subject poorly exploited so far. Five molecular networks have been generated and characterized by X-ray diffraction on single crystals. Interestingly, depending on the type of tecton used, different Po/DIFB ratio in the molecular network is observed. The number of fluorine atoms on the backbone influences the number and F---F contacts distances, thus, increase in the number of fluorine atoms in the periphery of the porphyrin, enhances the number of F---F contacts. For all the tectons used, crystals are stable during measurements; however, in air overnight, they decompose into amorphous powders. Attempts to introduce a third fluorinated partner are currently ongoing.

Our initial goal was to generate porous crystals composed of molecular networks capable of separating halogenated chiral molecules. We are not yet there. However, understanding interactions responsible for networks formation and their packing in the crystalline phase is an important step towards the design of porous materials for separation processes. The results presented in the manuscript are a first step towards that goal.



Experimental Part

Abbreviations

Å	Angström
°C	Celsius degree
δ	Chemical shift
DDQ	2,3-Dichloro-5,6-dicyano-1,4-benzoquinone
DPEPhos	(Oxydi-2,1-phenylene)bis(diphenylphosphine)
ESI	ElectroSpray Ionization
eq	Equivalent
g,mg	Gram, milligram
h	Hours
Hz, MHz	Hertz, megaHertz
J	Coupling constant
K	Kelvin
mL	Milliliter
mol, mmol	Mole, millimole
m/z	Mass/charge ratio
ppm	Part per million
βpyr	β-pyrrolic
NBS	N-bromosuccinimide
UV	Ultraviolet

1. Characterization techniques

$^1\text{H-NMR}$, $^{13}\text{C-NMR}$ and $^{19}\text{F-NMR}$ were recorded at room temperature on Bruker NMR spectrometers. The chemical shifts are given in ppm, for ^1H signal, δ values are followed by the multiplicity of the signal (s: singlet, d: doublet, t: triplet, dd: doublet of doublets, tt: triplet of triplets, br: broad signal, m: multiplet). UV-Vis absorption spectra were collected at room temperature on a UVIKON XL spectrometer. Mass spectra (ESI-MS) were recorded on microTOF LC spectrometer (Bruker Daltonics, Bremen).

X-Ray diffraction data were collected on a Bruker APEX8 CCD diffractometer equipped with an Oxford Cryosystem liquid N_2 device at 173(2) K device, using a molybdenum microfocus sealed tube generator with mirror-monochromated $\text{Mo-K}\alpha$ radiation ($\lambda = 0.71073 \text{ \AA}$), operated at 50 kV/600 μA . The structures were solved by using SHELXS-97 and refined by full-matrix least squares on F^2 using SHELXL-97. The hydrogen atoms were introduced at calculated positions and were not refined (riding model).

2. Synthesis

All reagents were purchased from commercial sources and used without further purification, except for pyrrole and NBS^1 . The support used for chromatography was Geduran, Silica Gel Si 60 (40-63 μm) from Merck.

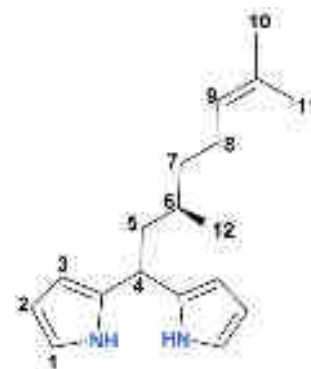
R-citronellyldipyrromethane 1

Chemical formula: $\text{C}_{18}\text{H}_{26}\text{N}_2$

Molecular weight: 270.21 g/mol

The synthesis was achieved by modifying a described procedure.²

Trifluoroacetic acid (0.110 mL, 1.4 mmol, 0.1 eq) was added to a solution of *R*-citronellal (2.59 mL, 14 mmol, 1 eq) in pyrrole (40 mL, 576 mmol, 40 eq) freshly filtered over an alumina pad. The mixture, protected from



light, was stirred under Argon at room temperature for 4h. Pyrrole was removed under reduced pressure and the green residue was diluted in 200 mL of chloroform. The solution was washed subsequently with water (2 x 100 mL) and 1M KOH (2 x 100 mL). The organic layer was dried over anhydrous Na_2SO_4 and evaporated. The dark oil thus obtained was purified by column chromatography (SiO_2 , cyclohexane: dichloromethane 1:1) to give the pure product as a yellow oil (2.6 g, 67%).

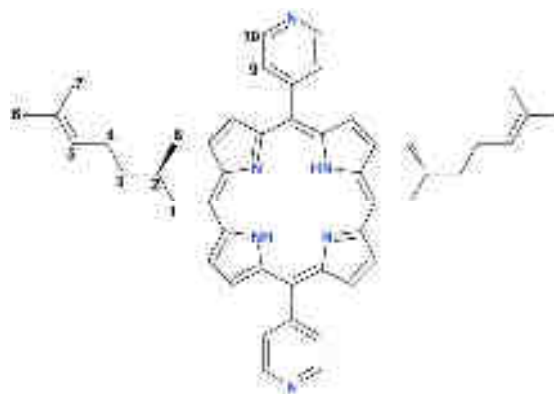
$^1\text{H-NMR}$ (400 MHz, CDCl_3) δ (ppm) : 0.92 (d, $J = 6.5 \text{ Hz}$, 3H, H_{12}), 1.18 (m, 1H, H_6), 1.38 (m, 2H, H_5), 1.6 (s, 3H, H_{10} or H_{11}), 1.74 (s, 3H, H_{10} or H_{11}), 1.95 (m, 4H, H_7 and H_8), 4.10 (t, $J = 7.5 \text{ Hz}$, 1H, H_4), 5.09 (t, $J = 7.5 \text{ Hz}$, 1H, H_9), 6.06 (br, 2H, H_2), 6.15 (m, 2H, H_3), 6.59 (m, 2H, H_1), 7.69 (br, 2H, NH).

5, 15-di (3*R*- citronellyl)-10, 20-dipyridylporphyrin **2**

Chemical formula: C₄₈H₅₂N₆

Molecular weight: 712.43g/mol

A solution of dipyrromethane **1** (0.26 g, 0.9 mmol, 1eq) and 4-pyridinecarboxaldehyde (0.09 mL, 0.9 mmol, 1eq) in CH₂Cl₂/MeOH (210:5mL) mixture was flushed with Ar for 15 min and treated with trifluoroacetic acid (0.21 mL, 2.7 mmol, 3 eq). The



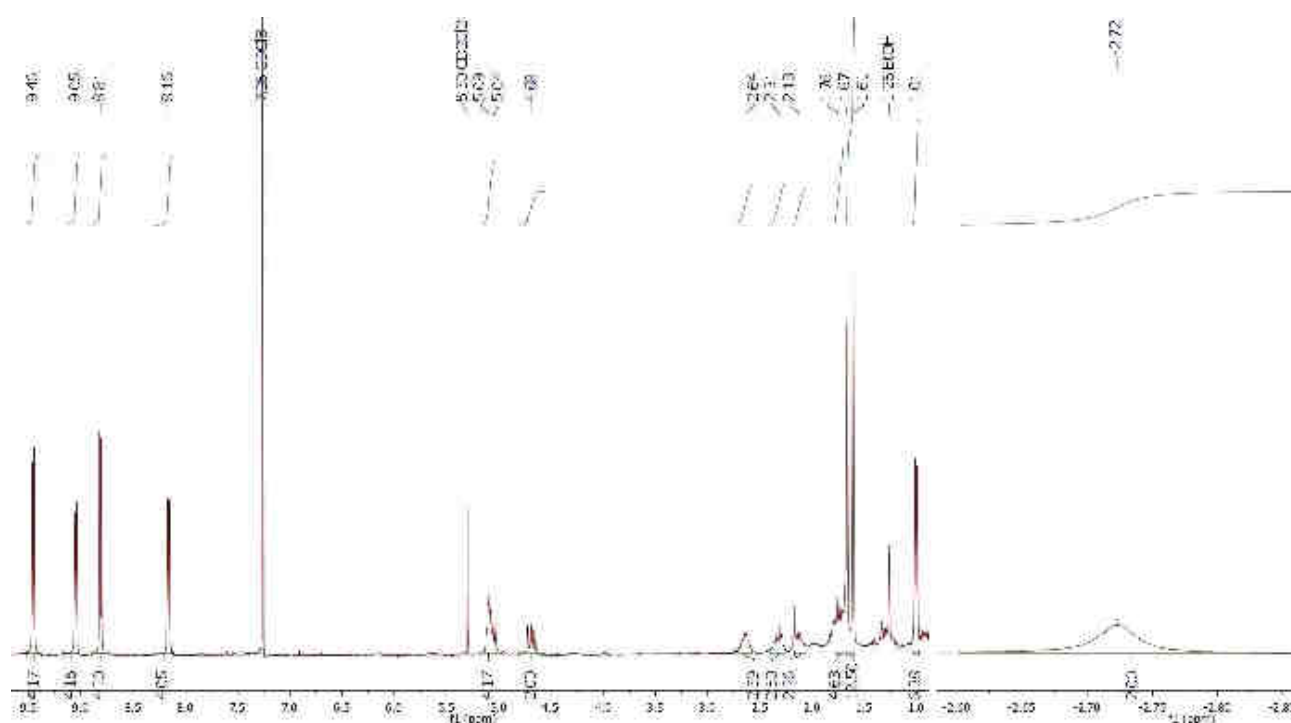
mixture protected from light, was stirred under Ar for 24h. DDQ (0.30 g, 1.35 mmol, 1.5 eq) was added to the reaction and stirred overnight. Triethylamine (0.07 mL, 0.54 mmol, 0.6 eq) was added and the solvent was evaporated under reduced pressure. The mixture was purified by column chromatography (SiO₂, dichloromethane 1% MeOH) to afford a pure purple solid (0.05 g, 16%).

¹H-NMR (300 MHz, CDCl₃) δ (ppm) : - 2.72 (s, br, 2H, NH), 1.01 (d, J = 6.6 Hz, 6H, H₈), 1.61 (s, 6H, H₆ or H₇), 1.67 (s, 6H, H₆ or H₇), 1.76 (m, 4H, H₄), 2.13 (m, 2H, H₃), 2.31 (m, 2H, H₃), 2.64 (m, 2H, H₂), 4.68 (m, 2H, H₁), 5.04 (m, 2H, H₁), 5.09 (m, 2H, H₅), 8.16 (dd, J = 5.9 and 2.7 Hz, 4H, H₉), 8.81 (d, J = 4.9 Hz, 4H, H_{βpyr}), 9.05 (dd, J = 5.7 and 2.8 Hz, 4H, H₁₀), 9.45 (d, J = 5 Hz, 4H, H_{βpyr}).

¹³C-NMR (125 MHz, CDCl₃) δ (ppm) : 17.73(CH₃), 20.17(CH₃), 25.70(CH₃), 25.91(CH₂), 38.00(CH₂), 41.35(CH₂), 116.01(CH), 119.61(CH), 124.70 (CH), 129.50 (CH), 131.72(CH), 148.26 (C), 151.32 (C).

λ_{max} (CH₂Cl₂)/nm (ε x 10⁴/L mol⁻¹ cm⁻¹) : 418 (45.07), 517 (0.2), 552 (0.09), 593 (0.062), 649 (0.063)

m/z (HRM⁺) [M+H⁺]_{calc} = 713.43, [M+H⁺]_{found} = 713.433.



3, 3, 3-trifluoropropylidipyrromethane **3**

Chemical formula: C₁₂H₁₃F₃N₂

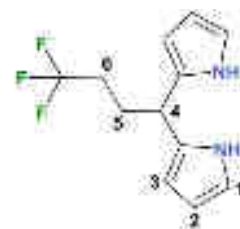
Molecular weight: 242.10 g/mol

The synthesis was achieved by modifying a described procedure.²

Trifluoroacetic acid (0.036 mL, 0.4 mmol, 0.1 eq) was added to a solution of **4**, 4, 4-trifluorobutanal (0.5 mL, 4.7 mmol, 1 eq) in pyrrole (13.2 mL, 190 mmol, 40 eq) freshly filtered over an alumina pad. The mixture, protected from light, was stirred under Ar at room temperature for 24 h. Pyrrole was removed under reduced pressure and the green residue was diluted in 100 mL of chloroform. The organic phase was washed with water (2 x 50 mL) and 1M KOH (2 x 50 mL) and then dried over anhydrous Na₂SO₄ and evaporated. The dark oil thus obtained was purified by column chromatography (SiO₂, cyclohexane: dichloromethane 1:1) to give the pure product as a white solid. (0.6 g, 53%)

¹H-NMR (300 MHz, CDCl₃) δ (ppm) : 2.10 (m, 2H, H₅), 2.19 (m, 2H, H₆), 4.05 (t, J = 7.4 Hz, 1H, H₄), 6.09 (br, 2H, H₂), 6.16 (dd, J = 8.8 and 3.1 Hz, 2H, H₃), 6.67(m, 2H, H₁), 7.82 (br, 2H, NH).

¹³C-NMR (100 CDCl₃) δ (ppm) : 32.04 (CH₂), 36.78 (CH₂), 105.90 (CH), 108.40 (CH), 117.67 (CH), 131.17 (C).



5,15-di (pyridin-4-yl)-10,20-bis (3,3,3-trifluoropropyl) porphyrin **4**

Chemical formula: C₃₆H₂₆F₆N₆

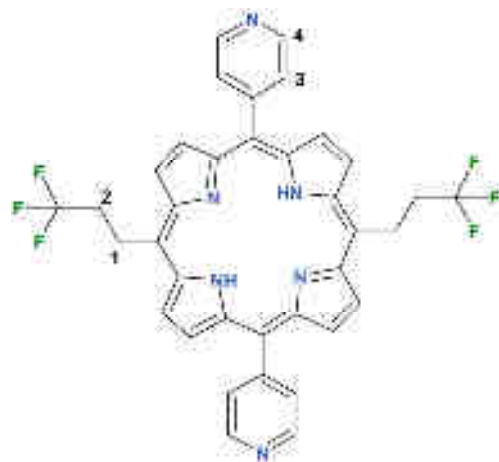
Molecular weight: 656.21g/mol

A solution of dipyrromethane **3** (0.38 g, 1.56 mmol, 1eq) and 4-pyridinecarboxaldehyde (0.143 mL, 1.56 mmol, 1eq) in CH₂Cl₂/MeOH (285:15) mixture was flushed with Argon for 15 min and treated with trifluoroacetic acid (0.35 mL, 4.68 mmol, 3 eq). The mixture, protected from light, was stirred under Ar for 72h. DDQ (0.54 g, 2.34 mmol, 1.5 eq) was added and the mixture further stirred overnight. Triethylamine (0.3 mL, 0.93 mmol, 0.6 eq) was added and volatiles were evaporated under reduced pressure. The mixture was purified by column chromatography (SiO₂, dichloromethane: acetone 7:3) to afford a pure purple solid (0.03 g, 6%).

¹H-NMR (500 MHz, CDCl₃) δ (ppm) : - 2.85 (s, br, 2H, NH), 3.30 (m, 4H, H₂), 5.27 (m, 4H, H₁), 8.14 (dd, J = 5.9 and 2.7 Hz, 4H, H₃), 8.89(d, J = 4.7 Hz, 4H, H_{βpyr}), 9.08 (dd, J = 5.8 and 2.7 Hz, 4H, H₄), 9.47 (d, J = 4.8 Hz, 4H, H_{βpyr}).

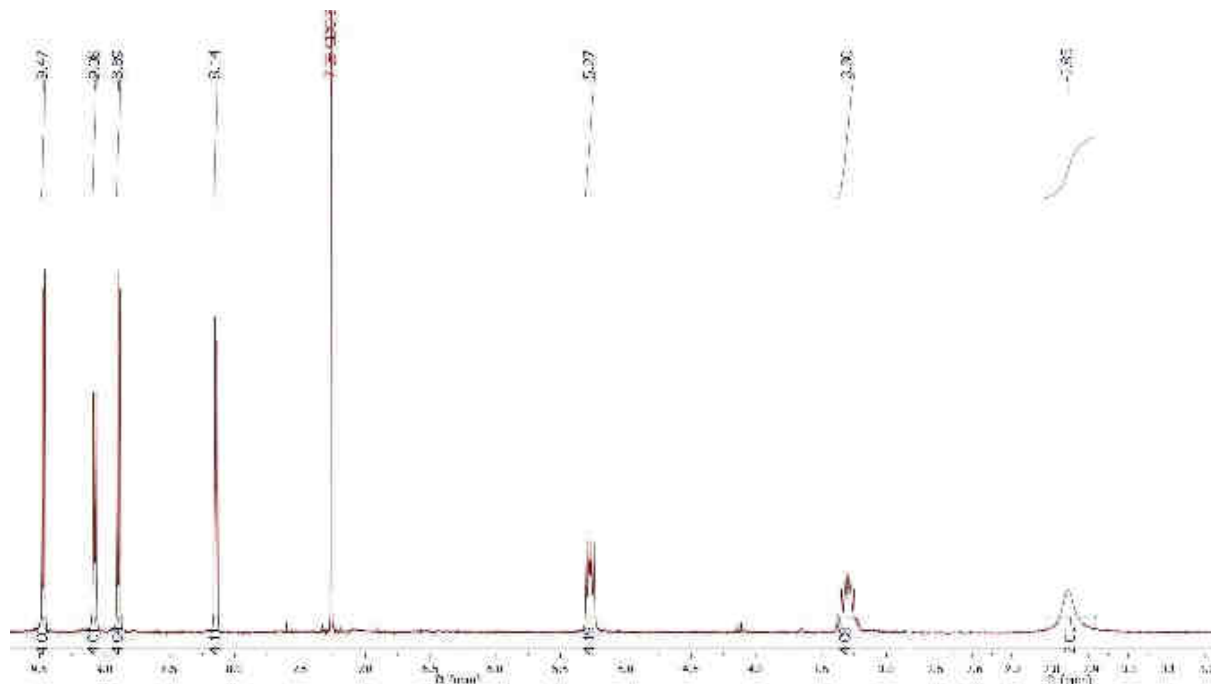
¹³C-NMR (125 MHz, CDCl₃) δ (ppm) : 27.79 (C₁), 41.19 (C₂), 116.16 (CH), 117.01 (CH), 128.32 (CH), 129.48 (CH), 132.25 (CH), 148.61 (C), 150.35 (C).

¹⁹F-NMR (282.4 MHz, CDCl₃) δ (ppm) : -67.63 (s, 6F).



λ_{max} (CH₂Cl₂)/nm ($\epsilon \times 10^4/\text{L mol}^{-1} \text{ cm}^{-1}$): 417 (12.50), 514 (1.46), 547 (0.46), 591 (0.44), 649(0.23).

m/z (HRM⁺) [M+H⁺]_{calc} = 657.21, [M+H⁺]_{found} = 657.2133.



4-Pyridyldipyrromethane **5**

Chemical formula: C₁₄H₁₃N₃

Molecular weight: 223.11 g/mol

The synthesis was achieved according to a described procedure.³ 4-pyridinecarboxaldehyde was added (1.75 mL, 18.5 mmol, 1 eq) to pyrrole (40 mL, 592 mmol, 32 eq) freshly filtered over an alumina pad and bubbled with Ar for 10 min. The mixture, protected from light, was refluxed under Argon at 85° overnight. Pyrrole was removed under reduced pressure and the purple residue was purified by column chromatography (Al₂O₃, cyclohexane: dichloromethane 1:1) to give the pure product as a yellow powder (2 g, 48%).



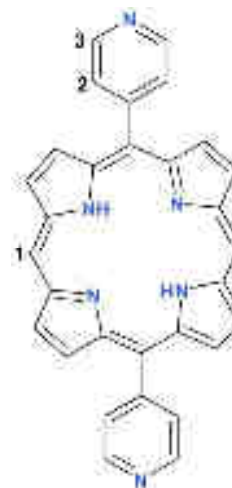
¹H-NMR (400 MHz, DMSO) δ (ppm) : 5.37 (s, 1H, H₄), 5.69 (br, 2H, H₂), 5.92 (dd, J = 6.6 and 2.6 Hz, 2H, H₃), 6.64 (dd, J = 6.5 and 2.4 Hz, 2H, H₁), 7.13 (d, J = 6.0 Hz, 2H, H₅), 8.45 (d, J = 6.0 Hz, 2H, H₆) 10.65 (br, 2H, NH).

5, 15-di (4-pyridyl) porphyrin **6**

Chemical formula: C₃₀H₂₀N₆

Molecular weight: 464.17 g/mol

The synthesis was achieved using a slightly modified reported procedure.⁴ A solution of dipyrromethane **5** (0.5 g, 2.24 mmol,) and trimethyl orthoformate (18 mL, 0.17 mol) in CH₂Cl₂ (500 mL) was flushed with Ar for 15 min and treated with trifluoroacetic acid (5 mL, 0.06 mol). The mixture, protected from light, was stirred under Ar for 8h. Triethylamine (7 mL) was added and the reaction mixture was further stirred overnight. The solution was purged with air for 15 min and



stirred under ambient conditions for 2h. Solvents were evaporated under reduced pressure. The mixture was pre-adsorbed on silica and separated by column chromatography (SiO₂, dichloromethane 1% methanol) to afford a pure purple solid (0.100 g, 19%).

¹H-NMR (300 MHz, CDCl₃) δ (ppm) : - 3.19 (s, br, 2H, NH), 8.27 (dd, J = 5.5 and 2.6 Hz, 4H, H₂), 9.05 (d, J = 4.9 Hz, 4H, H_{βpyr}), 9.10 (dd, J = 5.6 and 2.7 Hz, 4H, H₃), 9.47 (d, J = 4.8 Hz, 4H, H_{βpyr}), 10.40 (s, 2H, H₁).

¹³C-NMR: Owing to the low solubility of the compound, no ¹³C spectra could be acquired.

5, 15-dibromo-10, 20-di (pyridin-4-yl) porphyrin **7**

Chemical formula: C₃₀H₁₈Br₂N₆

Molecular weight: 620 g/mol

A solution of 5,15-di (4-pyridyl) porphyrin (0.100 g, 0.12 mmol, 1eq) in CHCl₃ (90 mL) and pyridine (0.8 mL) was treated with NBS¹ (0.080 g, 0.45 mmol, 2.1 eq). The mixture was stirred, at 0°C, for 5h and quenched with acetone (10 mL). Solvents were evaporated under reduced pressure and the mixture was purified by washing 3 times with MeOH to afford a pure purple solid (0.040 g, 54%).

¹H-NMR (300 MHz, CDCl₃) δ (ppm) : - 2.79 (s, br, 2H, NH), 8.11 (dd, J = 5.8 and 2.7 Hz, 4H, H₁), 8.78 (d, J = 5.2 Hz, 4H, H_{βpyr}), 9.06 (dd, J = 5.7 and 2.7 Hz, 4H, H₂), 9.66 (d, J = 5.1 Hz, 4H, H_{βpyr}).

¹³C-NMR: Owing to the low solubility of the compound, no ¹³C spectra could be acquired.



5, 15-di (pyridin-4-yl)-10, 20-bis (2,2,2-trifluoroethoxy) porphyrin **8**

Chemical formula: C₃₄H₂₂F₆N₆O₂

Molecular weight: 660.17 g/mol

A dried Schlenk tube connected to a vacuum line was degassed and purged with argon. Tube was charged with Pd₂(dba)₃ (4.6 mg, 0.005 mmol, 0.1 eq), phosphine ligand DPEPhos (13.5 mg, 0.01 mmol, 0.2 eq), di-bromoporphyrin **7** (30 mg, 0.05 mmol, 1 eq) and Cs₂CO₃ (65 mg, 0.2 mmol, 4 eq). The tube was backfilled with argon then 6 mL of toluene and 2,2,2-trifluoroethan-1-ol (30 μL, 0.2 mmol, 4 eq) is added. The tube was purged with argon for 2 min. and the mixture was heated in an oil bath for 48h at 100°C. After cooling to room temperature, the reaction mixture was diluted with ethyl acetate (100 mL) and washed with water (3 x 50 mL). Volatiles were evaporated under reduced pressure and the mixture was purified by column chromatography (SiO₂, ethyl acetate: cyclohexane 8:2) to afford the desired product **8** (0.010 g, 31%) as a pure purple solid.

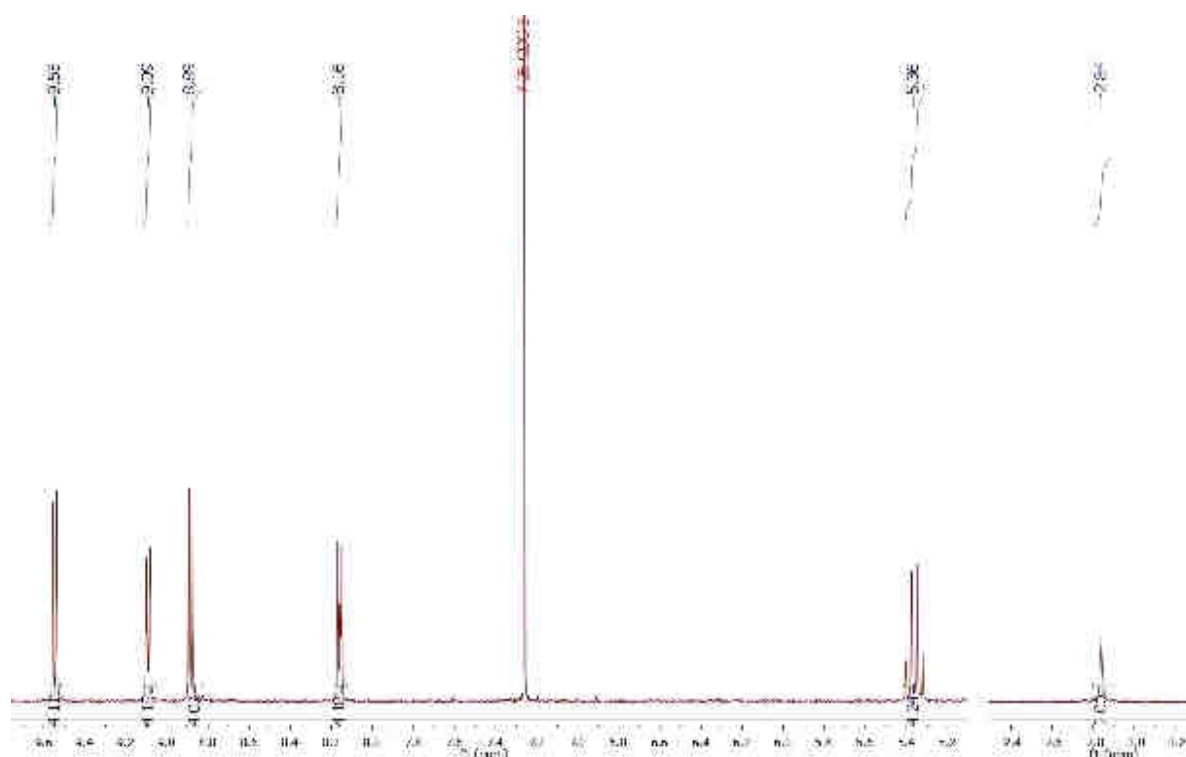
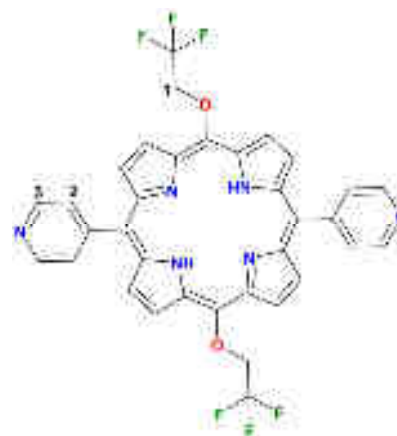
$^1\text{H-NMR}$ (300 MHz, CDCl_3) δ (ppm) : - 2.84 (s, br, 2H, NH), 5.36 (q, $J=8.2$ Hz, 4H, H_1), 8.16 (dd, $J = 5.9$ and 2.6 Hz, 4H, H_2), 8.89 (d, $J = 4.8$ Hz, 4H, $\text{H}_{\beta\text{pyr}}$), 9.09 (dd, $J = 5.8$ and 2.7 Hz, 4H, H_3), 9.55 (d, $J = 4.8$ Hz, 4H, $\text{H}_{\beta\text{pyr}}$).

$^{13}\text{C-NMR}$ (125 MHz, CDCl_3) δ (ppm) : 117.81 (CH), 127.68 (CH), 129.64 (CH), 131.39 (CH), 136.09 (CH), 148.69 (C), 149.45 (C).

$^{19}\text{F NMR}$ (282 MHz, CDCl_3) δ (ppm) : -73.55 (s, 6F).

λ_{max} (CH_2Cl_2)/nm ($\epsilon \times 10^4/\text{L mol}^{-1} \text{ cm}^{-1}$): 413 (17.02), 513 (0.58), 549 (0.34), 595 (0.14), 651 (0.23).

m/z (HRM^+) [$\text{M}+\text{H}^+$] $_{\text{calc}} = 661.17$, [$\text{M}+\text{H}^+$] $_{\text{found}} = 661.1722$.



5,15-bis(2,2,3,3,3-pentafluoropropoxy)-10,20-di(pyridin-4-yl)porphyrin **9**

Chemical formula: $\text{C}_{36}\text{H}_{22}\text{F}_{10}\text{N}_6\text{O}_2$

Molecular weight: 760.16 g/mol

A dried Schlenk tube connected to a vacuum line was degassed and purged with argon. The tube was charged with $\text{Pd}_2(\text{dba})_3$ (4.6 mg, 0.005 mmol, 0.1 eq), phosphine ligand DPEPhos (13.5 mg, 0.01 mmol, 0.2 eq), di-bromoporphyrin **7** (30 mg, 0.05 mmol, 1 eq) and Cs_2CO_3 (65 mg, 0.2 mmol, 4 eq). The tube was backfilled with argon before 6 mL of toluene and 2,2,3,3,3-pentafluoropropan-1-ol (30 μL , 0.2 mmol, 4eq) was added. The tube was purged with argon for 2 min. and the reaction mixture was heated in an oil bath at 80 $^\circ\text{C}$ for 5h. After cooling to room temperature, the reaction mixture was diluted with ethyl acetate (100 mL) and washed with water (3 x 50 mL). Volatiles were evaporated under reduced pressure and the mixture was purified by column chromatography (SiO_2 , CH_2Cl_2 : Acetone 7:3) to afford the desired compound **9** (0.010 g, 28%) as a purple solid.

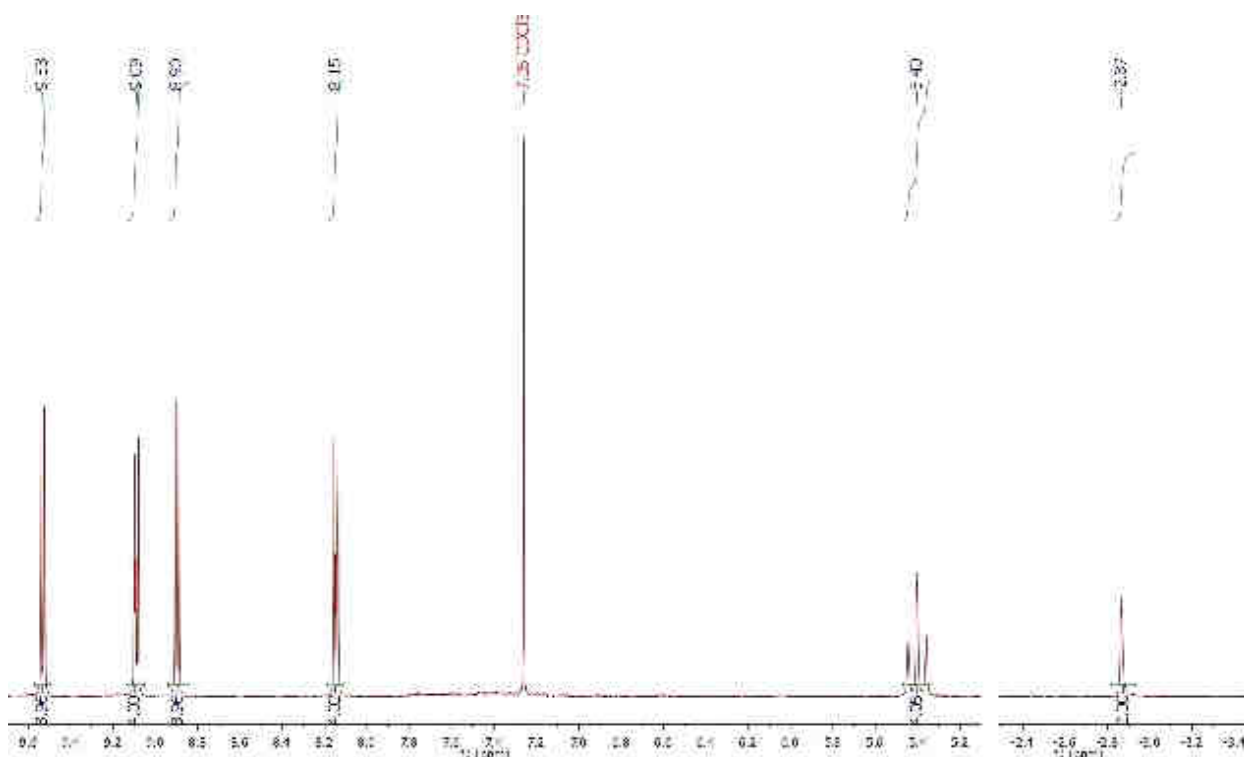
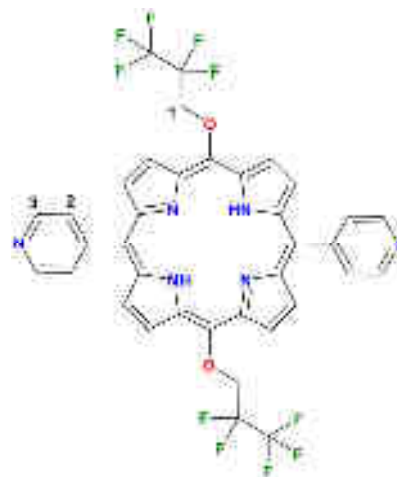
$^1\text{H-NMR}$ (300 MHz, CDCl_3) δ (ppm) : - 2.87 (s, br, 2H, NH), 5.40 (t, $J = 12.5$ Hz, 4H, H_1), 8.15 (dd, $J = 5.9$ and 2.6 Hz, 4H, H_2), 8.90 (d, $J = 4.8$ Hz, 4H, $\text{H}_{\beta\text{pyr}}$), 9.09 (dd, $J = 5.8$ and 2.7 Hz, 4H, H_3), 9.53 (d, $J = 4.8$ Hz, 4H, $\text{H}_{\beta\text{pyr}}$).

$^{13}\text{C-NMR}$ (125 MHz, CDCl_3) δ (ppm) : 117.71 (CH), 127.35 (CH), 129.43 (CH), 131.41 (CH), 135.65 (CH), 148.66 (C), 149.05 (C).

$^{19}\text{F-NMR}$ (282 MHz, CDCl_3) δ (ppm) : -124.12 (s, 4F), -83.82 (br, 6F).

λ_{max} (CH_2Cl_2)/nm ($\epsilon \times 10^4/\text{L mol}^{-1} \text{cm}^{-1}$): 413 (10.9), 512 (2.34), 547 (1.35), 593 (0.6), 650 (0.89).

m/z (HRM $^+$) [$\text{M}+\text{H}^+$] $_{\text{calc}} = 761.16$, [$\text{M}+\text{H}^+$] $_{\text{found}} = 761.1730$.



5,15-bis(2,2,3,3,4,4,4-heptafluorobutoxy)-10,20-di(pyridin-4-yl)porphyrin 10

Chemical formula: $\text{C}_{38}\text{H}_{22}\text{F}_{14}\text{N}_6\text{O}_2$

Molecular weight: 860.16 g/mol

A dried Schlenk tube connected to a vacuum line was degassed and purged with argon. The tube was charged with $\text{Pd}_2(\text{dba})_3$ (4.6 mg, 0.005 mmol, 0.1 eq), phosphine ligand DPEPhos (13.5 mg, 0.01 mmol, 0.2 eq), di-bromoporphyrin **7** (30 mg, 0.05 mmol, 1 eq) and Cs_2CO_3 (65 mg, 0.2 mmol, 4 eq). The tube was backfilled with argon then 6 mL of toluene and 2,2,3,3,4,4,4-heptafluorobutan-1-ol (30 μL , 0.2 mmol, 4 eq) was added. The tube was purged with argon for 2 min. and the reaction mixture was heated in an oil bath for 7h at 80 $^\circ\text{C}$. After cooling to room temperature, the reaction mixture was diluted with ethyl acetate (100 mL) and washed with water (3 x 50 mL). Volatiles were evaporated under reduced pressure and the mixture was purified by column

x 50mL). The solvent was evaporated under reduced pressure and the mixture was purified by column chromatography (SiO₂, CH₂Cl₂: Acetone 7:3) to afford the desired compound **11** (0.020 g, 45%) as a purple solid.

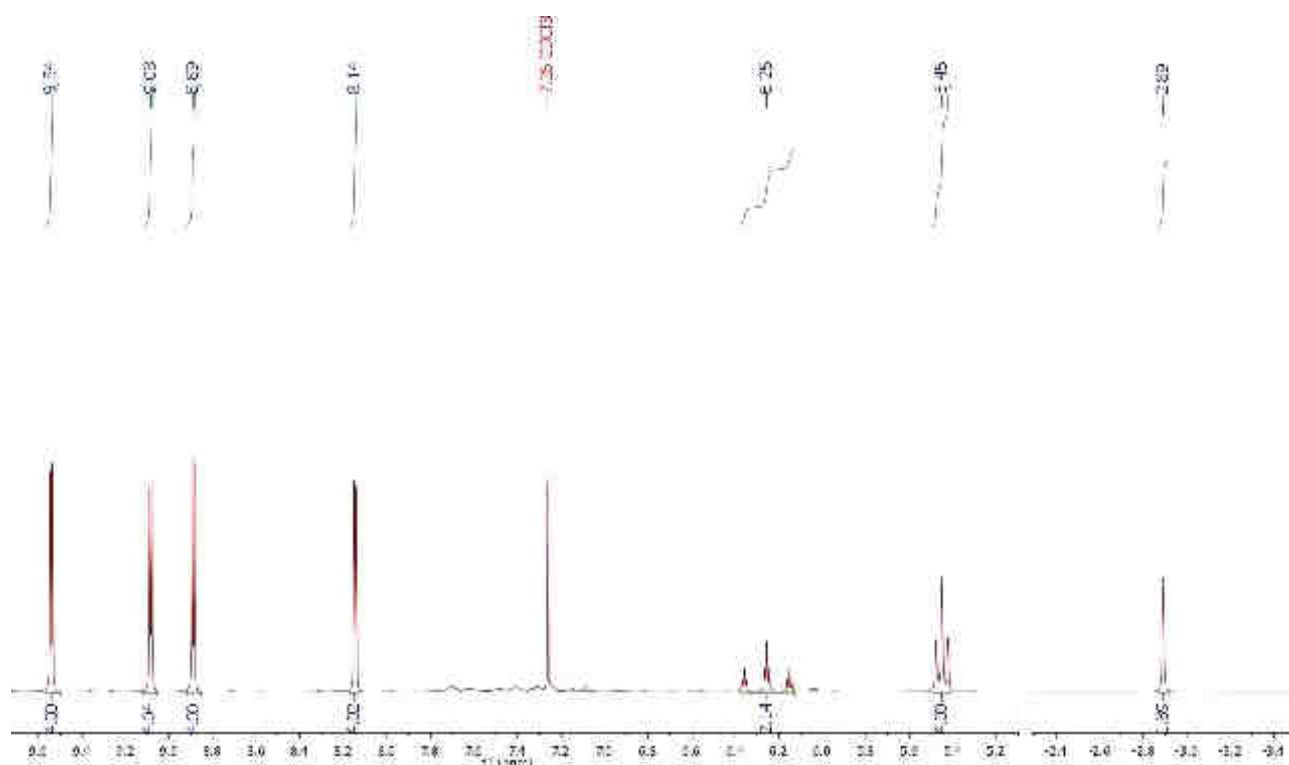
¹H-NMR (500 MHz, CDCl₃) δ (ppm) : - 2.89 (s, 2H, NH), 5.45 (t, J = 13.5 Hz, 4H, H₁), 6.25 (tt, J= 52 Hz and 5 Hz, 2H, H₂), 8.14 (dd, J = 5.7 and 2.6 Hz, 4H, H₃), 8.89 (d, J = 4.7 Hz, 4H, H_{βpyr}), 9.08 (dd, J= 5.7 and 2.8 Hz, 4H, H₄), 9.54 (d, J = 4.8 Hz, 4H, H_{βpyr}).

¹³C-NMR (125 MHz, CDCl₃) δ (ppm) : 107.93 (CF₂) 117.84 (CH), 127.61 (CH), 129.60 (CH), 131.61 (CH), 136.01 (CH), 148.81 (C), 149.24 (C).

¹⁹F-NMR (282 MHz, CDCl₃) δ (ppm) : -136.93 (m, 2F), -129.50 (m, 2F), -124.52 (m, 2F), -119.44 (m, 2F).

λ_{max} (CH₂Cl₂)/nm (ε x 10⁴/L mol⁻¹ cm⁻¹) : 413 (15.7), 512 (2.99), 547 (1.79), 593 (0.79), 650 (1.17).

m/z (HRM⁺) [M+H⁺]_{calc} = 925.17, [M+H⁺]_{found} = 925.1799.



(*R, R*)-5, 15-di-*sec*-butoxy-10, 20-di (pyridin-4-yl) porphyrin **12**-(*R, R*)

Chemical formula: C₃₈H₃₆N₆O₂

Molecular weight: 608.29 g/mol

A dried Schlenk tube connected to a vacuum line was degassed and purged with argon. The tube was charged with Pd₂(dba)₃ (4.6 mg, 0.005 mmol, 0.1 eq), phosphine ligand DPEPhos (13.5 mg, 0.01 mmol, 0.2 eq), di-bromoporphyrin **7** (30 mg, 0.05 mmol, 1 eq) and Cs₂CO₃ (65 mg, 0.2 mmol, 4 eq). The tube was backfilled with argon then 6 mL of toluene and (*R*)-butan-2-ol (30 μL, 0.2 mmol, 4 eq) was added. The tube was purged with argon for 2 min. and the reaction mixture was

heated in an oil bath for 4h at 80 °C. After cooling to room temperature, the reaction mixture was diluted with ethyl acetate (100 mL) and washed with water (3 x 50 mL). The solvent was evaporated under reduced pressure and the mixture was purified by column chromatography (SiO₂, ethyl acetate: cyclohexane 80:20) to afford the desired compound **12**-(R, R) (0.020 g, 69%) as a purple solid.

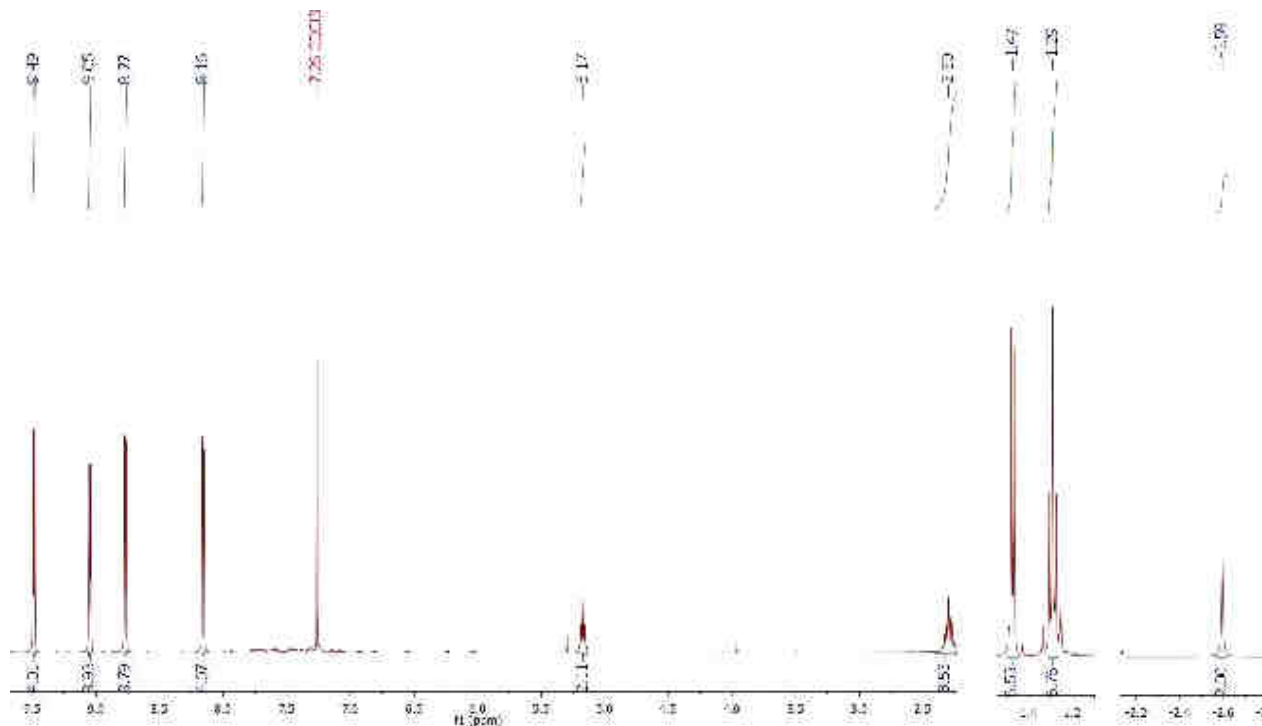


¹H-NMR (500 MHz, CDCl₃) δ (ppm) : - 2.59 (s, br, 2H, NH), 1.29 (t, J = 7.3 Hz, 6H, H₃), 1.47 (d, J = 6.2 Hz, 6H, H₄), 2.30 (m, 4H, H₂), 5.17 (m, 2H, H₁), 8.16 (dd, J = 5.8 and 2.7 Hz, 4H, H₅), 8.77 (d, J = 4.6 Hz, 4H, H_{βpyr}), 9.05 (dd, J = 5.6 and 2.6 Hz, 4H, H₆), 9.49(d, J = 4.5 Hz, 4H, H_{αpyr}).

¹³C-NMR (125 MHz, CDCl₃) δ (ppm) : 10.57 (CH₃), 20.16 (CH₃), 31.15 (CH₂), 90.65 (CH), 116.63 (CH), 128.40 (CH), 129.65 (CH), 136.79 (CH), 148.51 (C), 150.15 (C).

λ_{max} (CH₂Cl₂)/nm (ε x 10⁴/L mol⁻¹ cm⁻¹) : 418 (38.4), 520 (0.58), 557 (0.63), 602 (0.14), 661 (0.53).

m/z (HRM⁺) [M+H⁺]_{calc} = 609.29, [M+H⁺]_{found} = 609.2937.



(S, S)-5, 15-di-sec-butoxy-10, 20-di (pyridin-4-yl) porphyrin **12**-(*S, S*)

Chemical formula: C₃₈H₃₆N₆O₂

Molecular weight: 608.29 g/mol

A dried Schlenk tube connected to a vacuum line was degassed and purged with argon. The tube was charged with Pd₂(dba)₃ (4.6 mg, 0.005 mmol, 0.1 eq), phosphine ligand DPEPhos (13.5 mg, 0.01 mmol, 0.2 eq), di-bromoporphyrin **7** (30 mg, 0.05 mmol, 1 eq) and Cs₂CO₃ (65 mg, 0.2 mmol, 4 eq). The tube was backfilled with argon then 6 mL of toluene and (*S*)-butan-2-ol (30 μL, 0.2 mmol, 4 eq) was added.

The tube was purged with argon for 2 min. and the reaction mixture was heated in an oil bath for 4h at 80 °C. After cooling to room temperature, the reaction mixture was diluted with ethyl acetate (100 mL) and washed with water (3 x 50 mL). The solvent was evaporated under reduced pressure and the mixture was purified by column chromatography (SiO₂, ethyl acetate: cyclohexane 80:20) to afford the desired compound **12** (*S, S*) (0.020 g, 69%) as a purple solid.

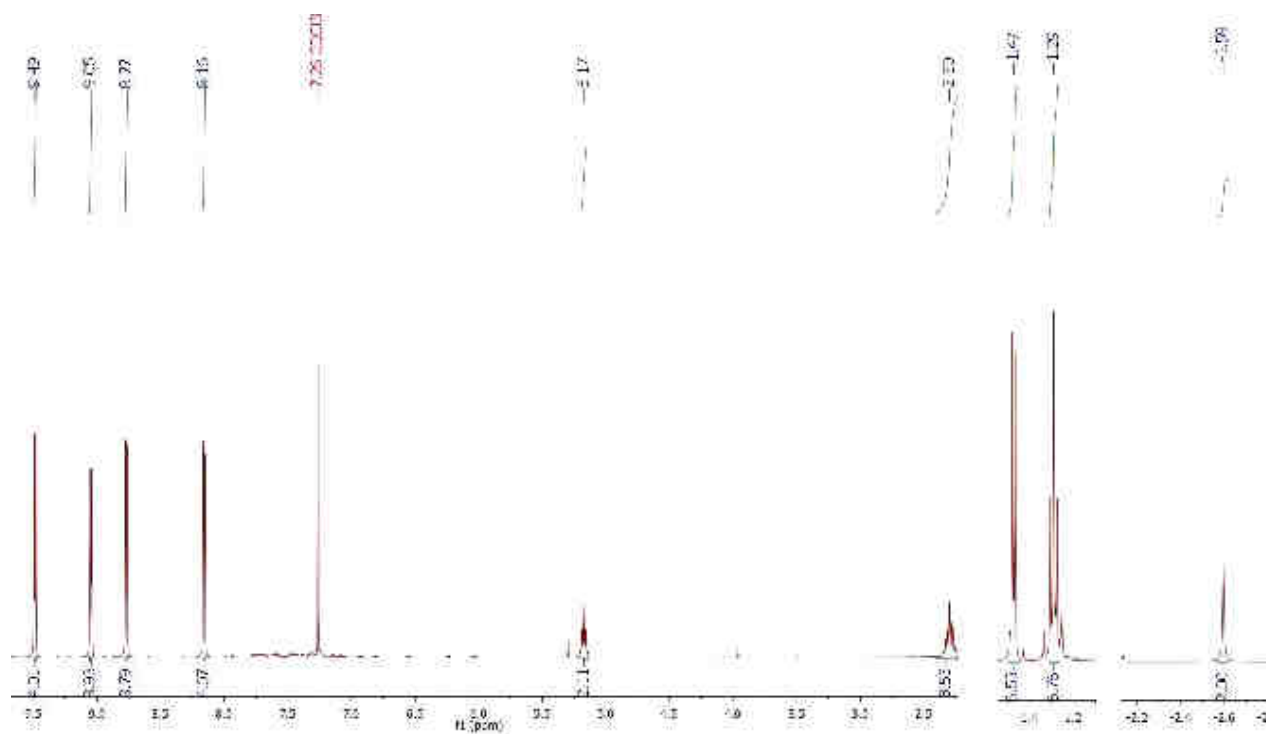


¹H-NMR (500 MHz, CDCl₃) δ (ppm) : - 2.59 (s, br, 2H, NH), 1.28 (t, J = 7.3 Hz, 6H, H₃), 1.47 (d, J = 6.2 Hz, 6H, H₄), 2.30 (m, 4H, H₂), 5.17 (m, 2H, H₁), 8.15 (dd, J = 5.8 and 2.7 Hz, 4H, H₅), 8.77 (d, J = 4.6 Hz, 4H, H_{βpyr}), 9.05 (dd, J = 5.6 and 2.6 Hz, 4H, H₆), 9.48(d, J = 4.5 Hz, 4H, H_{βpyr}).

¹³C-NMR (125 MHz, CDCl₃) δ (ppm) : 10.57 (CH₃), 20.16 (CH₃), 31.15 (CH₂), 90.65 (CH), 116.63 (CH), 128.40 (CH), 129.65 (CH), 130.17, 136.79 (CH), 148.51 (C), 150.15 (C).

λ_{max} (CH₂Cl₂)/nm (ε x 10⁴/L mol⁻¹ cm⁻¹) : 418 (38.4), 520 (0.58), 557 (0.63), 602 (0.14), 661 (0.53).

m/z (HRM⁺) [M+H⁺]_{calc} = 609.29, [M+H⁺]_{found} = 609.2967.

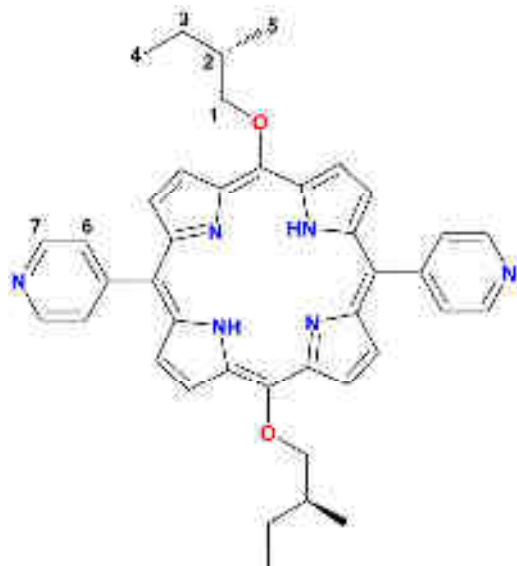


(S, S)-5,15-bis(2-methylbutoxy)-10,20-di(pyridin-4-yl) **13** (*S, S*)

Chemical formula: C₄₀H₄₀N₆O₂

Molecular weight: 636.32 g/mol

A dried Schlenk tube connected to a vacuum line was degassed and purged with argon. The tube was charged with Pd₂(dba)₃ (4.6 mg, 0.005 mmol, 0.1 eq), phosphine ligand DPEPhos (13.5 mg, 0.01 mmol, 0.2 eq), dibromoporphyrin **7** (30 mg, 0.05 mmol, 1 eq) and Cs₂CO₃ (65 mg, 0.2 mmol, 4 eq). The tube was backfilled with argon then 6 mL of toluene and (S)-2-methylbutan-1-ol (30 μL, 0.2 mmol, 4 eq) was added. The tube was purged with argon for 2 min. and the reaction mixture was heated in an oil bath for 5h at 80 °C. After cooling to room temperature, the reaction mixture was diluted with ethyl acetate (100 mL) and washed with water (3 x 50 mL). The solvent was evaporated under reduced pressure and the product is washed with MeOH to give a purple solid (0.027 g, 85%).

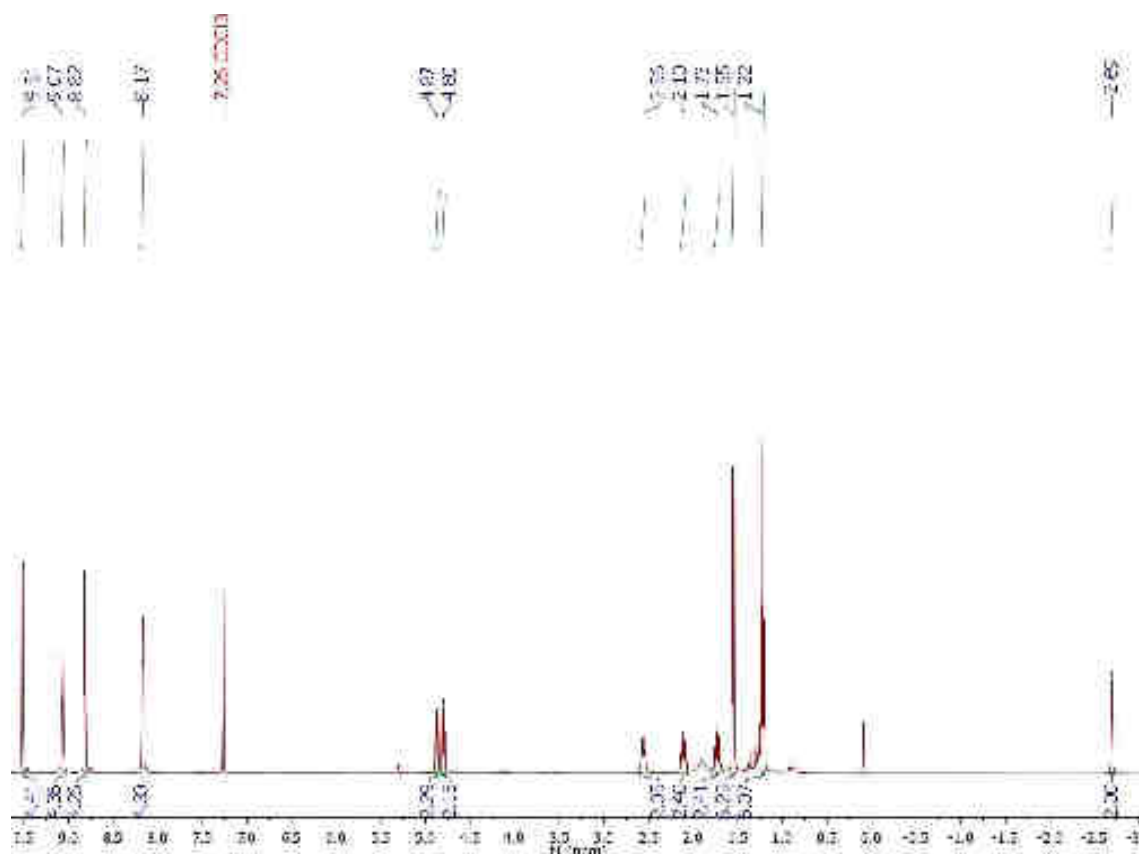


¹H-NMR (500 MHz, CDCl₃) δ (ppm) : - 2.69 (s, br, 2H, NH), 1.22 (t, J = 7.4 Hz, 6H, H₄), 1.55 (d, J = 6.4 Hz, 6H, H₅), 1.73 (m, 2H, H₃), 2.10 (m, 2H, H₃), 2.56 (m, 2H, H₂), 4.80 (dd, J= 9.1 and 5.8 Hz, 2H, H₁), 4.87 (dd, J= 9.1 and 5.8 Hz, 2H, H₁), 8.17 (d, J = 5.5 Hz, 4H, H₆), 8.82 (d, J = 4.6 Hz, 4H, H_{pyr}), 9.07 (d, J = 5.4 Hz, 4H, H₇), 9.51 (d, J = 4.8 Hz, 4H, H_{βpyr}).

¹³C-NMR (125 MHz, CDCl₃) δ (ppm) : 11.94 (CH₃), 17.34 (CH₃), 26.77 (CH₂), 37.04 (CH₂), 90.66 (CH), 116.64 (CH), 127.85 (CH), 129.72 (CH), 130.43, 138.58 (CH), 148.52 (C), 150.07 (C).

λ_{max} (CH₂Cl₂)/nm (ε x 10⁴/L mol⁻¹ cm⁻¹) : 416 (43.3), 517 (0.72), 553 (0.67), 599 (0.17), 656 (0.55).

m/z (HRM⁺) [M+H⁺] _{calc} = 637.32, [M+H⁺] _{found} = 637.3239.



5, 15-di (pyridin-4-yl)-10, 20-bis (4,4,4-trifluoro-3-methylbutoxy) porphyrin **14** (racemate+ meso)

Chemical formula: C₄₀H₃₄F₆N₆O₂

Molecular weight: 744.26 g/mol

Starting from a racemic mixture of 4,4,4-trifluoro-3-methylbutan-1-ol, the compound **14** was obtained as a mixture of the racemate (RR, SS) and the *meso* form (RS).

A dried Schlenk tube connected to a vacuum line was degassed and purged with argon. The tube was charged with Pd₂(dba)₃ (4.6 mg, 0.005 mmol, 0.1 eq), phosphine ligand DPEPhos (13.5 mg, 0.01 mmol, 0.2 eq), dibromoporphyrin **7** (30 mg, 0.05 mmol, 1 eq) and Cs₂CO₃ (65 mg, 0.2 mmol, 4 eq). The tube was backfilled with argon then 6 mL of toluene and 4,4,4-trifluoro-3-methylbutan-1-ol (30 μL, 0.2 mmol, 4 eq) was added. The tube was purged with argon for 2 min. and the reaction

mixture was heated to 100°C in an oil bath for 8h. After cooling to room temperature, the reaction mixture was diluted with ethyl acetate (100 mL) and washed with water (3 x 50 mL). The solvent was evaporated under reduced pressure and the mixture was purified by column chromatography (SiO₂, ethyl acetate: cyclohexane 8:2) to afford the desired compound **14** (0.020 g, 55%) as a purple solid.

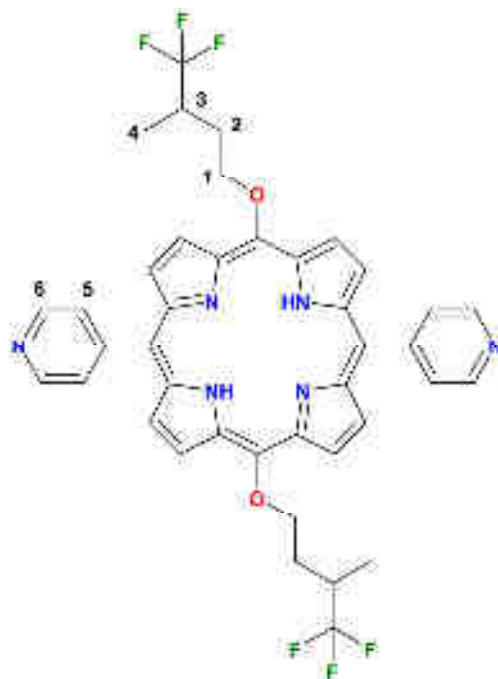
¹H-NMR (300 MHz, CDCl₃) δ (ppm) : - 2.72 (s, br, 2H, NH), 1.49 (d, J= 7.0Hz, 6H, H₄), 2.34 (m, 2H, H₂), 2.86 (m, 2H, H₂), 3.07 (m, 2H, H₃), 5.08 (t, J= 6.2Hz, 4H, H₁), 8.15 (dd, J = 5.9 and 2.7 Hz, 4H, H₅), 8.84 (d, J = 4.8 Hz, 4H, H_{βpyr}), 9.07 (dd, J = 5.8 and 2.7 Hz, 4H, H₆), 9.46 (d, J = 4.8 Hz, 4H, H_{βpyr}).

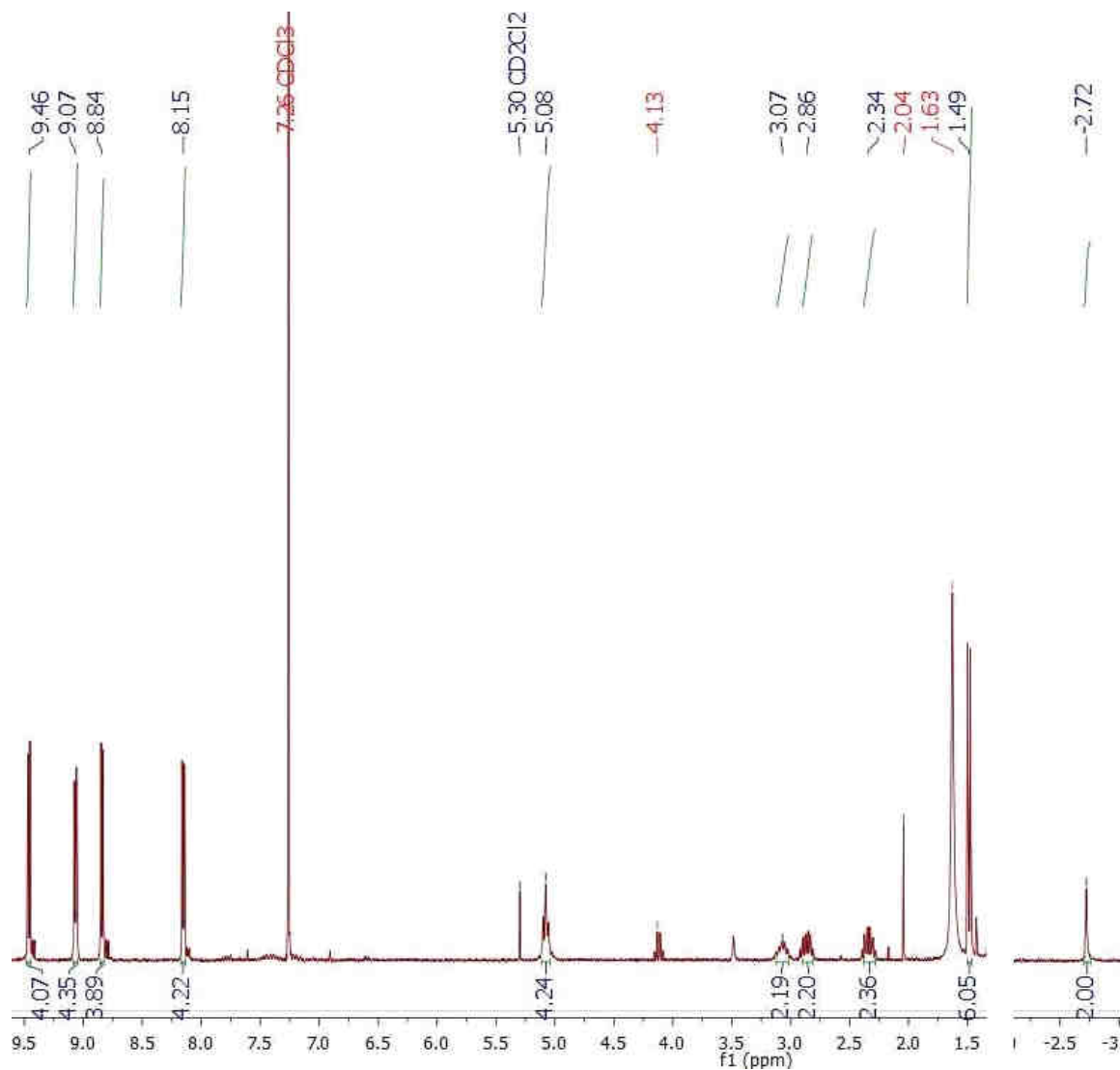
¹³C-NMR (125 MHz, CDCl₃) δ (ppm) : 12.21 (CH₃), 30.15 (CH₂), 34.28 (CH₂), 80.20 (CH), 115.89 (CH), 126.36 (CH), 128.42 (CH), 129.60, 136.61 (CH), 147.51 (C), 148.49 (C).

¹⁹F-NMR (282 MHz, CDCl₃) δ (ppm) : -72.93 (s, 6F).

λ_{max} (CH₂Cl₂)/nm (ε x 10⁴/L mol⁻¹ cm⁻¹) : 415 (40.85), 516 (0.61), 552 (0.49), 597 (0.23), 655 (0.45).

m/z (HRM⁺) [M+H⁺]_{calc} = 745. 26, [M+H⁺]_{found} = 745.2702.



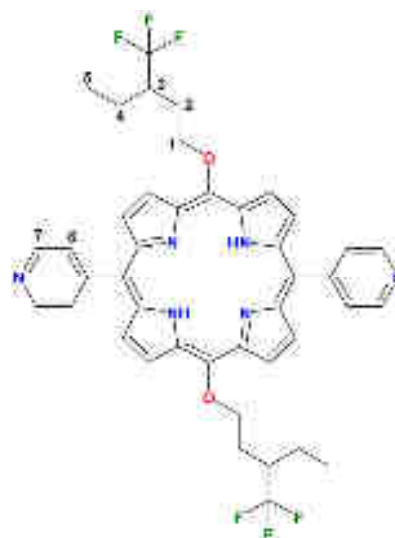


5,15-di(pyridin-4-yl)-10, 20-bis ((3-(trifluoromethyl) pentyl)oxy) porphyrin **15**(racemate+ meso)

Chemical formula: C₄₂H₃₈F₆N₆O₂

Molecular weight: 772.30 g/mol

Starting from a racemic mixture of 3-(trifluoromethyl) pentan-1-ol, the Compound **15** was obtained as a mixture of the racemate (RR, SS) and the *meso* form (RS). A dried Schlenk tube connected to a vacuum line was degassed and purged with argon. The tube was charged with Pd₂(dba)₃ (4.6 mg, 0.005 mmol, 0.1 eq), phosphine ligand DPEPhos (13.5 mg, 0.01 mmol, 0.2 eq), di-bromoporphyrin **7** (30 mg, 0.05 mmol, 1 eq) and Cs₂CO₃ (65 mg, 0.2 mmol, 4 eq). The tube was backfilled with argon then 6 mL of toluene and 3-(trifluoromethyl) pentan-1-ol (30 μL, 0.2 mmol, 4 eq) was added. The tube was purged with argon for 2 min. and the reaction mixture was heated in an oil bath for 48h to 100°C. After cooling to room temperature, the reaction mixture was diluted with ethyl acetate (100 mL) and washed with water (3 x 50 mL). The solvent was evaporated under reduced pressure and the mixture was purified by column



chromatography (SiO₂, ethyl acetate: cyclohexane 8:2) to afford the desired compound **15** (0.015 g, 40%) as a purple solid.

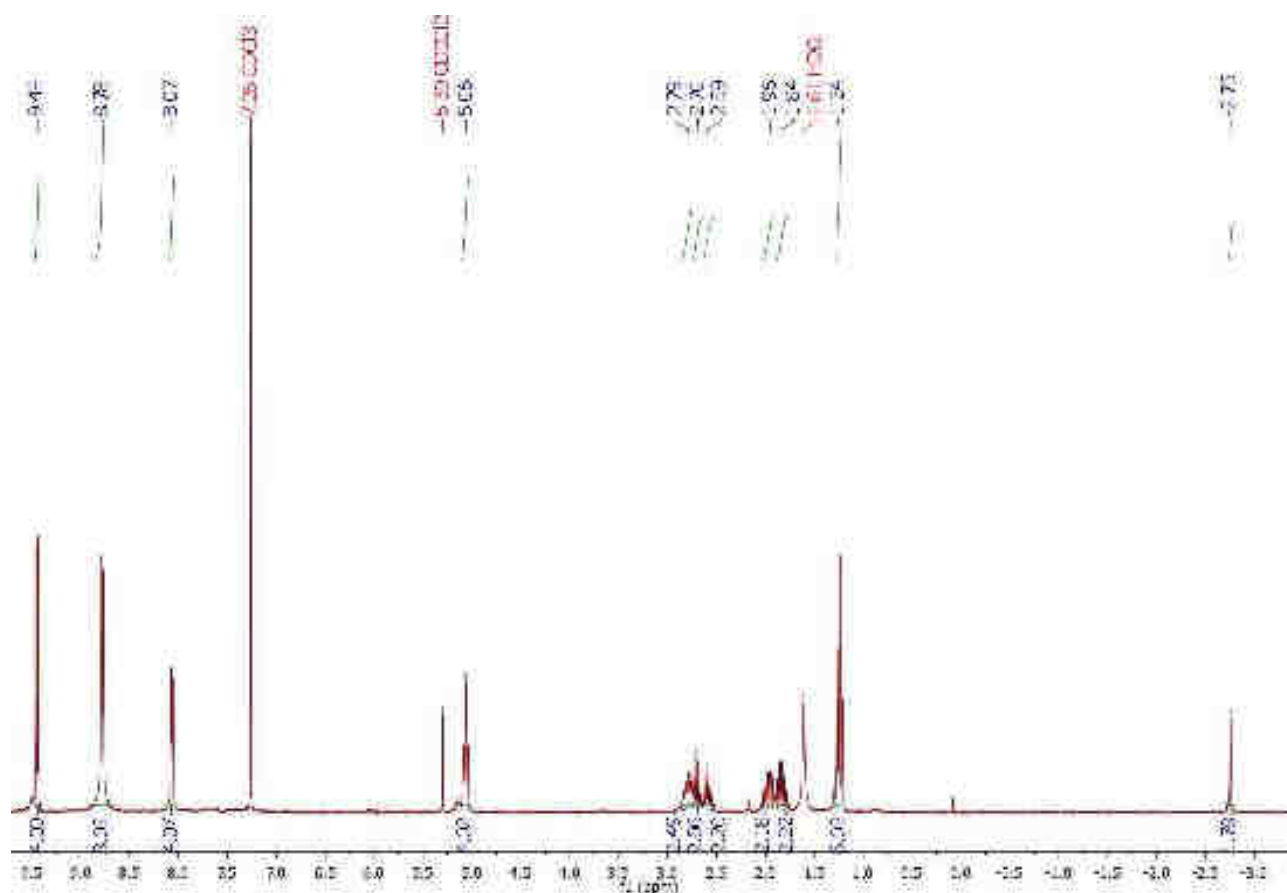
¹H-NMR (300 MHz, CDCl₃) δ (ppm) : - 2.75 (s, br, 2H, NH), 1.24 (t, J=7.3 Hz, 6H, H₅), 1.84 (m, 2H, H₂ or H₄), 1.96 (m, 2H, H₂ or H₄), 2.59 (m, 2H, H₄ or H₂), 2.70 (m, 2H, H₄ or H₂), 2.79 (m, 2H, H₃), 5.06 (t, J=6.6 Hz, 4H, H₁), 8.07 (dd, J = 5.8 and 2.6 Hz, 4H, H₆), 8.78 (8H, H_{βpyr} and H₇), 9.44 (d, J = 4.8 Hz, 4H, H_{βpyr}).

¹³C-NMR (90 MHz, CDCl₃) δ (ppm) : 11.45 (CH₃), 15.75 (CH₂), 21.43 (CH₂), 29.03 (CH₂), 41.16, 81.66 (CH), 116.78 (CH), 127.45 (CH), 129.39 (CH), 130.52 (CH), 137.72 (CH), 148.20 (C), 149.60 (C).

¹⁹F-NMR (282 MHz, CDCl₃) δ (ppm) : -69.66 (s, 6F).

λ_{max} (CH₂Cl₂)/nm (ε x 10⁴/L mol⁻¹ cm⁻¹) : 414 (43.07), 516 (0.59), 552 (0.55), 597 (0.18), 655 (0.39).

m/z (HRM⁺) [M+H⁺]_{calc} = 773.30 [M+H⁺]_{found} = 773.09



5,15-bis(2,2,3,4,4,4-hexafluorobutoxy)-10,20-di(pyridin-4-yl)porphyrin 16 (racemate + meso)

Chemical formula: C₃₈H₂₄F₁₂N₆O₂

Molecular weight: 824.63 g/mol

Starting from a racemic mixture of 2,2,3,4,4,4-hexafluorobutan-1-ol, the Compound **16** was obtained as a mixture of the racemate (RR, SS) and the *meso* form (RS). A dried Schlenk tube connected to a vacuum line was degassed and purged with argon. The tube was charged with Pd₂(dba)₃ (4.6 mg, 0.005 mmol, 0.1 eq), phosphine ligand DPEPhos (13.5 mg, 0.01 mmol, 0.2 eq), di-bromoporphyrin **7** (30 mg, 0.05 mmol, 1 eq) and Cs₂CO₃ (65 mg, 0.2 mmol, 4 eq). The tube was

backfilled with argon then 6 mL of toluene and 2,2,3,4,4,4-hexafluorobutan-1-ol (30 μ L, 0.2 mmol, 4 eq) was added. The tube was purged with argon for 2 min. and the reaction mixture was heated in an oil bath for 24h at 100°C. After cooling to room temperature, the reaction mixture was diluted with ethyl acetate (100 mL) and washed with water (3 x 50 mL). The solvent was evaporated under reduced pressure and the mixture was purified by column chromatography (SiO₂, ethyl acetate: cyclohexane 8:2) to afford the desired compound **16** (0.020 g, 51%) as a purple solid.



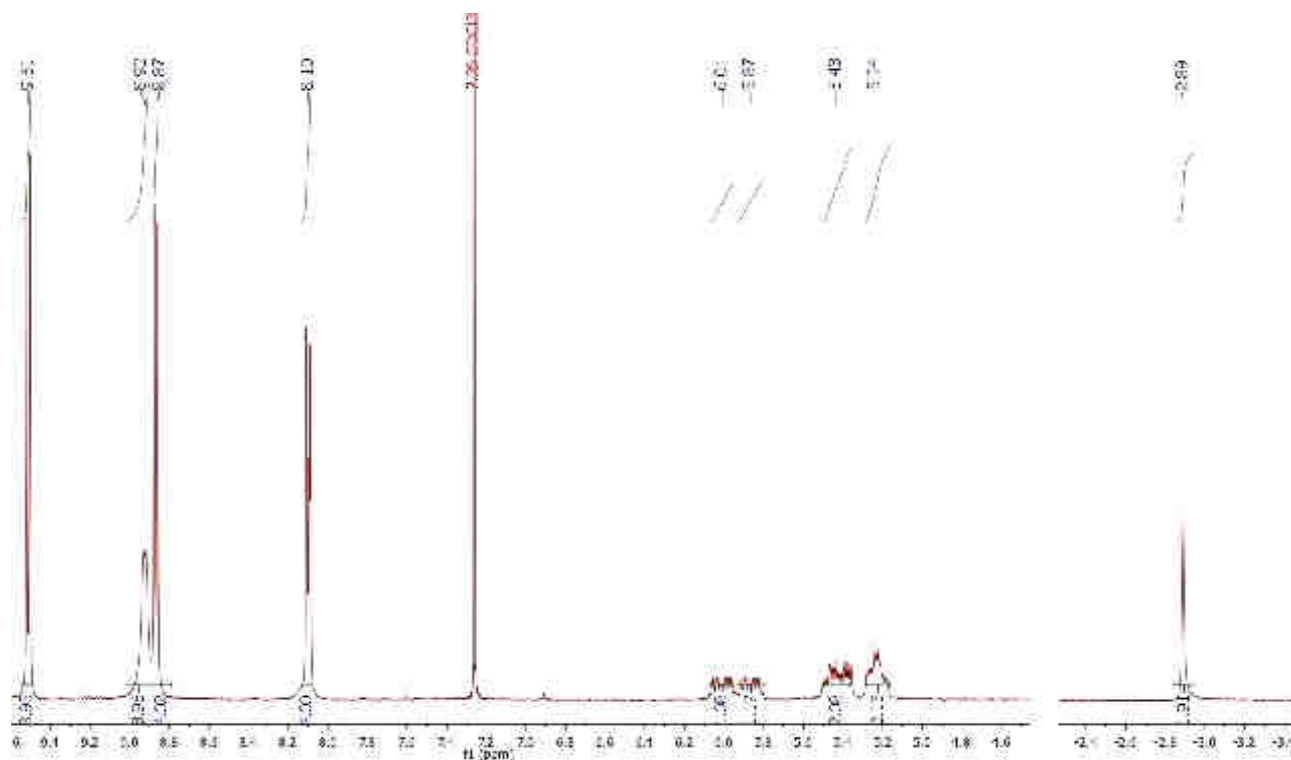
¹H-NMR (400 MHz, CDCl₃) δ (ppm) : - 2.89 (s, br, 2H, NH), 5.24 (m, 2H, H₁), 5.43 (m, 2H, H₁), 5.87 (m, 1H, H₂), 6.01 (m, 1H, H₂), 8.10 (dd, J = 5.9 and 2.6 Hz, 4H, H₃), 8.87 (d, J = 4.8 Hz, 4H, H _{β pyr}), 8.92 (dd, J = 5.9 and 2.8 Hz, 4H, H₄), 9.51 (d, J = 4.7 Hz, 4H, H _{β pyr}).

¹³C-NMR (90 MHz, CDCl₃) δ (ppm) : 117.83 (CH), 127.39(CH), 129.52(CH), 131.57(CH), 135.29(CH), 148.76(C), 149.15(C).

¹⁹F-NMR (282.4 MHz, CDCl₃) δ (ppm) : -211.92 (m, 2F), -122.60 (m, 1F), -121, 61 (m, 1F), -115.25 (m, 1F), -114.26 (m, 1F), -73.45 (m, 6F).

λ_{\max} (CH₂Cl₂)/nm ($\epsilon \times 10^4$ /L mol⁻¹ cm⁻¹) : 414 (18.35), 513 (3.82), 548 (2.32), 594 (1.14), 650 (1.46).

m/z (HRM⁺) [M+H⁺]_{calc} = 825.63, [M+H⁺]_{found} = 825.1820.

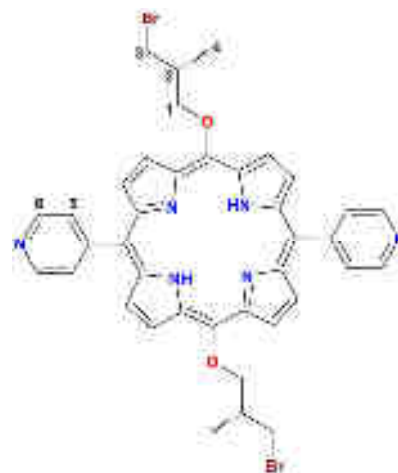


(R, R)-5,15-bis(3-bromo-2-methylpropoxy)-10,20-di(pyridin-4-yl)porphyrin **17**-*(R, R)*

Chemical formula: C₃₈H₃₄Br₂N₆O₂

Molecular weight: 766.11 g/mol

A dried Schlenk tube connected to a vacuum line was degassed and purged with argon. The tube was charged with Pd₂(dba)₃ (4.6 mg, 0.005 mmol, 0.1 eq), phosphine ligand DPEPhos (13.5 mg, 0.01 mmol, 0.2 eq), di-bromoporphyrin **7** (30 mg, 0.05 mmol, 1 eq) and Cs₂CO₃ (65 mg, 0.2 mmol, 4 eq). The tube was backfilled with argon then 6 mL of toluene and *(R)*-3-bromo-2-methylpropan-1-ol (30 μL, 0.2 mmol, 4 eq) was added. The tube was purged with argon for 2 min. and the reaction mixture was heated in an oil bath for 4h at 80 °C. After cooling to room temperature, the reaction mixture was diluted with ethyl acetate (100 mL) and washed with water (3 x 50 mL). The solvent was evaporated under reduced pressure and the solid thus obtained was washed with MeOH to afford a purple solid (0.025 g, 68%).

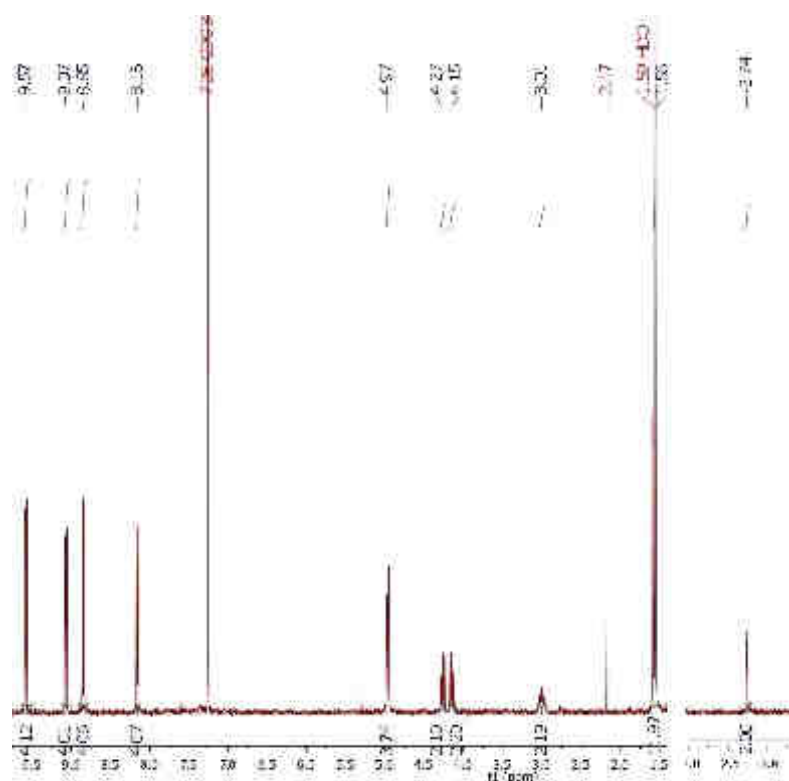


¹H-NMR (300 MHz, CDCl₃) δ (ppm) : - 2.74 (s, br, 2H, NH), 1.56 (d, J = 6.9 Hz, 6H, H₄), 3.01 (m, 2H, H₂), 4.15 (dd, J= 10.0 and 4.3 Hz, 2H, H₃), 4.27 (dd, J= 10.0 and 4.3 Hz, 2H, H₃), 4.97 (d, J = 5.7 Hz, 4H, H₁), 8.16 (dd, J = 5.5 and 3.0 Hz, 4H, H₅), 8.85 (d, J = 4.5 Hz, 4H, H_{βpyr}), 9.07 (dd, J = 5.7 and 2.9 Hz, 4H, H₆), 9.57 (d, J = 4.6 Hz, 4H, H_{βpyr}).

¹³C-NMR (90 MHz, CDCl₃) δ (ppm) : 16.50 (CH₃), 37.06 (CH₂), 37.72 (CH₂), 86.36 (CH), 116.74 (CH), 127.68 (CH), 129.49 (CH), 130.53, 137.75 (CH), 148.47 (C), 149.69 (C).

λ_{max} (CH₂Cl₂)/nm (ε x 10⁴/L mol⁻¹ cm⁻¹) : 415 (50.1), 516 (0.2), 552 (0.64), 596 (0.2), 655 (0.5).

m/z (HRM⁺) [M+H⁺]_{calc} = 767.11, [M+H⁺]_{found} = 767.1183.



References:

1. W. L. F. P. Armarego, D. D. ; B ; , *Butterworth Heinemann,Ed. 1997; Vol. Butterworth Heinemann.*, 1997.
2. B. J. Littler, M. A. Miller, C.-H. Hung, R. W. Wagner, D. F. O'Shea, P. D. Boyle and J. S. Lindsey, *J. Org. Chem*, 1999, **64**, 1391-1396.
3. D. Gryko and J. S. Lindsey, *J. Org. Chem*, 2000, **65**, 2249-2252.
4. D. P. N. Goncalves, S. Ladame, S. Balasubramanian and J. K. M. Sanders, *Org. Biomol. Chem.* , 2006, **4**, 3337-3342.



Crystallographic Data

A. General

1. Crystallizations

The solvents used for crystallization reactions were purchased as analytical grades and used without further purification. Liquid-liquid diffusions were conducted in glass crystallization tubes (height~15-17 cm, diameter = 0.4 cm) at ambient temperature.

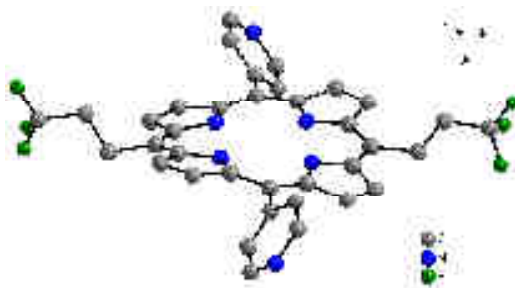
For vapor diffusion technique, a solution of the reagent contained in a glass vial (height = 4.7 cm, diameter = 1.1 cm) was placed into another closed vial (height = 6.3 cm, diameter 1.9 cm) containing the volatile solvent at ambient temperature.

2. Instruments

X-Ray analysis were collected on a Bruker APEX8 CCD diffractometer equipped with an Oxford Cryosystem liquid N₂ device at 173(2) K using graphite-monochromated Mo-K α ($\lambda = 0.71073$ Å) radiation operating at 50kv and 600 μ A. The structures were solved by using SHELXS-97 and refined by full-matrix least squares on F² using SHELXL-97 with anisotropic thermal parameters for all non-hydrogen atoms. The hydrogen atoms were introduced at calculated positions and were not refined (riding model).

B. Single crystal X-Ray diffraction data

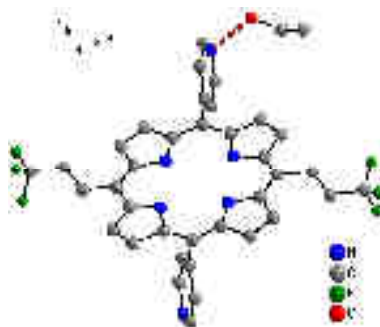
Tecton 4-Structure 1



Crystallization conditions: Crystals were obtained by diffusion of ether into a chloroform solution of the porphyrin.

Identification code	e2856a
Empirical formula	C ₃₆ H ₂₆ F ₆ N ₆
Formula weight	656.63
Temperature	173(2) K
Wavelength	0.71073 Å
Crystal system	Triclinic
Space group	P-1
Unit cell dimensions	a = 9.3714(2) Å α = 78.7430(10) ° b = 13.7838(4) Å β = 85.9520(10) ° c = 24.7238(7) Å γ = 72.5090(10) °
Volume	2987.16(14) Å ³
Z	4
Density (calculated)	1.460 Mg/m ³
Absorption coefficient	0.115 mm ⁻¹
F (000)	1352
Crystal size	0.12 x 0.08 x 0.03 mm ³
Theta range for data collection	1.58 to 29.51°
Index ranges	-7 ≤ h ≤ 12, -19 ≤ k ≤ 19, -34 ≤ l ≤ 34
Reflections collected	51762
Independent reflections	16046 [R (int) = 0.0280]
Completeness to theta = 29.51°	96.4 %
Absorption correction	Semi-empirical from equivalents
Max. and min. transmission	0.9966 and 0.9864
Refinement method	Full-matrix least-squares on F ²
Data / restraints / parameters	16046 / 2 / 865
Goodness-of-fit on F ²	1.041
Final R indices [I > 2σ(I)]	R1 = 0.0758, wR2 = 0.1955
R indices (all data)	R1 = 0.1044, wR2 = 0.2168
Largest diff. peak and hole	0.827 and -0.650 e.Å ⁻³

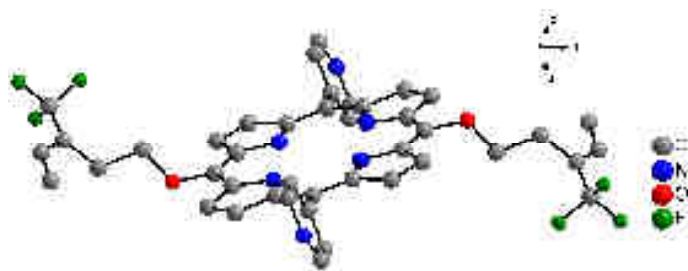
Tecton 4-Structure 2



Crystallization conditions: Crystals were obtained upon slow diffusion of ethanol into a chloroform solution of the porphyrin.

Identification code	e3589	
Empirical formula	C ₃₆ H ₂₆ F ₆ N ₆ O	
Formula weight	702.69	
Temperature	173(2) K	
Wavelength	0.71073 Å	
Crystal system	Monoclinic	
Space group	P 1 21/c 1	
Unit cell dimensions	a = 12.4161(5) Å	α = 90 °.
	b = 26.6146(10) Å	β = 98.137(3) °.
	c = 10.3672(6) Å	γ = 90 °.
Volume	3391.3(3) Å ³	
Z	4	
Density (calculated)	1.376 Mg/m ³	
Absorption coefficient	0.108 mm ⁻¹	
F (000)	1456	
Crystal size	0.030 x 0.030 x 0.060 mm ³	
Theta range for data collection	1.66 to 27.54°	
Index ranges	-16 ≤ h ≤ 16, -34 ≤ k ≤ 27, -13 ≤ l ≤ 13	
Reflections collected	37245	
Independent reflections	7814 [R (int) = 0.0572]	
Completeness to theta = 27.54°	99.7 %	
Absorption correction	Semi-empirical from equivalents	
Max. and min. transmission	0.9910 and 0.9960	
Refinement method	Full-matrix least-squares on F ²	
Data / restraints / parameters	7814 / 0 / 462	
Goodness-of-fit on F ²	1.019	
Final R indices [I > 2σ(I)]	R1 = 0.0657, wR2 = 0.1685	
R indices (all data)	R1 = 0.1189, wR2 = 0.1982	
Largest diff. peak and hole	0.372 and -0.393 eÅ ⁻³	

Tecton 15

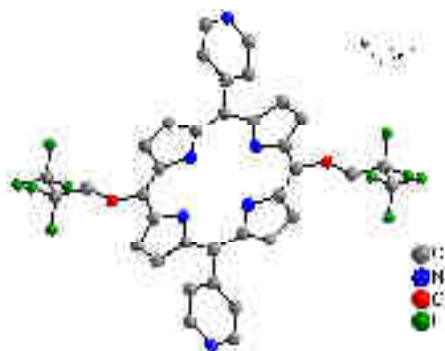


Crystallization conditions: Crystals were obtained upon diffusion of acetonitrile into a chloroform solution of the porphyrin.

Crystals obtained were of poor quality. The refinement parameters could not be optimized

Identification code	e3053a	
Empirical formula	C ₄₂ H ₃₈ F ₆ N ₆ O ₂	
Formula weight	772.30	
Temperature	173(2) K	
Wavelength	0.71073 Å	
Crystal system	Monoclinic	
Space group	P2 ₁ /n	
Unit cell dimensions	a = 7.3141(3) Å	α = 90 °.
	b = 15.0105(7) Å	β = 96.2430(10) °.
	c = 16.9532(9) Å	γ = 90 °.
Volume	1850.22(15) Å ³	
Z	2	
Density (calculated)	1.168 Mg/m ³	
Absorption coefficient	0.073 mm ⁻¹	
F (000)	650	
Crystal size	0.12 x 0.04 x 0.04 mm ³	
Theta range for data collection	1.82 to 30.06°	
Index ranges	-9 ≤ h ≤ 6, -21 ≤ k ≤ 21, -23 ≤ l ≤ 23	
Reflections collected	17606	
Independent reflections	5188 [R (int) = 0.0307]	
Completeness to theta = 30.06°	95.6 %	
Absorption correction	Semi-empirical from equivalents	
Max. and min. transmission	0.9971 and 0.9912	
Refinement method	Full-matrix least-squares on F ²	
Data / restraints / parameters	5188 / 0 / 254	
Goodness-of-fit on F ²	1.163	
Final R indices [I > 2σ(I)]	R1 = 0.1025, wR2 = 0.2717	
R indices (all data)	R1 = 0.1375, wR2 = 0.3026	
Largest diff. peak and hole	1.352 and -1.301 e.Å ⁻³	

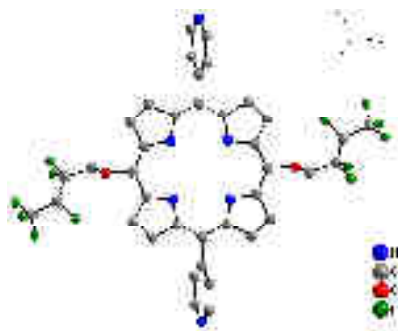
Tecton 9



Crystallization conditions: Crystals were obtained by slow diffusion of EtOH into a chloroform solution of the porphyrin.

Identification code	e3371a	
Empirical formula	C ₃₆ H ₂₂ F ₁₀ N ₆ O ₂	
Formula weight	760.60	
Temperature	173(2) K	
Wavelength	0.71073 Å	
Crystal system	Triclinic	
Space group	P-1	
Unit cell dimensions	a = 6.4816(2) Å	α = 99.3786(15) °
	b = 10.2199(4) Å	β = 95.1672(15) °
	c = 13.1508(5) Å	γ = 100.5480(15) °
Volume	838.48(5) Å ³	
Z	1	
Density (calculated)	1.506 Mg/m ³	
Absorption coefficient	0.134 mm ⁻¹	
F (000)	386	
Crystal size	0.12 x 0.10 x 0.08 mm ³	
Theta range for data collection	1.58 to 29.35°	
Index ranges	-9 ≤ h ≤ 8, -12 ≤ k ≤ 14, -18 ≤ l ≤ 18	
Reflections collected	15254	
Independent reflections	4489 [R (int) = 0.0191]	
Completeness to theta = 29.35°	98.0 %	
Absorption correction	Semi-empirical from equivalents	
Max. and min. transmission	0.9893 and 0.9841	
Refinement method	Full-matrix least-squares on F ²	
Data / restraints / parameters	4489 / 0 / 244	
Goodness-of-fit on F ²	1.071	
Final R indices [I > 2σ(I)]	R1 = 0.0531, wR2 = 0.1472	
R indices (all data)	R1 = 0.0634, wR2 = 0.1553	
Largest diff. peak and hole	0.620 and -0.292 e.Å ⁻³	

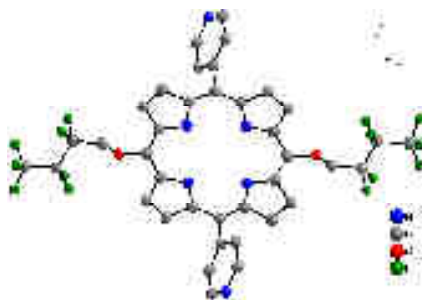
Tecton 16



Crystallization conditions: Crystals were obtained by diffusion of ethanol into a chloroform solution of the porphyrin.

Identification code	e3593
Empirical formula	'2(C ₃₈ H ₂₄ N ₆ O ₂)'
Formula weight	1649.26 g/mol
Temperature	173(2) K
Wavelength	0.71073 Å
Crystal system	triclinic
Space group	P -1
Unit cell dimensions	a = 6.3119(4) Å α = 95.4060(10)° b = 13.5452(8) Å β = 97.9570(10)° c = 21.2665(9) Å γ = 99.4090(10)°
Volume	1763.72(17) Å ³
Z	1
Density (calculated)	1.553 g/cm ³
Absorption coefficient	0.142 mm ⁻¹
F (000)	836
Crystal size	0.050 x 0.050 x 0.060 mm
Theta range for data collection	1.53 to 30.04°
Index ranges	-8 ≤ h ≤ 8, -19 ≤ k ≤ 19, -24 ≤ l ≤ 27
Reflections collected	44884
Independent reflections	9441 [R (int) = 0.0332]
Completeness to theta = 30.04°	91.8%
Absorption correction	Semi-empirical from equivalents
Max. and min. transmission	0.9960 and 0.9900
Refinement method	Full-matrix least-squares on F ²
Data / restraints / parameters	9441 / 20 / 554
Goodness-of-fit on F ²	1.072
Final R indices [I > 2σ(I)]	R1 = 0.1016, wR2 = 0.2528
R indices (all data)	R1 = 0.1267, wR2 = 0.2846
Largest diff. peak and hole	1.091 and -0.647 eÅ ⁻³

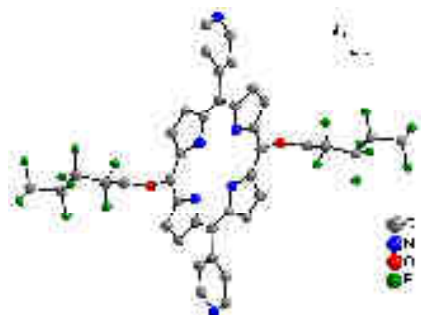
Tecton 10



Crystallization conditions: Crystals were obtained by diffusion of EtOH into a chloroform solution of the porphyrin.

Identification code	e3595	
Empirical formula	$C_{38}H_{22}F_{14}N_6O_2$	
Formula weight	860.61 g/ mol	
Temperature	173(2) K	
Wavelength	0.71073 Å	
Crystal system	Monoclinic	
Space group	P 1 21/n 1	
Unit cell dimensions	$a = 6.8740(3)$ Å	$\alpha = 90^\circ$.
	$b = 28.0707(11)$ Å	$\beta = 102.4410(10)^\circ$
	$c = 9.5776(3)$ Å	$\gamma = 90^\circ$.
Volume	$1804.68(12)$ Å ³	
Z	2	
Density (calculated)	1.584 g/cm ³	
Absorption coefficient	0.150 mm ⁻¹	
F (000)	868	
Crystal size	$0.040 \times 0.040 \times 0.050$ mm ³	
Theta range for data collection	1.45 to 30.12°	
Index ranges	$-8 \leq h \leq 9$, $-39 \leq k \leq 39$, $-13 \leq l \leq 13$	
Reflections collected	40461	
Independent reflections	5260 [R (int) = 0.0529]	
Completeness to theta = 30.12°	98.8%	
Absorption correction	Semi-empirical from equivalents	
Max. and min. transmission	0.9910 and 0.9960.	
Refinement method	Full-matrix least-squares on F ²	
Data / restraints / parameters	5260 / 12 / 292	
Goodness-of-fit on F ²	1.027	
Final R indices [I > 2sigma (I)]	R1 = 0.0933, wR2 = 0.2596	
R indices (all data)	R1 = 0.1173, wR2 = 0.2806	
Largest diff. peak and hole	1.171 and -0.860	eÅ ⁻³

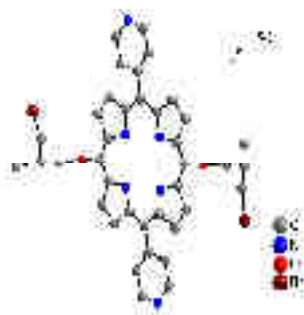
Tecton 11



Crystallization conditions: Crystals were obtained by slow diffusion of EtOH into a chloroform solution of the porphyrin.

Identification code	e3367a
Empirical formula	C ₄₀ H ₂₄ F ₁₆ N ₆ O ₂
Formula weight	924.65
Temperature	173(2) K
Wavelength	0.71073 Å
Crystal system	Triclinic
Space group	P-1
Unit cell dimensions	a = 6.8436(4) Å α = 82.126(3) ° b = 9.7863(6) Å β = 77.574(3) ° c = 14.9256(9) Å γ = 73.678(3) °
Volume	933.73(10) Å ³
Z	1
Density (calculated)	1.644 Mg/m ³
Absorption coefficient	0.159 mm ⁻¹
F (000)	466
Crystal size	0.12 x 0.08 x 0.02 mm ³
Theta range for data collection	1.40 to 29.21°
Index ranges	-9 ≤ h ≤ 8, -13 ≤ k ≤ 11, -21 ≤ l ≤ 18
Reflections collected	13266
Independent reflections	4977 [R (int) = 0.0582]
Completeness to theta = 29.21°	98.1 %
Absorption correction	Semi-empirical from equivalents
Max. and min. transmission	0.9968 and 0.9812
Refinement method	Full-matrix least-squares on F ²
Data / restraints / parameters	4977 / 0 / 289
Goodness-of-fit on F ²	1.163
Final R indices [I > 2σ(I)]	R1 = 0.0754, wR2 = 0.1525
R indices (all data)	R1 = 0.1125, wR2 = 0.1648
Largest diff. peak and hole	0.415 and -0.284 e.Å ⁻³

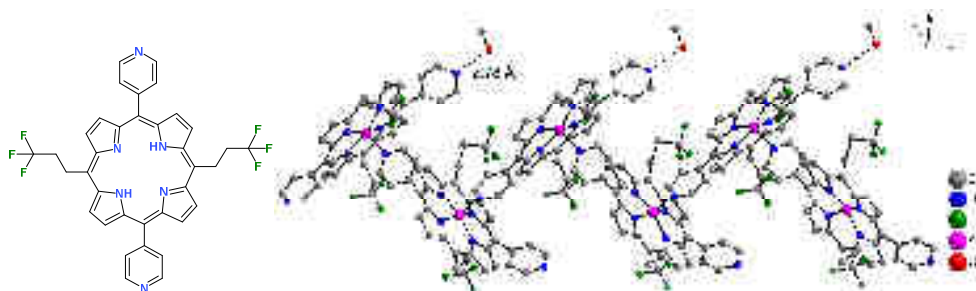
Tecton 17



Crystallization conditions: Crystals were obtained by slow diffusion of EtOH into a chloroform solution of the porphyrin.

Identification code	e3394a
Empirical formula	C ₃₈ H ₃₄ Br ₂ N ₆ O ₂
Formula weight	766.53
Temperature	173(2) K
Wavelength	0.71073 Å
Crystal system	Triclinic
Space group	P1
Unit cell dimensions	a = 6.9278(4) Å α = 106.6287(18) ° b = 9.8384(4) Å β = 90.748(2) ° c = 13.3784(7) Å γ = 103.4956(13) °
Volume	846.47(7) Å ³
Z	1
Density (calculated)	1.504 Mg/m ³
Absorption coefficient	2.438 mm ⁻¹
F (000)	390
Crystal size	0.12 x 0.10 x 0.04 mm ³
Theta range for data collection	1.59 to 27.00°
Index ranges	-5 ≤ h ≤ 8, -12 ≤ k ≤ 12, -17 ≤ l ≤ 17
Reflections collected	14000
Independent reflections	6348 [R (int) = 0.0210]
Completeness to theta = 27.00°	95.0 %
Absorption correction	Semi-empirical from equivalents
Max. and min. transmission	0.9088 and 0.7585
Refinement method	Full-matrix least-squares on F ²
Data / restraints / parameters	6348 / 3 / 435
Goodness-of-fit on F ²	1.545
Final R indices [I > 2σ(I)]	R1 = 0.0458, wR2 = 0.1227
R indices (all data)	R1 = 0.0514, wR2 = 0.1264
Absolute structure parameter	0.006(8)
Largest diff. peak and hole	1.367 and -0.580 e.Å ⁻³

Zn-Tecton 4: 1D network with MeOH

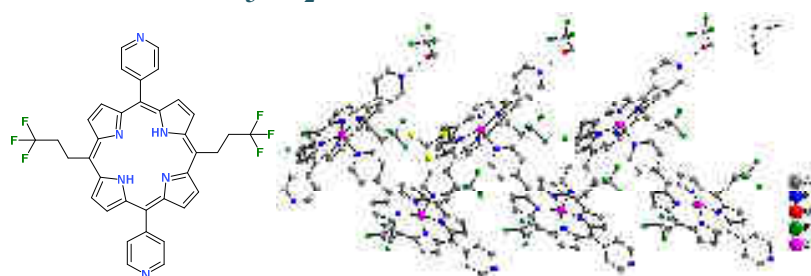


Crystallization conditions: Slow diffusion of Zn(OAc)₂·2H₂O in MeOH ($C = 2 \cdot 10^{-2}$ mol/L) into a chloroform solution of tecton 4 ($C = 2 \cdot 10^{-3}$ mol/L), between layers: CHCl₃:MeOH

Crystals obtained were of poor quality. The refinement parameters could not be optimized

Identification code	e2710a
Empirical formula	C ₃₆ H ₆ F ₆ N ₆ O ₃ Zn
Formula weight	744.80
Temperature	296(2) K
Wavelength	0.71073 Å
Crystal system	Monoclinic
Space group	P2 (1)/c
Unit cell dimensions	a = 14.5481(6) Å α = 90°. b = 20.0694(8) Å β = 105.275(2) °. c = 13.3405(4) Å γ = 90°.
Volume	3757.4(2) Å ³
Z	4
Density (calculated)	1.317 Mg/m ³
Absorption coefficient	0.724mm ⁻¹
F (000)	1468
Crystal size	0.11 x 0.10 x 0.03 mm ³
Theta range for data collection	1.45 to 30.13 °
Index ranges	-20 ≤ h ≤ 20, -28 ≤ k ≤ 28, -14 ≤ l ≤ 18
Reflections collected	56015
Independent reflections	10228 [R (int) = 0.0548]
Completeness to theta = 30.13 °	92.3 %
Absorption correction	Semi-empirical from equivalents
Max. and min. transmission	0.9971 and 0.9912
Refinement method	Full-matrix least-squares on F ²
Data / restraints / parameters	10228 / 16 / 487
Goodness-of-fit on F ²	2.604
Final R indices [I > 2σ(I)]	R1 = 0.1700, wR2 = 0.4352
R indices (all data)	R1 = 0.2639, wR2 = 0.4630
Largest diff. peak and hole	2.212 and -2.100 e.Å ⁻³

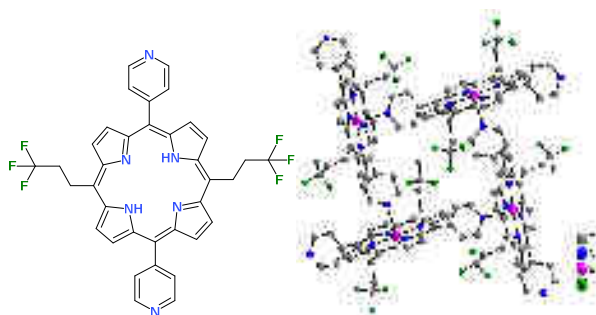
Zn-Tecton 4: 1D Network with CF₃CH₂OH



Crystallization conditions: Slow diffusion of Zn(OAc)₂ · 2H₂O in MeOH (C = 2 · 10⁻² mol/L) into a chloroform solution of tecton **4** (C = 2 · 10⁻³ mol/L), between layers: DMSO and drops of trifluoroethanol.

Identification code	e2805a	
Empirical formula	C ₃₉ H ₂₈ Cl ₃ F ₉ N ₆ O Zn	
Formula weight	939.39	
Temperature	173(2) K	
Wavelength	0.71073 Å	
Crystal system	Monoclinic	
Space group	P2 (1)/c	
Unit cell dimensions	a = 15.1982(3) Å	α = 90°.
	b = 20.4972(5) Å	β = 102.2590(10) °.
	c = 13.1012(2) Å	γ = 90°.
Volume	3988.23(14) Å ³	
Z	4	
Density (calculated)	1.565 Mg/m ³	
Absorption coefficient	0.900 mm ⁻¹	
F (000)	1896	
Crystal size	0.12 x 0.10 x 0.07 mm ³	
Theta range for data collection	1.88 to 30.10°	
Index ranges	-20 ≤ h ≤ 21, -28 ≤ k ≤ 28, -18 ≤ l ≤ 15	
Reflections collected	72931	
Independent reflections	11102 [R (int) = 0.0585]	
Completeness to theta = 30.10°	94.5 %	
Absorption correction	Semi-empirical from equivalents	
Max. and min. transmission	0.9397 and 0.8997	
Refinement method	Full-matrix least-squares on F ²	
Data / restraints / parameters	11102 / 0 / 512	
Goodness-of-fit on F ²	1.040	
Final R indices [I > 2σ(I)]	R1 = 0.0759, wR2 = 0.2139	
R indices (all data)	R1 = 0.1166, wR2 = 0.2444	
Largest diff. peak and hole	1.662 and -1.310 e.Å ⁻³	

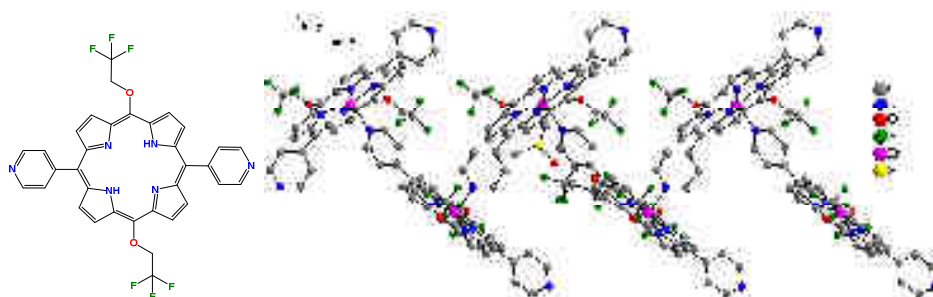
Zn-Tecton 4: 2D network



Crystallization conditions: Slow diffusion of ZnSiF_6 in MeOH ($C = 2 \cdot 10^{-2}$ mol/L) into a chloroform solution of tecton **4** ($C = 2 \cdot 10^{-3}$ mol/L), between layers: DMSO.

Identification code	e2824a
Empirical formula	$\text{C}_{36} \text{H}_{24} \text{F}_6 \text{N}_6 \text{Zn}$
Formula weight	719.98
Temperature	173(2) K
Wavelength	0.71073 Å
Crystal system	Monoclinic
Space group	$P2 (1)/n$
Unit cell dimensions	$a = 8.5148(2)$ Å $\alpha = 90^\circ$. $b = 12.1643(3)$ Å $\beta = 105.0180(10)^\circ$. $c = 15.4226(3)$ Å $\gamma = 90^\circ$.
Volume	$1542.86(6)$ Å ³
Z	2
Density (calculated)	1.550 Mg/m ³
Absorption coefficient	0.871 mm ⁻¹
F (000)	732
Crystal size	$0.10 \times 0.08 \times 0.06$ mm ³
Theta range for data collection	2.16 to 30.10°
Index ranges	$-12 \leq h \leq 10$, $-17 \leq k \leq 17$, $-17 \leq l \leq 21$
Reflections collected	16864
Independent reflections	4337 [R (int) = 0.0196]
Completeness to theta = 30.10°	95.8 %
Absorption correction	Semi-empirical from equivalents
Max. and min. transmission	0.9496 and 0.9180
Refinement method	Full-matrix least-squares on F^2
Data / restraints / parameters	4337 / 0 / 223
Goodness-of-fit on F^2	1.057
Final R indices [$I > 2\sigma(I)$]	$R1 = 0.0337$, $wR2 = 0.0984$
R indices (all data)	$R1 = 0.0391$, $wR2 = 0.1029$
Largest diff. peak and hole	0.550 and -0.336 e.Å ⁻³

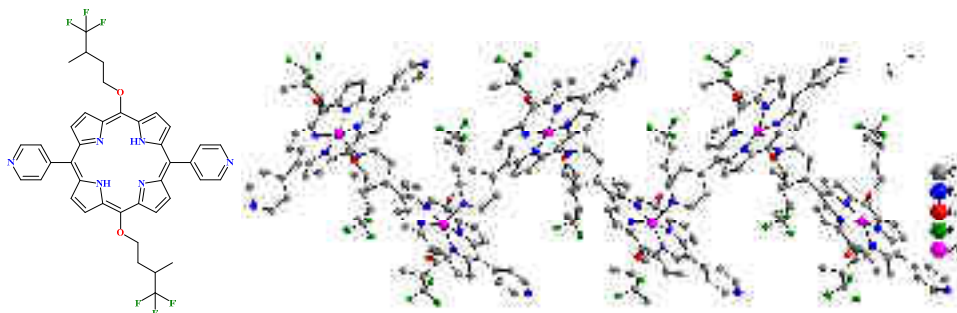
Zn-Tecton 8 : 1D network



Crystallization conditions: Slow diffusion of ZnSiF_6 in MeOH ($C = 2 \cdot 10^{-2}$ mol/L) into a chloroform solution of tecton **8** ($C = 2 \cdot 10^{-3}$ mol/L), between layers: DMSO and few drops of 2,2,3,4,4,4-hexafluorobutan-1-ol (racemic mixture).

Identification code	e3343a
Empirical formula	$\text{C}_{40} \text{H}_{30} \text{F}_{12} \text{N}_6 \text{O}_4 \text{S Zn}$
Formula weight	984.13
Temperature	173(2) K
Wavelength	0.71073 Å
Crystal system	Monoclinic
Space group	$P2 (1)/n$
Unit cell dimensions	$a = 17.8909(5)$ Å $\alpha = 90^\circ$. $b = 13.4778(5)$ Å $\beta = 112.3386(11)^\circ$. $c = 18.0010(5)$ Å $\gamma = 90^\circ$.
Volume	$4014.8(2)$ Å ³
Z	4
Density (calculated)	1.628 Mg/m ³
Absorption coefficient	0.771 mm ⁻¹
F (000)	1992
Crystal size	$0.12 \times 0.12 \times 0.04$ mm ³
Theta range for data collection	1.94 to 30.09°
Index ranges	$-23 \leq h \leq 25$, $-18 \leq k \leq 19$, $-25 \leq l \leq 25$
Reflections collected	41525
Independent reflections	11648 [R (int) = 0.0436]
Completeness to theta = 30.09°	98.7 %
Absorption correction	Semi-empirical from equivalents
Max. and min. transmission	0.9698 and 0.9132
Refinement method	Full-matrix least-squares on F^2
Data / restraints / parameters	11648 / 0 / 580
Goodness-of-fit on F^2	0.945
Final R indices [$I > 2\sigma(I)$]	R1 = 0.0534, wR2 = 0.1186
R indices (all data)	R1 = 0.0886, wR2 = 0.1362
Largest diff. peak and hole	0.976 and -0.586 e.Å ⁻³

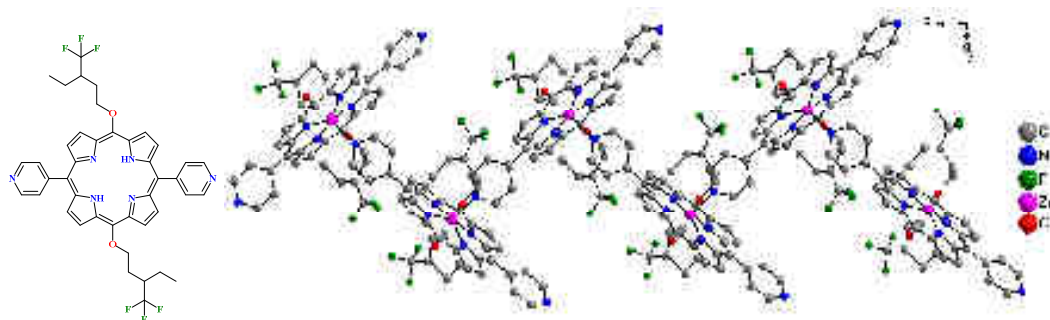
Zn-Tecton 14 : 1D network



Crystallization conditions: Slow diffusion of Zn(OAc)₂·2H₂O in MeOH ($C = 2 \cdot 10^{-2}$ mol/L) into a chloroform solution of tecton **14** ($C = 2 \cdot 10^{-3}$ mol/L), between layers: CHCl₃: MeOH (1:1). Crystals obtained were of poor quality. The refinement parameters could not be optimized

Identification code	e3066a	
Empirical formula	C ₄₀ H ₃₄ F ₆ N ₆ O ₂ Zn	
Formula weight	1316.39	
Temperature	173(2) K	
Wavelength	0.71073 Å	
Crystal system	Monoclinic	
Space group	P2 (1)/n	
Unit cell dimensions	a = 12.2095(4) Å	α = 90°.
	b = 14.7693(4) Å	β = 96.6530(10) °.
	c = 19.6115(6) Å	γ = 90°.
Volume	3512.64(18) Å ³	
Z	2	
Density (calculated)	1.245 Mg/m ³	
Absorption coefficient	0.405 mm ⁻¹	
F (000)	1310	
Crystal size	0.11 x 0.10 x 0.06 mm ³	
Theta range for data collection	2.08 to 30.07 °	
Index ranges	-15 ≤ h ≤ 17, -20 ≤ k ≤ 20, -26 ≤ l ≤ 27	
Reflections collected	40228	
Independent reflections	10228 [R (int) = 0.0557]	
Completeness to theta = 30.07 °	99.2 %	
Absorption correction	Semi-empirical from equivalents	
Max. and min. transmission	0.9971 and 0.9912	
Refinement method	Full-matrix least-squares on F ²	
Data / restraints / parameters	10228 / 18 / 481	
Goodness-of-fit on F ²	1.827	
Final R indices [I > 2σ(I)]	R1 = 0.1028, wR2 = 0.2875	
R indices (all data)	R1 = 0.1471, wR2 = 0.3069	
Largest diff. peak and hole	2.120 and -1.368 e.Å ⁻³	

Zn-Tecton 15 : 1D network

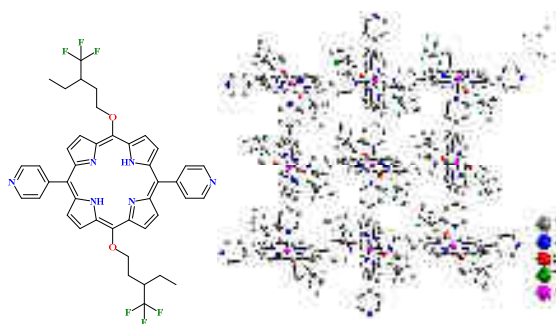


Crystallization conditions: Slow diffusion of $\text{Zn}(\text{OAc})_2 \cdot 2\text{H}_2\text{O}$ in MeOH ($C = 2 \cdot 10^{-2}$ mol/L) into a chloroform solution of tecton **15** ($C = 2 \cdot 10^{-3}$ mol/L), between layers: DMSO.

Crystals obtained were of poor quality. The refinement parameters could not be optimized

Identification code	e3032a
Empirical formula	$\text{C}_{42} \text{H}_{36} \text{F}_6 \text{N}_6 \text{O}_2 \text{Zn}$
Formula weight	836.14
Temperature	173(2) K
Wavelength	0.71073 Å
Crystal system	Monoclinic
Space group	$P2 (1)/n$
Unit cell dimensions	$a = 12.5112(3)$ Å $\alpha = 90^\circ$. $b = 15.1510(3)$ Å $\beta = 98.3520(10)^\circ$. $c = 19.5867(4)$ Å $\gamma = 90^\circ$.
Volume	$3673.42(14)$ Å ³
Z	4
Density (calculated)	1.512 Mg/m ³
Absorption coefficient	0.747 mm ⁻¹
F (000)	1720
Crystal size	$0.10 \times 0.10 \times 0.04$ mm ³
Theta range for data collection	1.71 to 30.13 °
Index ranges	$-17 \leq h \leq 17$, $-19 \leq k \leq 13$, $-27 \leq l \leq 27$
Reflections collected	63616
Independent reflections	10318 [R (int) = 0.0452]
Completeness to theta = 30.13 °	95.1 %
Absorption correction	Semi-empirical from equivalents
Max. and min. transmission	0.8971 and 0.9912
Refinement method	Full-matrix least-squares on F^2
Data / restraints / parameters	10318 / 2 / 516
Goodness-of-fit on F^2	1.871
Final R indices [$I > 2\sigma(I)$]	$R1 = 0.0830$, $wR2 = 0.2511$
R indices (all data)	$R1 = 0.1068$, $wR2 = 0.2650$
Largest diff. peak and hole	2.083 and -0.899 e.Å ⁻³

Zn-Tecton 15 : 2D network

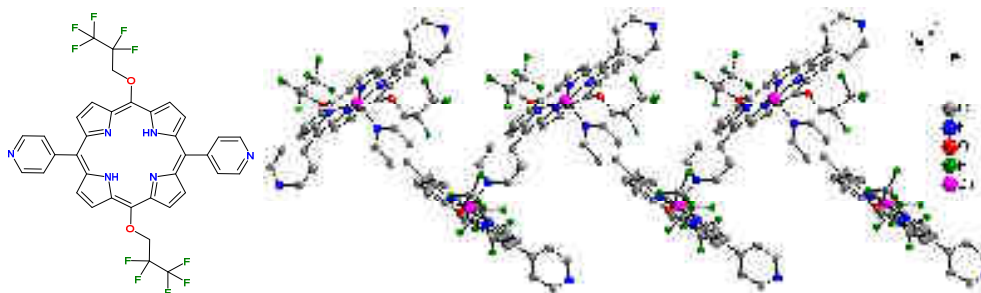


Crystallization conditions: Slow diffusion of ZnSiF_6 in MeOH ($C = 2 \cdot 10^{-2}$ mol/L) into a chloroform solution of tecton **15** ($C = 2 \cdot 10^{-3}$ mol/L), between layers: DMSO + 2,2,3,4,4,4-hexafluorobutan-1-ol.

Crystals obtained were of poor quality. The refinement parameters could not be optimized.

Identification code	e3077a		
Empirical formula	$\text{C}_{21} \text{H}_{18} \text{F}_3 \text{N}_3 \text{O}_{2.38} \text{Zn}$		
Formula weight	472.75		
Temperature	173(2) K		
Wavelength	0.71073 Å		
Crystal system	Monoclinic		
Space group	C2/c		
Unit cell dimensions	$a = 21.6259(6)$ Å	$\alpha = 90^\circ$.	
	$b = 14.4348(6)$ Å	$\beta = 101.836(2)^\circ$.	
	$c = 14.1530(4)$ Å	$\gamma = 90^\circ$.	
Volume	4324.1(2) Å ³		
Z	8		
Density (calculated)	1.452 Mg/m ³		
Absorption coefficient	1.185 mm ⁻¹		
F (000)	1928		
Crystal size	0.10 x 0.08 x 0.06 mm ³		
Theta range for data collection	2.38 to 30.11 °		
Index ranges	-30 ≤ h ≤ 30, -19 ≤ k ≤ 20, -17 ≤ l ≤ 19		
Reflections collected	49730		
Independent reflections	6364 [R (int) = 0.0292]		
Completeness to theta = 30.11 °	99.8 %		
Absorption correction	Semi-empirical from equivalents		
Max. and min. transmission	0.9496 and 0.9180		
Refinement method	Full-matrix least-squares on F ²		
Data / restraints / parameters	6364 / 7 / 280		
Goodness-of-fit on F ²	1.015		
Final R indices [I > 2σ(I)]	R1 = 0.0788, wR2 = 0.2436		
R indices (all data)	R1 = 0.0953, wR2 = 0.2643		
Largest diff. peak and hole	1.028	and -0.703	e.Å ⁻³

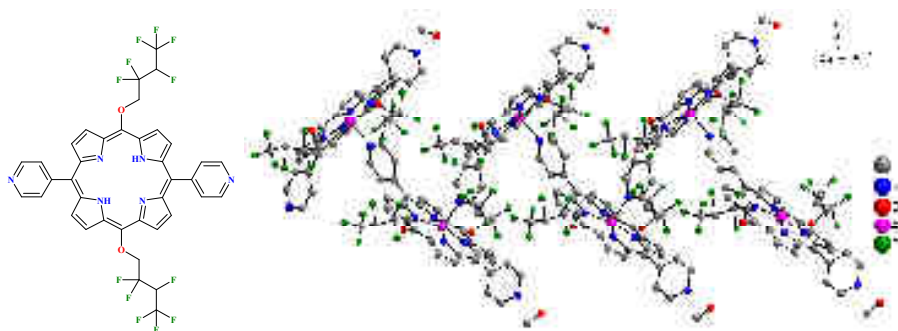
Zn-Tecton 9 : 1D network



Crystallization conditions: Slow diffusion of $\text{Zn}(\text{OAc})_2 \cdot 2\text{H}_2\text{O}$ in MeOH ($C = 2 \cdot 10^{-2}$ mol/L) into a chloroform solution of tecton **9** ($C = 1 \cdot 10^{-3}$ mol/L), between layers: DMSO.

Identification code	e3318a	
Empirical formula	$\text{C}_{36} \text{H}_{20} \text{F}_{10} \text{N}_6 \text{O}_2 \text{Zn}$	
Formula weight	823.95	
Temperature	296(2) K	
Wavelength	0.71073 Å	
Crystal system	Monoclinic	
Space group	$P2 (1)/n$	
Unit cell dimensions	$a = 13.5991(4)$ Å	$\alpha = 90^\circ$.
	$b = 13.8324(4)$ Å	$\beta = 105.7689(7)^\circ$.
	$c = 17.8046(4)$ Å	$\gamma = 90^\circ$.
Volume	$3223.15(15)$ Å ³	
Z	4	
Density (calculated)	1.698 Mg/m ³	
Absorption coefficient	0.867 mm ⁻¹	
F(000)	1656	
Crystal size	0.12 x 0.12 x 0.06 mm ³	
Theta range for data collection	1.89 to 29.40°	
Index ranges	$-19 \leq h \leq 19, -19 \leq k \leq 19, -22 \leq l \leq 24$	
Reflections collected	35376	
Independent reflections	8849 [R (int) = 0.0369]	
Completeness to theta = 29.40°	99.4 %	
Absorption correction	Semi-empirical from equivalents	
Max. and min. transmission	0.9498 and 0.9031	
Refinement method	Full-matrix least-squares on F ²	
Data / restraints / parameters	8849 / 0 / 496	
Goodness-of-fit on F ²	1.036	
Final R indices [I > 2sigma (I)]	R1 = 0.0484, wR2 = 0.1191	
R indices (all data)	R1 = 0.0629, wR2 = 0.1287	
Largest diff. peak and hole	1.659 and -1.380 e.Å ⁻³	

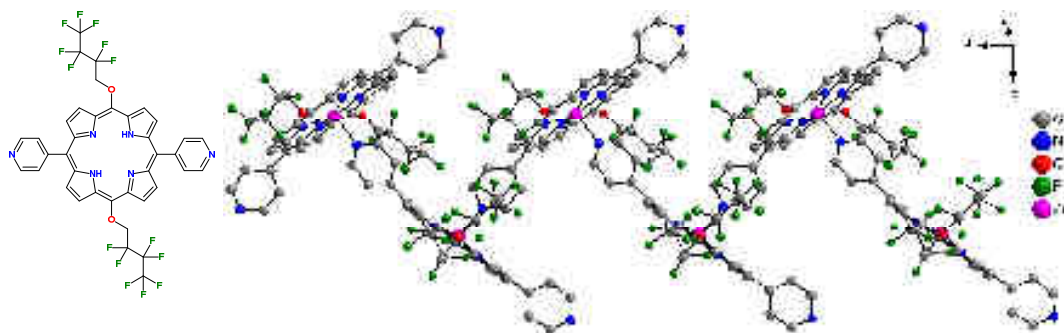
Zn-Tecton 16 : 1D network



Crystallization conditions: Slow diffusion of ZnSiF_6 in MeOH ($C = 2 \cdot 10^{-2}$ mol/L) into a chloroform solution of tecton **16** ($C = 2 \cdot 10^{-3}$ mol/L), between layers: CHCl_3 : MeOH (1:1).

Identification code	e2880a	
Empirical formula	$\text{C}_{39} \text{H}_{26} \text{F}_{12} \text{N}_6 \text{O}_3 \text{Zn}$	
Formula weight	920.03	
Temperature	173(2) K	
Wavelength	0.71073 Å	
Crystal system	Orthorhombic	
Space group	Pccn	
Unit cell dimensions	$a = 19.9221(5)$ Å	$\alpha = 90^\circ$.
	$b = 28.6865(9)$ Å	$\beta = 90^\circ$.
	$c = 13.2544(3)$ Å	$\gamma = 90^\circ$.
Volume	$7574.8(3)$ Å ³	
Z	8	
Density (calculated)	1.613 Mg/m ³	
Absorption coefficient	0.756 mm^{-1}	
F (000)	3712	
Crystal size	$0.12 \times 0.10 \times 0.03 \text{ mm}^3$	
Theta range for data collection	2.04 to 30.07°	
Index ranges	$-25 \leq h \leq 27, -40 \leq k \leq 12, -18 \leq l \leq 18$	
Reflections collected	43569	
Independent reflections	10943 [R (int) = 0.0572]	
Completeness to theta = 30.07°	98.3 %	
Absorption correction	Semi-empirical from equivalents	
Max. and min. transmission	0.9777 and 0.9148	
Refinement method	Full-matrix least-squares on F ²	
Data / restraints / parameters	10943 / 12 / 552	
Goodness-of-fit on F ²	1.001	
Final R indices [I > 2σ(I)]	R1 = 0.0639, wR2 = 0.1357	
R indices (all data)	R1 = 0.1046, wR2 = 0.1549	
Largest diff. peak and hole	1.372 and -1.014 e.Å ⁻³	

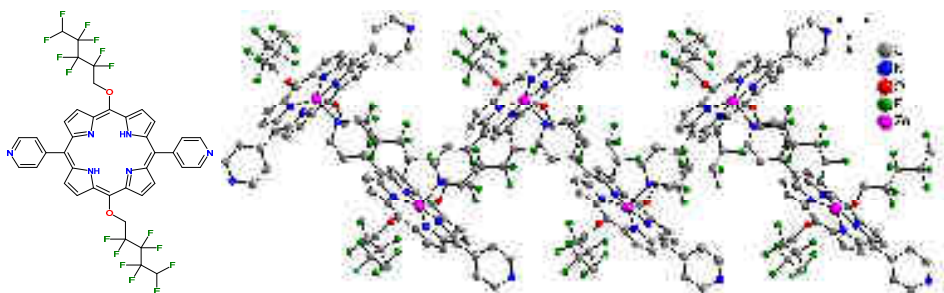
Zn-Tecton **10** : 1D network



Crystallization conditions: Slow diffusion of ZnSiF_6 in MeOH ($C = 2 \cdot 10^{-2}$ mol/L) into a chloroform solution of tecton **10** ($C = 1.7 \cdot 10^{-3}$ mol/L), between layers: DMSO.

Identification code	e3252a	
Empirical formula	$\text{C}_{38} \text{H}_{20} \text{F}_{14} \text{N}_6 \text{O}_2 \text{Zn}$	
Formula weight	923.97	
Temperature	173(2) K	
Wavelength	0.71073 Å	
Crystal system	Monoclinic	
Space group	$P2_1/c$	
Unit cell dimensions	$a = 19.0357(8)$ Å	$\alpha = 90^\circ$.
	$b = 13.6514(4)$ Å	$\beta = 113.5634(14)^\circ$.
	$c = 19.3560(7)$ Å	$\gamma = 90^\circ$.
Volume	$4610.5(3)$ Å ³	
Z	4	
Density (calculated)	1.331 Mg/m ³	
Absorption coefficient	0.626 mm^{-1}	
F(000)	1848	
Crystal size	0.12 x 0.08 x 0.06 mm ³	
Theta range for data collection	1.88 to 30.09°	
Index ranges	$-26 \leq h \leq 24, 0 \leq k \leq 16, 0 \leq l \leq 27$	
Reflections collected	12822	
Independent reflections	12822 [R (int) = 0.0000]	
Completeness to theta = 30.09°	94.6 %	
Absorption correction	Semi-empirical from equivalents	
Max. and min. transmission	0.9634 and 0.9287	
Refinement method	Full-matrix least-squares on F^2	
Data / restraints / parameters	12822 / 3 / 532	
Goodness-of-fit on F^2	1.256	
Final R indices [$I > 2\sigma(I)$]	R1 = 0.0666, wR2 = 0.1866	
R indices (all data)	R1 = 0.0899, wR2 = 0.1988	
Largest diff. peak and hole	2.144 and -1.523 e.Å^{-3}	

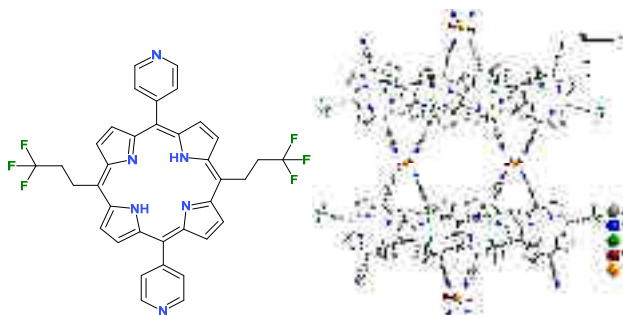
Zn-Tecton 11: 1D network



Crystallization conditions: Slow diffusion of $\text{Zn}(\text{OAc})_2 \cdot 2\text{H}_2\text{O}$ in MeOH ($C = 2 \cdot 10^{-2}$ mol/L) into a chloroform solution of Tecton **11** ($C = 1 \cdot 10^{-3}$ mol/L), between layers: DMSO.

Identification code	e3339a
Empirical formula	$\text{C}_{42} \text{H}_{28} \text{F}_{16} \text{N}_6 \text{O}_3 \text{S Zn}$
Formula weight	1066.13
Temperature	173(2) K
Wavelength	0.71073 Å
Crystal system	Monoclinic
Space group	$P2(1)/c$
Unit cell dimensions	$a = 15.8524(8)$ Å $\alpha = 90^\circ$. $b = 20.6796(9)$ Å $\beta = 113.8021(17)^\circ$. $c = 13.8820(7)$ Å $\gamma = 90^\circ$.
Volume	$4163.7(3)$ Å ³
Z	4
Density (calculated)	1.701 Mg/m ³
Absorption coefficient	0.762 mm^{-1}
F (000)	2144
Crystal size	$0.09 \times 0.07 \times 0.03 \text{ mm}^3$
Theta range for data collection	1.40 to 30.16°
Index ranges	$-22 \leq h \leq 22$, $-28 \leq k \leq 18$, $-19 \leq l \leq 19$
Reflections collected	42038
Independent reflections	12088 [R (int) = 0.0709]
Completeness to theta = 30.16°	98.1 %
Absorption correction	Semi-empirical from equivalents
Max. and min. transmission	0.9775 and 0.9346
Refinement method	Full-matrix least-squares on F^2
Data / restraints / parameters	12088 / 0 / 612
Goodness-of-fit on F^2	1.017
Final R indices [$I > 2\sigma(I)$]	$R1 = 0.0862$, $wR2 = 0.2172$
R indices (all data)	$R1 = 0.1524$, $wR2 = 0.2632$
Largest diff. peak and hole	1.876 and -1.292 e.Å^{-3}

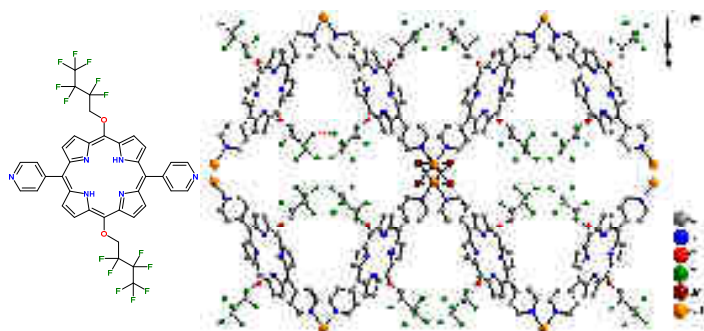
Cd-Tecton 4 : 2D network



Crystallization conditions: Slow diffusion of CdBr_2 in EtOH ($C = 3 \cdot 10^{-3}$ M) into a chloroform solution of Tecton 4 ($C = 1.6 \cdot 10^{-3}$ mol/L), between layers: DMSO and drops of trifluoroethanol.

Identification code	e3272a	
Empirical formula	$\text{C}_{72} \text{H}_{48} \text{Br}_2 \text{Cd} \text{F}_{12} \text{N}_{12}$	
Formula weight	1581.44	
Temperature	173(2) K	
Wavelength	0.71073 Å	
Crystal system	Orthorhombic	
Space group	Pnma	
Unit cell dimensions	$a = 15.7726(4)$ Å	$\alpha = 90^\circ$.
	$b = 36.3786(9)$ Å	$\beta = 90^\circ$.
	$c = 14.9386(3)$ Å	$\gamma = 90^\circ$.
Volume	$8571.5(3)$ Å ³	
Z	4	
Density (calculated)	1.225 Mg/m ³	
Absorption coefficient	1.255 mm ⁻¹	
F (000)	3160	
Crystal size	0.12 x 0.12 x 0.12 mm ³	
Theta range for data collection	1.96 to 30.09°	
Index ranges	$0 \leq h \leq 22, 0 \leq k \leq 51, 0 \leq l \leq 21$	
Reflections collected	12751	
Independent reflections	12751 [R (int) = 0.0000]	
Completeness to theta = 30.09°	99.8 %	
Absorption correction	Semi-empirical from equivalents	
Max. and min. transmission	0.8640 and 0.8640	
Refinement method	Full-matrix least-squares on F^2	
Data / restraints / parameters	12751 / 0 / 451	
Goodness-of-fit on F^2	1.068	
Final R indices [$I > 2\sigma(I)$]	R1 = 0.0388, wR2 = 0.1091	
R indices (all data)	R1 = 0.0592, wR2 = 0.1165	
Largest diff. peak and hole	0.655 and -1.008 e.Å ⁻³	

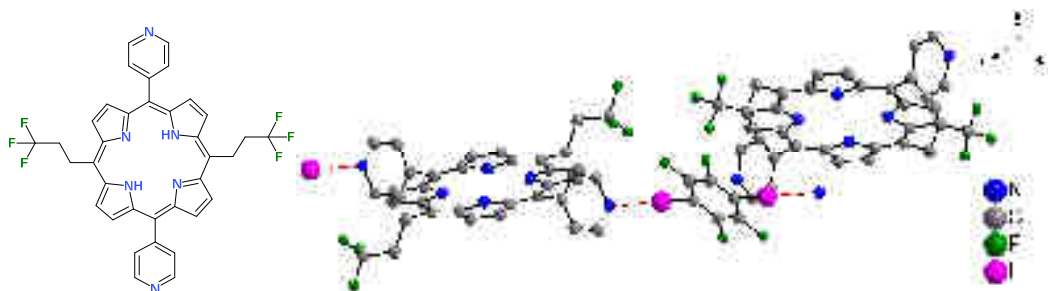
Cd-Tecton 10 : 3D network



Crystallization conditions: Slow diffusion of CdBr_2 in EtOH ($3 \cdot 10^{-3}$ M) into a chloroform solution of tecton **10** ($C = 1.7 \cdot 10^{-3}$ mol/L), between layers: DMSO and drops of trifluoroethanol.

Identification code	e3198a	
Empirical formula	$\text{C}_{38} \text{H}_{28} \text{Br}_2 \text{Cd} \text{F}_{14} \text{N}_6 \text{O}_6$	
Formula weight	1202.88	
Temperature	173(2) K	
Wavelength	0.71073 Å	
Crystal system	Monoclinic	
Space group	C2/c	
Unit cell dimensions	$a = 22.6302(7)$ Å	$\alpha = 90^\circ$.
	$b = 32.5452(9)$ Å	$\beta = 97.7913(13)^\circ$.
	$c = 6.7032(2)$ Å	$\gamma = 90^\circ$.
Volume	$4891.4(2)$ Å ³	
Z	4	
Density (calculated)	1.633 Mg/m ³	
Absorption coefficient	2.181 mm^{-1}	
F(000)	2360	
Crystal size	0.08 x 0.08 x 0.03 mm ³	
Theta range for data collection	2.80 to 30.19°	
Index ranges	$-31 \leq h \leq 31, -46 \leq k \leq 42, -7 \leq l \leq 9$	
Reflections collected	29244	
Independent reflections	7227 [R (int) = 0.0375]	
Completeness to theta = 30.19°	99.3 %	
Absorption correction	Semi-empirical from equivalents	
Max. and min. transmission	0.9375 and 0.8449	
Refinement method	Full-matrix least-squares on F ²	
Data / restraints / parameters	7227 / 10 / 288	
Goodness-of-fit on F ²	1.014	
Final R indices [I > 2sigma (I)]	R1 = 0.0592, wR2 = 0.1958	
R indices (all data)	R1 = 0.0777, wR2 = 0.2136	
Largest diff. peak and hole	2.926 and -1.087 e.Å ⁻³	

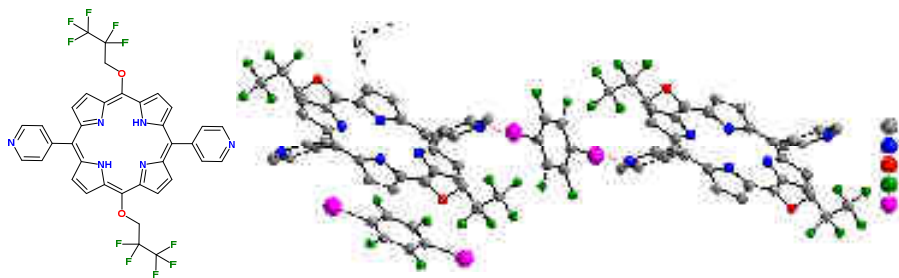
[(Tecton-4)₂ (DIFB)]



Crystallization conditions: To a solution of porphyrin ($C = 2.5 \cdot 10^{-3}$ M) in 0.5 mL in CHCl_3 was added a solution of 1,4-diiidotetrafluorobenzene, $C = 10^{-2}$ M in 0.5 mL of EtOH. Upon slow evaporation of the solvents, crystals appeared within 3-4 days.

Identification code	e3565	
Empirical formula	'C ₃₆ H ₂₆ F ₆ N ₆ , 0.5 (C ₆ F ₄ I ₂)	
Formula weight	857.56 g/ mol	
Temperature	173(2) K	
Wavelength	0.71073 Å	
Crystal system	Triclinic	
Space group	P-1	
Unit cell dimensions	$a = 11.0021(11)$ Å	$\alpha = 104.885(3)^\circ$.
	$b = 12.4397(8)$ Å	$\beta = 98.401(4)^\circ$
	$c = 13.6065(12)$ Å	$\gamma = \gamma = 101.249(3)^\circ$
Volume	$1726.9(3)$ Å ³	
Z	2	
Density (calculated)	1.649 g/cm ³	
Absorption coefficient	1.010 mm ⁻¹	
F(000)	854	
Crystal size	$0.030 \times 0.030 \times 0.050$ mm ³	
Theta range for data collection	1.58 to 30.11°	
Index ranges	$-15 \leq h \leq 15$, $-11 \leq k \leq 16$, $-19 \leq l \leq 18$	
Reflections collected	20786	
Independent reflections	9271 [R (int) = 0.0438]	
Completeness to theta = 30.11°	91.0%,	
Absorption correction	Semi-empirical from equivalents	
Max. and min. transmission	0.9730 and 0.9520	
Refinement method	Full-matrix least-squares on F ²	
Data / restraints / parameters	9271 / 0 / 487	
Goodness-of-fit on F ²	1.042	
Final R indices [I > 2σ(I)]	R1 = 0.0742, wR2 = 0.2067	
R indices (all data)	R1 = 0.1371, wR2 = 0.2454	
Largest diff. peak and hole	0.962 and -1.263 eÅ ⁻³	

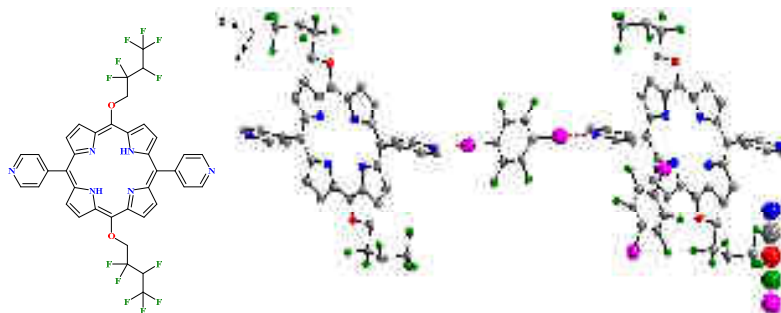
[(Tecton-9) (DIFB)₂]



Crystallization conditions: To a solution of porphyrin, $C = 3 \cdot 10^{-3}$ M in 0.5 mL of CHCl_3 was added a solution of 1,4-diiodotetrafluorobenzene ($C = 5 \cdot 10^{-3}$ M) in 0.5 mL of EtOH. Upon slow evaporation of solvents, crystals appeared within 3-4 days.

Identification code	e3425a	
Empirical formula	C ₄₈ H ₂₂ F ₁₈ I ₄ N ₆ O ₂	
Formula weight	1564.32	
Temperature	173(2) K	
Wavelength	0.71073 Å	
Crystal system	Triclinic	
Space group	P-1	
Unit cell dimensions	a = 9.2570(3) Å	$\alpha = 72.8416(12)^\circ$
	b = 9.6047(3) Å	$\beta = 83.1237(14)^\circ$
	c = 15.3601(4) Å	$\gamma = 78.8370(13)^\circ$
Volume	1277.35(7) Å ³	
Z	1	
Density (calculated)	2.034 Mg/m ³	
Absorption coefficient	2.552 mm ⁻¹	
F(000)	742	
Crystal size	0.10 x 0.07 x 0.05 mm ³	
Theta range for data collection	1.39 to 29.23°	
Index ranges	-13 ≤ h ≤ 13, -13 ≤ k ≤ 10, -21 ≤ l ≤ 21	
Reflections collected	25761	
Independent reflections	6818 [R (int) = 0.0197]	
Completeness to theta = 29.23°	98.3 %	
Absorption correction	Semi-empirical from equivalents	
Max. and min. transmission	0.8830 and 0.7844	
Refinement method	Full-matrix least-squares on F ²	
Data / restraints / parameters	6818 / 9 / 352	
Goodness-of-fit on F ²	1.052	
Final R indices [I > 2σ(I)]	R1 = 0.0314, wR2 = 0.0723	
R indices (all data)	R1 = 0.0423, wR2 = 0.0783	
Largest diff. peak and hole	1.642 and -1.079 e.Å ⁻³	

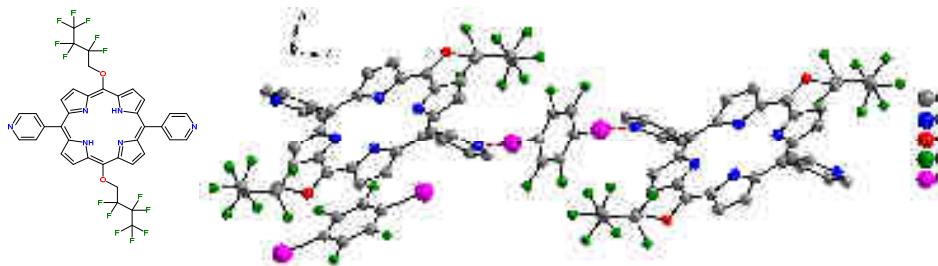
[(Tecton-16) (DIFB)₂]



Crystallization conditions: To a solution of porphyrin ($C = 1.8 \cdot 10^{-3}$ M) in 1 mL of CHCl_3 was added a solution of 1,4-diiodotetrafluorobenzene ($C = 1 \cdot 10^{-2}$ M) in 1 mL of EtOH. Upon slow evaporation of solvents, crystals appeared within 3-4 days.

Identification code	e3587	
Empirical formula	$\text{C}_{38} \text{H}_{24} \text{F}_{12} \text{N}_6 \text{O}_2$	$2(\text{C}_6 \text{F}_4 \text{I}_2)$
Formula weight	638.34 g/ mol	
Temperature	173(2) K	
Wavelength	0.71073 Å	
Crystal system	Triclinic	
Space group	P-1	
Unit cell dimensions	$a = 9.5361(5)$ Å	$\alpha = 73.330(2)^\circ$
	$b = 9.8469(5)$ Å	$\beta = 82.996(2)^\circ$
	$c = 15.0551(8)$ Å	$\gamma = 75.910(2)^\circ$
Volume	$1311.46(12)$ Å ³	
Z	2	
Density (calculated)	1.616 g/cm ³	
Absorption coefficient	1.293 mm ⁻¹	
F (000)	630	
Crystal size	0.050 x 0.050 x 0.060 mm	
Theta range for data collection	1.41 to 30.64°	
Index ranges	$-9 \leq h \leq 13$, $-12 \leq k \leq 13$, $-21 \leq l \leq 18$	
Reflections collected	11932	
Independent reflections	5990 [R (int) = 0.0207]	
Completeness to theta = 26.03°	73.9%	
Absorption correction	Semi-empirical from equivalents	
Max. and min. transmission	0.9380 and 0.9260	
Refinement method	Full-matrix least-squares on F ²	
Data / restraints / parameters	5990 / 14 / 346	
Goodness-of-fit on F ²	1.518	
Final R indices [I > 2sigma (I)]	R1 = 0.0603, wR2 = 0.1959	
R indices (all data)	R1 = 0.0712, wR2 = 0.2055	
Largest diff. peak and hole	4.350 and -2.568 eÅ ⁻³	

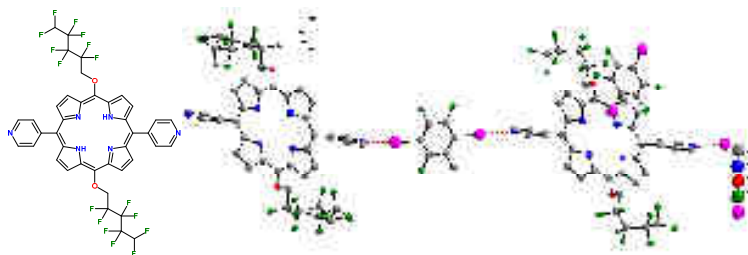
[(Tecton-10) (DIFB)₂]



Crystallization conditions: To a solution of porphyrin ($C = 2 \cdot 10^{-3}$ M) in 1 mL of CHCl_3 was added a solution of 1,4-diiodotetrafluorobenzene ($C = 1 \cdot 10^{-2}$ M) in 1 mL of EtOH. Upon slow evaporation of solvents, crystals appeared within 3-4 days.

Identification code	e3435a	
Empirical formula	$\text{C}_{50} \text{H}_{22} \text{F}_{22} \text{I}_4 \text{N}_6 \text{O}_2$	
Formula weight	1664.34	
Temperature	173(2) K	
Wavelength	0.71073 Å	
Crystal system	Triclinic	
Space group	P-1	
Unit cell dimensions	$a = 9.6049(7)$ Å	$\alpha = 74.832(2)^\circ$
	$b = 10.0508(6)$ Å	$\beta = 81.634(2)^\circ$
	$c = 14.7188(10)$ Å	$\gamma = 76.0088(19)^\circ$
Volume	$1325.58(15)$ Å ³	
Z	1	
Density (calculated)	2.085 Mg/m ³	
Absorption coefficient	2.476 mm ⁻¹	
F (000)	790	
Crystal size	0.12 x 0.08 x 0.00 mm ³	
Theta range for data collection	1.44 to 26.03°	
Index ranges	-13 ≤ h ≤ 13, -12 ≤ k ≤ 14, -20 ≤ l ≤ 20	
Reflections collected	17022	
Independent reflections	5048 [R (int) = 0.0591]	
Completeness to theta = 26.03°	96.6 %	
Absorption correction	Semi-empirical from equivalents	
Max. and min. transmission	0.9902 and 0.7554	
Refinement method	Full-matrix least-squares on F ²	
Data / restraints / parameters	5048 / 0 / 343	
Goodness-of-fit on F ²	1.062	
Final R indices [I > 2σ(I)]	R1 = 0.0651, wR2 = 0.1701	
R indices (all data)	R1 = 0.0959, wR2 = 0.1829	
Largest diff. peak and hole	1.658 and -1.140 e.Å ⁻³	

[(Tecton-11) (DIFB)₂]



Crystallization conditions: To a solution of porphyrin ($C = 1.8 \cdot 10^{-3}$ M) in 1 mL of CHCl_3 was added a solution of 1,4-diiodotetrafluorobenzene ($C = 1 \cdot 10^{-2}$ M) in 1 mL EtOH. Upon slow evaporation of solvents, crystals appeared within 3-4 days.

Identification code	e3566	
Empirical formula	$\text{C}_{40} \text{H}_{24} \text{F}_{16} \text{N}_6 \text{O}_2, 2(\text{C}_6 \text{F}_4 \text{I}_2)$	
Formula weight	1728.37 g/ mol	
Temperature	173(2) K	
Wavelength	0.71073 Å	
Crystal system	Triclinic	
Space group	P-1	
Unit cell dimensions	$a = 12.4883(5)$ Å	$\alpha = 75.729(2)^\circ$
	$b = 15.1129(6)$ Å	$\beta = 73.168(2)^\circ$
	$c = 15.5205(6)$ Å	$\gamma = 88.732(2)^\circ$
Volume	$2713.40(19)$ Å ³	
Z	2	
Density (calculated)	2.115 g/cm ³	
Absorption coefficient	2.429 mm ⁻¹	
F (000)	1644	
Crystal size	0.040 x 0.050 x 0.050 mm	
Theta range for data collection	1.39 to 29.00°	
Index ranges	$-16 \leq h \leq 15, -20 \leq k \leq 20, -21 \leq l \leq 19$	
Reflections collected	84408	
Independent reflections	13245 [R (int) = 0.0364]	
Completeness to theta = 29.00°	92.0%	
Absorption correction	Semi-empirical from equivalents	
Max. and min. transmission	0.9120 and 0.8900	
Refinement method	Full-matrix least-squares on F^2	
Data / restraints / parameters	13245 / 29 / 764	
Goodness-of-fit on F^2	1.136	
Final R indices [$I > 2\sigma(I)$]	R1 = 0.0625, wR2 = 0.1782	
R indices (all data)	R1 = 0.0810, wR2 = 0.1931	
Largest diff. peak and hole	4.632 and -3.537 eÅ ⁻³	

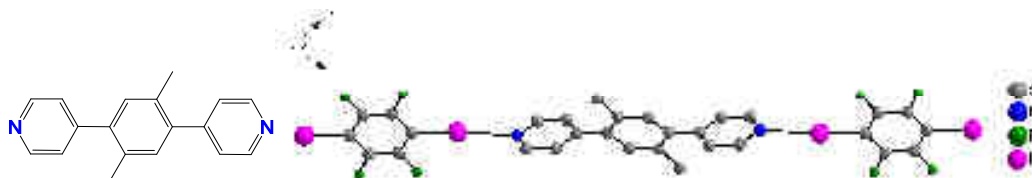
[(KIT-1) (IFB)₂]



Crystallization conditions: To 0.6 mL of H₂O few drops of iodopentafluorobenzene were added. To the mixture was added an EtOH solution of tecton KIT-1 ($C = 2 \cdot 10^{-2}$ M) in 1 mL of EtOH.

Identification code	e3335a	
Empirical formula	C ₃₀ H ₁₆ F ₁₀ I ₂ N ₂	
Formula weight	848.25	
Temperature	173(2) K	
Wavelength	0.71073 Å	
Crystal system	Monoclinic	
Space group	P2 (1)/c	
Unit cell dimensions	a = 4.02020(10) Å	α = 90°.
	b = 27.0920(11) Å	β = 93.8344(10) °.
	c = 13.0226(5) Å	γ = 90°.
Volume	1415.18(9) Å ³	
Z	2	
Density (calculated)	1.991 Mg/m ³	
Absorption coefficient	2.313 mm ⁻¹	
F (000)	812	
Crystal size	0.12 x 0.12 x 0.06 mm ³	
Theta range for data collection	2.17 to 30.09°	
Index ranges	-5 ≤ h ≤ 3, -38 ≤ k ≤ 38, -18 ≤ l ≤ 18	
Reflections collected	17279	
Independent reflections	3933 [R (int) = 0.0235]	
Completeness to theta = 30.09°	94.3 %	
Absorption correction	Semi-empirical from equivalents	
Max. and min. transmission	0.8737 and 0.7687	
Refinement method	Full-matrix least-squares on F ²	
Data / restraints / parameters	3933 / 0 / 200	
Goodness-of-fit on F ²	1.252	
Final R indices [I > 2σ(I)]	R1 = 0.0327, wR2 = 0.0589	
R indices (all data)	R1 = 0.0357, wR2 = 0.0598	
Largest diff. peak and hole	0.946 and -0.950 e.Å ⁻³	

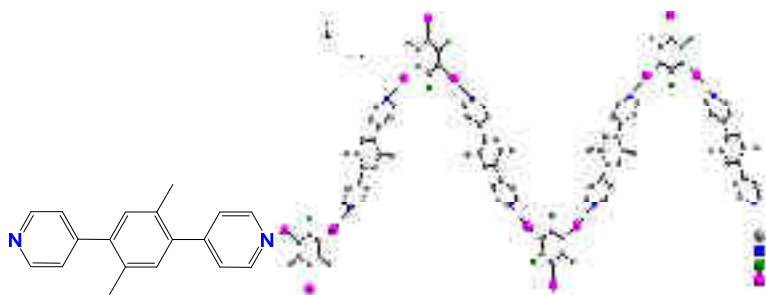
[(KIT-1) (DIFB)]



Crystallization conditions: To a solution of tecton KIT-1 ($C = 3 \cdot 10^{-3}$ M) in 1 mL of CHCl_3 was added a solution of 1,4-diiidotetrafluorobenzene ($C = 3 \cdot 10^{-3}$ M) in 1 mL of EtOH. Upon slow evaporation of solvents crystals appeared within 3-4 days.

Identification code	e3344	
Empirical formula	$\text{C}_{24} \text{H}_{16} \text{F}_4 \text{I}_2 \text{N}_2$	
Formula weight	662.19	
Temperature	173(2) K	
Wavelength	0.71073 Å	
Crystal system	Triclinic	
Space group	P-1	
Unit cell dimensions	$a = 6.8990(6)$ Å	$\alpha = 67.043(2)^\circ$.
	$b = 9.0065(8)$ Å	$\beta = 74.8130(19)^\circ$.
	$c = 10.5354(9)$ Å	$\gamma = 69.918(2)^\circ$.
Volume	$559.89(8)$ Å ³	
Z	1	
Density (calculated)	1.964 Mg/m ³	
Absorption coefficient	2.856 mm^{-1}	
F(000)	316	
Crystal size	$0.12 \times 0.12 \times 0.04 \text{ mm}^3$	
Theta range for data collection	2.12 to 29.46°	
Index ranges	$-9 \leq h \leq 9, -12 \leq k \leq 8, -14 \leq l \leq 14$	
Reflections collected	5755	
Independent reflections	3002 [R(int) = 0.0388]	
Completeness to theta = 29.46°	96.6 %	
Absorption correction	Semi-empirical from equivalents	
Max. and min. transmission	0.8943 and 0.7256	
Refinement method	Full-matrix least-squares on F^2	
Data / restraints / parameters	3002 / 0 / 146	
Goodness-of-fit on F^2	1.031	
Final R indices [$I > 2\sigma(I)$]	$R_1 = 0.0668, wR_2 = 0.1560$	
R indices (all data)	$R_1 = 0.0697, wR_2 = 0.1600$	
Largest diff. peak and hole	2.920 and -2.764 e.Å^{-3}	

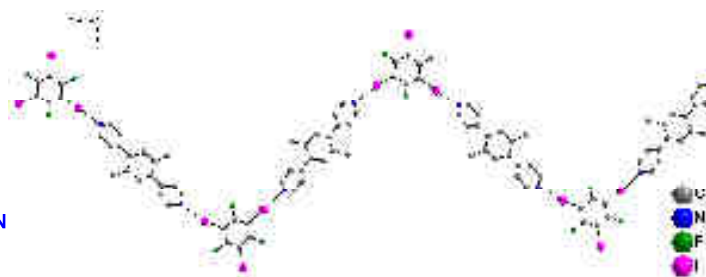
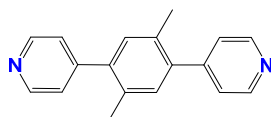
[(KIT-1) (TIFB)]



Crystallization conditions: To a solution of tecton KIT-1 ($C = 3 \cdot 10^{-3}$ M) in 0.5 mL of CHCl_3 was added a solution of 1,3,5-trifluoro-2,4,6-triiodobenzene ($C = 6 \cdot 10^{-3}$ M) in 0.5 mL of EtOH. Upon slow evaporation of solvents crystals appeared within 3-4 days.

Identification code	e3412a	
Empirical formula	$\text{C}_{24} \text{H}_{16} \text{F}_3 \text{I}_3 \text{N}_2$	
Formula weight	770.09	
Temperature	173(2) K	
Wavelength	0.71073 Å	
Crystal system	Orthorhombic	
Space group	Pbcn	
Unit cell dimensions	$a = 5.5110(3)$ Å	$\alpha = 90^\circ$.
	$b = 18.5899(11)$ Å	$\beta = 90^\circ$.
	$c = 23.7423(13)$ Å	$\gamma = 90^\circ$.
Volume	$2432.4(2)$ Å ³	
Z	4	
Density (calculated)	2.103 Mg/m ³	
Absorption coefficient	3.892 mm^{-1}	
F(000)	1440	
Crystal size	0.12 x 0.08 x 0.04 mm ³	
Theta range for data collection	1.72 to 30.04°	
Index ranges	$-4 \leq h \leq 7$, $-26 \leq k \leq 26$, $-33 \leq l \leq 30$	
Reflections collected	14054	
Independent reflections	3509 [R (int) = 0.0288]	
Completeness to theta = 30.04°	98.2 %	
Absorption correction	Semi-empirical from equivalents	
Max. and min. transmission	0.8599 and 0.6523	
Refinement method	Full-matrix least-squares on F^2	
Data / restraints / parameters	3509 / 0 / 148	
Goodness-of-fit on F^2	1.010	
Final R indices [$I > 2\sigma(I)$]	R1 = 0.0317, wR2 = 0.0626	
R indices (all data)	R1 = 0.0485, wR2 = 0.0706	
Largest diff. peak and hole	1.274 and -1.258 e.Å ⁻³	

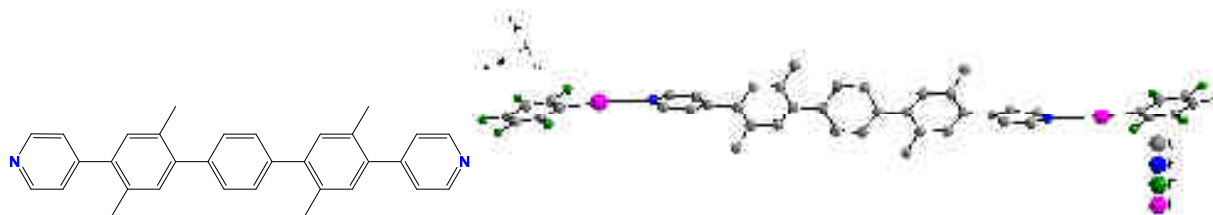
[(KIT-1) (TIFB)]



Crystallization conditions: To a solution of tecton KIT-1 ($C = 4.5 \cdot 10^{-3}$ M) in 1 mL of CHCl_3 was added a solution of 1,3,5-trifluoro-2,4,6-triiodobenzene ($C = 3 \cdot 10^{-3}$ M) in 1 mL of EtOH. Upon slow evaporation of solvents crystals appeared within 3-4 days.

Identification code	e3423a	
Empirical formula	$\text{C}_{24} \text{H}_{16} \text{F}_3 \text{I}_3 \text{N}_2$	
Formula weight	770.09	
Temperature	173(2) K	
Wavelength	0.71073 Å	
Crystal system	Orthorhombic	
Space group	Pbca	
Unit cell dimensions	$a = 7.4200(4)$ Å	$\alpha = 90^\circ$.
	$b = 17.8302(10)$ Å	$\beta = 90^\circ$.
	$c = 35.8919(19)$ Å	$\gamma = 90^\circ$.
Volume	$4748.5(4)$ Å ³	
Z	8	
Density (calculated)	2.154 Mg/m^3	
Absorption coefficient	3.988 mm^{-1}	
F(000)	2880	
Crystal size	$0.10 \times 0.10 \times 0.06 \text{ mm}^3$	
Theta range for data collection	2.27 to 30.01°	
Index ranges	$-8 \leq h \leq 10, -25 \leq k \leq 21, -50 \leq l \leq 50$	
Reflections collected	29156	
Independent reflections	6814 [R (int) = 0.0409]	
Completeness to theta = 30.01°	98.2 %	
Absorption correction	Semi-empirical from equivalents	
Max. and min. transmission	0.7959 and 0.6912	
Refinement method	Full-matrix least-squares on F^2	
Data / restraints / parameters	6814 / 0 / 291	
Goodness-of-fit on F^2	1.009	
Final R indices [I > 2sigma (I)]	$R_1 = 0.0358, wR_2 = 0.0712$	
R indices (all data)	$R_1 = 0.0507, wR_2 = 0.0768$	
Largest diff. peak and hole	1.769 and -1.797 e.Å^{-3}	

[(KIT-2) (IFB)₂]



Crystallization conditions: To 0.6 mL of H₂O few drops of iodopentafluorobenzene were added. To the mixture, an EtOH solution of tecton KIT-2 ($C = 1 \cdot 10^{-2}$ M) in 1 mL of EtOH was added.

Identification code	e3324b	
Empirical formula	C ₄₄ H ₂₈ F ₁₀ I ₂ N ₂	
Formula weight	1028.48	
Temperature	173(2) K	
Wavelength	0.71073 Å	
Crystal system	Triclinic	
Space group	P-1	
Unit cell dimensions	a = 7.68540(10) Å	α = 78.9336(8) °
	b = 9.3757(2) Å	β = 76.5682(8) °
	c = 14.3001(3) Å	γ = 76.3666(7) °
Volume	963.67(3) Å ³	
Z	1	
Density (calculated)	1.772 Mg/m ³	
Absorption coefficient	1.716 mm ⁻¹	
F (000)	502	
Crystal size	0.12 x 0.08 x 0.06 mm ³	
Theta range for data collection	2.26 to 29.51°	
Index ranges	-7 ≤ h ≤ 10, -13 ≤ k ≤ 13, -19 ≤ l ≤ 20	
Reflections collected	19292	
Independent reflections	5188 [R (int) = 0.0177]	
Completeness to theta = 29.51°	96.4 %	
Absorption correction	Semi-empirical from equivalents	
Max. and min. transmission	0.9040 and 0.8205	
Refinement method	Full-matrix least-squares on F ²	
Data / restraints / parameters	5188 / 0 / 264	
Goodness-of-fit on F ²	1.003	
Final R indices [I > 2σ(I)]	R1 = 0.0243, wR2 = 0.0534	
R indices (all data)	R1 = 0.0276, wR2 = 0.0549	
Largest diff. peak and hole	0.915 and -0.570 e.Å ⁻³	

[(KIT-2) (DIFB)]



Crystallization conditions: To a solution of tecton KIT-2 ($C = 3 \cdot 10^{-3}$ M) in 1 mL of CHCl_3 was added a solution of 1,4-diodotetrafluorobenzene ($C = 3 \cdot 10^{-3}$ M) in 1 mL of EtOH. Upon slow evaporation of solvents crystals appeared within 3-4 days.

Identification code	e3342b	
Empirical formula	$\text{C}_{38} \text{H}_{28} \text{F}_4 \text{I}_2 \text{N}_2$	
Formula weight	842.42	
Temperature	173(2) K	
Wavelength	0.71073 Å	
Crystal system	Triclinic	
Space group	P-1	
Unit cell dimensions	$a = 8.0484(4)$ Å	$\alpha = 107.7388(16)^\circ$.
	$b = 8.2258(4)$ Å	$\beta = 92.0288(17)^\circ$.
	$c = 13.2448(8)$ Å	$\gamma = 104.3100(17)^\circ$.
Volume	$803.42(7)$ Å ³	
Z	1	
Density (calculated)	1.741 Mg/m ³	
Absorption coefficient	2.011 mm^{-1}	
F(000)	412	
Crystal size	0.12 x 0.12 x 0.04 mm ³	
Theta range for data collection	1.63 to 29.42°	
Index ranges	$-9 \leq h \leq 11, -11 \leq k \leq 8, -18 \leq l \leq 18$	
Reflections collected	6965	
Independent reflections	4289 [R (int) = 0.0167]	
Completeness to theta = 29.42°	96.3 %	
Absorption correction	Semi-empirical from equivalents	
Max. and min. transmission	0.9239 and 0.7943	
Refinement method	Full-matrix least-squares on F^2	
Data / restraints / parameters	4289 / 0 / 210	
Goodness-of-fit on F^2	1.034	
Final R indices [$I > 2\sigma(I)$]	R1 = 0.0228, wR2 = 0.0567	
R indices (all data)	R1 = 0.0251, wR2 = 0.0581	
Largest diff. peak and hole	0.811 and -0.616 e.Å ⁻³	

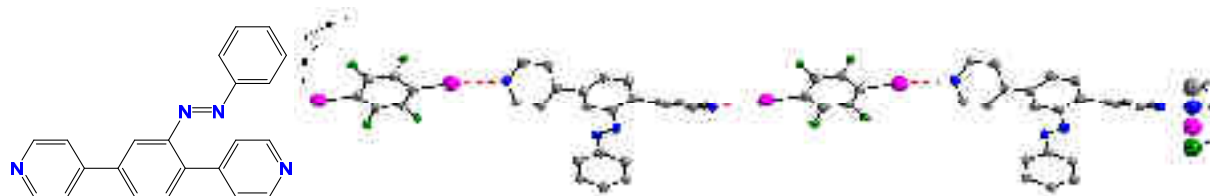
[(KIT-2) (TIFB)₂]



Crystallization conditions: To a solution of tecton KIT-2 ($C = 3 \cdot 10^{-3}$ M) in 0.5 mL of CHCl_3 was added a solution of 1,3,5-trifluoro-2,4,6-triiodobenzene ($C = 6 \cdot 10^{-3}$ M) in 0.5 mL of EtOH. Upon slow evaporation of solvents crystals appeared within 3-4 days.

Identification code	e3407a	
Empirical formula	C ₄₄ H ₂₈ F ₆ I ₆ N ₂	
Formula weight	1460.08	
Temperature	173(2) K	
Wavelength	0.71073 Å	
Crystal system	Monoclinic	
Space group	P2 (1)/c	
Unit cell dimensions	a = 7.7820(3) Å	$\alpha = 90^\circ$.
	b = 33.4952(14) Å	$\beta = 114.9896(11)^\circ$.
	c = 9.1815(4) Å	$\gamma = 90^\circ$.
Volume	2169.20(16) Å ³	
Z	2	
Density (calculated)	2.235 Mg/m ³	
Absorption coefficient	4.357 mm ⁻¹	
F (000)	1356	
Crystal size	0.12 x 0.08 x 0.04 mm ³	
Theta range for data collection	1.22 to 30.05°	
Index ranges	-9 ≤ h ≤ 10, -47 ≤ k ≤ 45, -12 ≤ l ≤ 12	
Reflections collected	22232	
Independent reflections	6291 [R (int) = 0.0235]	
Completeness to theta = 30.05°	99.5 %	
Absorption correction	Semi-empirical from equivalents	
Max. and min. transmission	0.8450 and 0.6229	
Refinement method	Full-matrix least-squares on F ²	
Data / restraints / parameters	6291 / 0 / 264	
Goodness-of-fit on F ²	1.048	
Final R indices [I > 2σ(I)]	R1 = 0.0353, wR2 = 0.0825	
R indices (all data)	R1 = 0.0432, wR2 = 0.0863	
Largest diff. peak and hole	1.500 and -1.203 e.Å ⁻³	

[(KIT-3) (DIFB)]



Crystallization conditions: To a solution of tecton KIT-3 ($C = 3 \cdot 10^{-3}$ M) in 1 mL of CHCl_3 was added a solution of 1,4-diiodotetrafluorobenzene ($C = 3 \cdot 10^{-3}$ M) in 1 mL of EtOH. Upon slow evaporation of solvents crystals appeared within 3-4 days.

Identification code	e3586	
Empirical formula	$\text{C}_{28}\text{H}_{16}\text{F}_4\text{I}_2\text{N}_4$	
Formula weight	738.25 g/mol	
Temperature	173(2) K	
Wavelength	0.71073 Å	
Crystal system	monoclinic	
Space group	$P 1 21/n 1$	
Unit cell dimensions	$a = 12.3957(5)$ Å	$\alpha = 90^\circ$
	$b = 17.8774(6)$ Å	$\beta = 115.9150(10)^\circ$
	$c = 13.0708(5)$ Å	$\gamma = 90^\circ$
Volume	$2605.26(17)$ Å ³	
Z	4	
Density (calculated)	1.882 g/cm ³	
Absorption coefficient	2.468 mm ⁻¹	
F(000)	1416	
Crystal size	$0.060 \times 0.060 \times 0.070$ mm	
Theta range for data collection	1.89 to 30.08°	
Index ranges	$-17 \leq h \leq 17$, $-23 \leq k \leq 21$, $-18 \leq l \leq 18$	
Reflections collected	25438	
Independent reflections	7479 [R (int) = 0.0261]	
Completeness to theta = 30.08°	97.5%,	
Absorption correction	Semi-empirical from equivalents	
Max. and min. transmission	0.8700 and 0.8400	
Refinement method	Full-matrix least-squares on F^2	
Data / restraints / parameters	7479 / 0 / 343	
Goodness-of-fit on F^2	1.023	
Final R indices [$I > 2\sigma(I)$]	$R1 = 0.0335$, $wR2 = 0.0843$	
R indices (all data)	$R1 = 0.0430$, $wR2 = 0.0908$	
Largest diff. peak and hole	2.703 and -0.498 eÅ ⁻³	



Résumé

La tectonique moléculaire^{1, 2} est un domaine qui combine la chimie supramoléculaire et la chimie de l'état solide. Il traite de la construction de réseaux moléculaires, systèmes périodiques de grande taille dans la phase cristalline, par auto-assemblage de tectons moléculaires (blocs de construction) en utilisant des processus de reconnaissance moléculaire basés sur des interactions spécifiques.

La formation de réseaux moléculaires se déroule dans des conditions d'auto-assemblage et des processus réversibles sont utilisés pour les activités de reconnaissance. Une variété d'interactions attractives réversibles est utilisée pour la construction d'ensembles supramoléculaires tels que les forces de van der Waals, les interactions électrostatiques, la liaison hydrogène ou la liaison de coordination. En faisant varier la nature chimique, le nombre et l'orientation des sites de reconnaissance des blocs de construction, il est possible de générer des réseaux moléculaires de différentes topologies par l'itération du processus de reconnaissance dans une, deux ou trois directions de l'espace (1-D, 2-D et 3-D). Ces architectures peuvent être obtenues en utilisant un tecton auto-complémentaire unique ou plusieurs tectons ayant des sites de reconnaissance complémentaires.

Un intérêt particulier dans ce domaine est la formation de MOF (Metal-Organic Frameworks ou réseaux métallo-organiques),³ résultant de l'assemblage de tectons organiques et des centres métalliques ou complexes, présentant des vides potentiels.

Durant ce projet de thèse, nous nous sommes intéressés à des briques moléculaires à base de porphyrines et plus particulièrement des porphyrines fluorées. En effet, la porphyrine est particulièrement adaptée du fait de sa stabilité thermique, sa nature robuste et une fonctionnalisation relativement aisée. Des travaux antérieurs effectués au laboratoire,^{4, 5} ont notamment permis la formation de réseaux de coordination particulièrement stables par auto-assemblage de complexes porphyriniques de Zn(II). L'échange des molécules de solvants présents à l'intérieur des cavités des MOFs ainsi formés a pu être effectué à l'état mono-cristallin. Dans la continuité de ce travail, nous nous sommes particulièrement intéressés à l'incorporation d'atomes de fluor et/ou des groupements chiraux à la périphérie du macrocycle porphyrinique. La formation de MOFs à partir de telles briques moléculaires pourrait conduire à des applications potentielles en imagerie médicale ou en catalyse. Les briques ciblées sont des porphyrines de type *trans*-A₂B₂ possédant deux groupements coordinants de type pyridine en position *méso trans* d'une part et des chaînes alkyles chirales et/ou fluorées sur les deux autres positions *méso*.

Le but ultime du projet est de générer des cristaux moléculaires poreux stables dont la structure poreuse inclurait des substituants chiraux fluorés, pouvant ainsi permettre la séparation chirale de mélanges racémiques hautement fluorés tels que les anesthésiques d'inhalation (enflurane, isoflurane, desflurane) grâce à des interactions spécifiques impliquant les fluors.

Le manuscrit est composé de trois parties. La première est consacrée à la synthèse de nouveaux tectons à base de porphyrines halogénées et/ou chirales. Dans la deuxième partie, nous

décrivons la formation de MOFs basés sur ces unités de construction. Enfin, la dernière partie est dédiée à la formation de réseaux à base des liaisons halogène.

I. Synthèse de porphyrines halogénées et/ou chirales.

Notre première approche pour la synthèse des porphyrines de type A_2B_2 a consisté en la formation préalable d'un dipyrrométhane portant le substituant chiral et/ou une chaîne alkyle fluorée (schéma 1). Le dipyrrométhane formé réagit dans une deuxième étape avec le 4-pyridylcarboxaldéhyde dans des conditions acides pour conduire au produit final avec des rendements modérés voire très faibles en fonction du réactif de départ.

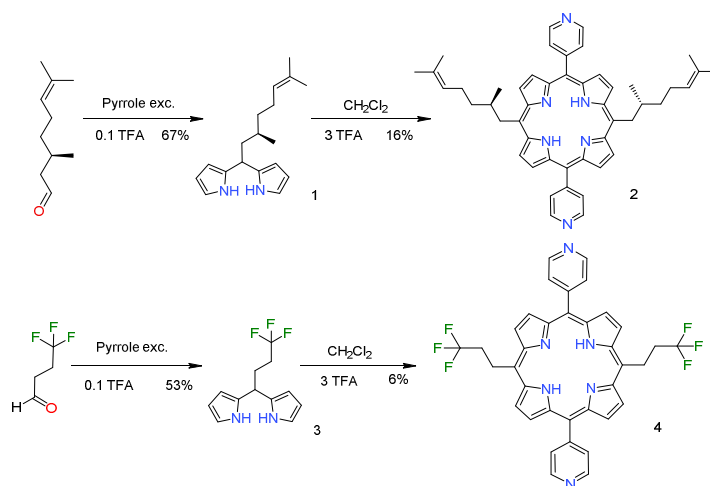


Schéma 1. Voie de synthèse conduisant aux porphyrines A_2B_2 ciblées.

Outre les rendements faibles dans les deux cas, cette approche présente deux inconvénients majeurs. Le premier est la nécessité d'utiliser des aldéhydes fluorés et/ou chiraux. En effet, très peu d'aldéhydes fluorés sont disponibles dans le commerce, et les dérivés fluorés et chiraux sont quasi inexistant, en outre, la synthèse d'aldéhydes fluorés est délicate car ce sont des composés extrêmement volatils

Le deuxième inconvénient est lié à l'utilisation d'aldéhydes chiraux fluorés et coûteux lors de la première étape alors que la deuxième étape conduit à des rendements très faibles ce qui conduit à une perte conséquente du réactif le plus onéreux.

En conséquence, nous avons développé une deuxième stratégie (représentée schéma 2) en nous inspirant des travaux antérieurs rapportés par les groupes de J. Sanders⁶ et P. Zhang.⁷ Cette stratégie en 4 étapes permet l'introduction des substituants chiraux et/ou fluorés dans la dernière étape de la voie de synthèse par un couplage au palladium entre la porphyrine *méso* di-bromée **7** et un alcool fluoré et/ou chiral. La porphyrine **7** est obtenue en trois étapes. La première consiste en la synthèse du dipyrrométhane **5** qui est ensuite mis à réagir avec le triméthylorthoformate (TMOF) pour conduire à la porphyrine **6** avec un rendement de 20%. La bromation des deux positions *méso trans* est effectuée par l'ajout de NBS avec un rendement de 54 % (schéma 2).

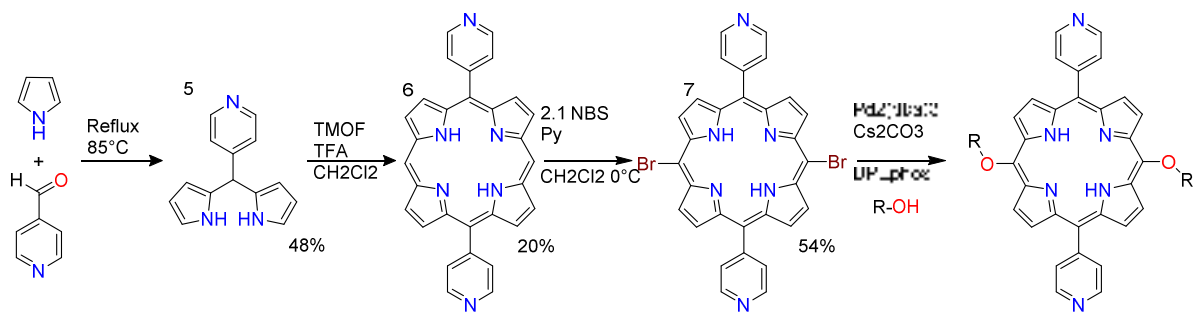


Schéma 2. Voie alternative pour porphyrines A₂B₂ substituées.

Cette voie de synthèse a permis la formation d'une nouvelle série de 11 tectons possédant deux pyridines en position *méso trans* et deux chaînes chirales et/ou fluorées sur les positions *méso* restantes (schéma 3) avec des rendements variant entre 28 et 85 % pour la dernière étape de couplage.

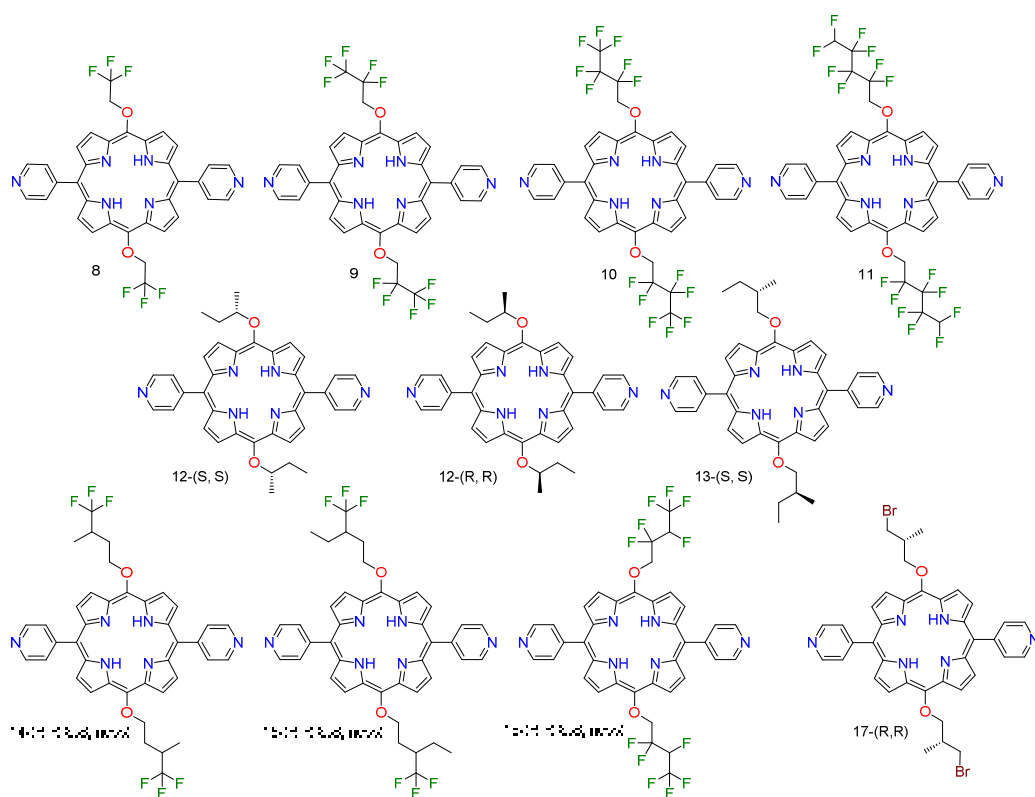


Schéma 3. 11 nouveaux tectons porphyriniques synthétisés.

Les tectons synthétisés par cette méthode peuvent être divisés en trois groupes; le premier (tectons **8-11**) est un ensemble de porphyrines avec un nombre croissant de fluorures sur les chaînes alkyles (de 6 à 16 atomes de fluor), un second groupe comprend les tectons chiraux **12** et **13**, le dernier ensemble est constitué de porphyrines chirales et halogénées (**14-17**). Cette voie de synthèse semble être appropriée à l'introduction d'une grande variété de substituants en positions *méso* de la porphyrine et elle sera utilisée dans le laboratoire dans un proche avenir afin de générer de nouveaux tectons porphyriniques

Les onze nouveaux tectons ont été caractérisés par ¹H-, ¹³C-, et ¹⁹F- RMN, UV-vis et spectrométrie de masse. Concernant **14**, **15** et **16**, un mélange racémique d'alcool a été utilisé lors

de la dernière étape, nous avons supposé qu'ils étaient composés d'un mélange statistique correspondant à 50% du racémate (25% de (R, R), 25% de (S, S)) et 50% de *méso* (R, S).

Des mono-cristaux ont été obtenus pour sept tectons. Leur analyse par diffraction de rayons X a permis de mettre en évidence les interactions intermoléculaires spécifiques à l'état solide en fonction de la structure des tectons et notamment du nombre de fluors présents à la périphérie du macrocycle. Concernant plus particulièrement les contacts F---F, nous constatons de nombreux contacts intermoléculaires F---F pour les deux tectons **16** et **11** avec des distances F---F de 2.72 à 2.94 Å.

II. Polymères de coordination.

Afin de générer des MOFs chiraux et/ou halogénés, les tectons porphyriniques obtenus ont été combinés avec des cations métalliques. De nombreux cations ont été utilisés et de multiples conditions de cristallisation testées.

La formation de réseaux de coordination peut résulter de deux stratégies : soit de l'auto-assemblage de tectons métallo-organiques auto-complémentaires, soit de la reconnaissance entre un tecton organique ou métallo-organique et un/ou des composants métalliques externes.

II.A. Réseaux de coordination à base de tectons auto-complémentaires.

L'utilisation de tectons auto-complémentaire neutre a pour avantage d'éviter l'inclusion de contre-ions dans le réseau formé. Dans ce cadre, une métalloporphyrine de Zn(II) substituée en position méso par des groupements de type pyridine est parfaitement adaptée.

Les porphyrines synthétisées (schéma 1 et schéma 3) ont trois pôles coordonnant: le noyau de la porphyrine (tétradentate) et les deux unités pyridyls monodentates.

L'insertion de Zn(II) dans la cavité conduit à la formation de tectons neutres auto-complémentaires pouvant générer des réseaux de coordination 1-D, 2-D ou 3-D en fonction de la sphère de coordination du cation Zn(II) (schéma 4).⁴ En effet, la coordination d'une seule pyridine en position axiale du Zn(II) conduit à la formation d'un réseau de 1D, tandis que la coordination de deux pyridines en position axiale du Zn²⁺ peut générer un réseau bi ou tridimensionnel en fonction de l'angle dièdre entre le plan moyen de la porphyrine et celui des pyridines apicales.

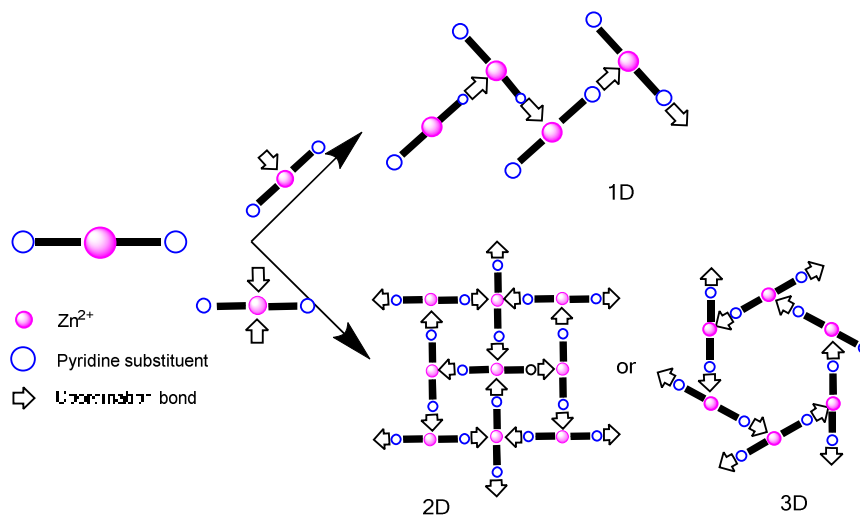


Schéma 4. Représentation schématique de la topologie des réseaux de coordination formés par auto-assemblage de tectons Zn-porphyrines.

Nous avons étudié la formation de réseaux de coordination à l'état monocristallin à partir des 13 tectons décrits précédemment en présence de Zn(II). La méthode de choix pour caractériser ces assemblages est la diffraction des rayons X sur monocristaux. Nous avons réalisé de multiples essais de cristallisation, en particulier dans le cas des ligands chiraux.

L'analyse des monocristaux obtenus a révélé dans tous les cas la formation de réseaux 1D dans lesquels seule une des *méso*-pyridines est coordonnée en position axiale du Zn^{2+} d'un tecton adjacent. Le cation métallique est donc pentacoordiné et adopte une géométrie pyramidale à base carrée. La seconde *méso*-pyridine est dans certains cas en interaction de type liaison H avec une molécule de solvant de cristallisation. A titre d'exemple, le tecton **4** conduit à la formation d'un réseau 1D en présence de MeOH ou de trifluoroéthanol. Dans les deux cas, une molécule d'alcool forme une liaison H avec l'azote de la pyridine non coordonnée. La structure du réseau obtenu en présence de trifluoroéthanol est représentée sur la figure 1.

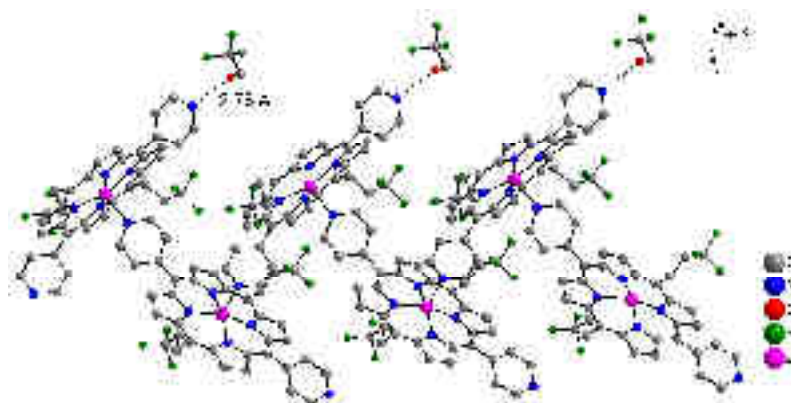


Figure 1. La structure 1-D formée par tecton **4** en présence de $Zn(OAc)_2$ et de trifluoroéthanol. Les atomes d'hydrogène ont été omis pour plus de clarté.

Toutefois, en modifiant légèrement les conditions de cristallisation, il a été possible de générer, à partir des tectons **4** et **15**, un mélange de deux types de monocristaux. Le produit majoritaire reste le réseau 1D, alors que le produit minoritaire correspond à un réseau 2D de type

grille (figure 2). La formation de cette architecture est possible grâce à la coordination de deux pyridines provenant de deux porphyrines adjacentes en position axiale de Zn^{2+} . L'ion métallique est donc hexacoordiné et les deux *méso*-pyridines sont impliquées dans des liaisons de coordination. Au sein du réseau, aucune molécule de solvant n'est présente et toutes nos tentatives pour remplir les cavités par diffusion de vapeur de solvant ont été infructueuses.

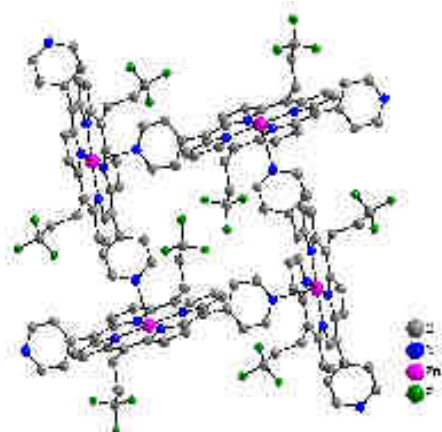


Figure 2. La grille 2D obtenue par auto-assemblage **4-Zn**. Les atomes d'hydrogène ont été omis pour plus de clarté.

L'analyse systématique des interactions intermoléculaires présentes dans les réseaux 1D formés à partir des porphyrines représentées sur le schéma 3 a mis en évidence la formation d'interactions π - π entre les macrocycles porphyriniques (figure 3), en particulier dans le cas des mono-cristaux ne contenant pas de molécules de solvant. Pour les porphyrines possédant 6 et 10 atomes de fluor (tecton **8** et **9** respectivement) sur le squelette de porphyrine, l'empilement cristallin révèle des interactions π - π (3.4 Å) entre les chaînes 1D adjacentes (figure 3). De plus, on note également la formation de liaison H faibles impliquant les atomes de fluor des chaînes alkyles (3.1 à 3.4 Å).

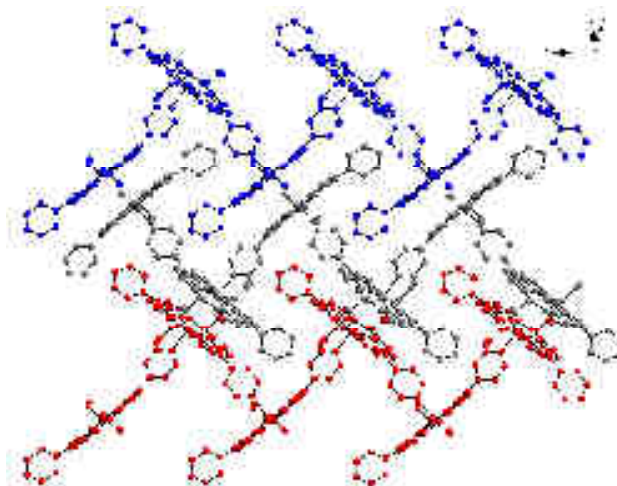


Figure 3. Empilement cristallin illustrant les interactions π - π présentes dans le réseau 1D obtenu à partir de l'autoassemblage de **8-Zn**.

En considérant plus spécifiquement les contacts F---F présents à l'état solide, ces interactions sont présentes dans les cristaux obtenus par auto-assemblage des tectons **8-Zn**, **16-Zn**, **10-Zn** et **11-Zn** portant 6, 12, 14 et 16 atomes de fluor. Alors que pour la **16-Zn** et **10-Zn**, le

nombre de contacts F---F (type I) par porphyrine est constant avec 3 contacts de type I, la distance F---F passe de 2.91 Å à 2.74 Å. Dans la structure de **11-Zn** (16 F/porphyrine), on observe 8 contacts F---F par porphyrine avec des distances F---F de *ca* 2.82 Å et des angles θ_1 et θ_2 indiquant des contacts F---F de type II.

L'analyse structurale des réseaux 1D obtenus à partir des complexes porphyriniques de Zn(II) semble indiquer que logiquement plus le nombre de fluors à la périphérie du macrocycle est important plus des interactions F---F sont présentes dans le cristal.

Nous avons effectué de nombreux tests de cristallisation en présence de solvants fluorés ou/et chiraux. Des tests sont toujours en cours, mais à ce jour, outre les cristaux obtenus pour **Zn-4** en présence de trifluoroéthanol (figure 1) nous n'avons isolé aucun monocristal contenant ces solvants.

Nous avons également tenté d'insérer ces solvants (chiraux et/ou fluorés) par une transformation de mono-cristal à mono-cristal, notamment sur les réseaux 2D formé par auto-assemblage de **4-Zn** et **15-Zn** pour lesquels les cavités sont vides. Malheureusement dans tous les cas, ceci n'a pas abouti.

II.B. Réseaux de coordination à base de deux tectons

Les porphyrines obtenues possèdent deux pyridines en position méso *trans* et peuvent donc générer des réseaux moléculaires par coordination à un cation métallique externe, c'est-à-dire non intégré dans la cavité porphyrinique. Selon la nature du cation métallique et ses préférences en termes de géométrie de coordination (nombre et la position relative des sites de coordination libres), la formation des architectures 1D, 2D ou 3D est possible. Dans notre cas, de nombreuses tentatives ont été effectuées afin de faire croître des monocristaux à partir des porphyrines décrites précédemment et de cations métalliques externes tels que Cu^{2+} , Co^{2+} , Ni^{2+} , Cd^{2+} , Hg^{2+} , Ag^+ . De nombreuses tentatives ont conduit à la formation de poudres amorphes et des essais sont toujours en cours.

Nous avons pu isoler des monocristaux dans deux cas en présence de Cd(II).

Leur analyse par diffraction des rayons X a révélé la formation d'un réseau de coordination 2D en présence de CdBr_2 et du tecton **4**. Le cation métallique est hexacoordiné avec quatre pyridines appartenant à 4 porphyrines adjacentes dans le plan équatorial et deux anions bromure en positions axiales. Chaque tecton est coordonné à deux Cd^{2+} par l'intermédiaire de liaisons Cd(II)-pyridine (figure 4a).

Dans le cas de porphyrine **10**, dans des conditions de cristallisation similaires, la formation d'un réseau 3D a été observée (figure 4b). Dans ce cas, les ions Cd(II) forment une chaîne polymérique (Cd_2Br_4) le long de l'axe *c*. Chaque Cd^{2+} est hexacoordiné, avec quatre bromures et deux pyridines en position cis. Tous les bromures sont pontants, ce qui conduit bien à une stœchiométrie de deux bromures pour un Cd(II). Cette disposition particulière des unités de

pyridyle conduit à la formation d'un polymère de coordination 3D. Fait intéressant, dans ce cas, on observe de contacts F---F de 2.6 Å dans les canaux (figure 4b).

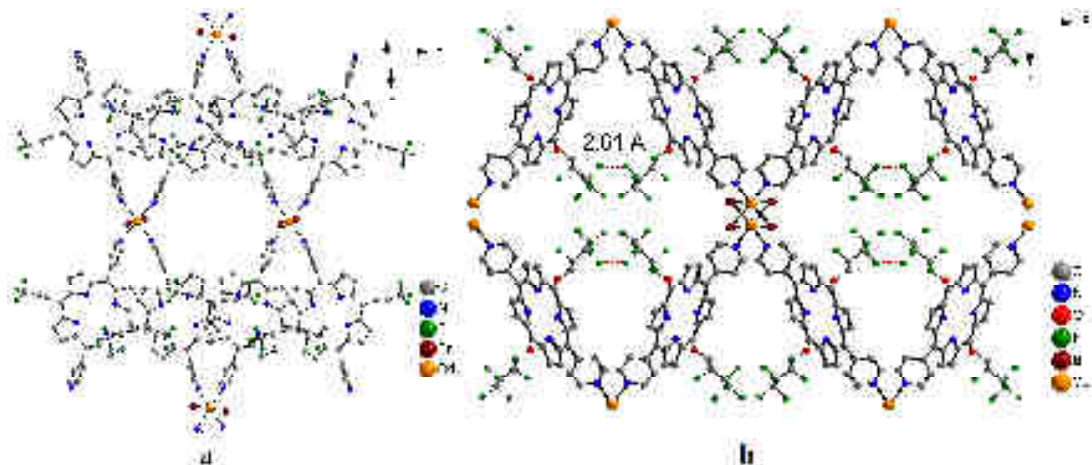


Figure 4. Réseaux de coordination obtenus en présence de CdBr_2 , a) avec le tecton **4**, b) avec le tecton **10**.

Dans les deux cas, les réseaux sont stables et les chaînes alkyles fluorées décorent les cavités. Nous avons tenté d'insérer divers solvants dans ces cavités, notamment des solvants fluorés, mais à ce jour aucun essai n'a abouti.

III. Réseaux moléculaires formés par liaisons halogène.

La dernière partie du manuscrit se concentre sur les réseaux moléculaires formés à partir de liaisons halogènes de type I---N.

Le 1,4-diiodotetrafluorobenzène (DIFB) et le 1,3,5-triiodotrifluorobenzène (TIFB) sont des briques moléculaires qui ont été largement utilisées pour générer des réseaux moléculaires avec différentes topologies et dimensionnalités en présence de composés de type 4,4'-bipyridine.

Nous avons étendu cette étude à deux types de tectons :

- des composés organiques obtenus dans le cadre d'une collaboration avec le groupe du Pr Stefan Bräse (Karlsruhe Institute of Technology, Allemagne). Il s'agit de deux tectons linéaires de type 4,4'-bipyridine de longueur différente, KIT-1 et KIT-2 (figure 5). Le tecton KIT-3 est de longueur similaire à KIT-1 mais la présence d'un substituant de type azobenzène pourrait conduire à la formation de réseaux moléculaires photo-commutables.

- l'ensemble des porphyrines décrites précédemment. En effet, ces tectons peuvent faire office d'accepteurs de liaisons halogènes par l'intermédiaire des atomes d'azotes des deux *méso*-pyridines et conduire, en présence de DIFB ou de TIFB, à la formation de réseaux moléculaires hautement fluorés et/ou chiraux.

III.A. Réseaux obtenus en présence de 4,4'-bipyridine « allongées »

Cette étude se concentre sur la formation de réseaux moléculaires à base de tectons bipyridyle des longueurs différentes avec des dérivés benzéniques iodofluorés (figure 5).

En présence du composé monoiodé (IFB), des cristaux ont été obtenus avec les tectons KIT-1 et KIT-2. Le tecton IFB étant monodentate, il agit comme un bouchon. On obtient logiquement une stoechiométrie tecton/IFB de 2/1 dans le cristal.

Dans le cas du DIFB, l'assemblage avec KIT-1, KIT-2 et KIT-3 conduit à la formation des chaînes 1D par des interactions N---I (2.78 Å) et des liaisons H (H---F de 3.1 à 3.5 Å) entre les chaînes consécutives.

Des études préliminaires d'irradiation des cristaux obtenus avec KIT-3 ont été effectuées. A ce jour, elles n'ont pas permis de mettre en évidence la photo-isomérisation Z/E à l'état solide de la fonction diazobenzène mais ces études seront approfondies.

Tous les réseaux obtenus en présence de 1,3,5-triiodotrifluorobenzène ont mis en évidence la formation de deux liaisons halogènes I---N sur les trois possibles, et des réseaux 1D sont formés dans le cas de KIT-1 et KIT-2.

Les cristaux obtenus ne contiennent pas de molécules de solvants et des essais de piégeage de solvants seront effectués au laboratoire.

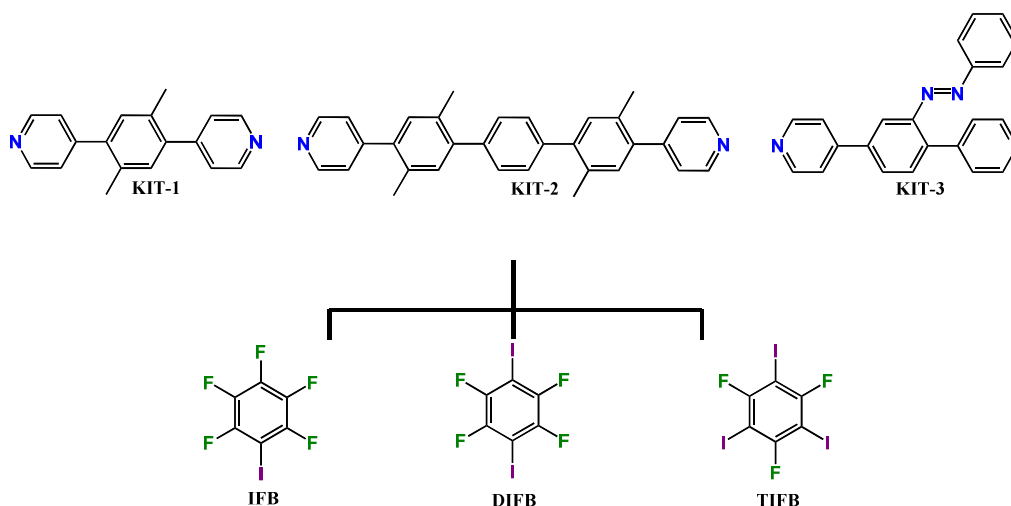


Figure 5. Tectons utilisés pour générer des réseaux supramoléculaires.

III.B. Réseaux à base de porphyrines chirales et/ou fluorés et de DIFB ou TIFB.

Nous avons voulu exploiter les tectons porphyriniques synthétisés comme accepteur de liaison halogènes et étudier leur cristallisation en présence de DIFB et TIFB. Des monocristaux adéquats pour la DRX ont été obtenus par combinaison DIFB avec les tectons fluorés **4**, **9**, **10**, **11** contenant respectivement 6, 10, 14, 16 et de **16** (mélange de racémate + méso) contenant 12 atomes de fluor. Les cristaux obtenus à partir de la tecton **4** ont un rapport Porphyrine/DIFB de 2:1, et ceux obtenus à partir des tectons **9**, **10**, **11** et **16** cristallisent en stoechiométries Porphyrine/DIFB de 1:2. De nombreuses tentatives ont été faites dans le but de modifier ces rapports et en particulier d'obtenir un adduit 1:1, mais dans tous les cas avec une concentration inférieure de DIFB, on observe la formation de cristaux composés uniquement de la porphyrine. D'autre part, des concentrations plus élevées de DIFB ne changent pas le rapport Po/DIFB.

Le tecton **4** conduit à un rapport Po/DIFB 2:1 (figure 6). On note la formation d'un réseau 1D impliquant des DIFB connectant deux porphyrines adjacentes ($N \cdots I = 3.00 \text{ \AA}$). La deuxième porphyrine ne forme pas de liaisons $N \cdots I$ mais est présente entre les chaînes 1D via des interactions de type liaison H entre les fluorures des DIFB et les *méso*-pyridines.

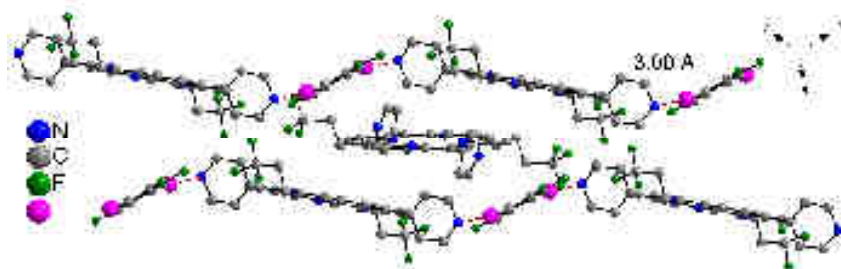


Figure 6. Une partie de la structure obtenue lors de la combinaison de tecton **4** avec DIFB se concentrant sur les interactions $N \cdots I$ (lignes pointillées rouges). Les atomes d'hydrogène ont été omis pour plus de clarté.

Dans tous les autres cas, le rapport porphyrine/DIFB est de $\frac{1}{2}$, une porphyrine et un DIFB forme un réseau 1D ($N \cdots I$ proche de 2.75 \AA). Pour les tectons **9**, **10**, **16**, et **11** le deuxième DIFB présent dans l'unité asymétrique forme des contacts $I \cdots I$ (3.81 \AA) avec les DIFB de deux chaînes adjacentes générant un réseau moléculaire 2-D (Figure 7).

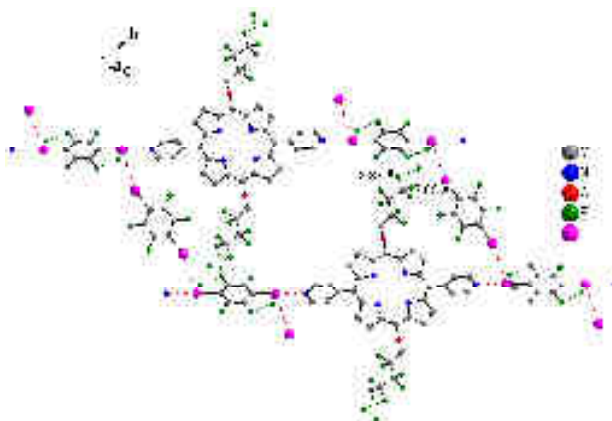


Figure 7. Une partie de la structure obtenue lors de la combinaison de la tecton **10** avec DIFB. Les interactions $N \cdots I$ et $I \cdots I$ apparaissent en pointillés rouges et les contacts $F \cdots F$ en vert pointillés.

Les atomes d'hydrogène ont été omis pour plus de clarté.

Comme pour les réseaux de coordination décrits précédemment, un nombre croissant d'atomes de fluorures présents à la périphérie du macrocycle porphyrinique conduit à une augmentation du nombre de contacts $F \cdots F$ entre les porphyrines et les DIFB. L'ensemble de ces cristaux se décomposent à l'air et forment un poudre amorphe.

Des tentatives visant à introduire un troisième composant lors de la cristallisation (solvant fluoré ou chiraux) sont encore en cours.

Conclusions.

Nous avons conçu, synthétisé et caractérisé 13 nouveaux tectons à base de porphyrines contenant des chaînes fluorés et /ou chirales en position *méso trans*. Tous ces nouveaux tectons ont été caractérisés par les méthodes classiques (RMN ^1H , RMN ^{19}F , Spectroscopie UV-Visible et Spectrométrie de masse) et pour certains d'entre eux par Diffraction des Rayons X sur monocristal.

Dans un deuxième temps, nous avons étudié la formation de réseaux de coordination à partir de ces tectons en testant deux approches: la première est basée sur l'assemblage de tectons auto-complémentaire neutre en utilisant les positions axiales du cation métallique présent à l'intérieur de la cavité porphyrinique. La deuxième approche est basée sur la génération du réseau de coordination grâce à la coordination d'un métal à l'extérieur de la cavité porphyrinique

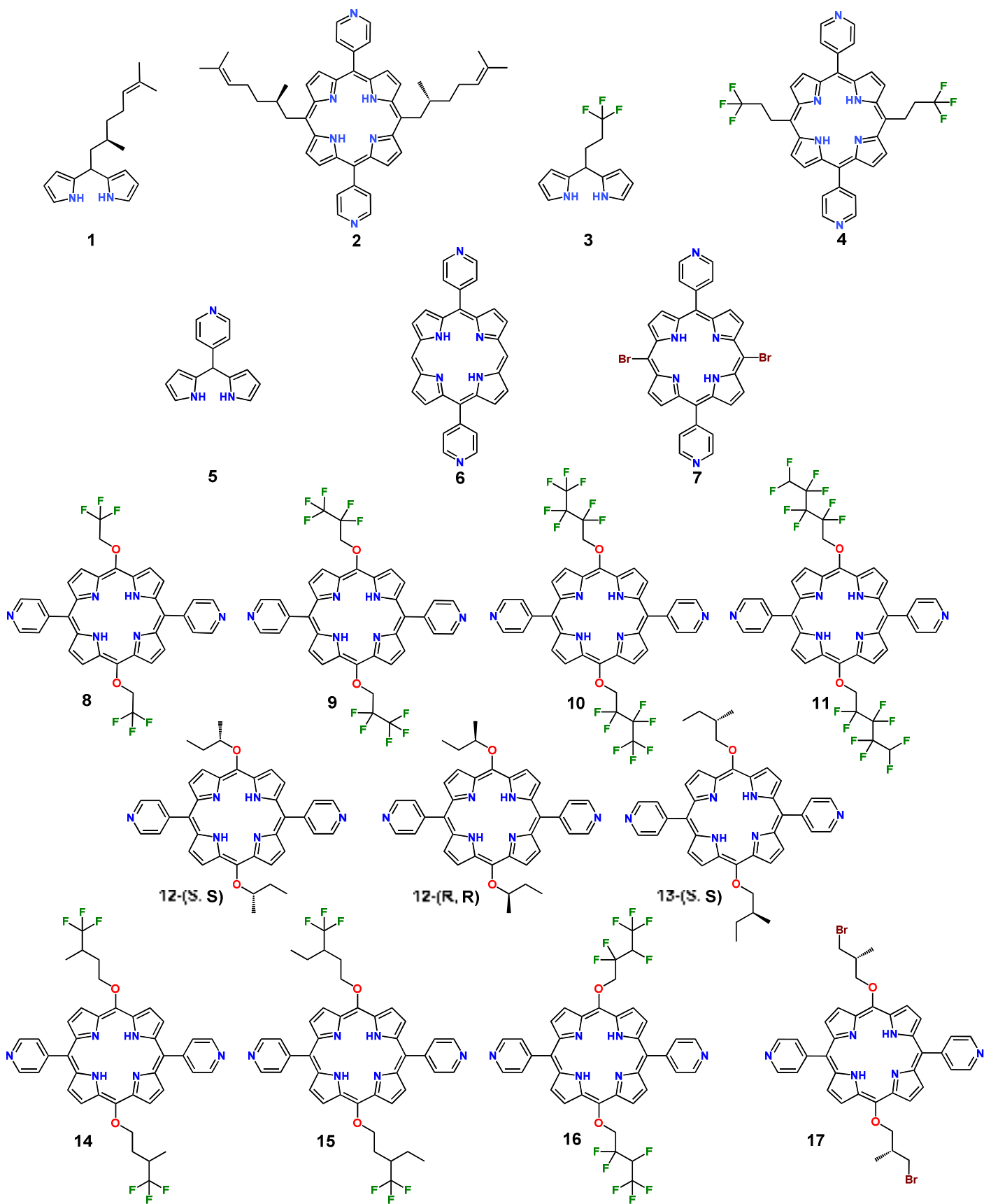
Dans le premier cas, l'auto-assemblage de porphyrines de Zn(II) a permis de générer des réseaux de coordination monodimensionnels hautement fluorés et/ou chiraux. Une étude systématique des interactions présentes à l'état solide en fonction de la nature des substituants en position *méso* a été effectuée. Pour les porphyrines contenant des chaînes alkyles fluorées liés à la position *méso* par une jonction d'éther, les chaînes 1-D affichent des caractéristiques intéressantes par rapport aux contacts F---F. En effet, lorsqu'on augmente le nombre d'atomes de fluor, des contacts F---F (type I) entre les chaînes sont observés et leur nombre augmente avec le nombre d'atomes de fluor présents à la périphérie de la porphyrine. Des études de piégeage de solvants chiraux et/ou fluorés dans tels assemblages sont toujours en cours. La deuxième approche a permis de générer des réseaux bi- et tri-dimensionnel en présence de Cd(II).

Nous avons également étendu cette étude à la formation d'architectures basées sur la liaison halogène et plus spécifiquement la liaison N---I et ce à partir des porphyrines synthétisées en présence de diiodo ou triodofluorobenzène. A nouveau des réseaux moléculaires hautement fluorés ont pu être obtenus et caractérisés par diffraction des RX. Des essais de piégeage de molécules fluorées et/ou chirales dans de tels édifices est toujours en cours.

Le but ultime de cette étude est d'obtenir des cristaux poreux capables de séparer les mélanges racémiques de molécules chirales halogénés. Bien que ce but n'ait pas été atteint à ce jour, cette étude a permis de poser les premières briques de l'édifice. En effet, la compréhension des interactions responsables de la formation de réseaux moléculaires et de leur empilement dans la phase cristalline est une étape importante vers la conception de matériaux poreux pour les procédés de séparation chirale. De nombreux assemblages ont été obtenus, caractérisés et analysés lors de ce travail. A ce jour, de nombreux essais sont toujours cours au laboratoire.

Références

1. M. W. Hosseini, *CrystEngComm*, 2004, **6**, 318-322.
2. M. W. Hosseini, *Acc. Chem. Res*, 2005, **38**, 313-323.
3. O. M. Yaghi and H. Li, *J. Am. Chem. Soc.*, 1995, **117**, 10401-10402.
4. V. Bulach and M. W. Hosseini, *Handbook of Porphyrin Science*, Eds. K. Kadish, K. Smith and R. Guilard, World Scientific, 2011, **13**, 299-391.
5. E. Kuhn, V. Bulach and M. W. Hosseini, *Chem. Commun.*, 2008, 5104-5106.
6. D. P. N. Goncalves, S. Ladame, S. Balasubramanian and J. K. M. Sanders, *Org. Biomol. Chem.*, 2006, **4**, 3337-3342.
7. G.-Y. Gao, A. J. Colvin, Y. Chen and X. P. Zhang, *Org. Lett.*, 2003, **5**, 3261-3264.



Poster Presentations

- “*Molecular tectonics: Coordination networks based on fluorinated porphyrins*”
Elena Vulpe, Véronique Bulach, Mir Wais Hosseini, *Gecom Concoord*, Lyon (France), 26 – 29 May, **2015**
- “*Molecular tectonics: fluorinated porphyrin based coordination networks*”
Elena Vulpe, Véronique Bulach, Mir Wais Hosseini, *Suprachim +*, Strasbourg (France), 8 - 12 September, **2014**.

Oral Communications

- “*Fluorinated porphyrin based coordination networks*”
Elena Vulpe, Véronique Bulach, Mir Wais Hosseini, *Chiranet Meeting*, Karlsruhe Institute of Technology (Germany), March 24, **2015**
- “*Fluorinated porphyrin based coordination networks*”
Elena Vulpe, Véronique Bulach, Mir Wais Hosseini, *Journée des Doctorants*, University of Strasbourg (France), November 7, **2014**
- “*Functionalized porphyrins and their networks*”
Elena Vulpe, Véronique Bulach, Mir Wais Hosseini, *Chiranet Meeting*, University of Kaiserslautern(Germany), October 15, **2014**
- “*Fluorinated porphyrin based coordination networks*”,
Elena Vulpe, Véronique Bulach, Mir Wais Hosseini, *Fujita-Hosseini Meeting*, University of Strasbourg(France), September 12, **2014**.
- “*Coordination networks based on chiral porphyrins*”
Elena Vulpe, Véronique Bulach, Mir Wais Hosseini, *Chiranet Meeting*, University of Strasbourg (France), March 11, **2014**
- “*Coordination networks based on chiral porphyrins*”
Elena Vulpe, Véronique Bulach, Mir Wais Hosseini, *Chiranet Meeting*, Karlsruhe Institute of Technology (Germany), October 1, **2013**
- “*Coordination networks based on chiral porphyrins*”
Elena Vulpe, Véronique Bulach, Mir Wais Hosseini, *Chiranet Meeting*, University of Kaiserslautern(Germany), March 22, **2013**

Tectonique Moléculaire à base de Porphyrines Fluorées

Résumé

Les travaux décrits dans ce manuscrit utilisent les principes de la tectonique moléculaire pour générer des polymères de coordination hautement fluorés et/ou chiraux pour une application potentielle en séparation chirale. La synthèse de 13 porphyrines de type A_2B_2 substituées en position *méso* par deux pyridines et par deux chaînes fluorées et/ou alkyles a été mise au point. Des réseaux de coordination ont été obtenus en présence de Zn(II) et de Cd(II) et caractérisés par diffraction des RX sur monocristal (DRX). Une analyse systématique des interactions supramoléculaires et notamment de interactions F---F présentes à l'état solide a été conduite. Des réseaux à base de liaisons halogènes ont également été obtenus en présence de di- et tri-iodoarènes et caractérisés par DRX.

Le premier chapitre est une introduction générale sur la tectonique moléculaire, le deuxième chapitre décrit les voies des synthèses utilisées pour générer les ligands chiraux et fluorés et leur caractérisation à l'état solide. Le troisième chapitre présente la structure des réseaux mono, bi, et tridimensionnels formés en présence de Zn(II) ou de Cd(II), l'analyse structurale met en évidence un nombre croissant d'interaction F---F en fonction du nombre de fluors présents à la périphérie du macrocycle porphyrinique. Le dernier chapitre se concentre sur l'utilisation des liaisons halogènes de type N---I impliquant des porphyrines ou des tectons de type bipyridine et une série d'iodofluoroarènes.

Mots-clés : Tectonique Moléculaire, Chimie Supramoléculaire, Polymères de Coordination, Porphyrine, Chiralité, Interactions halogène- halogène, Liaisons halogène, Fluor.

Abstract

This manuscript focuses on the use of molecular tectonics to generate chiral and / or fluorinated coordination polymers based on porphyrin building blocks for potential application in chiral separation. Synthesis of novel A_2B_2 fluorinated porphyrin tectons is described and their combinations with metal ions and haloarenes molecules are characterized by X-Ray diffraction.

The first chapter gives a general introduction on molecular tectonics; the second chapter focuses on the synthetic routes used for the synthesis of highly fluorinated and/or chiral porphyrins and their solid state characterization by X-Ray diffraction analysis, highlighting the importance of the number of fluorine atoms present at the periphery of the tecton on the crystal packing. The third chapter presents the mono-, bi- and three dimensional networks formed by a combination of the porphyrins with Zn(II) or Cd(II). In the solid state, short F---F contacts were observed depending on the number of fluorine atoms present on the porphyrin backbone. The last chapter focuses on the use of halogen bonds, by merging the neutral porphyrin or bipyridine tectons with a series of iodofluoroarenes. The crystalline materials described in this work can be used as potential candidates for the separation of chiral and fluorinated molecules.

Keywords : Molecular tectonics, Supramolecular Chemistry , Porphyrin chemistry, Halogen bonding, Coordination polymers, Halogen bonded networks, Halogen-halogen interactions, Fluorine.